

# CHEMICAL EVOLUTION OF NEARBY STELLAR SYSTEMS

## **Inauguraldissertation**

zur Erlangung der Würde des Doktorgrades der Philosophie

vorgelegt der  
Philosophisch-Naturwissenschaftlichen Fakultät  
der Universität Basel

von

ANDREA KAYSER

aus Iserlohn/Deutschland

Basel, 2007

Genehmigt von der Philosophisch-Naturwissenschaftlichen Fakultät

auf Antrag von  
Prof. Dr. Eva K. Grebel und Prof. Dr. John S. Gallagher

Basel, den 13. November 2007

Prof. Dr. Hans-Peter Hauri  
Dekan

”Es gibt ein großes und doch ganz alltägliches Geheimnis. Alle Menschen haben daran teil, jeder kennt es, aber die wenigsten denken je darüber nach. Die meisten Leute nehmen es einfach so hin und wundern sich kein bisschen darüber. Dieses Geheimnis ist die Zeit.”

*Michael Ende, Momo*



*”Für meine Eltern.”*



# Contents

<b>1</b>	<b>Motivation</b>	<b>1</b>
<b>2</b>	<b>Introduction</b>	<b>3</b>
2.1	The Local Group . . . . .	3
2.2	The Milky Way and its globular cluster system . . . . .	5
2.3	The Magellanic Clouds and their star clusters . . . . .	8
2.4	Theoretical chemical evolution models adapted to the SMC . . . . .	13
2.4.1	Simple closed box model by Da Costa & Hatzidimitriou (1998) . . . . .	13
2.4.2	Models by Pagel & Tautvaisiene (1998) including time delays . . . . .	14
<b>3</b>	<b>CN and CH in Galactic Globular Clusters</b>	<b>17</b>
3.1	Introduction . . . . .	18
3.2	Observations and data reduction . . . . .	22
3.2.1	Observations . . . . .	22
3.2.2	Data reduction . . . . .	22
3.3	CN and CH band strengths . . . . .	24
3.3.1	CN band strengths . . . . .	24
3.3.2	CN vs. CH . . . . .	27
3.3.3	Cyanogen excess parameter ( $\delta\text{CN}$ ) . . . . .	28
3.4	CN-CH - anticorrelation . . . . .	32
3.5	Trends with cluster parameters . . . . .	36
3.6	Summary and conclusions . . . . .	40
3.A	Appendix: Target stars in Galactic globular clusters . . . . .	43
<b>4</b>	<b>Structural Parameters of Star Clusters in the SMC</b>	<b>55</b>
4.1	Introduction . . . . .	56
4.2	Data and data reduction . . . . .	57
4.3	Cluster core radii . . . . .	61
4.3.1	Cluster centers . . . . .	62
4.3.2	Completeness test . . . . .	66
4.3.3	Surface brightness profiles and core radii . . . . .	68
4.3.4	Comparison with previous studies . . . . .	70
4.3.5	Cluster evolution . . . . .	70
4.4	Cluster radial velocities and velocity dispersions . . . . .	74
4.4.1	Comparison with previous studies . . . . .	79
4.5	Summary . . . . .	84

<b>5</b>	<b>The Age-Metallicity Relation and SF History of the SMC</b>	<b>85</b>
5.1	Introduction . . . . .	86
5.2	Data . . . . .	88
5.2.1	Target selection . . . . .	88
5.2.2	Observations . . . . .	90
5.2.3	Data reduction . . . . .	91
5.3	Calcium triplet metallicities . . . . .	93
5.4	Metallicity determination . . . . .	95
5.4.1	$(V - V_{HB})$ . . . . .	95
5.4.2	Velocities . . . . .	97
5.4.3	[Fe/H] for individual RBs . . . . .	97
5.5	Analysis of the star clusters . . . . .	99
5.5.1	Membership . . . . .	99
5.5.2	Considering outliers . . . . .	101
5.5.3	Metallicities . . . . .	110
5.6	Results . . . . .	113
5.6.1	Spatial distribution . . . . .	113
5.6.2	Age-metallicity relation . . . . .	116
5.6.3	Comparison with theoretical models of chemical evolution . . . . .	119
5.6.4	Discussion . . . . .	123
5.7	Summary and Conclusions . . . . .	131
5.A	Appendix: Target stars in SMC star clusters . . . . .	133
<b>6</b>	<b>Summary, Conclusions, and Outlook</b>	<b>151</b>
<b>A</b>	<b>Chemical Evolution Models</b>	<b>155</b>
A.1	Basic assumptions and equations . . . . .	155
A.2	Instantaneous recycling approximation . . . . .	156
A.3	Simple closed-box model . . . . .	157
A.3.1	The G-dwarf problem . . . . .	157
A.4	Leaky box model . . . . .	158
A.5	Accreting box model . . . . .	159
<b>B</b>	<b>List of Abbreviations</b>	<b>161</b>
	<b>Bibliography</b>	<b>163</b>
	<b>Acknowledgments</b>	<b>173</b>
	<b>Curriculum Vitae</b>	<b>175</b>



# List of Figures

2.1	The Local Group . . . . .	4
2.2	The Milky Way . . . . .	5
2.3	Omega Centauri . . . . .	7
2.4	The Magellanic Clouds . . . . .	9
2.5	Star clusters in the Magellanic Clouds . . . . .	10
2.6	Cartoon of SMC-LMC-MW interaction . . . . .	12
2.7	Simple closed box model by Da Costa & Hatzidimitriou (1998) . . . . .	14
2.8	Smooth chemical evolution model by Pagel & Tautvaisiene (1998) . . . . .	15
2.9	Bursting chemical evolution model by Pagel & Tautvaisiene (1998) . . . . .	16
3.1	Typical spectrum of a RGB star in the globular cluster NGC 288 . . . . .	20
3.2	Color magnitude diagrams for the globular clusters in our sample . . . . .	21
3.3	Distribution of the stars of the different clusters in the CN vs. $M_V$ diagram . . . . .	25
3.4	Distribution of the RGB stars in the CN vs. CH diagram . . . . .	27
3.5	Fitting of the lower envelope and definition of $\delta\text{CN}$ . . . . .	28
3.6	Distributions of the CN-excess parameter in the RGB stars . . . . .	29
3.7	Combined histograms of the CN-excess parameter . . . . .	30
3.8	Combined distributions of the CN-excess parameters for SGB and MS stars . . . . .	32
3.9	CN vs. $M_V$ and CH vs. $M_V$ diagrams for the eight clusters in our sample . . . . .	33
3.10	Ratio of CN-strong/CN-weak stars vs. various cluster parameters . . . . .	37
3.11	Combining our r-parameter with literature values . . . . .	39
4.1	Quality of the photometric data . . . . .	60
4.2	Comparison of our photometry with the catalog of Zaritsky et al. (2002) . . . . .	61
4.3	Area plots and CMDs of twelve SMC star clusters . . . . .	63
4.4	Selection of member candidates from the CMD of the cluster NGC 411 . . . . .	64
4.5	Determination of the star cluster centers . . . . .	66
4.6	CMD of the inner region of the cluster Ln 116 . . . . .	67
4.7	Completeness depending on brightness of the star and distance from the cluster center . . . . .	68
4.8	Annuli for the radius determinations . . . . .	69
4.9	Surface brightness profiles of SMC star clusters . . . . .	71
4.9	Surface brightness profiles of SMC star clusters - <i>continued</i> . . . . .	72
4.10	Comparison of core radii derived in previous studies with our results . . . . .	73
4.11	Age vs. core radius diagram for the SMC star clusters . . . . .	74
4.12	Contour plots of through slit acquisition image of NGC 416 . . . . .	75

4.13	Heliocentric velocity vs. distance from the cluster center . . . . .	77
4.13	Heliocentric velocity vs. distance from the cluster center - <i>continued</i> . . . . .	78
4.14	Comparison of measured velocities with literature values . . . . .	80
4.15	Heliocentric velocity vs. position angle . . . . .	81
4.16	Velocity distribution frequency of star clusters in the SMC . . . . .	82
5.1	Optical image of the SMC . . . . .	87
5.2	Position of the SMC clusters . . . . .	89
5.3	Target selection for L11 . . . . .	90
5.4	Example of CaII triplet spectra . . . . .	92
5.5	Comparison of measured horizontal branch/red clump magnitudes with literature data . . . . .	95
5.6	Comparison of measured red clump magnitudes with theoretical horizontal branch magnitudes . . . . .	96
5.7	Consistency check with calibration by Cole et al. (2004) . . . . .	98
5.8	Velocity distributions for stars in and around SMC star clusters . . . . .	102
5.8	Velocity distributions for stars in and around SMC star clusters - <i>continued</i> . . . . .	103
5.9	CMDs for SMC star clusters and their surrounding fields . . . . .	104
5.9	CMDs for SMC star clusters and their surrounding fields - <i>continued</i> . . . . .	105
5.10	Summed equivalent width vs. $V - V_{\text{HB}}$ . . . . .	106
5.10	Summed equivalent width vs. $V - V_{\text{HB}}$ - <i>continued</i> . . . . .	107
5.11	Stellar metallicity as a function of distance from the cluster center . . . . .	108
5.11	Stellar metallicity as a function of distance from the cluster center - <i>continued</i> . . . . .	109
5.12	Comparison of the newly derived spectroscopic metallicities with literature values from various sources . . . . .	110
5.13	Frequency distribution of cluster metallicities . . . . .	111
5.14	Comparing photometric literature values on different metallicity scales . . . . .	113
5.15	Positions of the SMC clusters color-coded by their metallicities . . . . .	114
5.16	Metallicity and age gradients in the SMC . . . . .	115
5.17	Age-metallicity relation of the SMC . . . . .	116
5.18	Age-metallicity relation of the SMC in comparison with the chemical evolution models by Da Costa & Hatzidimitriou (1998) . . . . .	120
5.19	Separation between inner and outer star clusters . . . . .	120
5.20	The age-metallicity relation of the SMC in comparison with chemical evolution models by Pagel & Tautvaisiene (1998) . . . . .	121
5.21	Distances in the LMC/SMC/MW system . . . . .	122
A.1	Schematic overview of the behavior of total mass, gas mass, and stellar mass and the metallicity for the Simple closed-box and balanced accretion model . . . . .	158

# List of Tables

2.1	Parameters of the Magellanic Clouds . . . . .	11
3.1	Log of observations . . . . .	19
3.2	Reddening, distance modulus, and photometric parameters of the MSTO for our sample globular clusters . . . . .	23
3.3	CN number ratios . . . . .	31
3.4	Global parameters of globular clusters of our sample . . . . .	35
3.A	Parameters of stars in NGC 288 . . . . .	43
3.B	Parameters of stars in NGC 362 . . . . .	45
3.C	Parameters of stars in NGC 5286 . . . . .	46
3.D	Parameters of stars in M 15 . . . . .	47
3.E	Parameters of stars in M 22 . . . . .	48
3.F	Parameters of stars in M 55 . . . . .	50
3.G	Parameters of stars in Pal 12 . . . . .	51
3.H	Parameters of stars in Ter 7 . . . . .	52
4.1	Observation log of photometry of SMC and MW clusters . . . . .	58
4.2	Zero points in photometric calibration . . . . .	59
4.3	Extinction coefficients and color terms of the photometric calibration . . . . .	59
4.4	Star cluster centers . . . . .	65
4.5	Derived properties of SMC clusters and literature values . . . . .	83
5.1	Log of spectroscopic observations of SMC star clusters . . . . .	91
5.2	Bandpass definitions . . . . .	97
5.3	Parameters of calibrating Galactic globular clusters . . . . .	99
5.4	Derived metallicities and adopted ages for SMC clusters . . . . .	117
5.5	Compilation of available SMC cluster data . . . . .	126
5.6	Overview of result and possible explanations . . . . .	130
5.A	Parameters of stars in Kron 28 . . . . .	134
5.B	Parameters of stars in Kron 44 . . . . .	135
5.C	Parameters of stars in Lindsay 11 . . . . .	136
5.D	Parameters of stars in Lindsay 32 . . . . .	138
5.E	Parameters of stars in Lindsay 38 . . . . .	139
5.F	Parameters of stars in Lindsay 116 . . . . .	140
5.G	Parameters of stars in NGC 152 . . . . .	141
5.H	Parameters of stars in NGC 339 . . . . .	142
5.I	Parameters of stars in NGC 361 . . . . .	144

5.J	Parameters of stars in NGC 411 . . . . .	145
5.K	Parameters of stars in NGC 416 . . . . .	146
5.L	Parameters of stars in NGC 419 . . . . .	148

# Chapter 1

## Motivation

One of the fundamental topics in astrophysical research is the formation and evolution of galaxies. It has been widely recognized that star clusters and especially globular clusters are cornerstones for the solution of a large variety of problems concerning the formation and evolution of galaxies. These dense concentrations of stars can be very luminous objects. With typical total luminosities of the order of  $M_V = -5$  to  $-10$  mag globular clusters are, unlike individual stars, observable even in galaxies far beyond our nearest neighborhood - the Local Group. Another valuable property is their ubiquity. Globular clusters are present in all morphological types of galaxies, ranging from none or very few in dwarf galaxies to ten-thousands in giant elliptical galaxies. It is widely accepted that star clusters form via contraction and fragmentation of molecular clouds. They consist of stars of the same age and chemical composition and are therefore good examples for simple stellar populations. Star clusters are thus considered as tracers of the environment of which they were formed. Whereas the Galactic globular clusters are all very old, in other galaxies, such as our closed neighboring galaxies, the Magellanic Clouds, massive and populous star clusters of different ages can be found. Since the globular-cluster-type clusters are among the most ancient objects in galaxies they mirror the early stages of their host. The youngest open clusters have just formed and resemble today's conditions. Thus studying the star cluster system of a galaxy is like a time travel through the different chemical and dynamical evolutionary phases of the host galaxy. This makes star clusters important objects in order to constrain models of the formation and evolution of galaxies.

Besides for galaxy evolution, star clusters are interesting objects in order to understand the evolution of stars and star clusters themselves. Since they host stars of different mass but the same age, one finds stars of all different evolutionary phases located roughly at the same distance. This makes them natural laboratories to confront stellar evolutionary theory with observations.

For a long time Galactic globular clusters have been considered to be very simple objects. The new generation of telescope and spectrographic facilities like the Hubble Space Telescope (HST) and the 8m- class terrestrial telescopes such as the Very Large Telescope (VLT) lead to the discovery of a number of peculiarities in star cluster properties. The more knowledge was gained about globular clusters the more became clear, that these objects are far more complex than initially imagined. Photometric data of excellent quality revealed substructures in the color-magnitude diagrams all the way from the red giant branch down to the main sequence of the largest Galactic globular clusters  $\omega$  Centauri (e.g., Lee et al. 1999; Bedin et al. 2004).

Spectroscopic studies showed that star clusters are not as chemically homogeneous as adopted for a long time (e.g., Cohen 1978). Although iron shows a single abundance distribution for most of the globular clusters, variations in many light element abundances have been recognized for many objects.

The detection of abundance patterns in some clusters that differ from those of the rest of the cluster population and those of the field stars suggested that some globular clusters are not native to our Milky Way (MW). This scenario is supported by the discovery of the Sagittarius dwarf spheroidal galaxy which is currently in process of merging with the Galaxy and will eventually contribute about five globular clusters to the MW system.

In order to use star clusters as tools in various fields in astrophysical research it is essential to understand how these systems form and evolve and what role their environments play. This thesis provides a contribution towards a better understanding of the formation and evolution of the globular clusters in our own Galaxy and star clusters in neighboring galaxies. We study the absorption features of the CN and CH molecule at 3883 and 4300 Å in stars of different evolutionary stages in eight Galactic globular clusters. In order to search for a possible origin of the detected abundance variations we differentiate between evolutionary stages and cluster types (halo, disk or accreted cluster). We join the abundance measurements with various cluster parameters.

Furthermore, the star cluster system of one of our nearest neighboring galaxies, the Small Magellanic Cloud, is studied. This galaxy contains a fairly rich star clusters system comprising about 700 objects. However, despite its proximity to the MW this system is only poorly studied. We determine the core radii and radial velocities of twelve star clusters associated with this galaxy and compare the results with the few previous results from the literature.

Concerning the star cluster formation history the SMC is an outstanding object among the dwarf galaxies in the Local Group. It is the only dwarf galaxy known to have formed and preserved star clusters continuously over its entire lifetime. Thus, these clusters provide a unique closely spaced set of single-age single-metallicity tracers for a detailed study of the age-metallicity relation. Spectroscopic metallicity measurements, however, existed up to date only for the small subsample of six clusters. The aim of this project is to determine a homogeneous set of accurate metallicities of twelve clusters via spectroscopy of the near IR CaII triplet lines. In order to trace the chemical evolution history, the derived mean metallicities are combined with age estimates from the literature. We are able to provide for the first time an age-metallicity relation of the Small Magellanic Cloud fully based on a statically significant sample of spectroscopic measurements. For a better understanding of the possible evolution of this galaxy we compare our results with the outcome of theoretical models.

This thesis is organized as follows:

- Chapter 2 gives an introduction to our local Universe.
- Chapter 3 is dedicated to the abundance variations in Galactic globular clusters.
- In Chapter 4 we determine the radial velocities and core radii of twelve star clusters in the Small Magellanic Cloud.
- Chapter 5 deals with the metallicity determination of these clusters and the age-metallicity relation of the Small Magellanic Cloud.
- In Chapter 6 we summarize the major results of this work.

# Chapter 2

## Introduction

### 2.1 The Local Group

The Local Group is the denotation for the small, gravitationally bound group of galaxies in our immediate cosmic neighborhood. It was first introduced in the early days of cosmic distance measurements and embossed by Edwin Hubble. Most member galaxies lie within a diameter of 2 Mpc in space. This small galaxy group itself is part of a larger structure - the Virgo-Supercluster.

Currently more than 40 galaxies are believed to be members of the Local Group, whereas new members are continuously being discovered. The largest members are the two spiral galaxies Andromeda and the Milky Way (MW). The third-largest galaxy is another, yet smaller, spiral galaxy - Triangulum. These large spiral galaxies are rich in gas and dust and have ongoing star formation. Besides the three large spirals the Local Group hosts about 40 smaller dwarf galaxies. The majority of these smaller objects can be found in the proximity of the two largest spirals. The discovery of the Sagittarius dwarf spheroidal galaxy (Ibata et al. 1994), and the subsequent detection of its tidal debris in the MW halo (Ibata et al. 2001) clearly shows that the dwarf companions play an important role in the evolution of the large galaxies.

Within the entirety of the dwarf galaxies in the Local Group one further distinguishes between various types of galaxies: Three dwarf elliptical galaxies (dE) are known. These are compact bright galaxies that host stars of old and intermediate ages and some gas. Their stellar densities are highly centrally concentrated and can even contain conspicuous nuclei. In addition nine galaxies of irregular shape (Irr/dIrr) have been found. These galaxies are gas-rich and experience recent or ongoing star formation. They host stars of various ages. The largest fraction is made of dwarf spheroidal galaxies (dSph), which are diffuse and faint objects. These low mass and gas-deficient galaxies are built up by old and intermediate stars, which formed in extended star formation histories. DSphs have no ongoing star formation. Their stellar content shows only a weak central concentration. Often sub-populations can be found in these object, with the tendency of the younger population being more concentrated (Harbeck et al. 2001). For a more detailed review on the Local Group galaxies see Grebel (2001).

The new dwarf members of the Local Group that are still being discovered all have low optical brightnesses and tend to be gas-deficient (e.g., Willman et al. 2005). Therefore they all have been classified as low mass dSph galaxies. On the other side the Irr and dIrr census

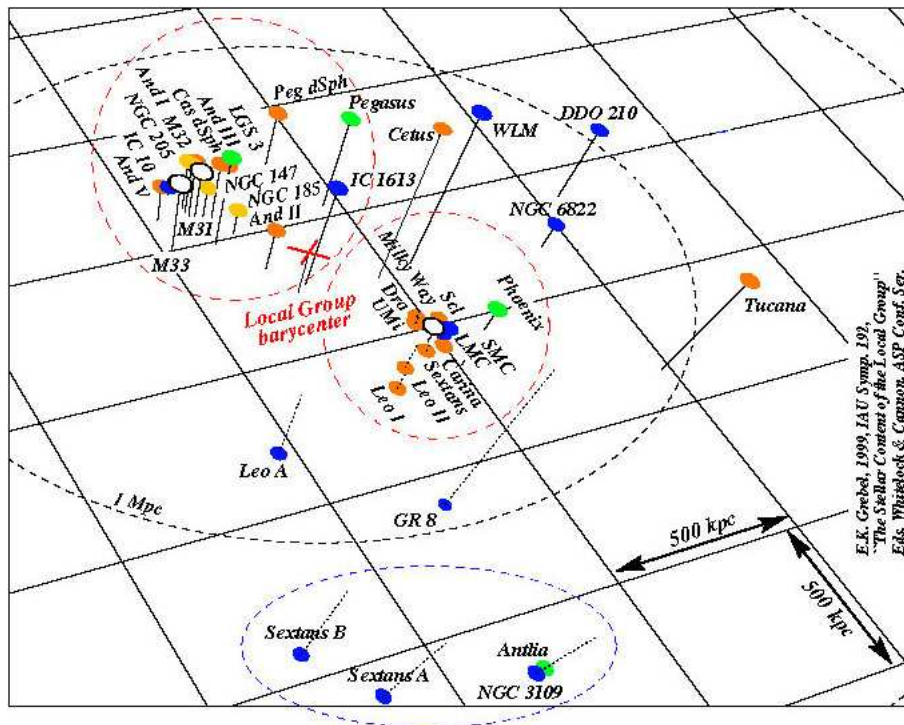


**Figure 2.1:** A three-dimensional view of the Local Group. The color classifies the galaxies as follows: dSph - orange, dE - yellow, dSph/dIrr - green, dIrr - blue. This figure was published by Eva K. Grebel in the framework of the IAU Symposium 192.

of the Local Group appears to be complete.

In a detailed comparison of the individual star formation histories of a large number of Local Group dwarf galaxies, Grebel (1999) could show that the star formation histories of all galaxies are unique. In fact no two galaxies have been found with star formation histories that are alike, irrespectively of morphological type. It was found that an old population is ubiquitous in all galaxies. Nevertheless the fraction varies, which these stars make of the entire galaxy. This can be understood as a sign of a common epoch of early star formation of the Local Group galaxies.

The study of the spatial distribution of the galaxies in the Local Group revealed a pronounced concentration of gas-poor, early-type dwarfs around the closest massive primary galaxy. Gas-rich, late-type dwarfs show less concentration and are more widely distributed. This has been interpreted as a signature of the impact of environmental effects. Figure 2.1 shows a three-dimensional view of the Local Group.

Comparisons with other galaxy groups have shown that the Local Group resembles other nearby groups in many ways. Galaxy content, structure, mass, and other properties are found to be similar (e.g., Karachentsev et al. 2002b,a). However, in contrast to other groups of galaxies the Local Group objects are the only galaxies for which current observations can resolve sufficiently faint stars, e.g., red giant branch (RGB) stars, that allows to constrain both recent and ancient star formation histories. Even among the Local Group members this becomes difficult with larger distances to the MW. Nevertheless the immediate proximity and variety of galaxies make the Local Group an ideal laboratory to study galaxy evolution at



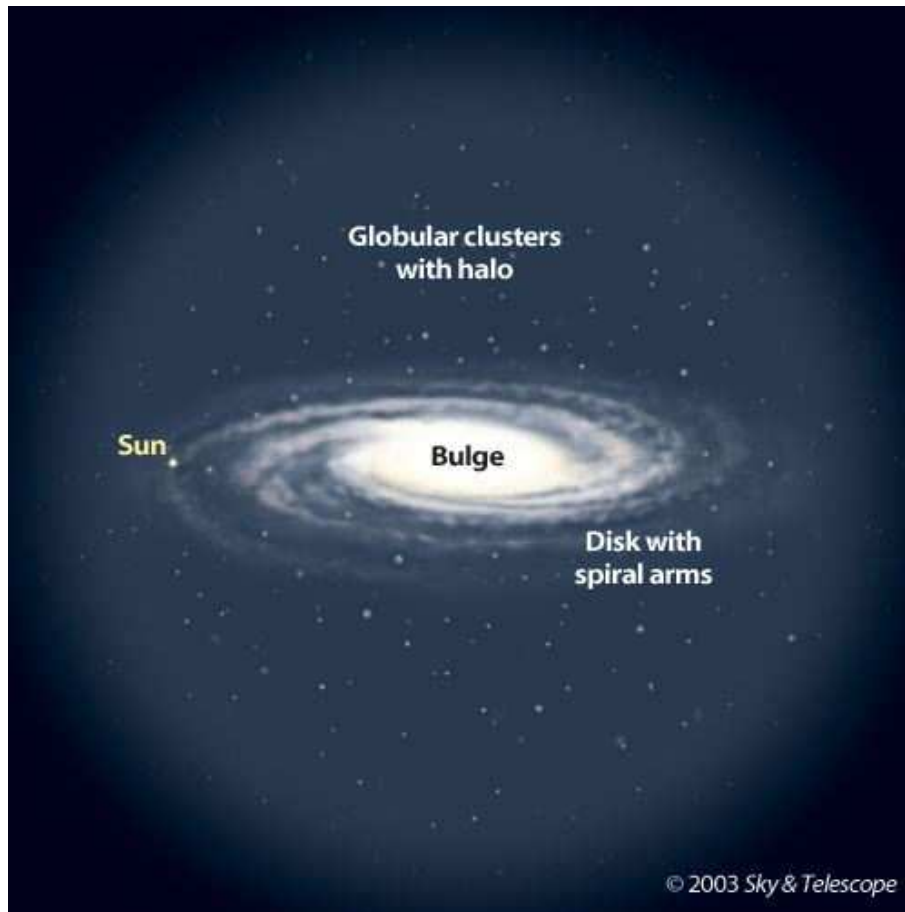


**Figure 2.2:** A simplified schematic structure of the Milky Way. Image Credit: Sky&Telescope, Steven Simpson: <http://www.skyandtelescope.com/howto/basics>

the highest possible resolution and in the greatest possible detail. Only by studying our local environment in detail we can gain the knowledge that can finally be transferred to larger scales.

## 2.2 The Milky Way and its globular cluster system

The MW is besides the Andromeda galaxy one of the two large spiral galaxies in the Local Group. It has a visible mass of about  $2 \cdot 10^{11} M_{\odot}$ . For a simplistic view the entire galaxy can be subdivided into three major components: a flattened disk, a bulge and a halo component. Figure 2.2 gives a schematic overview of the different Galactic components.

The disk and spiral arms of the MW contain gas, dust, and stars. Since the vertical density profile cannot be fitted by a single exponential, it was presumed that the Galactic disk is actually made up of two disks (Gilmore & Reid 1983). Evidence for this was further given by the stellar populations of these two components. Differences have been found in various parameters like position, kinematic, chemical abundance, and age. The thin disk has a scale height of 300 – 400 pc and contains 95% of the stars. It is characterized by past and present star formation prolonging over several Gyr. Consequently stars of a wide range

in age can be found in this component - the youngest associated with the spiral arms. The metallicity of thin disk stars is high and extends up to super-solar values. Nearly all the rest of the stars are located in the thick disk (scale height 1000 – 1500 pc). With intermediate metallicities ranging between  $-0.6$  to  $-1$  dex the stellar population is more metal-poor than those of the thin disk. Higher ratios of  $\alpha$ -elements at a given  $[\text{Fe}/\text{H}]$  suggest that the thick disk is influenced mainly by supernova type II (e.g., Feltzing et al. 2003, and references therein). The stars in the thick disk are found to be older (10 – 12 Gyr) than those in the thin disk. Moreover both disk components are also kinematically distinct. The thin disk is kinematically cooler and has a Galactic rotation velocity of 220 km/s whereas the thick disk rotates with a velocity of 180 km/s.

The bulge is a flattened spheroidal region with a high density of stars located around the center of the MW. More recent investigations suggest that the central region of the Galaxy is actually a bar (Blitz & Spergel 1991). While the disk of the Galaxy is made up of stars of all ages, the bulge contains only stars older than 10 Gyr. Zoccali et al. (2003) found no trace of younger populations and argued that the bulge has formed rapidly when the Galaxy/Universe was very young. The detected metallicity distribution ranges from about  $-1$  dex to slightly above solar.

The entire galaxy is surrounded by a nearly spherical Galactic halo with a diameter of about 50 kpc. Besides very few old and metal-poor stars the halo contains most of the Galactic globular clusters.

In the MW about 150 objects are classified as globular clusters. Globular clusters are spherical aggregates of up to a million ( $10^6$ ) stars, held together by gravity. Their stellar densities are very high. In the central regions of some clusters stellar densities are about  $10^7$  times higher than in the solar neighborhood. The most massive cluster known is  $\omega$  Centauri, which has a mass of about  $3 \cdot 10^6 M_{\odot}$  (Merritt et al. 1997). All globular clusters in the MW have been found to be very old. In fact we do not see any of these objects forming in the MW at the present time. With ages of about 10 – 12 Gyr they belong to the oldest Galactic object. Compared to the sun, they are generally deficient in most of the heavier chemical elements. However, the most metal-rich clusters are found to have metallicities of the order of solar values. On the other hand the most metal-poor clusters have metallicities as low as  $[\text{Fe}/\text{H}] = -2.5$  dex. An overview on the Galactic globular cluster parameters can be found in Harris (1996).

The detailed analysis of the MW globular cluster system revealed a bimodal distribution in metallicity. Two rather distinct groups clearly exist. The clusters more metal-rich than  $[\text{Fe}/\text{H}] \sim -0.8$  dex are confined to the bulge and disk. They form a highly flattened spatial distribution and have a significant rotation velocity. The scale height and rotational velocity of the system is comparable to that of the thick disk. The more metal-poor clusters form the familiar halo population. They are spherically distributed about the Galactic center, with a small rotation velocity and a large velocity dispersion (Zinn 1985). Studying their metallicities and horizontal branch morphologies, Zinn (1993) further proposed the existence of two groups within the halo cluster component. On one side an old halo cluster component, which are those clusters that formed in the MW halo during a rapid dissipative collapse phase. On the other hand a younger halo cluster component, which are clusters that formed in satellite systems which were subsequently accreted and disrupted by the MW. This suggestion is supported by the detection of the Sagittarius dwarf galaxy by Ibata et al. (1994), one of our nearest neighboring galaxies. Five globular clusters are suggested to be spatially and kinematically connected to this galaxy (e.g., Da Costa & Armandroff 1995). Since the



**Figure 2.3:** An image of the most massive Galactic globular cluster  $\omega$  Centauri. The picture was taken by a member of the Southern Astronomical Society/Australia: Julian West: <http://www.sas.org.au>

Sagittarius dSph is in process of being destroyed by tidal forces, the clusters associated with this galaxy will eventually be absorbed by the MW. The detection of large substructures in the MW halo (e.g., Ibata et al. 2001; Martínez-Delgado et al. 2001; Newberg et al. 2002), generally understood as the tidal debris of disrupted dwarf galaxies, further strengthens this theory. An overdensity of stars in the direction of Monoceros is also discussed to be the remains of a dwarf galaxy (Martin et al. 2004). Again various globular clusters are suggested to share kinematic properties with this dwarf galaxy candidate.

Additional support for the idea that some clusters might not share a common origin with the majority of the Galactic globular clusters comes from abundance measurement. The majority of globular clusters (and also open clusters) have the same  $\alpha$ -abundance as the field stars of similar metallicities. The general observed trend is that  $[\alpha/\text{Fe}]$  increases as  $[\text{Fe}/\text{H}]$  declines from 0 to  $-1$ . For metallicities below  $-1$ , the  $\alpha$ -abundance remains constant at about 0.3 dex. The interpretation of this trend is that in the early MW (i.e., for low metallicities) the contributions from supernovae type II dominated. Consequently the objects forming at that time are over-abundant in  $\alpha$ -elements with respect to solar values. By and

by supernovae type Ia contributed Fe, resulting in the decrease of  $[\alpha/\text{Fe}]$  towards higher metallicities. Nevertheless, some clusters show an under-abundance in  $\alpha$ -elements compared to the other objects of similar metallicities (e.g., Brown et al. 1997). This is also typically observed in the MW dwarf satellites. Those clusters are thus further candidates that may have been contributed to the MW stellar halo and globular cluster population by Galaxy interaction/accretion.

Besides the above mentioned inter-cluster differences, extensive research of the last decades with modern telescope facilities revealed various intra-cluster variations. A detailed overview is presented by Gratton et al. (2004). Globular clusters appear to be chemically homogeneous with respect to the iron-group (Mn, Fe, Ni, Cu). Furthermore, they generally show only a very weak scatter and the same trends as field stars for the neutron-capture elements (both  $s$ - and  $r$ - process elements). The only widely accepted example that does not show this internal homogeneity in heavy elements but a significant spread in  $[\text{Fe}/\text{H}]$  abundances is  $\omega$  Centauri. There are other candidates for  $[\text{Fe}/\text{H}]$  variations (e.g., M 22 and M 92), however they are very controversially discussed in the literature (e.g., Langer et al. 1998; Richter et al. 1999). In contrast to the homogeneity in heavy element abundances, complex variations have been detected in the abundances of many light elements (C, N, O, Na, Mg, Al) in all globular clusters studied so far. These are not shared by their field counterparts.

The surface abundance variations in light elements were first detected in RGB stars (e.g., Osborn 1971; Cohen 1978). Typically C, O, and Na were found to be anticorrelated with N, Na, and Mg, respectively. One of the best known inhomogeneities are those detected in the absorption band strengths of the cyanogen (CN) and CH molecules (e.g., Norris 1987). Since CN and CH are good tracers of N and C, respectively, one observed an anticorrelation between CN and CH for stars on the RGB. Furthermore, the variations of the CN band strengths within various globular clusters exhibit the surprising property of being clearly bimodally distributed. For many clusters, stars on the RGB of similar magnitude were found to be either strong or weak in CN absorption. The ratio of this dichotomy varies from clusters to cluster and its origin is still unknown. Two scenarios are mostly discussed in the literature as possible origin for the observations: 1 - evolution scenario: This scenario states that the chemical anomalies are generated inside the stars themselves (e.g., Sweigart & Mengel 1979; Charbonnel 1994). display also on the sub giant branch and near the main sequence turn off. 2 - primordial origin: This scenario states that the variations were built in when the star clusters were born. Stellar ejecta from asymptotic giant branch stars and fast rotation massive stars have been considered to play a key role in the pollution of the early cluster material (e.g., Cottrell & Da Costa 1981; Weiss et al. 2000; Ventura et al. 2001; Maeder & Meynet 2006).

## 2.3 The Magellanic Clouds and their star clusters

The Magellanic Clouds (MCs), named after the Portuguese seafarer Ferdinand Magellan (1480-1521), are two dwarf galaxy companions of the MW. These galaxies can be seen with the unaided eye as hazy patches in the constellations Dorado and Tucana in the Southern Hemisphere. In the night sky they are roughly  $22^\circ$  apart, which corresponds to a true distance of about 20 kpc. Both, the Small and the Large Magellanic Cloud, are classified as dIrr. Similar to other dIrr galaxies they are rich in gas and dust and exhibit a higher star formation activity than galaxies like the MW. Until the discovery of the Sagittarius dSph, they were



**Figure 2.4:** An image of the Magellanic Clouds taken by Fred Espenak. The larger of the two clouds is located on the left and the smaller cloud can be seen to the right. Furthermore, to the right of the SMC one can clearly see the Milky Way globular cluster 47 Tucane. <http://www.mreclipse.com/Astrophoto/SS97galleryB.html>

the closest known galaxies to our own. Given their close proximity, they offer the unique opportunity to study the dynamics and composition of other galaxies besides our own in detail. Observations have revealed that aside from their structure and lower mass the MCs differ from the MW in their chemical abundances. The youngest stars in the two clouds have been found to have metallicities of  $-0.2$  and  $-0.5$  dex, respectively. A compilation of the major parameters of the two clouds is listed in Table 2.1.

Both clouds host a large number of star clusters. Mistakenly these clusters were long suspected of being similar to MW globular clusters. In fact, the MCs host besides globular cluster counterparts, a population of very blue (i.e., young) and very populous star clusters. It is important to point out that these star clusters are not comparable to either type of MW star clusters. With masses of the order of  $10\,000 - 100\,000 M_{\odot}$  they are more massive than open clusters ( $\approx 1\,000 M_{\odot}$ ), but still less massive than globular clusters. Moreover, whereas the MW globular clusters are nearly spherical, the MC star clusters were found to be significantly elliptical. In this thesis they are therefore simply referred to as populous star clusters. Similar star clusters are found in star burst galaxies and in interacting/merging systems.

The relatively low metal abundances and large number of star clusters of all ages indicate that the evolution of the MCs is less advanced than those of the MW. Furthermore, their position in the sky at high Galactic latitudes implies that the observations of these systems suffer only very little from foreground extinction. In addition, their proximity allows to resolve stellar populations well below the oldest main sequence turn-off points which enables



**Figure 2.5:** Two young and populous star clusters (NGC 265 and NGC 290). These composite images were taken with the Advanced Camera for Surveys on board the NASA/ESA Hubble Space Telescope. <http://hubblesite.org/gallery>

accurate age-dating. All this makes the Magellanic Clouds an excellent probe towards a better understanding of the characteristics of the stellar populations in a vigorously evolving system.

In terms of star cluster studies the MCs also provide an ideal laboratory. Since massive star clusters can be destroyed by several processes one assumes that the old globular cluster system we see in the MW now, does not include all of those that were initially formed. As the MW is not forming any massive stars clusters today, we have to refer to close-by, extragalactic systems in order to understand how these objects form and evolve. The rich star cluster systems in the MCs provide a snapshot of all phases of star cluster evolution.

### The LMC

As the name says the Large Magellanic Cloud (LMC) is with a mass of  $\approx 10^{10} M_{\odot}$  the larger of the two clouds. The LMC is located about 50 kpc from our MW and has been intensively studied in the past. Originally classified as an irregular galaxy it turned out to be a very complex system. Various observational studies revealed the existence of a pronounced bar and possible relics of some spiral structure (Westerlund 1997). The quite numerous system of star clusters of the LMC is well studied. One has identified a well established population of old, metal-poor star clusters, which are comparable to Galactic halo globular clusters. In addition the LMC hosts a large number of intermediate age clusters with ages younger than 3–4 Gyr. The age distribution of the LMC star clusters shows a prominent age gap from 3 to 9 Gyr between these two populations (e.g., Da Costa 1991; Olszewski et al. 1991; Geisler et al. 1997). Only one cluster is known so far, that falls in this time range. The gap is now frequently confirmed by various observations, which leaves little doubt that it is real and not merely due to some statistical fluke (e.g., Olszewski et al. 1996). This is further supported

**Table 2.1:** Compilation of major parameters of the Magellanic Clouds.

	LMC	SMC	Reference
Right Ascension [J2000]	05 23 34.6	00 52 38.0	Paturel et al. (2002) Karachentsev et al. (2004)
Declination [J2000]	−69 45 22	−72 48 01	Paturel et al. (2002) Karachentsev et al. (2004)
Galactic longitude [J2000]	280.4652	302.8084	Paturel et al. (2002) Karachentsev et al. (2004)
Galactic latitude [J2000]	−32.8884	−44.3277	Paturel et al. (2002) Karachentsev et al. (2004)
Distance modulus [mag]	18.5	18.9	Westerlund (1997)
Distance [kpc]	63	50	Westerlund (1997)
Visual Brightness [mag]	0.1	2.3	Westerlund (1997)
Total Mass [ $M_{\odot}$ ]	$\approx 10^{10}$	$\approx 10^9$	Westerlund (1997)
Radial velocity [km/s]	257	158	Cole et al. (2005) Stanimirović et al. (2004)
Angular Size [arcmin <sup>2</sup> ]	$> 10^6$	$> 6 \cdot 10^4$	SIMBAD <sup>1</sup>
Number of Star Clusters	$\approx 4200$	$\approx 700$	Bica et al. (1999) Bica & Dutra (2000)
Metallicity [dex]	−0.2	−0.5	Cole et al. (2005) Rolleston et al. (2003)

<sup>1</sup><http://simbad.u-strasbg.fr/simbad/sim-fid>

by Olszewski et al. (1991), who noted that the age gap is also a metallicity gap. Obviously the LMC has undergone two major epochs of cluster formation in its past. It seems as if the LMC did lie relatively dormant for a substantial fraction of a Hubble time.

In order to receive a more complete view on the structure and history of this galaxy, Cole et al. (2000) began to fill up this gap by field star observations. The spectroscopy of field red giants suggested that the dominant population in the LMC field has a metallicity similar to the one observed for the intermediate cluster populations. Cole et al. (2005) found strong evidence for a radial variation in the relative fraction of metal-rich to metal-poor stars and the presence of an old, thicker disk or halo population.

### The SMC

The Small Magellanic Cloud (SMC) lies with a distance of 63 kpc about 20% farther away from the MW than the LMC. In contrast to the LMC, the SMC has no spiral structure and is unbarred (Zaritsky et al. 2000). Thus, there is no apparent internal mechanism that can drive the global star formation modes. The SMC has an asymmetric appearance with an irregular main body and an extension in the direction towards the LMC. Population studies revealed that the old population is rather smoothly distributed while the asymmetric appearance is primarily caused by the distribution of young stars (Zaritsky et al. 2000; Cioni et al. 2000). The interstellar medium of the SMC shows a fractal structure. Complex shell structures have been found in the neutral Hydrogen map (HI), which are all apparently very young (Staveley-Smith et al. 1997). The true origin of these structures are still under discussion. However the vast majority of the shells is associated with young objects (Chiosi et al. 2006).

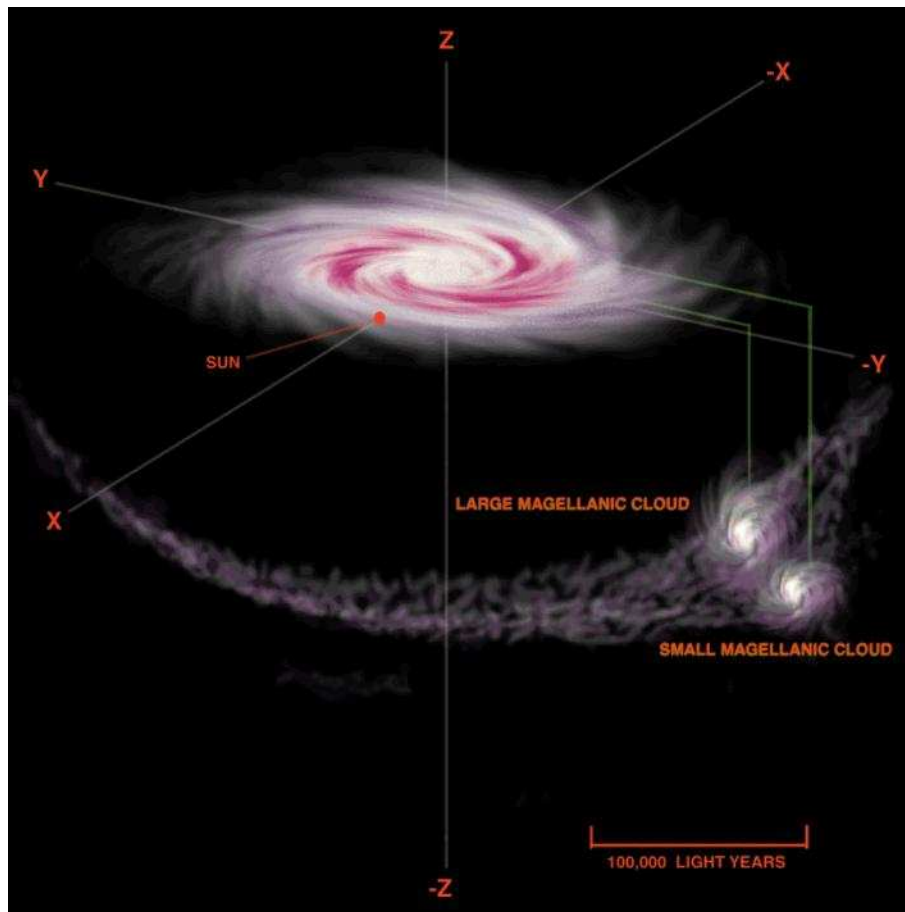


**Figure 2.6:** A schematic view of the Magellanic Clouds and the Milky Way. Furthermore the stream of gas which results from the interaction between those galaxies is shown. Illustration Credit: Dallas Parr (CSIRO) <http://www.csiro.au/news/mediare1/mr1998/mr98194.html>

Although both clouds have the same galaxy classification and are located close together in the same direction on the sky their star formation histories differ significantly. Compared to the LMC, the SMC has experienced a more constant star forming past. In contrast to the larger neighbor, the SMC star cluster system does not show any sign of a substantial age gap, i.e., a period where no clusters were formed. In fact, it is the only dwarf galaxy in the Local Group that has continued to form and preserve populous star clusters over its entire lifetime. However, whereas the LMC hosts many globular-cluster-like objects, the only cluster in the SMC older than 11 Gyr is NGC 121. This cluster is still significantly younger than the ancient Galactic globular clusters and LMC clusters.

### The SMC-LMC-MW system

Observations and theoretical studies suggested that the LMC and SMC are greatly distorted by the tidal interaction with the MW. The streams detected in HI provide clear observational evidence of the LMC/SMC interaction. Hindman et al. (1963) were the first who discovered the Magellanic Bridge - a connection between the two clouds. This bridge consists of very low metallicity material. Interestingly, signs for recent star formation were found within the



bridge (Muller et al. 2003). About a decade after the detection of the bridge, the picture of gaseous streams was further extended. Mathewson et al. (1974) mapped the Magellanic Stream, a tidal stream of atomic hydrogen stretching  $120^\circ$  around the sky from the Magellanic Clouds. It builds a connection between the clouds and the MW.

It is now widely accepted that the tidal interaction between the MCs and the MW played the key role in the formation of the Magellanic Bridge and the Stream. The theoretical models (e.g., Bekki & Chiba 2005, and references therein) predict even more than that. It is also conceivable that these now irregular galaxies have been disrupted through repeated interactions with the MW. The consequences of this process are dramatic changes in their appearance and the emergence of vigorous star-forming activity throughout the clouds. Some of the star clusters may very well owe their existence to these close encounters with the MW. Thus, the interaction with the Galaxy may have importantly influenced both the dynamical and the chemical evolution of the MC. It is therefore tempting to use dynamical models of the MC-MW encounters as a vehicle for the understanding of the LMC/SMC star and clusters formation histories. Fig. 2.6 gives a schematic view of the gas tidally stripped from the LMC and SMC as they approach the MW.

## 2.4 Theoretical chemical evolution models adapted to the SMC

For a better understanding of the evolution of stellar populations many researchers all around the world are putting a lot of effort in generating theoretical models of the chemical enrichment of the interstellar medium (ISM) in various types of evolving stellar systems. All models rely on basic principles of chemical evolution such as star formation, nucleosynthesis, mass loss from evolving and dying stars, and gas flows. Moreover one considers sub-regions of stellar systems to assume an ISM of uniform composition.

### 2.4.1 Simple closed box model by Da Costa & Hatzidimitriou (1998)

The most simple chemical evolution model adapted to the SMC is the closed-box model by Da Costa & Hatzidimitriou (1998). This model is based on the fundamental equations explained in the appendix to this thesis.  $Z(t) = y \ln \mu^{-1}$  is the abundance at the time  $t$  and  $\mu(t)$  is the gas fraction of the SMC. This equation is solved by specifying  $Z = Z_1$  at a time  $t = t_1$ . For the present day conditions of the SMC they adopted the abundance of  $\log(Z_1/Z_\odot) = -0.7$  dex and  $t_1 = 16$  Gyr. They assumed that the gas fraction depends on time as  $u(t) = 1 - \frac{1-u_1}{t_1}t$ , where  $u_1 = 0.3$  is the present day gas fraction. Combining these equations with the assumed present day values gives:

$$Z(t) = -3.31 \cdot 10^{-3} \ln(1 - 4.38 \cdot 10^{-2} t). \quad (2.1)$$

The resulting curve is given in Figure 2.7 by the blue line.

In order to be more consistent with recent scientific results we derived another curve adopting the latest parameters from the literature. According to the results of NASA's Wilkinson Microwave Anisotropy Probe mission (WMAP), which calculated the age of the universe to be  $13.7 \pm 0.2$  Gyr (Spergel et al. 2003), we approximate  $t_1 = 14$  Gyr. Furthermore, the recent study by Rolleston et al. (2003) suggested a present day abundance of the SMC of  $\log(Z_1/Z_\odot) = -0.5$  dex. In contrast to previous studies this result is based on high

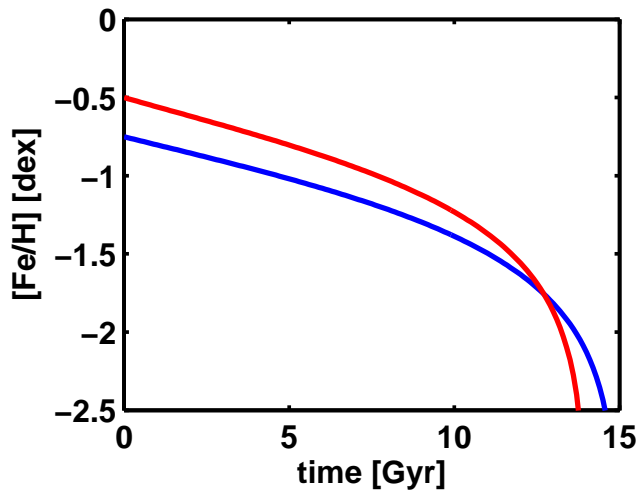


**Figure 2.7:** Simple closed-box model of the age-metallicity relation of the SMC by Da Costa & Hatzidimitriou (1998).

resolution spectroscopy of a B-dwarf star and therefore provides a more reliable estimate to the present day SMC abundance than previous estimates based on supergiant observations. The atmospheres of supergiants may be contaminated by products of nucleosynthesis, dredged up to the stellar surfaces. The resulting equation for the metallicity dependence of the SMC with time is:

$$Z(t) = -5.25 \cdot 10^{-3} \ln(1 - 0.05 t). \quad (2.2)$$

This curve is indicated by the red line in Figure 2.7. The slope of the two curves are very similar.

#### 2.4.2 Models by Pagel & Tautvaisiene (1998) including time delays

In their paper, Pagel & Tautvaisiene (1998) provided two different models to explain the observed chemical evolution of the SMC: a simple smooth model and a bursting model of star formation.

In order to alleviate the G-dwarf problem, they assumed for both models the SMC to have been built up by gradual infall of primordial gas. The accretion of unprocessed material decreases the fraction of metal-poor to metal-rich stars (see A.5). Since for the investigation of abundances of iron-peak elements with time the instantaneous recycling approximation does not hold, they introduced for both models a time delay  $\Delta$ . This assumes that the production of a certain element takes place at a fixed time after the star formation. The delay parameter for iron was set to  $\Delta = 1.33$  Gyr to reflect the typical time-scale for type Ia supernovae. Although the majority of iron is produced in those dying low and intermediate mass stars, core-collapse supernovae resulting from massive stars also contribute to the iron abundances. For these type of supernovae no time-delay was assumed. The yields for iron were identical to those adopted to fit the chemical evolution of the solar neighborhood:  $y/Z_{\odot} = 0.28$  and  $0.42$  for 0 and 1.33 Gyr time delay, respectively. Another approximation adopted is the sudden mass loss of the stars at the end of their lifetime.

Besides the above, Pagel & Tautvaisiene (1998) forwent other assumptions made by various

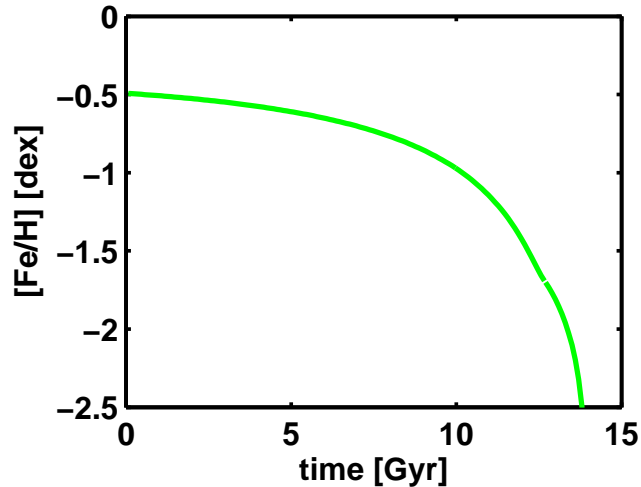


**Figure 2.8:** Smooth chemical evolution model of the age-metallicity relation of the SMC by Pagel & Tautvaišienė (1998).

authors in order to explain the observed differences to the solar neighborhood abundance patterns. In the Magellanic Clouds the  $[\alpha/\text{Fe}]$  ratio was found to be lower than in Galactic stars with the same  $[\text{Fe}/\text{H}]$ . Russell & Dopita (1992) and Tsujimoto et al. (1995), for example, introduced a steeper IMF to bring down the  $[\alpha/\text{Fe}]$ . Pilyugin (1996) used selective winds associated with star bursts. Despite the observed abundance differences, Pagel & Tautvaišienė (1998) found no necessity in changing the IMF or selective winds. They assumed a IMF similar to the solar-neighborhood and non-selective wind proportional to SFR.

### Smooth model

The first and simpler model developed by Pagel & Tautvaišienė (1998), is a model assuming a smooth star formation rate. This was implied in the calculation by introducing the parameter  $\omega(t)$ , the transition probability for diffuse material to change into stars in a unit time. For the smooth model  $\omega(t) = 0.115 \text{ Gyr}^{-1}$  was assumed to be constant for the entire past of the SMC. The final gas fraction was chosen to be in accordance with the value by Westerlund (1997). The resulting slope for the metallicity as a function of time of this model is shown in Figure 2.8. Compared with the closed-box model by Da Costa & Hatzidimitriou (1998) the slope is shallower after the first few Gyr. This indicates a slower enrichment with time, as expected due to the assumption of gas infall.

### Bursting model

In the bursting model, Pagel & Tautvaišienė (1998) assumed  $\omega(t)$  to be constant over certain time periods. They divided the star formation history into three episodes. For the initial starburst e.g., up to a time of  $t_1 = 1.33 \text{ Gyr}$  they assumed  $\omega_1 = 0.10 \text{ Gyr}^{-1}$ , which is of the order of the average value of  $\langle\omega\rangle = 0.115 \text{ Gyr}^{-1}$ . For the time between  $t_1$  and  $t_2 = 10 \text{ Gyr}$  they supposed the SMC to be in a quiescent phase and therefore adopted a low value for the star-formation efficiency of  $\omega_2 = 0.01 \text{ Gyr}^{-1}$ . For the recent past they assumed a second stronger starburst. Therefore, for the period between  $t_2$  and  $t_3 = 14 \text{ Gyr}^{-1}$ , a value of

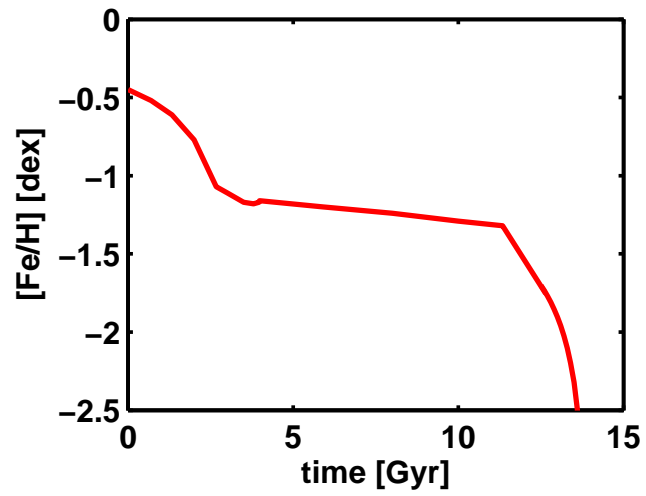


**Figure 2.9:** Bursting chemical evolution model of the age-metallicity relation of the SMC by Pagel & Tautvaišienė (1998).

$\omega_3 = 0.35 \text{ Gyr}^{-1}$  was chosen. The resulting slope for the metallicity as a function of this model is shown in Fig. 2.9.

## Chapter 3

# CN and CH Line Strength in Galactic Globular Clusters

### Abstract

Our work focuses on the understanding of the origin of CNO-anomalies, which have been detected in several Galactic globular clusters. The novelty and advantage of this study is that it is based on a homogeneous data set of hundreds of medium resolution spectra of stars in eight Galactic globular clusters (M 15, M 22, M 55, NGC 288, NGC 362, NGC 5286, Palomar 12 and Terzan 7). Two of the clusters (Palomar 12 and Terzan 7) are believed to be former members of the Sagittarius dwarf spheroidal (Sgr dSph) galaxy. The large homogeneous data set allows for a detailed differential study of the line strengths in the stellar spectra of the observed clusters. Our sample comprises stars in different evolutionary states, namely the main-sequence turn-off (MSTO) region, the subgiant branch (SGB) and the base of the red giant branch (RGB). We compare the relative CN and CH line strengths of stars in the same evolutionary states (with similar  $\log g$  and  $T_{\text{eff}}$ ). The majority of the examined clusters show significant variations in their CN and CH abundances at the base of the RGB. We confirm the presence of a bimodal distribution in CN for the second parameter pair of the clusters (NGC 288 and NGC 362). The two probable former Sgr dSph clusters do not exhibit any CN-strong stars. Overall, our results suggest that the environment in which the clusters formed is responsible for the existence of CN-strong stars. We can confirm the known anticorrelation between CN and CH for most of the observed clusters. Although the signal of CN absorption is weaker for the hotter stars on the MSTO and SGB we observed the same anticorrelation in these less evolved stars for the CN-bimodal clusters. Including structural parameters taken from literature reveals that the existence of the CN-bifurcation seems to be independent from most other cluster characteristics. In particular, we do not confirm the correlation between cluster ellipticity and number of CN-strong stars. However, there may be a trend of an increased percentage of CN-strong stars with increasing cluster tidal radius and total luminosity. We argue that our findings are consistent with pollution by AGB stars or fast rotating massive stars and two generations of star formation in luminous clusters with larger tidal radii at larger Galactocentric distances.

*This project was done in collaboration with Michael Hilker, Eva K. Grebel and Philip G. Willemsen*

### 3.1 Introduction

Among the about 150 known Galactic globular clusters (GC) there exist several clusters that show star-to-star abundance variations for certain chemical elements (see review from Gratton et al. 2004). These variations are ubiquitous particularly for light elements such as C and N and are seen mainly for stars on the red giant branch (RGB). Stars with significantly stronger cyanogen (CN) bands as compared to other stars in the same cluster have been detected as early as 1971 by Osborn in M5 and M10 (Osborn 1971). The existence of such stars in these and many other clusters has been confirmed repeatedly (e.g., Cohen 1978; Smith & Norris 1982, 1983; Briley et al. 1989). However, the fraction of red giants showing enriched CN bands differs from cluster to cluster (Norris 1987).

Over the last three decades spectroscopic studies of the CN and CH absorption bands often revealed a bimodality in CN that is accompanied by a broadened distribution in CH. For the majority of the CN-bimodal clusters (e.g., M2, M3, M5, M13, 47 Tuc) a CN-CH anticorrelation was detected (e.g., Smith et al. 1996). Since CN is a double-metal molecule, it can be more easily observed in stars with a higher metallicity. Nevertheless, the CN-CH anticorrelation seems to be present also in the very metal-poor cluster M15 where no clear bimodality of CN could be detected so far (Lee 2000).

Although this topic has been studied extensively in the last decades no self-consistent model has been found to satisfactorily explain the observed chemical variations. Two main scenarios are discussed as possible origins of these abundance patterns:

1) The ‘evolutionary mixing’ scenario: In this scenario the chemical composition in the surfaces of the stars is altered due to deep mixing effects. Material from the stellar interior is dredged-up through regions of active CNO element nucleosynthesis to the upper layers of H-burning. During the H-burning phase via the CNO-cycle N is enriched at the cost of C and O. One would therefore expect a CN-CH anticorrelation if CNO-processed material is dredged up to the stellar surface. The so-called first dredge-up, however, is not able to explain the observed abundance patterns of light elements in RGB stars, especially for metal-poor stars that do not possess deep enough convective envelopes according to standard models (see references in Gratton et al. 2004). An additional mixing episode is needed to explain those patterns. This can either be rotation-induced mixing (e.g., Sweigart & Mengel 1979; Charbonnel 1995) or so-called ‘canonical extra-mixing’ (Denissenkov & Vandenberg 2003). These mechanisms naturally explain the [C/Fe]-[N/Fe] anticorrelation observed in RGB stars, however will not work for stars below the RGB bump due the increased molecular weight barrier (e.g., Iben 1968). Based on low resolution spectroscopy, various studies showed that the CN-band strength is a good indicator for the [N/Fe] abundances whereas CH traces [C/Fe] (e.g., Smith et al. 1996). As a consequence, the CN bimodality and the CN-CH anticorrelation observed on the upper RGB stars of many clusters are often interpreted as a result of deep mixing that takes place in certain stars while not in other stars.

2) The ‘primordial’ and ‘self-enrichment’ scenarios: In both cases the abundance variations are not due to internal stellar evolutionary effects. The ‘primordial’ scenario assumes that there exists a ‘primordial floor of abundance variations’ (Gratton et al. 2004) that was in place when the star cluster formed (i.e., an inhomogeneously mixed molecular cloud). In the ‘self-enrichment’ scenario the abundance variations are caused by successive generations of stars that formed within the same star cluster. Theoretical nucleosynthesis models show that the observed abundance mix can be provided either by intermediate-mass (4–5  $M_{\odot}$ ) asymptotic giant branch (AGB) stars (e.g., Cottrell & Da Costa 1981; Ventura et al. 2001;

**Table 3.1:** Log of observations.

Date	Target	Position (RA; DEC (J2000))		Exp.time
May 2002	M55 MSTO	294.99564	-30.88307	1800 s
	M55 SGB	294.99646	-30.88368	2160 s
	M55 RGB	294.99559	-30.88235	480 s
July 2004	NGC 288 MSTO	13.23313	-26.57845	5140 s
	NGC 288 SGB	13.23630	-26.57807	2700 s
	NGC 362 MSTO	15.67363	-70.84870	5400 s
	NGC 362 SGB	15.67209	-70.84886	2800 s
	NGC 5286 SGB	206.54375	-51.37364	2700 s
	M 22 MS	279.04539	-23.90313	5400 s
	M 22 SGB	279.04539	-23.90311	3000 s
	Ter 7 SGB	289.43484	-34.65680	5400 s
	Ter 7 RGB	289.43488	-34.65773	4500 s
	M 15 SGB	322.54426	12.16722	2400 s
	Pal 12 RGB	326.66087	-21.25134	2400 s

Denissenkov & Herwig 2003), or by fast rotating massive (20–120  $M_{\odot}$ ) stars (e.g., Maeder & Meynet 2006; Decressin et al. 2007). Both types of objects expel their ejecta via slow stellar winds, which is important in order to not sweep out the gas from which the second generation shall be formed. There are mainly two ways how the enriched stars got to their peculiar abundance pattern: either, the AGB ejecta mixed well with the intracluster medium out of which the second generation formed within the cluster (Cottrell & Da Costa 1981). Or, the AGB ejecta polluted the surfaces of a certain fraction of already existing stars with well-developed radiative cores (e.g., D’Antona et al. 1983; Thoul et al. 2002). The pollution scenario, however, has difficulties to explain the sharp bimodality of CN abundances and the similarity of abundance patterns of evolved as well as unevolved stars.

Lately, the evolutionary mixing scenario has been more and more challenged as correlations/anticorrelations among these elements and the range of variations of each element appear to be independent of stellar evolutionary states (with exception of enhanced depletion of C and O seen on the RGB) (e.g., Harbeck et al. 2003a). Recent spectroscopic studies near and below the main sequence turn-off (MSTO) in the GCs M 71, 47 Tuc and NGC 6752 showed that abundance variations are already present among stars that are expected to be unaffected from deep mixing mechanisms (e.g., Cohen 1999b; Harbeck et al. 2003a; Briley et al. 2004). This suggests that at least some of the abundance variations observed in evolved stars were present before the stars reached the RGB, i.e. mixing can not be the only driving mechanism of the observed abundance variations.

The ‘self-enrichment’ scenario also is strengthened by the recent findings of multiple sub-giant branches (SGB) and main sequences (MS) in several massive GCs (Bedin et al. 2004; Piotto et al. 2007), which require stellar populations with distinct abundance patterns (and ages) within the clusters. Interestingly, the multiple SGBs and MSs can best be explained by a large helium enhancement in the second/third subpopulation of a cluster (D’Antona et al. 2005), which is consistent with the expected abundances of ejecta from intermediate-mass AGB stars (e.g., D’Antona et al. 2002). Actually, these AGB stars need not have been members of the same star cluster. Bekki et al. (2007) recently suggested that massive GCs might

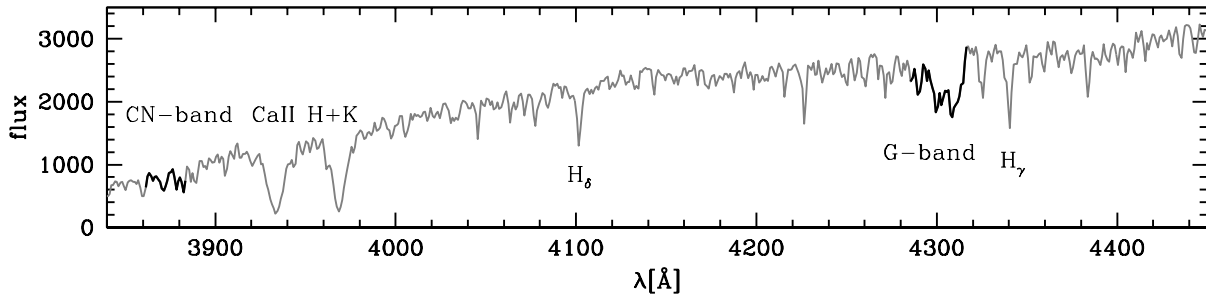


**Figure 3.1:** Typical spectrum of a RGB star in the globular cluster NGC288. The regions of the measured indices are marked by darker lines. Furthermore the positions of the prominent CaII H and K and Hydrogen lines are indicated.

have formed in low mass dwarfs embedded in a dark matter halo. In this scenario, the later generations of stars then was created out of ejecta from the external ‘field’ AGB stars.

Coming back to the overall CNO abundances, the work by Smith et al. (1996) has shown that the total  $[(C + N + O)/Fe]$  for giants in the globular clusters M3 and M13 is the same for both CN-strong and CN-weak stars, which would be expected from deep mixing, dredging up CNO processed material to the stellar surfaces. Thus although mixing effects are not existent in unevolved stars they seem to play a role for red giants when studying the CN and CH bands.

If the environment in which a cluster formed (e.g., in the disk of a galaxy vs. the center of a dark matter substructure) defines the enrichment history of a cluster, the observed abundance patterns would provide an indication of the origin of the cluster. In his groundbreaking work Zinn proposed that the Galactic globular cluster system consists of various sub-systems (Zinn 1985, 1993): bulge/disk (BD), old halo (OH), young halo (YH) globular clusters. He furthermore suggested that most YH clusters might have been accreted from satellite galaxies. However, the Milky Way companions have been found to show, on average, systematically lower  $[\alpha/Fe]$  ratios than Galactic halo stars and globular clusters (e.g., Shetrone et al. 2001; Fulbright 2002; Pritzl et al. 2005; Sbordone et al. 2007). Hence the present-day dwarfs do not seem to have contributed in a significant way to the build-up of the Galactic halo and to the YH clusters.

The aim of this work is to gain further insight into the mechanism responsible for the strong CN enhancement in some stars. We therefore concentrate on regions in the color magnitude diagrams (CMDs) where stars are believed to be unaffected by mixing effects, i.e. stars on the MS, MSTO, SGB, and lower RGB. In particular, we investigate whether there is a dependence of the CN enhancement on the overall globular cluster properties and/or the sub-class they are belonging to. We investigate if CN-CH variations are different in genuine halo clusters as compared to possibly accreted globular clusters.

This chapter is structured as follows. Section 3.2 describes our data and their reduction. Section 3.3 explains the measurements of the CN and CH band strength and the definition of the cyanogen excess parameter. Sections 3.4 and 3.5 present the investigation of the CN/CH anticorrelation and the search for correlations between other cluster properties and the number ratio of CN-strong/CN-weak stars. The final section 3.6 gives our summary and conclusions.



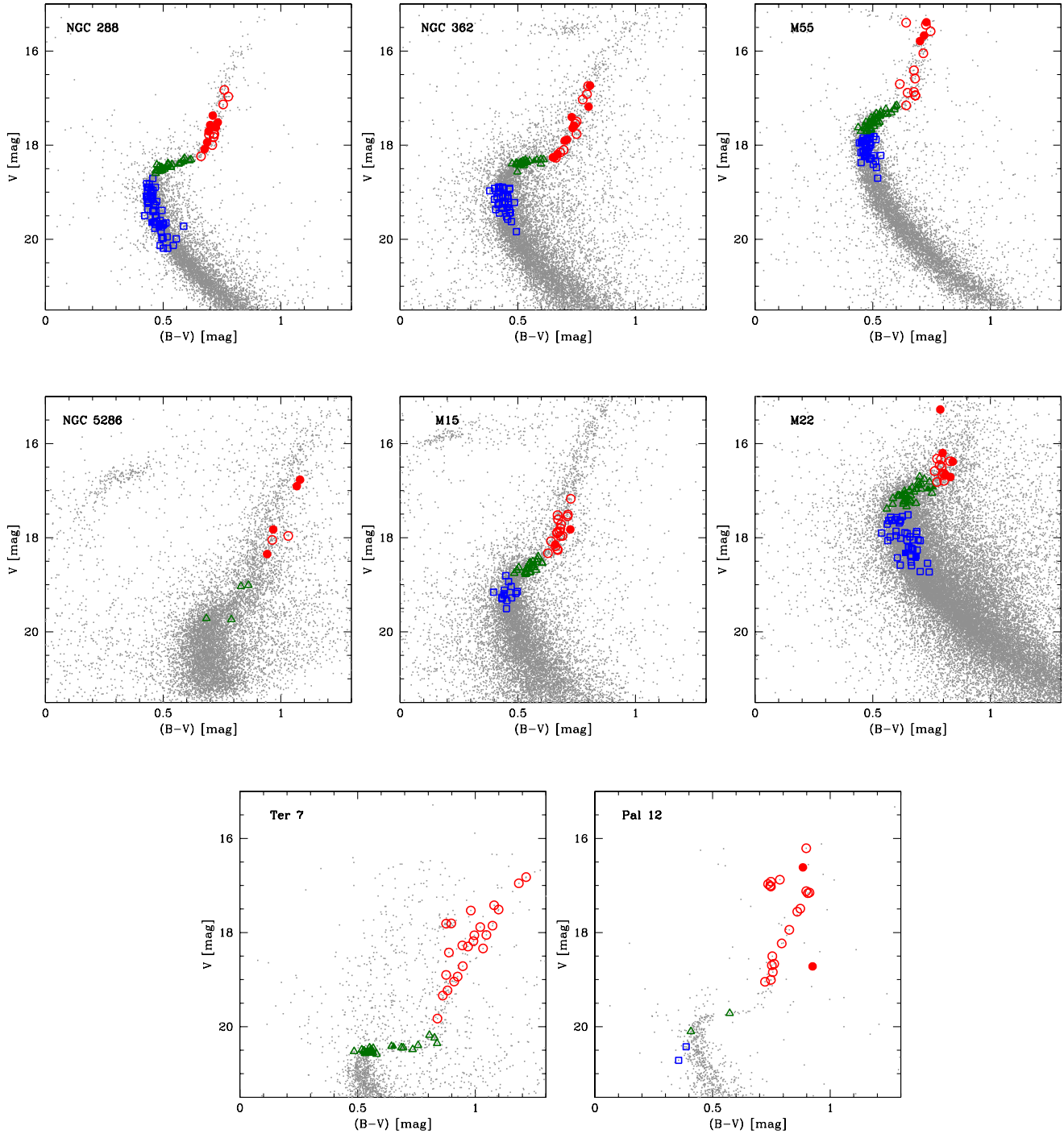


**Figure 3.2:** The color magnitude diagrams for the globular clusters in our sample. Those stars for which line strength measurements are available are marked in color. We distinguish between stars of different evolutionary states. MS stars are indicated by blue squares, SGB stars by green triangles, and RGB stars by red circles. CN-weak and CN-strong stars are denoted by open and filled symbols, respectively. Note that in all diagrams the calibrated pre-image  $B$  and  $V$  magnitudes are shown. Our sample comprises clusters spanning a large range in metallicity ( $-2.26 < [\text{Fe}/\text{H}] < -0.58$  dex). The clusters Palomar 12 and Terzan 7 are believed to be part of the Sgr dSph, which is currently being disrupted by its tidal interaction with the Milky Way.

## 3.2 Observations and data reduction

### 3.2.1 Observations

The data were obtained in May 2002 and July 2004 at the Very Large Telescope (VLT) at ESO/Paranal (Chile) with the FOcal Reducer and low dispersion Spectrograph FORS2. FORS2 is equipped with the multi-slit spectroscopy facility MXU and provides a field of view of  $6'.8 \times 6'.8$ . The observations of M 55 were obtained in 2002 and were also used for calibration purposes in a study of  $\omega$  Cen (Hilker et al. 2004; Willemsen et al. 2005; Kayser et al. 2006). The observations obtained in 2004 were dedicated to CN and CH measurements in seven further Galactic globular clusters (M 15, M 22, M 55, NGC 288, NGC 362, NGC 5286, Palomar 12, and Terzan 7) spanning a large range in metallicity ( $-2.26 < [\text{Fe}/\text{H}] < -0.58$  dex). Two of the clusters (Palomar 12 and Terzan 7) are suggested to have originated from the Sagittarius dwarf spheroidal (Sgr dSph) galaxy (Bellazzini et al. 2003; Sbordone et al. 2005).

For both observing runs, the candidate stars for the spectroscopy were selected from pre-images in Johnson  $B$  and  $V$ . We selected target stars from the upper MS, the SGB, and the lower RGB in the cluster CMDs. On the RGB we focused on stars fainter than the RGB bump, the point where deep mixing is believed to set in (Sweigart & Mengel 1979; Charbonnel 1995).

For each cluster up to three slit masks were defined using the FORS Instrument Mask Simulator (FIMS) provided by ESO. Each mask was dedicated to the observation of stars of a certain part of the CMD. This enabled the choice of the optimal integration time for each mask, according to the stellar brightnesses. Typically each slit mask contained  $\sim 50$ – $70$  slits. We selected slit lengths of  $4$ – $8''$  to make local sky subtraction possible. The slit width was fixed to  $1''.0$ . For the spectroscopic observations we chose the grating with the ESO denotation 660I+25 (second order) with a dispersion of  $0.58 \text{ \AA pix}^{-1}$ . The spectral region covers  $\sim 3700$  to  $5800 \text{ \AA}$  including the CN band at  $3885 \text{ \AA}$  and the G-band at  $4300 \text{ \AA}$ . The final actual wavelength coverage depends on the location of the star/slit on the mask with respect to the dispersion direction.

The total exposure time per mask varied between 360 and 5400 s depending on the cluster and the brightness of the target stars. To facilitate cosmic ray removal the observations were split into multiple (2–3) exposures. The central coordinates of the observed fields as well as the total exposure times are listed in Table 3.1. In addition to the science observations, calibration exposures were obtained during daytime. These consisted of five bias and five dome flat-field frames. For the wavelength calibration for each mask an exposure of the emission-lines spectra of an arc lamp (He-Hg-Cd) was taken.

### 3.2.2 Data reduction

The data reduction was carried out using standard routines within IRAF<sup>1</sup>.

For each night the bias frames were combined using the IRAF task `imcombine` and subtracted off the raw science, flat field, and wavelength calibration images of the corresponding night. Afterwards the bias-corrected flat fields were also combined. We used a sigma-clipping algorithm in order to remove hits from cosmic rays. The science and lamp exposures were

---

<sup>1</sup>IRAF is distributed by the National Optical Astronomy Observatories, which are operated by the Association of Universities for Research in Astronomy, Inc., under cooperative agreement with the National Science Foundation.

cleaned from cosmic rays individually. Herefore we used the task `bclean` from the `STARLINK` package. In order to increase the signal-to-noise ratio the individual science exposures were stacked using `imcombine`.

Before the extraction of the spectra, the remaining pixel-to-pixel variations resulting from the sensitivity of the telescope optic had to be removed in all lamp and science exposures. This was done by dividing each exposure by the corresponding normalized flatfield. In case of spectroscopy the response function in the dispersion direction of each slit has to be determined separately in order to normalize the spectra. With the tasks `apall` and `response`, `IRAF` provides a very useful means for the tracing, response curve fitting and extraction of the spectra.

For each spectrum an adequate local sky background was selected for the sky subtraction. In most cases, object and sky could be extracted from the same slit. The wavelength calibration was achieved using the well known, strong emission lines in the spectra of the He-Hg-Cd arc lamps taken after each set of observations. For every spectrum about ten lines were identified. The transformation from the pixel to the wavelength scale is based on the fit of the dispersion function. Generally the RMS was lower than  $0.01 \text{ \AA}$ . Note that the final spectra were neither flux-calibrated nor normalized by the continuum. All spectra were binned to a spectral scale of  $1 \text{ \AA pix}^{-1}$ . Considering the seeing the final spectral resolution (FWHM) for narrow lines is  $\sim 2 \text{ \AA}$ .

All spectra were corrected for their radial velocities by cross-correlating them with five high quality template spectra taken from the  $\omega$  Cen dataset using `IRAF/fxcor`. We adopted the mean value of the five measurements as the radial velocity of the star. The scatter of the velocity measurements is of the order of  $20 \text{ km/s}$ , which reflects the uncertainties given by the spectral resolution. In the resulting velocity distributions the globular clusters clearly stand out against the Galactic foreground. Possible non cluster member stars were identified by their radial velocities and rejected from the further analysis. In a final step, we examined each spectrum individually and rejected those spectra with bad quality (e.g., due to tracing errors). In total about 500 spectra are suitable for our analysis, whereof 120 spectra are from lower RGB stars.

**Table 3.2:** Reddening, distance modulus, and photometric parameters of the MSTO for our sample GCs.

Cluster	$E_{B-V}^a$	$(m - M)_V^a$	$V_{MSTO}$	$(B - V)_{MSTO}$
NGC 288	0.03	14.83	18.90 <sup>b</sup>	0.46 <sup>b</sup>
NGC 362	0.05	14.81	similar to NGC 288 <sup>c</sup>	
NGC 5286	0.24	15.95	20.05 <sup>d</sup>	0.73 <sup>d</sup>
M 22	0.34	13.60	17.70 <sup>e</sup>	0.75 <sup>e</sup>
Ter 7	0.07	17.05	20.96 <sup>f</sup>	0.52 <sup>f</sup>
M 55	0.08	13.87	17.89 <sup>g</sup>	0.50 <sup>g</sup>
M 15	0.10	15.37	0.50 <sup>h</sup>	19.40 <sup>h</sup>
Pal 12	0.02	16.47	$\sim 20.5^i$	0.452 <sup>i</sup>

<sup>a</sup>Harris (1996) <sup>b</sup>Alcaino et al. (1997) <sup>c</sup>Bellazzini et al. (2001) <sup>d</sup>Samus et al. (1995a) <sup>e</sup>Samus et al. (1995b)

<sup>f</sup>Buonanno et al. (1995) <sup>g</sup>Alcaino et al. (1992) <sup>h</sup>Durrell & Harris (1993) <sup>i</sup>Stetson et al. (1989)

The photometric data are based on the pre-image observations of the target fields in the  $B$  and  $V$  band, taken several months prior to the spectroscopic observations. The identification and psf-photometry was performed on the pipeline reduced images (provided by ESO) using the the IRAF package DAOPHOT.  $B$  and  $V$  magnitudes were matched to create the CMDs. For this work, a precise photometric calibration is not necessary since we are mainly interested in a comparative study of stars in different evolutionary states, which can easily be identified in the CMDs. A rough calibration was done by adjusting the zeropoints such that the MSTO ( $B - V$ ) colors and  $V$  magnitudes taken from the literature were matched (see Table 3.2).

Based on the location in the CMDs we assigned stars to the MS, SGB, and RGB. Figure 3.2 shows the CMDs for all clusters in our sample. The stars with available spectra are symbol-coded according to their position in the CMD. Only those stars are shown that were identified as radial velocity members and that passed our quality check of the spectra. For the two Sgr clusters Ter 7 and Pal 12 some stars near the RGB bump have been observed. These stars are included in the Figures 3.2, 3.3, and 3.4 but neglected in the further analysis.

### 3.3 CN and CH band strengths

For all spectra, we measured line indices covering the absorption features of the CN and CH molecules at about 3883 Å and 4300 Å, respectively. This is a simple way to quantify the molecule content in the stellar atmospheres for medium and small resolution spectra. In order to determine the strengths of the absorption bands via indices, two or three bandpass region need to be defined: One central bandpass, comprising the actual absorption band to be measured and at least one neighboring bandpass on one - if possible on both sides of the central bandpass. These continuum bandpasses should be close to the measured absorption band and should not contain any major line feature. For the measurements of the band strengths of the CN and CH absorption various authors defined various sets of line indices (e.g., Norris et al. 1981; Cohen 1999a; Harbeck et al. 2003a; Stanford et al. 2004). The definition of the individual indices are very similar and mainly based on the early work by Norris et al. (1981). Generally, for the CH band a line index involving two continuum regions is applied. For the CN band, which is located towards the ultraviolet part of the spectrum where the line density is very high, only a red continuum can be defined.

In this project the CN and CH band strengths is quantified by the modified S3839 and CH4300 indices used by Harbeck et al. (2003a), because their study is based on observations from the same instrumental setup as ours. These are defined as:

$$S3839 = -2.5 \log \frac{F_{3861-3884}}{F_{3894-3910}}, \quad (3.1)$$

$$CH4300 = -2.5 \log \frac{F_{4285-4315}}{0.5F_{4240-4280} + 0.5F_{4390-4460}}, \quad (3.2)$$

where  $F_\lambda$  are the fluxes in the different bandpass regions. Larger determined index values mean stronger absorption features of the corresponding molecule. Our error estimates assume Poisson statistics in the flux measurements.

#### 3.3.1 CN band strengths

In order to investigate the behavior of the strengths of the CN index as a function of evolutionary state (or stellar mass) we plotted CN against the absolute  $V$  magnitude,  $M_V$ , for all

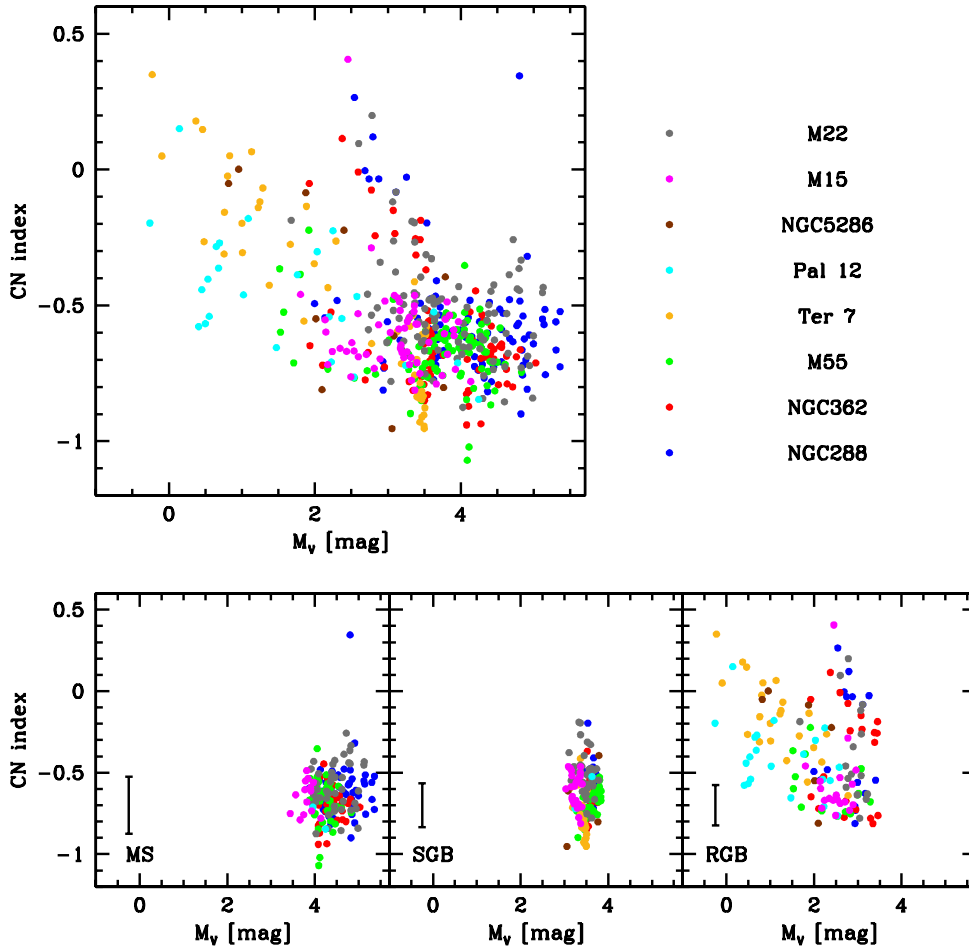


**Figure 3.3:** The distribution of the stars of the different clusters in the CN vs.  $M_V$  diagram. The upper left panel illustrates the overall distribution of our sample stars. In the lower panels we distinguished between different evolutionary states of the stars. The color coding of the data points corresponds to stars from the different clusters as indicated in the figure legend in the upper right. Whereas for the MS all clusters show roughly the same distribution, for the RGB the distribution shows a large scatter. For the clusters NGC288 and NGC362 a bimodal distribution in CN band strength is visible. In the lower left corner of the bottom panels the median errors of the measurements are shown.

clusters (Figure 3.3). We adopted the distance moduli and extinction values of Harris (1996).

Looking at the whole sample of stars a wide spread in CN and a continuous increase of CN with decreasing  $M_V$  can be seen in the upper panel of this figure. This is caused by the fact that the formation of molecules in stellar atmospheres strongly depends on the effective temperature,  $T_{\text{eff}}$ , and the surface gravity,  $\log g$  of the stars. The efficiency of CN formation is higher in stars with lower  $T_{\text{eff}}$  and lower  $\log g$ . To further illustrate this effect we subdivided our sample into MS ( $\log g \sim 4.5$ ,  $T_{\text{eff}} \sim 6000$  K), SGB ( $\log g \sim 4.5-3$ ,  $T_{\text{eff}} \sim 5000-6000$  K), and RGB stars ( $\log g \sim 3$ ,  $T_{\text{eff}} \sim 5000$  K). The different distributions for the different evolutionary states are shown in the lower panels. One can clearly see that the line strengths of CN on average increase as stars evolve from the MS to the RGB. This can be understood by the augmented formation of molecules in cooler atmospheres.

Looking at the globular clusters individually one recognizes that they show very different behaviors in the  $M_V$  vs. CN diagram. Whereas for the MS and the SGB all clusters show roughly the same pattern, the distributions on the RGB deviate between the clusters. For some clusters like e.g., NGC 288 and NGC 362, we clearly see a bifurcation in CN band strengths as we reach the RGB. Either part of the bifurcation contains roughly equal numbers of stars. This is worth to keep in mind as the two clusters are a so called “second-parameter pair”: both clusters have similar metallicities but show a very distinct horizontal branch morphology. In NGC 288, most of the core helium burning stars can be found on the blue horizontal branch whereas almost no stars are located on the red part. Exactly the opposite is the case for NGC 362. For this cluster the red part of the horizontal branch is densely populated. Some authors proposed that deep mixing and the consequently increased mass loss could be an explanation for the different horizontal branch morphologies as well as the observed abundance anomalies (e.g., Weiss et al. 2000). For other second parameter pairs like e.g., M 3 and M 13, which also show differences in light abundance elements this might be a possible explanation for the observed patterns. Both clusters have similar age and metallicities. However, the RGB in M 3 is dominated by CN-weak stars, whereas the majority of stars in M 13 are found to be CN-strong (e.g., Suntzeff 1981).

Nevertheless, the fact that we do not observe significant differences in the CN distributions indicates that deep mixing cannot be a major cause of the horizontal branch morphology. Similarly, based on the CN and CH measurements of stars in the second parameter cluster NGC 7006, Harbeck et al. (2003b) argued against the hypothesis that CN-variations are directly correlated with the second parameter effect. They found the scatter in CN to be similar to those in other GCs of the same metallicity but different horizontal branch ratios.

In contrast to NGC 288 and NGC 362, the clusters Ter 7, Pal 12, and M 55 seem to exhibit no or only very few stars with strong CN band strengths. In the clusters NGC 5286, M 22, and M 15, stars can be found on both the CN-weak and the CN-strong regime in this diagram. For M 15 and M 22, the majority of the stars are associated with the CN-weak group. For NGC 5286, we have only six measurements. Four of these stars are found to be CN-strong and two CN-weak.

We cannot assess whether similar abundance variations on the SGB and the MS region are not present or can not be detected due to a too weak signal caused by the higher effective temperatures of these stars. The observed scatter in the CN measurements of MS and SGB stars (rms  $\sim$  0.13 and 0.14, respectively) is found to be of the same order as the errors in the index measurements (0.17 and 0.13, respectively).

CN as a double-metal molecule is easier to observe in more metal-rich clusters due to the stronger equivalent widths at higher metallicities. Our work as well as former studies on the RGB show that whatever process is responsible for the formation of the CN-strong stars, it seems to occur in the majority of Galactic globular clusters. In contrast to this, in both fairly metal-rich Sgr dSph clusters (Pal 12 and Ter 7) we found no sign for this process to be present. All stars in these clusters are located in the CN-weak branch in Fig. 3.3. From the fact that, if present, CN-strong stars should show up easily in these clusters we conclude that they actually lack those stars. This suggests that probably the environment in which the clusters formed had an effect on the presence or absence of the CN variations.

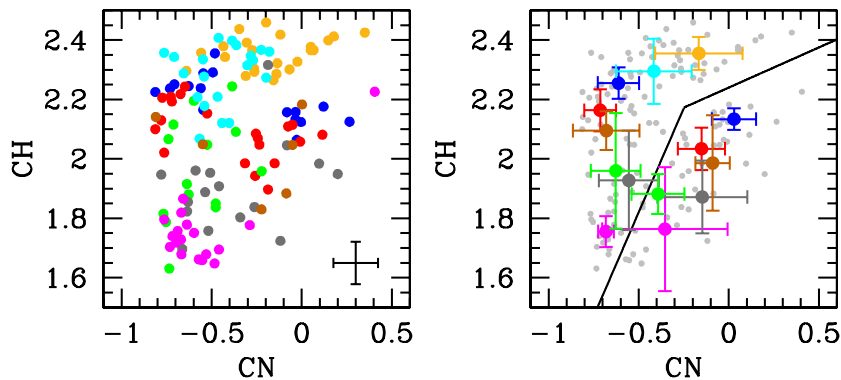


**Figure 3.4:** The distribution of the stars in the CN vs. CH diagram for the RGB star in our sample clusters. The stars of different clusters are indicated by different colors as listed in Fig 3.3. The left panel illustrates the overall distribution of our sample stars, with a typical error given in the lower right corner. The solid line indicated a possible differentiation between CN-strong and CN-weak stars in this diagram, drawn by eye. In right panel we calculated the mean CN and CH of both, the CN-strong and CN-weak stars. The original overall distribution is plotted in gray, while the mean values are color-coded as defined before.

### 3.3.2 CN vs. CH

The CN vs. CH diagram also allows us to study CN bimodalities. In Fig. 3.4 (left panel) we plot the measured CN vs. the CH band strengths for the RGB stars in our sample clusters. The overall patterns found for RGB stars in Fig. 3.3 also show up in Fig. 3.4. A clear bifurcation into two branches is detected in the CN vs. CH diagram for stars on the RGB. NGC 288 and NGC 362 show the strong bimodality in the distribution of CN line strength, seen before. In contrast, the RGB data points of Ter 7 and Pal 12 again are both located on the CN-weak branch in Fig. 3.4. Due to their fairly high metallicities these clusters are found in the CH-strong regime in this diagram. It seems as if the two Sgr clusters are more homogeneous in their CN abundances than the Galactic globular clusters in our sample.

Interestingly, the stars in M 15, which showed no indication for a bifurcation in Fig. 3.3, show a weak indication of a bimodal distribution (two clumps separated at  $CN \sim -0.6$ ) in the CN-CH plane (Fig. 3.4). However, this needs further confirmation since the observational errors of such weak lines are large compared to the separation of the two clumps. Assuming that the clump at  $CN = -0.5$  and  $CH = 1.65$  defines the CN-rich population, this would strongly change the number ratio of CN-strong to CN-weak stars in M 15 (see next section). In order to further illustrate the dichotomy in this plot we separated CN-strong from CN-weak stars (see Fig. 3.4 right panel) and calculated the mean CN- and CH-indices for each sub-population in the different clusters (large dots).

As we introduced earlier, one of the scenarios proposed to explain the variations in C and N in RGB stars in globular clusters is the dredge-up of material processed in the CNO cycle. In our case, the origin of the observed patterns/bimodalities can not only lie in such mixing effects as the analyzed stars are considerably fainter than the red bump at which the deep mixing mechanism is expected to set in. Although we did not find evidence for CN bimodalities among our SGB and MS stars (cf. Harbeck et al. 2003a) we favor a scenario in which the cluster formed out of chemically inhomogeneous material that was polluted by the

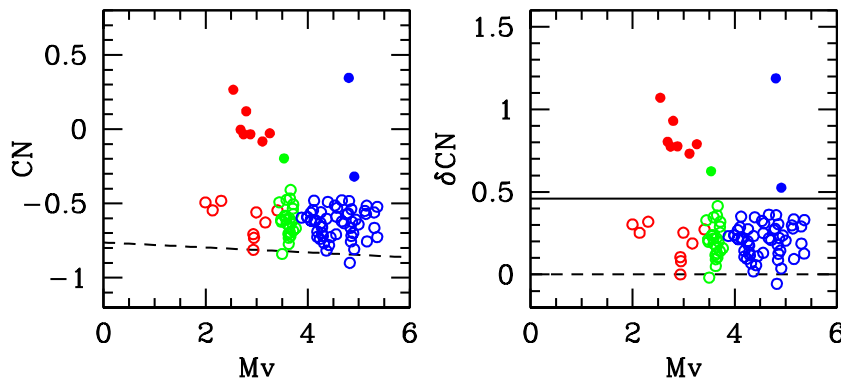


**Figure 3.5:** Left: The  $M_V$  vs. CN diagram for the RGB (red), SGB (green) and MS (blue) stars for the cluster NGC 288. The bimodal distribution is clearly visible. The dashed line illustrates the lower envelope fitted to this distribution. Right: Plotted is  $M_V$  vs. the CN excess parameter  $\delta\text{CN}$ . Stars with  $\delta\text{CN} > 0.46$  are defined as CN-strong and indicated by filled circles. CN-weak stars are indicated by open circles. The solid line indicates the separation between CN-strong and CN-weak stars.

outflows of fast rotating massive stars or AGB stars (e.g., Cottrell & Da Costa 1981; Ventura et al. 2001; Decressin et al. 2007).

### 3.3.3 Cyanogen excess parameter ( $\delta\text{CN}$ )

As a measure to quantify the large range of CN line strengths we used a CN excess parameter ( $\delta\text{CN}$ ) similar to the one introduced by Norris & Smith (1981). This minimizes the effects of effective temperature and surface gravity existent in the CN measurements. The  $\delta\text{CN}$  parameter is defined as the CN strength with respect to a baseline. This baseline is defined by the lower envelope fitted for each individual cluster in the CN vs.  $M_V$  distribution. The left panel in Fig. 3.5 illustrates the baseline fit and right panel shows the resulting  $\delta\text{CN}$  vs.  $M_V$  distribution for the cluster NGC 288.

In the previous sections we saw that the bimodality is only clearly detected for stars on the lower RGB. Therefore, in the following we concentrate on this part of the CMD. Fig. 3.6 shows the histograms of the CN excess parameter for the RGB stars in all eight globular clusters in our sample, sorted by their metallicity. We selected a bin width of 0.13, comparable to the median uncertainties of the CN index for these stars.

Most of the metal-poor clusters (M 15, M 55, and M 22) show a distinct main CN-weak peak with a weak extension towards higher  $\delta\text{CN}$  values. For NGC 5286, we observe a fairly flat distribution. However, due to the small sample size we cannot definitely comment on any distribution pattern. For NGC 288 and NGC 362, which have similar intermediate metallicities, the bimodal distribution clearly shows up in these plots. Both peaks are roughly equally pronounced. The two probable Sgr dSph clusters (Pal 12 and Ter 7) show a single peak and a fairly broad distribution around the CN-weak peak. The broadness is a consequence of the larger errors in the CN measurements of these two most remote clusters in our sample. Pal 12 and Ter 7 are furthermore the most metal-rich clusters in our sample. As mentioned before, if CN-strong stars and a bimodality were present we expect them to clearly show up in these diagrams.

In Fig. 3.7 we show combined histograms of the  $\delta\text{CN}$  measurements of the clusters in our



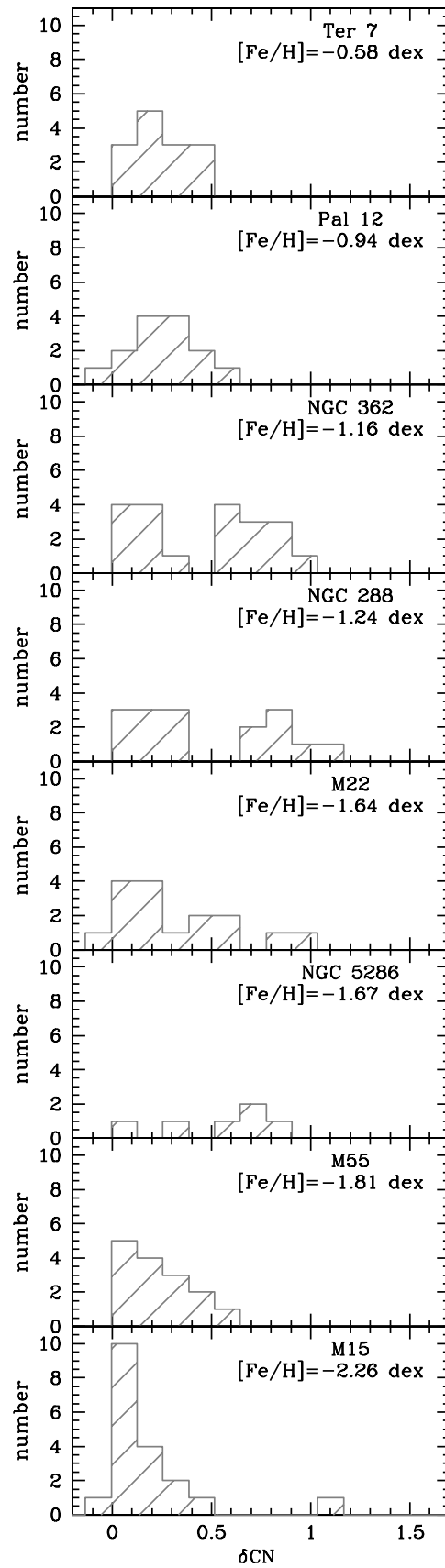


**Figure 3.6:** Distributions of CN-band strength in the RGB stars of our sample clusters. The histograms of the CN-excess parameter  $\delta\text{CN}$  are plotted. The clusters are sorted by their metallicity. The two fairly metal-rich Sgr clusters are found in the two uppermost panels.

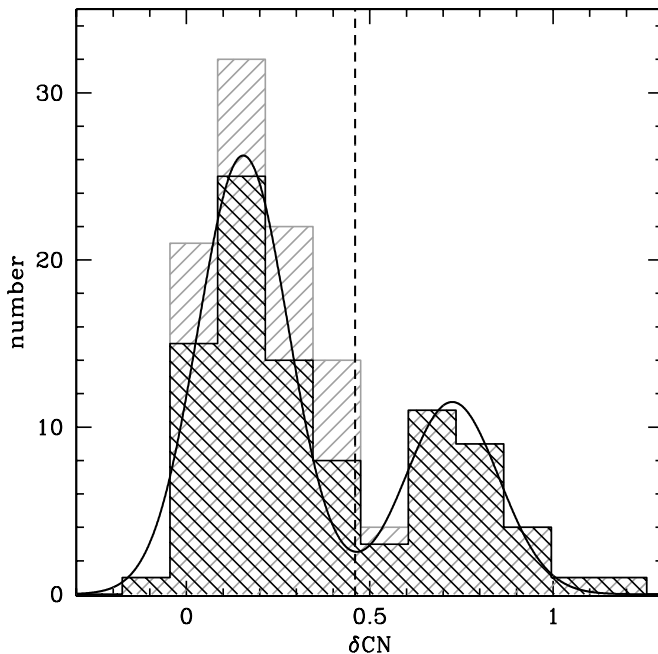


**Figure 3.7:** Combined histograms of the CN-excess parameter for the clusters in our sample. The gray histogram comprises all eight clusters. In the black histogram Pal 12 and Ter 7, which are believed to belong to the Sgr dSph, are not included. Here we only consider stars on the lower RGB.  $\delta\text{CN}$  shows a bimodal distribution, which was fitted by two Gaussians. The minimum between the two Gaussians was chosen as the criterion to differentiate between CN-strong and CN-weak stars.

sample. We distinguish between a histogram of all eight clusters and one where we did not include the two Sgr dSph clusters, Ter 7 and Pal 12. In both cases a clear bimodal distribution is visible. As Ter 7 and Pal 12 are of extragalactic origin and also show a broader distribution in  $\delta\text{CN}$  we focused on the histogram based on six globular clusters. This distribution was used for the differentiation between CN-strong and CN-weak stars. We fitted a double Gaussian to the distribution and selected the minimum as the differential criteria between CN-strong and CN-weak stars. CN-strong stars are then those that have a CN excess larger than  $\delta\text{CN}=0.46$ .

In order to quantify the observed bimodality in the CN line strength, we determined the parameter  $r$  introduced by Norris (1987). It gives the number ratio of CN-strong to CN-weak stars.

$$r = N_{\text{strong}}/N_{\text{weak}}, \quad (3.3)$$

Errors in  $r$  have been estimated from statistical uncertainties (adopting  $\Delta N = \sqrt{N}$ ):

$$\Delta r = r \sqrt{1/N_{\text{weak}} + 1/N_{\text{strong}}}, \quad (3.4)$$

where  $N_{\text{weak}}$  and  $N_{\text{strong}}$  give the number of CN-weak and CN-strong stars, respectively.

For the further analysis, we included two additional data from literature sources. Briley (1997) determined the ratio of CN-strong to CN-weak stars for stars on the RGB in 47 Tuc. He distinguished between RGB stars below and above the RGB bump and found very similar values of 1.9 and 1.8, respectively. For this work, we adopted the value of 1.9. Penny et al. (1992) and Lee (2005), who found the  $r$ -parameter in the cluster M 71 for stars on the lower RGB to be 0.8 and 0.69, respectively. We adopted the more recent result by Lee (2005).

Table 3.3: CN number ratios.

Cluster	$\frac{\text{CN}_{\text{weak}}}{\text{CN}_{\text{strong}}}$	$r_{\text{lowerRGB}}$	$r_{\text{upperRGB}}$
NGC 288	9/7	$0.78 \pm 0.39$	
NGC 362	9/11	$1.22 \pm 0.55$	2.46 <sup>a</sup>
NGC 5286	2/4	$2.00 \pm 1.73$	
NGC 6656 (M 22)	10/6	$0.60 \pm 0.31$	0.41 <sup>b</sup>
Ter 7	14/0	$0.00 \pm 0.00$	
NGC 6809 (M 55)	13/2	$0.15 \pm 0.12$	0.22 <sup>c</sup>
NGC 7078 (M 15)	18/1	$0.06 \pm 0.06$	
	(12/7)	( $0.60 \pm 0.29$ )	
Pal 12	13/1	$0.07 \pm 0.07$	
NGC 104 (47 Tuc)		1.90 <sup>d</sup>	1.8 <sup>d</sup>
NGC 6839 (M 71)	13/9	0.69 <sup>e</sup>	1.0 <sup>e</sup> , 0.63 <sup>g</sup> , 0.3 <sup>h</sup>
NGC 1904 (M 79)			2.6 <sup>b</sup>
NGC 2808			2.4 <sup>f</sup>
NGC 3201			1.1 <sup>f</sup>
NGC 5272 (M 3)			0.6 <sup>f</sup>
NGC 5904 (M 5)			3.0 <sup>f</sup>
NGC 6121 (M 4)			1.4 <sup>f</sup>
NGC 6171 (M 107)			1.4 <sup>f</sup>
NGC 6205 (M 13)			3.2 <sup>f</sup>
NGC 6254 (M 10)			0.5 <sup>f</sup>
NGC 6637			1.2 <sup>f</sup>
NGC 6752			1.6 <sup>f</sup>
NGC 6934			0.6 <sup>f</sup>
NGC 7006			2-3.5 <sup>b</sup>
NGC 7089 (M 2)			3.8 <sup>f</sup>

<sup>a</sup>Smith & Mateo (1990), <sup>b</sup>Harbeck et al. (2003b), <sup>c</sup>Norris (1987), <sup>d</sup>Briley (1997), <sup>e</sup>Lee (2005),  
<sup>f</sup>Smith (2002), <sup>g</sup>Cohen (1999b), <sup>h</sup>Penny et al. (1992)

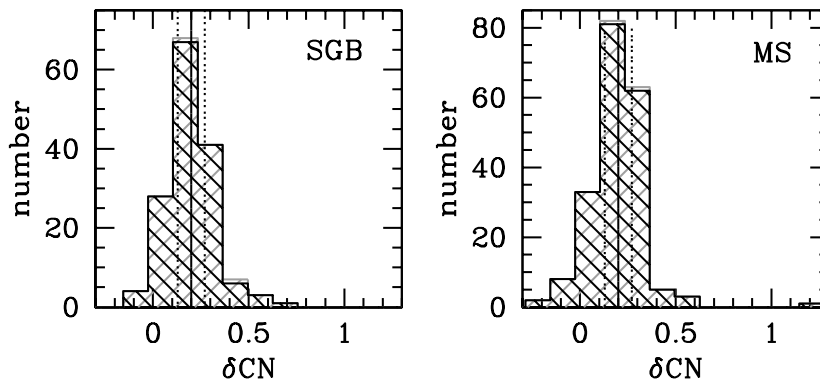


**Figure 3.8:** The combined distributions of the CN-excess parameters measured for stars on the SGB and MS. The gray histogram comprises all eight clusters. In the black histogram Pal 12 and Ter 7 are not included. The solid lines indicate the median values of the distributions. The dashed lines indicate the selection limits for CN-strong and CN-weak stars. Stars with  $\delta\text{CN}$  smaller than the position of the first dashed line are considered as CN-weak, stars with  $\delta\text{CN}$  larger than the position of the second dashed line as CN-strong.

The measurements of the number ratio of CN-strong stars on the upper RGB of M 71 range between 0.3 (Penny et al. 1992), 0.63 (Cohen 1999b), and 1.0 (Lee 2005). The average value is 0.64, similar to those found on the lower RGB. Nevertheless, we have to keep in mind that the additional r-parameters are based on observations obtained with a different instrument and different index definitions.

In the upper part of Table 3.3 an overview of the number of stars identified as CN-strong and CN-weak is given. In the third column the r-parameters for the lower RGB of our clusters and M 71 and 47 Tuc are listed. The r-parameters range from 0.0 for Ter 7 to 2.00 for NGC 5286. The uncertainties vary from 0.07 for Pal 12 to 1.73 for NGC 5286. The large uncertainty for NGC 5286 is due to the small sample size. If one would divide the stars of M 15 into CN-weak and CN-strong according to Fig. 3.4 its r-parameter would be 0.6 (given in brackets in Table 3.3). For those clusters that were part of previous studies the r-parameters for the upper RGB are given in the last column. We find for two out of the three clusters of our sample, for which RGB studies exist, a good agreement of the number ratios found on the SGB with those on the RGB. The values for NGC 362 differ by a factor of 2. The reason for this remains unclear and requires the repetition of the measurement on the RGB.

### 3.4 CN-CH - anticorrelation

In many clusters the bimodal distribution in CN is accompanied by an anticorrelation of CN and CH. A summary on this can be found in e.g., Kraft (1994). As these abundance patterns are similar to those expected by the nucleosynthesis of material in the CNO cycle they have been attributed to a dredge-up of processed material to the stellar surfaces. In the meantime CN-CH anticorrelations have been found to be very common for clusters with a bimodal distribution in CN (see, e.g., the recent review paper by Gratton et al. 2004).

In order to examine possible CN-CH anticorrelations we used the distinction criteria between CN-strong and CN-weak RGB stars as described in Section 3.3.1. Although no clear bimodality in CN absorption strength was detected on the SGB and MS, we observe a scatter

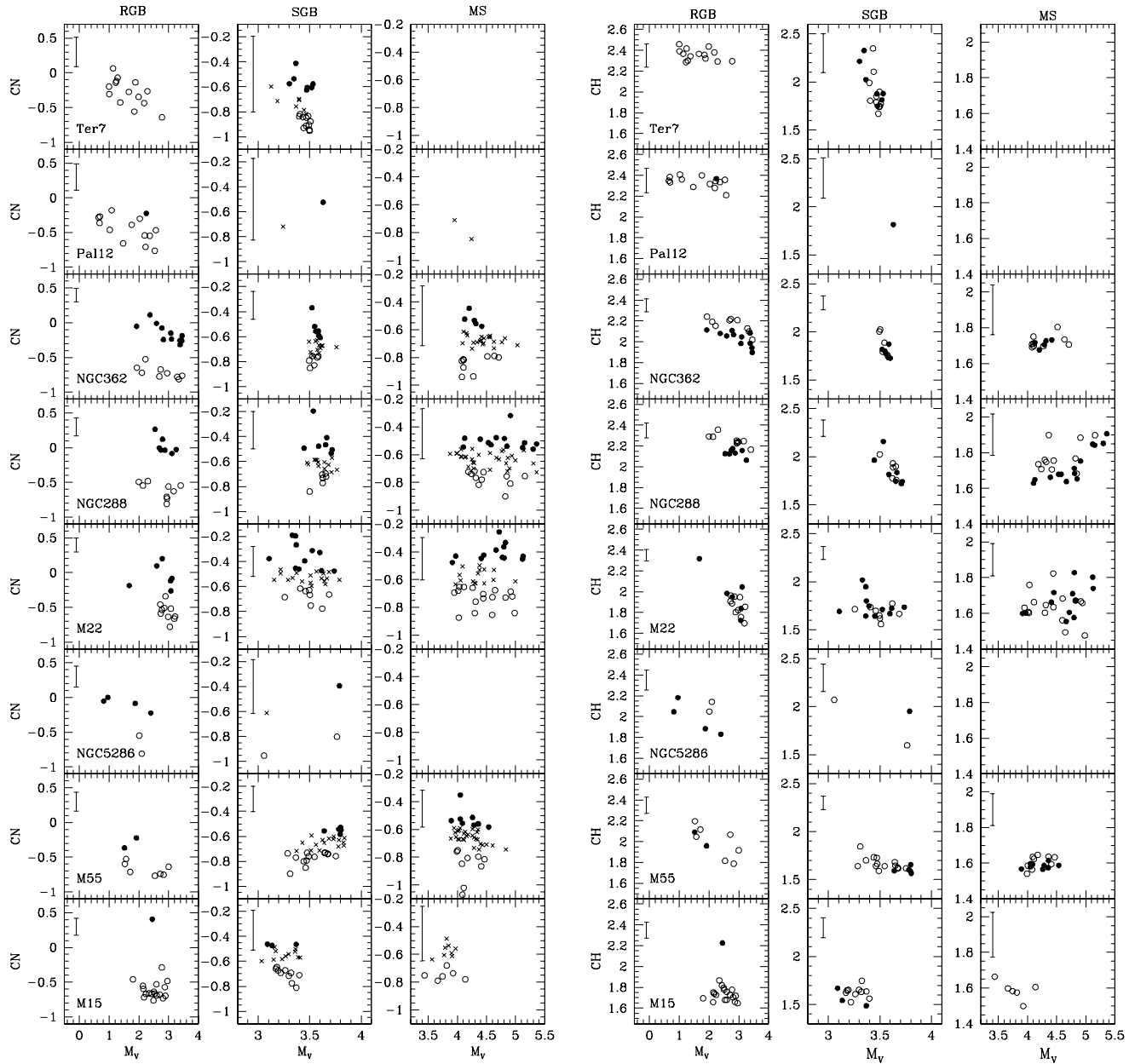


**Figure 3.9:** The CN vs.  $M_V$  and CH vs.  $M_V$  diagrams for the eight clusters in our sample. We differentiate between RGB, SGB, and MS stars for all clusters. The CN-strong and CN-weak stars are marked by filled and open symbols, respectively. SGB and MS stars with intermediate  $\delta$ CN strength are plotted as crosses. For reasons of clarity these stars are only plotted in the CN vs.  $M_V$  diagrams. The median error of the measurements are given in the upper left corners of each panel. We do not plot the errors for SGB and MS stars in Pal 12 as they exceed the limit of the diagrams.

in CN larger than expected from measurement errors alone in all evolutionary states.

Since cyanogen dichotomies have been detected before on the MS on 47 Tuc (Harbeck et al. 2003a) and M 71 (Cohen 1999b) it is quite conceivable that abundance variations among the less evolved stars exist in our sample as well. At the precision of our measurements, however, the signal might be simply too weak due to the higher temperatures and/or low metallicities, which inhibit the formation efficiency of the CN molecule. Nevertheless, in order to check for anticorrelations, we determined the CN excess parameter for the SGB and MS stars analogously to the RGB stars. The resulting  $\delta\text{CN}$  distributions are shown in Fig. 3.8. In analogy to the RGB analysis we neglected the Sgr clusters Palomar 12 and Terzan 7. The median  $\delta\text{CN}$  values were found to be 0.20 both for the SGB and MS. The standard deviation is  $\sigma = 0.08$  in both cases. We considered those stars with  $\delta\text{CN}$  higher than  $1\sigma$  above and below the median as CN-strong and CN-weak, i.e., CN-strong:  $\delta\text{CN} > \text{median} + \sigma$ ; CN-weak:  $\delta\text{CN} < \text{median} - \sigma$ .

A comparison of CN vs.  $M_V$  and CH vs.  $M_V$  is shown in Fig. 3.9. We differentiate between RGB, SGB, and MS stars for all clusters. Stars with stronger and weaker CN absorption band features are highlighted by filled and open symbols, respectively. SGB and MS stars with intermediate  $\delta\text{CN}$  strength are plotted as crosses and are shown in the CN vs.  $M_V$  diagrams only. A bimodal distribution in CH is not detected for any of the clusters. Note that even for NGC 288 and NGC 362, which showed the strongest dichotomy in CN, we do not observe a bimodality in CH. However, the CN-strong RGB stars of these two GCs clearly have smaller CH indices than the CN-weak RGB stars of similar  $M_V$ . This is not seen for the other clusters, except maybe for NGC 5286. In case of M 22, larger uncertainties due the significant differential reddening (Richter et al. 1999) might dilute a possible CN-CH anticorrelation. In the very metal-poor cluster, M 15, one RGB star with high CN absorption bands was identified, which also seems to be quite rich in CH. This CN- and CH-strong star in M 15 stands out from the rest of the datapoints by more than 1 in  $\delta\text{CN}$ . Since this star lies slightly off the RGB we suggest that this star is not a cluster member (although it has the right radial velocity).

Moving from the RGB to the SGB and the MS, the CN-CH anticorrelation still is visible for NGC 288 and NGC 362. Due to the smaller signal to noise ratio, it is less pronounced but on average the more CN-strong stars are more CH-weak. For the other clusters, no clear statement can be made.

We conclude that in case of clearly bimodal clusters like NGC 288 and NGC 362 the differences in the band strengths and the CN/CH anticorrelation do exist among stars of all evolutionary states. Deep mixing is believed to set in at the level of the RGB bump and does not take place in stars on the lower RGB, SGB, and MS. Furthermore low-mass MS stars burn hydrogen in their cores only. Thus the observed patterns can not be caused by the transport of CNO cycle processed material from the interior to the stellar surfaces. We can therefore rule out evolutionary effects within the stars as the origin of the observed anticorrelation.

Table 3.4: Global parameters of globular clusters of our sample.

Cluster	$D_{GC}^{1a}$ (kpc)	$M_V^a$ (mag)	HBR <sup>2a</sup>	[Fe/H] <sup>a</sup> (dex)	$c^{3a}$	$e^{4a}$	$r_{core}^{5a}$ (pc)	$r_{tidal}^{6a}$ (pc)	$\mu_{0,V}^{7a}$ (mag/'' <sup>2</sup> )	$\sigma^{8b}$ (km/s)	(M/L) <sup>b</sup>	age <sup>c,d</sup>	class <sup>f</sup> (Gyr)
NGC 288	12.0	-6.74	0.98	-1.24	0.96	0.09 <sup>e</sup>	3.64	33.12	19.95	2.9	3.0	11.3	OH
NGC 362	9.4	-8.41	-0.87	-1.16	1.94	0.01	0.47	39.83	14.88	6.4	1.1	8.7	YH
NGC 5286	8.4	-8.61	0.80	-1.67	1.46	0.12	0.93	26.75	16.07	8.0	2.1	NA	OH
M 22	4.9	-8.50	0.91	-1.64	1.31	0.14	1.32	26.97	17.32	9.0	3.3	12.3	OH
Terzan 7	16.0	-5.05	-1.00	-0.58	1.08	NA	4.12	49.06	20.65	NA	NA	7.4	SG
M 55	3.9	-7.55	0.87	-1.81	0.76	0.02	4.36	25.10	19.13	4.9	3.4	12.3	OH
M 15	10.4	-9.17	0.67	-2.26	2.50	0.05	0.21	64.42	14.21	12.0	2.2	12.3	YH
Palomar 12	15.9	-4.48	-1.00	-0.94	1.94	NA	1.11	96.78	20.59	NA	NA	6.4	SG
47 Tuc	7.4	-9.42	-0.99	-0.76	2.03	0.09	0.52	56.1	14.43	11.5	2.0	10.7	BD
M 71	6.7	-5.60	-1.00	-0.73	1.15	0.00	0.73	10.43	19.22	2.3	1.1	10.2	BD
NGC 1904	18.8	-7.86	0.89	-1.57	1.72	0.01	0.60	31.3	16.23	5.4	2.2	11.7	OH
NGC 2808	11.1	-9.39	-0.49	-1.15	1.77	0.12	0.73	43.42	15.17	13.4	2.4	9.3	OH
NGC 3201	8.9	-7.46	0.08	-1.58	1.30	0.12	2.08	41.38	18.77	5.2	4.1	11.3	YH
NGC 5272	12.2	-8.93	0.08	-1.57	1.84	0.04	1.66	115.5	16.34	5.6	1.2	11.3	YH
NGC 5904	6.2	-8.81	0.31	-1.27	1.83	0.14	0.92	61.96	16.05	5.7	1.4	10.9	OH
NGC 6121	5.9	-7.20	-0.06	-1.20	1.59	0.00	0.53	20.79	17.88	4.2	2.6	11.7	OH
NGC 6171	3.3	-7.13	-0.73	-1.04	1.51	0.02	1.01	32.47	18.84	4.1	3.9	11.7	OH
NGC 6205	8.7	-8.70	0.97	-1.54	1.51	0.11	1.75	56.4	16.80	7.1	2.2	11.9	OH
NGC 6254	4.6	-7.48	0.98	-1.52	1.40	0.00	1.10	27.49	17.69	6.6	3.5	11.8	OH
NGC 6637	1.9	-7.64	-1.00	-0.70	1.39	0.01	0.90	22.10	16.83	NA	NA	10.6	BD
NGC 6752	5.2	-7.73	1.00	-1.56	2.50	0.04	0.20	64.39	15.20	4.5	1.1	12.2	OH
NGC 6934	12.8	-7.46	0.25	-1.54	1.53	0.01	1.14	38.23	17.26	5.1	2.5	9.6	YH
NGC 7089	10.4	-9.02	0.96	-1.62	1.80	0.11	1.14	71.75	15.92	8.2	1.9	NA	OH
NGC 7006	38.8	-7.68	-0.28	-1.63	1.42	0.01	2.90	76.54	18.50	NA	NA	NA	YH

<sup>1</sup>distance from Galactic center, <sup>2</sup>horizontal branch ratio:  $HBR = (B - R)/(B + V + R)$ , <sup>3</sup>concentration, <sup>4</sup>ellipticity  $e = 1 - (b/a)$ ,  
<sup>5</sup>core radius, <sup>6</sup>tidal radius, <sup>7</sup>central surface brightness, <sup>8</sup>central velocity dispersion, <sup>a</sup>Harris (1996), <sup>b</sup>Pryor & Meylan (1993),  
<sup>c</sup>Rosenberg et al. (1999), <sup>d</sup>Buonanno et al. (1998), <sup>e</sup>Frenk & Fall (1982), <sup>f</sup>Mackey & van den Bergh (2005)

### 3.5 Trends with cluster parameters

In order to explore possible correlations of the CN distribution with global parameters of the globular clusters we combine our observations to quantities available in the literature. A similar analysis was done before by, e.g., Norris (1987), Smith & Mateo (1990), Smith (2002) and Harbeck et al. (2003b). However their studies were based on compilations of upper RGB star measurements in various clusters from different sources and therefore different techniques. We now provide a sample that is based on a very homogeneous data set of eight star clusters. The cluster quantities were selected from the 2003 version of the McMaster (Harris 1996) and Pryor & Meylan (1993) globular cluster catalogs<sup>2</sup>. As no ellipticity is listed in these catalogs for NGC 288, we adopted the value given by Frenk & Fall (1982). The age estimates were adopted from Rosenberg et al. (1999) and Buonanno et al. (1998). Moreover, we adopted the subdivision of our globular clusters into objects belonging to different Galactic components (namely OH, YH, BD, and those accreted from the Sgr dSph (SG)) from Mackey & van den Bergh (2005). Table 3.4 gives an overview of the extracted parameters.

In order to quantify the statistical significance of possible correlations between the number ratio of CN-strong stars with various structural parameters we computed for each parameter the Spearman coefficient of rank correlation,  $r_s$ . This correlation coefficient is a technique that can be used to characterize the strength and direction of a relationship of two random variables  $X$  and  $Y$ . It gives a measure of the dependence of  $X$  on  $Y$ , based on the rankings of ascending  $X_i$  and  $Y_i$  values. The Spearman rank coefficient is defined as:

$$r_s = 1 - \frac{6}{n(n^2 - 1)} \sum_{i=1}^n d_i^2, \quad (3.5)$$

where  $d_i$  gives the difference between the ranks of  $X_i$  and  $Y_i$ . The values of  $r_s$  lie between +1 and -1, the extremes where the rank sequences completely coincide and are completely opposite, respectively. For the clusters in our sample we do not find a clear correlation between the majority of the cluster parameters and the percentage of CN-strong stars (Fig. 3.10).

Norris (1987) observed a correlation between the percentage of CN-rich stars and the apparent flattening of the individual clusters, which he proposed to be associated with the clusters' rotation. He suggested that the high systematic cluster rotation is linked, via exchange of angular momentum, to a higher initial angular momentum of the individual stars. Within giants the rotation may drive circulation currents that are capable of cycling the material in the envelope through the interior hydrogen-burning shell where the CNO process is active (Sweigart & Mengel 1979). Consequently a larger percentage of CN-strong stars is expected to be observed in clusters with larger mean stellar rotation velocities and thus larger overall cluster rotational velocities and hence possibly larger ellipticities. Since there is little information on cluster rotation for the globulars in our sample, we use ellipticity as a proxy for rotation. This correlation was confirmed by Smith & Mateo (1990) and Smith (2002). The computed Spearman rank coefficient of 0.26 suggests that the number ratio of CN-strong stars is mostly independent of the cluster ellipticity. We conclude that the effect proposed by Sweigart & Mengel (1979) is probably not as relevant as thought so far.

Another correlation detected by Smith & Mateo (1990) is between the r-parameter and the central velocity dispersion. Our analysis reveals  $r_s = -0.07$ , which makes such a correlation

---

<sup>2</sup><http://coihue.rutgers.edu/~andresj/gccat.html>



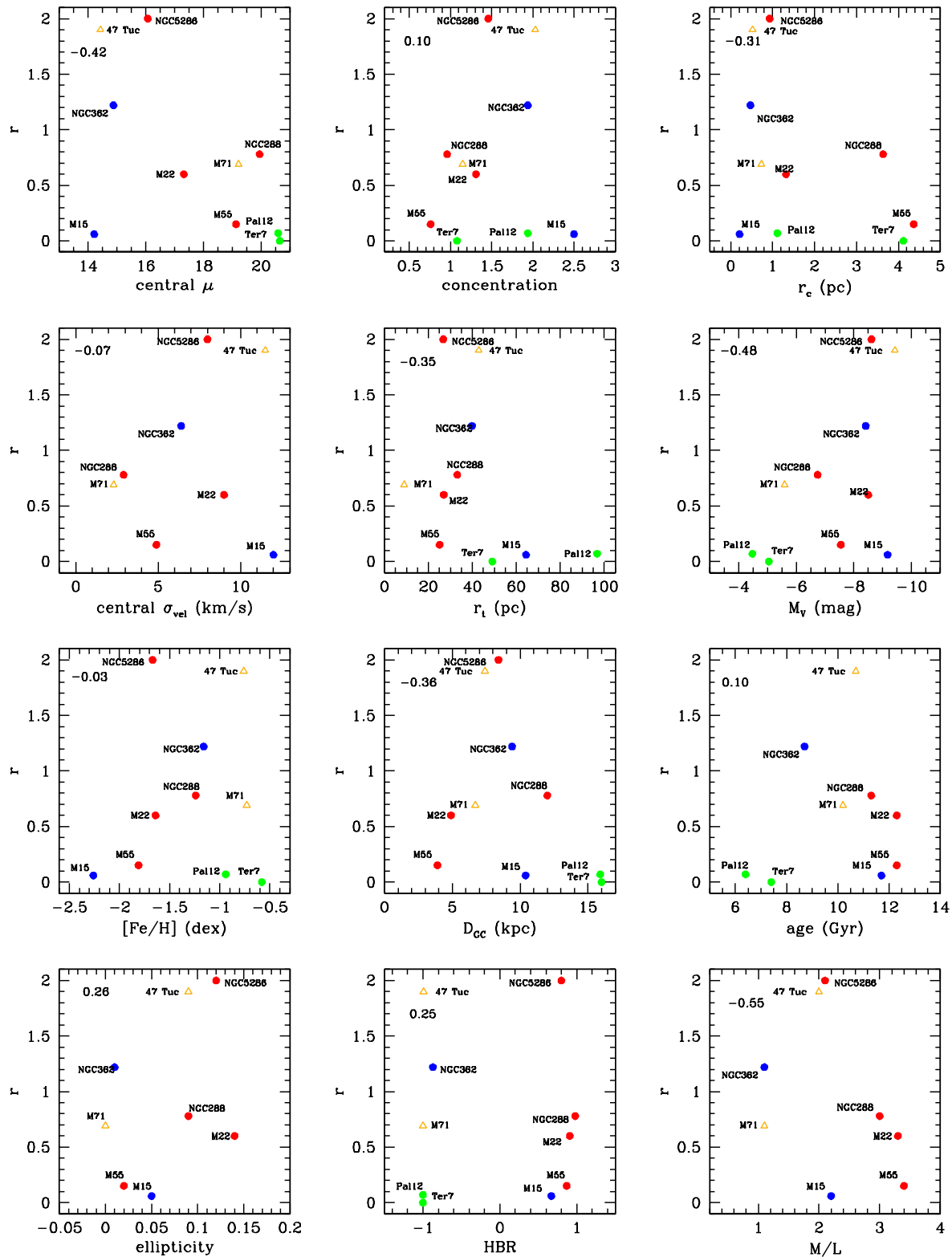


**Figure 3.10:** The number ratio of CN-strong to CN-weak stars ( $r$ -parameter) vs. various cluster parameters (see Tab. 3.4). Our targets are indicated by the filled circles. The two results taken from the literature are marked by open triangles. Red, blue, yellow and green colors indicate OH, YH, BD and Sgr GCs, respectively. In the upper left corner the calculated Spearman rank correlation coefficient is given.

rather unlikely. Furthermore, Smith & Mateo (1990) found the largest percentages of CN-strong stars to be restricted to the more luminous/massive clusters. They suggest an inter-cluster self-pollution scenario as a possible origin. Due to the higher binding energies in more massive clusters, the ability to retain enriched ejecta of massive and intermediate-mass stars is expected to be higher than in lower mass clusters. Our cluster sample supports the correlation with the total absolute magnitude. The calculated Spearman coefficient of  $r_s = -0.48$  is actually among the highest found in our analysis.

In order to perform a more statistically complete investigation we combined our results with those by Smith (2002) and Harbeck et al. (2003b). In Section 3.3.1 we have seen that for the majority of the studied clusters the r-parameter on the upper RGB is consistent with those on the lower RGB. We are thus confident that we may combine our results with those from the literature. Nevertheless we keep in mind that this leads to a more heterogeneous sample, since values of different evolutionary states and different measurements are combined.

For most parameters the lack of any clear trends is confirmed. In particular, the inclusion of our results with those listed in Smith (2002) and Harbeck et al. (2003b) further confirms the lack of a correlation between cluster ellipticity  $\epsilon$  and the number ratio of CN-strong stars. We observe a large scatter in Fig. 3.11 (lower right panel). It can, however, not be ruled out that some clusters with low  $\epsilon$  and high r values are actually more elliptical but appear round due to projection effects. This would dilute a possible correlation. GCs with high  $\epsilon$  and low r values would then be clear outliers.

We see a possible connection between the r-parameter and the tidal radius (Fig. 3.11, lower left panel). Clusters with larger tidal radii seem to possess a larger percentage of CN-strong stars. Interestingly, those clusters that do not follow this trend are those that are thought to be linked to the Sgr dSph (Palomar 12 and Terzan 7) as well as the very metal-poor clusters M15 and NGC 5272, which belong to the young halo GCs. We computed the Spearman coefficient including and excluding these cluster. The resulting values are 0.19 and 0.67, respectively. This is an interesting finding, since Zinn (1993) postulated that the young halo population of globular clusters was predominantly formed by accretion of extragalactic objects. We therefore put forward the hypothesis that, among other parameters, environmental differences due to different cluster formation sites may influence the today observed abundance patterns. Carretta (2006) showed that apart from differences in the environmental properties during the time of formation also differences in the evolution of clusters have probably influenced the light element abundance ratios. Using a set of high resolution spectroscopic abundance measurements he found that clusters with larger orbital semi major axes, i.e., extended orbits and revolution periods, exhibit a larger amount of inhomogeneities. From this he concluded that for clusters on orbits reaching large Galactocentric distances the lack of disturbance by the Galactic disk helps to retain pre-enriched material. In contrast, clusters close to the Galactic center might have suffered early and frequent disk/bulge shocks that enforced rapid gas loss and prohibited the formation of a second enriched subpopulation. Those clusters also show smaller tidal radii due to the even stronger tidal forces towards the center of the Galaxy.

In the upper right panel of Fig. 3.11 we plotted the r-parameter as a function of the absolute magnitude, representing the present-day cluster mass. It seems that the maximum number ratio of CN-strong to CN-weak stars increases with increasing  $M_V$  (cf. Smith 2002). Only the brightest clusters have formed CN-strong stars. This supports the idea that the more massive objects can more efficiently retain processed material ejected from evolved stars.

The possible CN-bimodality of M15 as described in Sect. 3.3.2 and shown in Fig. 3.4 increases the r-parameter of this cluster to 0.6. As a consequence the correlations of r with

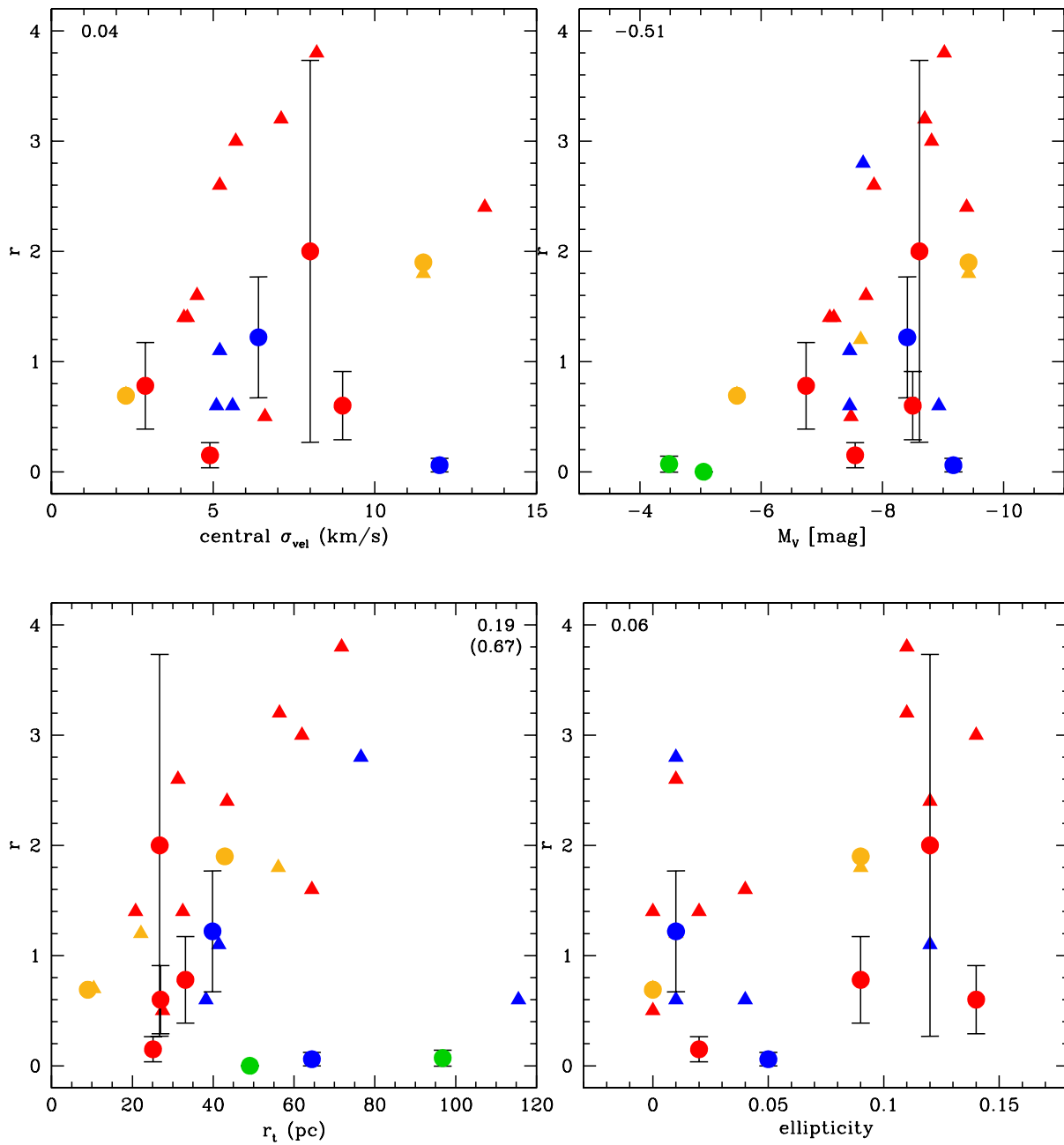


**Figure 3.11:** Plot of the  $r$ -parameter vs. those globular cluster parameters that showed a promising correlation in Fig. 3.10 or in previous studies by e.g., Smith (2002), such as ellipticity, central velocity dispersion ( $\sigma_{\text{vel}}$ ), absolute brightness ( $M_V$ ) and tidal radius  $r_t$ . We also included the results by Smith (2002) (triangles). The results of our study are plotted as filled circles. In this figure we furthermore differentiate between the different MW cluster populations. Old and young halo clusters are colored in red and blue, respectively. Bulge and disk clusters are plotted in yellow and accreted clusters from dwarf galaxies such as the Sagittarius dSph in green.

absolute magnitude,  $M_V$  and tidal radius  $r_t$  become slightly more significant with Spearman rank values of  $r_s = -0.56$  and  $-0.68$ , respectively. The low correlations with central velocity dispersion and ellipticity, however, remain nearly unchanged. More accurate CN/CH index measurements of this very metal-poor cluster are needed to confirm these findings.

### 3.6 Summary and conclusions

We analyzed the absorption bands of the CN and CH molecule in eight Galactic globular clusters via line index measurements. In each cluster, stars of various evolutionary stages were studied, from the lower RGB and SGB to the upper MS. Our sample comprises clusters belonging to different Milky Way components, e.g., young and old halo. In particular, two of our studied objects are associated with a disrupting Galactic companion, the Sagittarius dwarf spheroidal (Sgr dSph). We could show that the majority of the studied clusters shows significant CN/CH variations at the base of the RGB. For the two most prominent CN-bimodal GCs, NGC 288 and NGC 362, CN anticorrelates with CH. A weak signal for a CN/CH anticorrelation was detected also in the least evolved stars in these clusters. From this we conclude that purely evolutionary effects within the stellar interior cannot be the main driver of the observed abundance patterns. Our findings therefore favor a scenario in which a certain fraction of most clusters was formed out of material that was enriched or polluted by ejecta of a prior generation of massive stars. In fact, the existence of star-to-star variations among those slightly evolved stars favors self-enrichment as the probable origin. One possible explanation could be that the nowadays observed stars in globular clusters formed out of protocluster material that was to some degree inhomogeneously enriched in light elements. Such a pollution might have originated from ejecta of a prior generation of massive and therefore fast evolving stars, either belonging to the cluster itself or to the field population of a larger (dwarf sized) galaxy in which the cluster was embedded (e.g., Bekki et al. 2007). Possible candidates for the polluters discussed in the literature are massive AGB stars (e.g., Cottrell & Da Costa 1981; Ventura et al. 2001) and more recently fast rotating massive stars (Decressin et al. 2007). AGBs eject material via slow winds that are processed through the hot CNO cycle but are not enriched in iron. Fast rotating massive stars lose large amounts of material through slow winds, which are also enriched in H-burning products.

For the clusters NGC 288 and NGC 362 we found a clear bimodal distribution in CN with similar numbers of CN-strong and CN-weak stars. As the two clusters are a second-parameter pair, we conclude that the horizontal branch morphology is not correlated with this phenomenon. A possible explanation for such a pronounced dichotomy is given by a prolonged star formation in these globular clusters. The second, enriched stellar population formed well after the first generation had expelled and homogeneously distributed their AGB ejecta. The existence of such multiple stellar populations within globular clusters is further supported by the recent discoveries of complex CMD morphologies (e.g., multiple SGBs and MSs with age spreads) in some massive objects (Bedin et al. 2004; Piotto et al. 2007).

The two probable former Sgr dSph clusters (Terzan 7 and Palomar 12) do not exhibit any CN-strong stars. They are the most metal-rich clusters in our sample and therefore the double metal molecule CN should be easy to detect. We conclude that these clusters actually lack stars with strong CN absorption. Our results suggest that the accreted Sgr globular clusters might be more chemically homogeneous than those native to the Milky Way. This is supported by the abundance analysis of 21 elements for four Sgr stars by Cohen (2004), who

do not find a significant star-to-star scatter. Probably environmental conditions during the formation of the clusters played a major role for the observed abundance pattern. Another reason might be the low mass of Ter 7 and Pal 12. Maybe very low mass clusters are not able to build up a second enriched generation of stars at all. For further conclusions a thorough investigation of the abundance patterns of more low mass GCs and all probable Sgr clusters (M 54, Arp 2, Ter 7, Ter 8, and Pal 12) is desirable.

In order to search for possible drivers for the abundance anomalies we studied the ratio of CN-strong/CN-weak stars as a function of various cluster parameters. We do not confirm the correlation with the cluster ellipticity that was observed before (Norris 1987). Our study therefore does not support cluster rotation and the associated enhanced deep mixing (Sweigart & Mengel 1979) as a main source of the production of CN-strong stars. Although we hardly see correlations of the number ratio of CN-strong stars with the majority of cluster parameters, some dependencies do seem to exist. We find evidence for an increase of the CN-strong star fraction with cluster tidal radius. Since GCs with large tidal radii are mostly found in the weak tidal field of the Galaxy (well outside the bulge and disk potential) they might occupy orbits that avoid bulge/disk shocks. Thus they might keep their gas longer, which favors the build-up of a second generation of enriched stars. Furthermore, we find that preferably the more luminous/massive clusters exhibit a large number of CN-strong stars. This may be an indication that the CNO processed ejecta could be more efficiently retained by more massive objects, independent of their tidal radius. The picture emerges that there are two basic channels that lead to a high fraction of CN-rich stars in GCs: 1) the cluster formed and lived in a remote environment, which allowed it to keep/regain its gas, and 2) the gravitational potential of the cluster itself was large enough to trap the enriched ejecta of slow velocity winds out of which a new generation of stars was formed.

Interestingly, those clusters that do not follow the observed trend are either associated with the young halo or accreted from the Sgr dSph. This might indicate that, as third parameter, the environmental conditions in which the clusters formed might had a non-negligible influence on the abundance patterns we observe today.

Nevertheless we point out that our study is limited to a small sample of clusters. For a statistically better supported study a larger cluster sample is necessary. Furthermore a complete set of cluster parameters are needed to search for the significance of the CN-CH differences between genuine halo globular clusters and accreted objects.



# Appendix 3.A

## Target stars in Galactic globular clusters

**Table 3.A:** Parameters of stars in NGC 288.

Star ID	x-position	y-position	$V$	$(B - V)$	S3839	CH4300
MS-1.1	943.25	320.46	19.63	0.45	$0.345 \pm 0.200$	$1.712 \pm 0.125$
MS-2.1	1072.45	344.91	19.41	0.46	$-0.529 \pm 0.173$	$1.679 \pm 0.114$
MS-3.1	1103.77	367.80	19.09	0.43	$-0.559 \pm 0.141$	$1.648 \pm 0.095$
MS-5.1	1009.16	435.73	19.64	0.46	$-0.484 \pm 0.197$	$1.684 \pm 0.124$
MS-6.1	981.53	463.59	19.11	0.43	$-0.658 \pm 0.148$	$1.685 \pm 0.096$
MS-8.1	981.45	501.24	19.83	0.49	$-0.641 \pm 0.250$	$1.678 \pm 0.150$
MS-9.1	1001.27	532.91	19.98	0.50	$-0.515 \pm 0.263$	$1.841 \pm 0.166$
MS-10.1	1010.25	558.94	19.68	0.47	$-0.539 \pm 0.199$	$1.653 \pm 0.128$
MS-11.1	1011.76	580.78	19.97	0.49	$-0.570 \pm 0.236$	$1.796 \pm 0.153$
MS-12.1	1134.00	611.82	19.68	0.48	$-0.756 \pm 0.209$	$1.682 \pm 0.133$
MS-13.1	912.68	641.70	19.77	0.47	$-0.609 \pm 0.229$	$1.889 \pm 0.150$
MS-14.1	947.37	666.26	19.08	0.43	$-0.632 \pm 0.162$	$1.759 \pm 0.102$
MS-15.1	966.58	687.98	19.36	0.43	$-0.514 \pm 0.181$	$1.679 \pm 0.113$
MS-17.1	1167.54	743.09	19.02	0.46	$-0.689 \pm 0.150$	$1.704 \pm 0.097$
MS-18.1	879.54	766.42	18.96	0.46	$-0.619 \pm 0.147$	$1.739 \pm 0.096$
MS-19.1	1034.84	800.01	18.93	0.45	$-0.545 \pm 0.142$	$1.629 \pm 0.090$
MS-20.1	1190.55	825.61	19.07	0.45	$-0.739 \pm 0.160$	$1.707 \pm 0.102$
MS-21.1	1195.81	851.13	19.11	0.46	$-0.700 \pm 0.161$	$1.716 \pm 0.104$
MS-22.1	984.09	878.45	19.50	0.42	$-0.478 \pm 0.207$	$1.638 \pm 0.132$
MS-23.1	1069.59	897.63	18.96	0.43	$-0.481 \pm 0.138$	$1.648 \pm 0.090$
MS-24.1	1036.46	925.06	18.89	0.47	$-0.562 \pm 0.139$	$1.705 \pm 0.090$
MS-25.1	1179.83	952.25	19.65	0.51	$-0.900 \pm 0.205$	$1.768 \pm 0.131$
MS-26.1	963.81	979.70	20.19	0.52	$-0.523 \pm 0.244$	$1.906 \pm 0.159$
MS-26.2	963.15	982.86	20.14	0.49	$-0.664 \pm 0.243$	$1.848 \pm 0.162$
MS-27.1	1058.41	1003.80	18.98	0.45	$-0.614 \pm 0.140$	$1.671 \pm 0.093$
MS-29.1	1040.95	1097.66	19.20	0.47	$-0.603 \pm 0.176$	$1.735 \pm 0.110$
MS-30.1	1061.13	1124.04	18.82	0.43	$-0.591 \pm 0.140$	$1.774 \pm 0.089$
MS-32.1	1020.30	1170.62	19.10	0.45	$-0.656 \pm 0.172$	$1.780 \pm 0.106$
MS-33.1	1011.40	1188.18	19.67	0.50	$-0.664 \pm 0.219$	$1.744 \pm 0.136$
MS-35.1	1157.22	1234.17	19.72	0.59	$-0.700 \pm 0.228$	$1.911 \pm 0.144$
MS-36.1	1022.37	1268.96	19.28	0.47	$-0.726 \pm 0.188$	$1.756 \pm 0.116$
MS-38.1	1156.55	1310.83	19.70	0.50	$-0.623 \pm 0.214$	$1.801 \pm 0.135$
MS-39.1	900.83	1330.27	20.13	0.54	$-0.560 \pm 0.279$	$1.852 \pm 0.175$
MS-40.1	1171.31	1362.37	19.22	0.44	$-0.489 \pm 0.179$	$1.662 \pm 0.108$
MS-41.1	1185.31	1380.32	19.60	0.49	$-0.575 \pm 0.208$	$1.706 \pm 0.129$
MS-42.1	1190.31	1405.40	19.74	0.48	$-0.319 \pm 0.240$	$1.753 \pm 0.145$

*Continued on next page*

Parameters of stars in NGC 288 - *continued*

MS-43.1	1141.22	1430.89	19.99	0.56	$-0.755 \pm 0.262$	$1.898 \pm 0.164$
MS-45.1	1045.14	1480.24	19.39	0.49	$-0.708 \pm 0.179$	$1.801 \pm 0.116$
MS-46.1	1072.95	1504.67	19.69	0.50	$-0.719 \pm 0.211$	$1.774 \pm 0.135$
MS-47.1	1252.73	1534.11	19.74	0.49	$-0.809 \pm 0.236$	$1.884 \pm 0.152$
MS-48.1	1228.92	1556.29	18.90	0.43	$-0.617 \pm 0.143$	$1.708 \pm 0.089$
MS-49.1	1312.96	1582.56	19.50	0.47	$-0.621 \pm 0.193$	$1.796 \pm 0.121$
MS-51.1	1317.48	1640.79	19.13	0.45	$-0.718 \pm 0.155$	$1.760 \pm 0.099$
MS-52.1	1251.11	1661.10	19.39	0.46	$-0.589 \pm 0.176$	$1.725 \pm 0.111$
MS-53.1	1326.23	1689.57	19.25	0.46	$-0.781 \pm 0.178$	$1.706 \pm 0.110$
MS-54.1	1290.11	1713.63	19.20	0.43	$-0.818 \pm 0.157$	$1.898 \pm 0.102$
MS-55.1	1087.69	1734.31	18.83	0.44	$-0.592 \pm 0.141$	$1.722 \pm 0.088$
MS-56.1	1104.58	1764.54	19.62	0.47	$-0.566 \pm 0.223$	$1.714 \pm 0.134$
MS-57.1	1022.00	1783.84	20.19	0.50	$-0.726 \pm 0.318$	$1.793 \pm 0.187$
MS-58.1	1286.60	1806.80	19.02	0.45	$-0.725 \pm 0.151$	$1.735 \pm 0.095$
MS-59.1	1131.00	1824.31	18.71	0.46	$-0.595 \pm 0.134$	$1.749 \pm 0.083$
MS-60.1	1327.37	1857.82	19.15	0.44	$-0.767 \pm 0.159$	$1.748 \pm 0.100$
MS-61.1	1098.49	1873.09	18.89	0.44	$-0.613 \pm 0.147$	$1.697 \pm 0.092$
MS-62.1	1201.43	1908.53	19.54	0.47	$-0.634 \pm 0.195$	$1.660 \pm 0.123$
MS-65.1	1131.37	1976.64	19.95	0.52	$-0.551 \pm 0.268$	$1.847 \pm 0.171$
SGB-2.1	1157.79	344.19	18.49	0.50	$-0.720 \pm 0.139$	$1.758 \pm 0.083$
SGB-4.1	1515.72	409.83	18.41	0.54	$-0.605 \pm 0.115$	$1.853 \pm 0.072$
SGB-7.1	1177.91	492.68	18.39	0.52	$-0.584 \pm 0.143$	$1.824 \pm 0.081$
SGB-8.1	1056.45	520.16	18.45	0.48	$-0.704 \pm 0.151$	$1.776 \pm 0.086$
SGB-11.1	1230.93	603.26	18.48	0.49	$-0.466 \pm 0.152$	$1.744 \pm 0.087$
SGB-12.1	1141.44	625.99	18.54	0.47	$-0.535 \pm 0.140$	$1.720 \pm 0.081$
SGB-13.1	904.52	666.58	18.27	0.59	$-0.492 \pm 0.162$	$1.964 \pm 0.087$
SGB-14.1	1173.49	687.06	18.47	0.49	$-0.604 \pm 0.156$	$1.764 \pm 0.088$
SGB-15.1	983.68	724.36	18.32	0.59	$-0.623 \pm 0.146$	$1.970 \pm 0.084$
SGB-24.1	1133.67	991.18	18.33	0.61	$-0.840 \pm 0.139$	$2.025 \pm 0.081$
SGB-26.2	1150.09	1081.94	18.38	0.58	$-0.585 \pm 0.149$	$1.842 \pm 0.083$
SGB-27.1	1262.81	1106.76	18.47	0.53	$-0.658 \pm 0.167$	$1.879 \pm 0.092$
SGB-28.1	1156.97	1128.29	18.40	0.57	$-0.588 \pm 0.152$	$1.994 \pm 0.088$
SGB-29.1	1073.86	1151.96	18.46	0.53	$-0.731 \pm 0.164$	$1.889 \pm 0.093$
SGB-34.1	1167.90	1312.03	18.50	0.50	$-0.409 \pm 0.148$	$1.837 \pm 0.086$
SGB-35.1	1062.25	1340.67	18.51	0.51	$-0.626 \pm 0.162$	$1.883 \pm 0.090$
SGB-38.1	1355.30	1433.65	18.55	0.49	$-0.506 \pm 0.144$	$1.741 \pm 0.082$
SGB-39.1	1529.54	1458.98	18.54	0.49	$-0.684 \pm 0.147$	$1.859 \pm 0.085$
SGB-42.1	1495.32	1528.09	18.60	0.47	$-0.666 \pm 0.135$	$1.742 \pm 0.080$
SGB-45.2	1518.06	1623.74	18.48	0.49	$-0.695 \pm 0.143$	$1.899 \pm 0.084$
SGB-46.1	1207.55	1642.82	18.42	0.52	$-0.636 \pm 0.155$	$1.942 \pm 0.087$
SGB-48.1	1260.67	1710.36	18.46	0.52	$-0.773 \pm 0.153$	$1.932 \pm 0.087$
SGB-49.1	1222.93	1739.30	18.36	0.59	$-0.197 \pm 0.174$	$2.158 \pm 0.094$
SGB-50.1	1170.66	1766.35	18.31	0.62	$-0.610 \pm 0.169$	$2.078 \pm 0.095$
SGB-51.1	1125.80	1782.97	18.42	0.47	$-0.476 \pm 0.136$	$1.815 \pm 0.080$
SGB-56.1	1208.61	1940.66	18.55	0.48	$-0.571 \pm 0.146$	$1.786 \pm 0.086$
RGB-3.1	1524.67	369.42	17.14	0.76	$-0.482 \pm 0.082$	$2.355 \pm 0.049$
RGB-6.1	1165.10	454.40	17.77	0.72	$-0.812 \pm 0.115$	$2.225 \pm 0.067$
RGB-10.1	1305.81	586.43	18.00	0.71	$-0.628 \pm 0.155$	$2.245 \pm 0.086$
RGB-16.1	1278.18	744.43	17.52	0.73	$-0.004 \pm 0.120$	$2.124 \pm 0.063$
RGB-21.1	1293.97	894.58	16.97	0.78	$-0.546 \pm 0.094$	$2.288 \pm 0.052$
RGB-22.2	1135.57	934.33	17.78	0.69	$-0.731 \pm 0.125$	$2.237 \pm 0.071$
RGB-25.1	1178.04	1005.82	18.09	0.68	$-0.028 \pm 0.144$	$2.064 \pm 0.078$
RGB-30.1	1148.99	1187.90	17.82	0.72	$-0.560 \pm 0.136$	$2.238 \pm 0.075$
RGB-32.2	1194.84	1261.21	17.62	0.72	$0.121 \pm 0.110$	$2.176 \pm 0.060$
RGB-36.1	1400.00	1362.54	18.24	0.66	$-0.547 \pm 0.158$	$2.165 \pm 0.087$
RGB-37.1	1290.59	1397.84	17.76	0.72	$-0.707 \pm 0.159$	$2.251 \pm 0.085$

*Continued on next page*



Parameters of stars in NGC 288 - *continued*

RGB-44.1	1142.57	1592.80	17.94	0.69	$-0.083 \pm 0.142$	$2.157 \pm 0.076$
RGB-47.1	1327.35	1676.14	17.37	0.71	$0.265 \pm 0.130$	$2.125 \pm 0.063$
RGB-52.1	1154.67	1831.40	16.83	0.76	$-0.493 \pm 0.105$	$2.291 \pm 0.056$
RGB-53.1	997.54	1857.01	17.71	0.69	$-0.034 \pm 0.137$	$2.133 \pm 0.071$
RGB-54.1	1111.51	1884.63	17.57	0.70	$-0.034 \pm 0.128$	$2.158 \pm 0.066$

Table 3.B: Parameters of stars in NGC 362.

Star ID	x-position	y-position	V	(B - V)	S3839	CH4300
MS-2.1	941.82	367.85	18.89	0.44	$-0.940 \pm 0.173$	$1.690 \pm 0.114$
MS-5.1	945.55	450.55	19.25	0.44	$-0.706 \pm 0.209$	$1.701 \pm 0.139$
MS-6.1	1167.80	473.12	19.52	0.45	$-0.800 \pm 0.276$	$1.706 \pm 0.172$
MS-7.1	1005.48	503.15	19.37	0.47	$-0.654 \pm 0.215$	$1.696 \pm 0.140$
MS-8.1	1016.13	529.10	19.84	0.49	$-0.712 \pm 0.297$	$1.671 \pm 0.185$
MS-11.1	1095.22	607.05	19.37	0.41	$-0.642 \pm 0.228$	$1.810 \pm 0.153$
MS-12.1	1166.80	626.60	19.44	0.42	$-0.789 \pm 0.235$	$1.735 \pm 0.155$
MS-13.1	931.06	675.28	19.26	0.42	$-0.661 \pm 0.235$	$1.693 \pm 0.151$
MS-14.1	1068.11	687.64	19.10	0.41	$-0.534 \pm 0.199$	$1.704 \pm 0.132$
MS-15.1	935.15	714.64	18.92	0.40	$-0.818 \pm 0.192$	$1.697 \pm 0.126$
MS-16.1	891.98	739.13	19.33	0.45	$-0.792 \pm 0.279$	$1.804 \pm 0.174$
MS-17.1	1219.25	773.41	19.23	0.42	$-0.576 \pm 0.226$	$1.731 \pm 0.143$
MS-23.1	1052.08	926.38	19.01	0.42	$-0.446 \pm 0.185$	$1.675 \pm 0.116$
MS-25.1	885.51	986.28	19.15	0.40	$-0.690 \pm 0.171$	$1.736 \pm 0.113$
MS-26.1	865.74	1008.83	18.90	0.42	$-0.698 \pm 0.185$	$1.617 \pm 0.121$
MS-28.1	995.76	1090.82	18.94	0.47	$-0.524 \pm 0.209$	$1.716 \pm 0.129$
MS-29.1	1102.62	1114.41	19.44	0.47	$-0.687 \pm 0.257$	$1.888 \pm 0.167$
MS-30.1	1111.33	1138.33	19.20	0.44	$-0.684 \pm 0.226$	$1.639 \pm 0.142$
MS-31.1	792.32	1170.66	19.22	0.49	$-0.677 \pm 0.256$	$1.828 \pm 0.161$
MS-34.1	1121.22	1239.61	18.89	0.42	$-0.826 \pm 0.213$	$1.708 \pm 0.135$
MS-35.1	1026.40	1261.28	18.92	0.47	$-0.871 \pm 0.194$	$1.711 \pm 0.127$
MS-36.1	901.17	1287.83	19.09	0.46	$-0.936 \pm 0.223$	$1.697 \pm 0.142$
MS-39.1	860.21	1363.48	18.97	0.38	$-0.627 \pm 0.199$	$1.712 \pm 0.128$
MS-42.1	788.00	1426.07	19.34	0.43	$-0.650 \pm 0.223$	$1.668 \pm 0.146$
MS-44.1	925.08	1485.68	19.22	0.45	$-0.650 \pm 0.216$	$1.573 \pm 0.137$
MS-46.1	870.05	1534.21	19.06	0.44	$-0.737 \pm 0.237$	$1.688 \pm 0.154$
MS-47.1	831.38	1557.51	19.09	0.45	$-0.695 \pm 0.200$	$1.651 \pm 0.130$
MS-48.1	959.24	1589.02	18.98	0.42	$-0.639 \pm 0.194$	$1.684 \pm 0.126$
MS-49.1	901.55	1626.91	19.62	0.47	$-0.663 \pm 0.274$	$1.806 \pm 0.186$
MS-51.1	734.24	1668.44	19.43	0.46	$-0.735 \pm 0.280$	$1.656 \pm 0.183$
MS-53.1	744.32	1715.74	19.13	0.46	$-0.556 \pm 0.199$	$1.727 \pm 0.133$
MS-54.1	761.01	1745.65	18.92	0.44	$-0.616 \pm 0.189$	$1.668 \pm 0.123$
MS-56.2	1049.02	1802.77	18.91	0.42	$-0.814 \pm 0.216$	$1.750 \pm 0.140$
MS-57.1	972.89	1812.41	19.26	0.46	$-0.697 \pm 0.228$	$1.658 \pm 0.147$
MS-61.1	951.94	1928.09	19.57	0.46	$-0.689 \pm 0.270$	$1.618 \pm 0.181$
SGB-6.1	1037.71	461.51	18.57	0.50	$-0.683 \pm 0.114$	$1.813 \pm 0.076$
SGB-9.1	1101.19	537.26	18.37	0.51	$-0.558 \pm 0.107$	$1.773 \pm 0.070$
SGB-11.1	865.65	583.44	18.34	0.52	$-0.756 \pm 0.109$	$1.793 \pm 0.073$
SGB-13.1	1227.50	646.02	18.31	0.58	$-0.851 \pm 0.111$	$2.026 \pm 0.073$
SGB-14.2	1147.27	669.99	18.39	0.48	$-0.756 \pm 0.115$	$1.739 \pm 0.075$
SGB-18.1	893.29	766.30	18.41	0.51	$-0.608 \pm 0.112$	$1.724 \pm 0.074$
SGB-23.1	893.68	898.36	18.42	0.51	$-0.674 \pm 0.106$	$1.660 \pm 0.071$
SGB-25.1	765.15	966.59	18.30	0.60	$-0.642 \pm 0.106$	$1.849 \pm 0.070$
SGB-26.1	891.92	986.83	18.30	0.61	$-0.791 \pm 0.110$	$2.003 \pm 0.074$
SGB-28.1	685.72	1074.47	18.38	0.49	$-0.629 \pm 0.116$	$1.703 \pm 0.075$

*Continued on next page*

Parameters of stars in NGC 362 - *continued*

SGB-30.1	787.03	1129.67	18.38	0.50	$-0.705 \pm 0.111$	$1.796 \pm 0.072$
SGB-31.1	783.18	1159.27	18.43	0.53	$-0.671 \pm 0.116$	$1.672 \pm 0.075$
SGB-33.1	1168.47	1209.90	18.40	0.51	$-0.733 \pm 0.116$	$1.695 \pm 0.071$
SGB-34.1	826.74	1244.48	18.40	0.60	$-0.592 \pm 0.112$	$1.871 \pm 0.073$
SGB-38.1	1265.35	1362.47	18.36	0.54	$-0.519 \pm 0.109$	$1.799 \pm 0.069$
SGB-42.1	1038.49	1451.19	18.34	0.55	$-0.751 \pm 0.112$	$1.875 \pm 0.072$
SGB-44.1	913.14	1502.64	18.37	0.54	$-0.637 \pm 0.111$	$1.704 \pm 0.071$
SGB-46.1	767.04	1558.94	18.39	0.51	$-0.555 \pm 0.110$	$1.733 \pm 0.073$
SGB-48.1	661.78	1621.89	18.38	0.53	$-0.768 \pm 0.113$	$1.762 \pm 0.074$
SGB-50.1	1228.37	1667.74	18.33	0.57	$-0.369 \pm 0.110$	$1.817 \pm 0.070$
SGB-54.1	1298.51	1772.44	18.40	0.52	$-0.669 \pm 0.108$	$1.742 \pm 0.071$
SGB-55.1	1148.98	1788.49	18.41	0.50	$-0.694 \pm 0.112$	$1.762 \pm 0.072$
SGB-56.1	1078.11	1813.08	18.35	0.54	$-0.829 \pm 0.110$	$1.887 \pm 0.072$
SGB-58.1	1000.13	1855.87	18.32	0.53	$-0.723 \pm 0.108$	$1.773 \pm 0.071$
RGB-2.1	1196.66	347.02	16.74	0.80	$-0.648 \pm 0.064$	$2.243 \pm 0.040$
RGB-7.1	1236.14	476.40	18.19	0.67	$-0.254 \pm 0.119$	$2.085 \pm 0.072$
RGB-8.1	1052.24	515.64	17.91	0.70	$-0.235 \pm 0.107$	$2.048 \pm 0.065$
RGB-10.1	685.97	564.45	18.27	0.66	$-0.763 \pm 0.114$	$2.021 \pm 0.075$
RGB-16.1	840.41	714.10	17.03	0.78	$-0.525 \pm 0.072$	$2.153 \pm 0.046$
RGB-19.1	1036.96	797.50	17.40	0.73	$-0.009 \pm 0.087$	$2.058 \pm 0.051$
RGB-20.1	1086.92	813.56	17.54	0.74	$-0.673 \pm 0.089$	$2.218 \pm 0.056$
RGB-22.1	854.39	863.31	17.76	0.75	$-0.727 \pm 0.094$	$2.209 \pm 0.064$
RGB-24.1	818.98	929.50	16.73	0.81	$-0.051 \pm 0.066$	$2.115 \pm 0.039$
RGB-27.1	721.55	1003.86	18.15	0.68	$-0.813 \pm 0.115$	$2.100 \pm 0.075$
RGB-32.1	638.81	1189.32	17.18	0.80	$0.115 \pm 0.087$	$2.081 \pm 0.049$
RGB-35.1	1089.35	1268.46	17.64	0.73	$-0.243 \pm 0.098$	$2.070 \pm 0.059$
RGB-36.1	733.26	1291.73	18.26	0.65	$-0.187 \pm 0.124$	$1.897 \pm 0.075$
RGB-37.2	916.33	1333.53	17.50	0.75	$-0.774 \pm 0.090$	$2.206 \pm 0.057$
RGB-39.1	785.01	1390.31	16.92	0.79	$-0.720 \pm 0.071$	$2.193 \pm 0.044$
RGB-40.1	841.08	1399.36	18.19	0.67	$-0.314 \pm 0.124$	$1.985 \pm 0.075$
RGB-41.2	1160.89	1437.64	18.10	0.70	$-0.780 \pm 0.116$	$2.130 \pm 0.073$
RGB-45.1	996.97	1531.88	17.88	0.71	$-0.150 \pm 0.107$	$1.985 \pm 0.063$
RGB-47.1	762.57	1584.26	18.25	0.66	$-0.258 \pm 0.118$	$1.943 \pm 0.073$
RGB-49.1	880.34	1636.83	17.59	0.74	$-0.075 \pm 0.097$	$2.109 \pm 0.057$

Table 3.C: Parameters of stars in NGC 5286.

Star ID	x-position	y-position	$V$	$(B - V)$	S3839	CH4300
SGB-19.1	736.70	518.78	19.71	0.68	$-0.802 \pm 0.216$	$1.598 \pm 0.141$
SGB-38.1	767.46	271.35	19.01	0.86	$-0.953 \pm 0.216$	$2.071 \pm 0.139$
SGB-48.1	844.54	520.94	19.74	0.79	$-0.395 \pm 0.298$	$1.952 \pm 0.190$
SGB-51.1	865.13	610.95	19.03	0.83	$-0.612 \pm 0.209$	$1.854 \pm 0.133$
RGB-4.1	650.90	87.59	17.96	1.03	$-0.549 \pm 0.150$	$2.049 \pm 0.096$
RGB-5.1	754.54	138.64	16.77	1.08	$-0.051 \pm 0.099$	$2.047 \pm 0.057$
RGB-6.1	594.31	161.42	18.05	0.96	$-0.810 \pm 0.152$	$2.141 \pm 0.096$
RGB-15.1	915.66	386.49	17.83	0.97	$-0.085 \pm 0.144$	$1.884 \pm 0.083$
RGB-16.1	800.56	411.74	16.91	1.07	$0.002 \pm 0.104$	$2.183 \pm 0.059$
RGB-21.1	916.00	573.42	18.35	0.94	$-0.223 \pm 0.172$	$1.830 \pm 0.102$

Table 3.D: Parameters of stars in M 15.

Star ID	x-position	y-position	$V$	$(B - V)$	S3839	CH4300
MS-1.1	869.77	324.32	19.34	0.45	$-0.560 \pm 0.217$	$1.559 \pm 0.134$
MS-2.1	1166.40	351.60	19.19	0.44	$-0.680 \pm 0.186$	$1.575 \pm 0.124$
MS-6.1	975.03	454.58	19.27	0.43	$-0.590 \pm 0.185$	$1.569 \pm 0.126$
MS-9.1	931.95	531.82	18.93	0.46	$-0.636 \pm 0.168$	$1.551 \pm 0.112$
MS-11.1	942.19	588.60	19.30	0.43	$-0.735 \pm 0.206$	$1.499 \pm 0.134$
MS-14.1	1400.05	667.35	19.22	0.44	$-0.536 \pm 0.197$	$1.607 \pm 0.127$
MS-16.1	1016.32	723.20	19.11	0.44	$-0.758 \pm 0.179$	$1.583 \pm 0.119$
MS-18.2	1206.32	779.61	18.81	0.45	$-0.751 \pm 0.161$	$1.664 \pm 0.107$
MS-33.1	722.33	1223.58	19.14	0.50	$-0.604 \pm 0.201$	$1.522 \pm 0.129$
MS-49.1	899.18	1609.17	19.28	0.47	$-0.612 \pm 0.207$	$1.602 \pm 0.138$
MS-51.1	908.00	1655.32	19.51	0.45	$-0.780 \pm 0.236$	$1.606 \pm 0.153$
MS-60.1	739.73	1895.66	19.18	0.49	$-0.487 \pm 0.198$	$1.566 \pm 0.126$
MS-62.1	1037.64	1946.21	19.16	0.40	$-0.551 \pm 0.192$	$1.522 \pm 0.122$
MS-63.1	1166.62	1976.77	19.03	0.47	$-0.789 \pm 0.187$	$1.598 \pm 0.121$
SGB-5.1	1116.49	437.73	18.40	0.59	$-0.600 \pm 0.142$	$1.644 \pm 0.093$
SGB-8.1	1077.24	511.98	18.55	0.55	$-0.646 \pm 0.149$	$1.646 \pm 0.097$
SGB-10.1	1439.04	568.35	18.56	0.55	$-0.673 \pm 0.145$	$1.653 \pm 0.096$
SGB-12.1	921.93	608.16	18.64	0.50	$-0.560 \pm 0.149$	$1.541 \pm 0.098$
SGB-15.1	1136.67	706.17	18.46	0.58	$-0.463 \pm 0.144$	$1.670 \pm 0.095$
SGB-19.1	1117.40	806.14	18.51	0.56	$-0.473 \pm 0.145$	$1.543 \pm 0.095$
SGB-22.1	1037.52	895.58	18.67	0.54	$-0.717 \pm 0.165$	$1.655 \pm 0.107$
SGB-23.1	1303.37	912.15	18.70	0.50	$-0.776 \pm 0.147$	$1.747 \pm 0.093$
SGB-25.1	1270.05	966.16	18.74	0.55	$-0.812 \pm 0.162$	$1.636 \pm 0.106$
SGB-27.1	1182.74	1011.64	18.66	0.54	$-0.543 \pm 0.153$	$1.559 \pm 0.101$
SGB-30.1	966.09	1152.43	18.77	0.53	$-0.569 \pm 0.176$	$1.606 \pm 0.113$
SGB-32.1	968.87	1191.26	18.54	0.60	$-0.659 \pm 0.163$	$1.622 \pm 0.106$
SGB-37.1	1114.86	1316.83	18.77	0.54	$-0.711 \pm 0.169$	$1.562 \pm 0.112$
SGB-38.1	818.01	1342.41	18.73	0.55	$-0.523 \pm 0.166$	$1.551 \pm 0.108$
SGB-39.1	1020.10	1369.29	18.59	0.57	$-0.692 \pm 0.163$	$1.524 \pm 0.104$
SGB-40.1	967.16	1388.81	18.63	0.57	$-0.671 \pm 0.164$	$1.609 \pm 0.103$
SGB-41.1	720.26	1401.00	18.54	0.60	$-0.518 \pm 0.164$	$1.641 \pm 0.105$
SGB-46.1	890.97	1541.85	18.69	0.58	$-0.692 \pm 0.167$	$1.633 \pm 0.110$
SGB-48.1	972.46	1577.92	18.52	0.58	$-0.587 \pm 0.157$	$1.661 \pm 0.101$
SGB-52.1	976.61	1687.57	18.73	0.53	$-0.501 \pm 0.160$	$1.625 \pm 0.108$
SGB-54.1	1040.61	1738.18	18.53	0.55	$-0.487 \pm 0.149$	$1.578 \pm 0.099$
SGB-55.1	1280.38	1760.25	18.74	0.53	$-0.463 \pm 0.166$	$1.488 \pm 0.106$
SGB-59.1	1060.51	1863.66	18.60	0.56	$-0.584 \pm 0.151$	$1.547 \pm 0.099$
SGB-61.1	1268.03	1917.95	18.75	0.49	$-0.568 \pm 0.159$	$1.542 \pm 0.102$
RGB-3.1	1096.88	371.62	17.81	0.68	$-0.669 \pm 0.115$	$1.819 \pm 0.075$
RGB-4.1	1417.29	403.07	17.88	0.67	$-0.637 \pm 0.115$	$1.779 \pm 0.075$
RGB-7.1	1169.17	482.70	17.72	0.68	$-0.658 \pm 0.110$	$1.866 \pm 0.072$
RGB-13.1	1138.79	646.57	17.52	0.67	$-0.598 \pm 0.097$	$1.751 \pm 0.064$
RGB-17.1	814.66	751.60	18.08	0.64	$-0.680 \pm 0.124$	$1.729 \pm 0.082$
RGB-21.1	862.28	855.18	17.82	0.72	$0.406 \pm 0.135$	$2.226 \pm 0.082$
RGB-24.1	1057.88	945.56	17.61	0.67	$-0.670 \pm 0.113$	$1.729 \pm 0.072$
RGB-26.1	1217.68	986.55	17.91	0.67	$-0.667 \pm 0.120$	$1.679 \pm 0.077$
RGB-28.2	886.99	1097.94	17.96	0.69	$-0.530 \pm 0.132$	$1.679 \pm 0.084$
RGB-35.1	941.47	1275.39	18.24	0.67	$-0.571 \pm 0.145$	$1.662 \pm 0.093$
RGB-42.1	1185.71	1427.51	17.55	0.71	$-0.718 \pm 0.111$	$1.740 \pm 0.070$
RGB-43.1	1115.69	1457.35	18.26	0.67	$-0.697 \pm 0.143$	$1.718 \pm 0.091$
RGB-44.1	1266.20	1487.03	18.18	0.66	$-0.732 \pm 0.136$	$1.704 \pm 0.086$
RGB-45.1	1094.67	1511.35	17.97	0.68	$-0.689 \pm 0.130$	$1.757 \pm 0.083$
RGB-47.1	1254.95	1558.40	17.17	0.72	$-0.459 \pm 0.093$	$1.695 \pm 0.057$

Continued on next page

Parameters of stars in M15 - *continued*

RGB-50.1	1342.11	1631.70	18.14	0.66	$-0.288 \pm 0.148$	$1.777 \pm 0.093$
RGB-53.1	1394.34	1712.13	17.86	0.68	$-0.763 \pm 0.119$	$1.796 \pm 0.077$
RGB-56.1	729.96	1778.57	17.51	0.71	$-0.553 \pm 0.105$	$1.659 \pm 0.066$
RGB-58.1	1024.26	1846.18	18.33	0.63	$-0.484 \pm 0.144$	$1.648 \pm 0.093$

Table 3.E: Parameters of stars in M22.

Star ID	x-position	y-position	V	(B - V)	S3839	CH4300
MS-1.1	1080.04	343.62	17.65	0.62	$-0.605 \pm 0.117$	$1.708 \pm 0.074$
MS-2.2	1056.44	363.16	18.59	0.62	$-0.841 \pm 0.187$	$1.476 \pm 0.115$
MS-4.1	1115.50	390.26	18.40	0.66	$-0.445 \pm 0.176$	$1.828 \pm 0.111$
MS-5.1	1118.07	416.62	18.60	0.66	$-0.612 \pm 0.137$	$1.809 \pm 0.091$
MS-7.1	912.72	475.57	18.72	0.70	$-0.453 \pm 0.196$	$1.802 \pm 0.123$
MS-10.1	1013.33	553.71	18.20	0.65	$-0.726 \pm 0.093$	$1.683 \pm 0.062$
MS-12.2	1142.53	610.89	17.98	0.66	$-0.530 \pm 0.076$	$1.680 \pm 0.049$
MS-14.1	1181.02	652.87	17.62	0.60	$-0.680 \pm 0.137$	$1.608 \pm 0.084$
MS-15.2	1188.13	681.57	17.96	0.60	$-0.555 \pm 0.144$	$1.675 \pm 0.087$
MS-16.2	1187.59	707.21	17.98	0.57	$-0.498 \pm 0.144$	$1.596 \pm 0.091$
MS-17.1	941.22	729.04	18.01	0.62	$-0.448 \pm 0.136$	$1.662 \pm 0.083$
MS-18.1	962.56	748.24	18.52	0.66	$-0.687 \pm 0.216$	$1.667 \pm 0.130$
MS-19.1	1215.23	768.44	17.71	0.56	$-0.653 \pm 0.141$	$1.662 \pm 0.088$
MS-20.1	1224.23	796.21	17.57	0.58	$-0.635 \pm 0.125$	$1.640 \pm 0.077$
MS-21.1	1046.49	813.09	17.55	0.63	$-0.695 \pm 0.126$	$1.631 \pm 0.077$
MS-22.1	1154.29	832.02	18.06	0.56	$-0.627 \pm 0.162$	$1.603 \pm 0.101$
MS-24.1	1260.28	882.95	17.63	0.58	$-0.653 \pm 0.143$	$1.759 \pm 0.087$
MS-25.2	992.49	905.79	17.89	0.64	$-0.623 \pm 0.147$	$1.729 \pm 0.088$
MS-28.2	1073.21	974.72	17.64	0.57	$-0.566 \pm 0.119$	$1.587 \pm 0.071$
MS-29.1	1149.28	990.47	18.32	0.64	$-0.258 \pm 0.192$	$1.605 \pm 0.113$
MS-30.1	1212.48	1000.75	18.43	0.61	$-0.729 \pm 0.192$	$1.672 \pm 0.122$
MS-31.2	1310.65	1077.11	17.69	0.61	$-0.507 \pm 0.134$	$1.628 \pm 0.081$
MS-32.1	973.53	1085.68	17.86	0.60	$-0.659 \pm 0.128$	$1.343 \pm 0.080$
MS-33.1	1002.82	1108.68	17.91	0.68	$-0.759 \pm 0.153$	$1.646 \pm 0.094$
MS-36.1	978.91	1190.94	18.20	0.65	$-0.855 \pm 0.176$	$1.561 \pm 0.110$
MS-37.2	946.31	1236.48	18.05	0.67	$-0.736 \pm 0.196$	$1.635 \pm 0.119$
MS-38.2	1321.84	1261.33	18.43	0.68	$-0.333 \pm 0.206$	$1.671 \pm 0.122$
MS-39.1	1037.76	1270.90	18.40	0.69	$-0.364 \pm 0.201$	$1.576 \pm 0.121$
MS-41.2	1145.89	1329.72	17.90	0.54	$-0.843 \pm 0.127$	$1.603 \pm 0.080$
MS-42.1	1020.11	1353.89	18.73	0.74	$-0.433 \pm 0.198$	$1.739 \pm 0.117$
MS-44.1	1181.81	1387.77	17.63	0.62	$-0.875 \pm 0.118$	$1.602 \pm 0.072$
MS-45.1	1084.76	1418.77	18.05	0.65	$-0.424 \pm 0.155$	$1.716 \pm 0.091$
MS-47.1	846.86	1459.91	18.06	0.70	$-0.528 \pm 0.143$	$1.589 \pm 0.091$
MS-49.1	1092.85	1505.59	18.04	0.69	$-0.706 \pm 0.166$	$1.823 \pm 0.105$
MS-51.1	858.45	1541.45	17.51	0.65	$-0.477 \pm 0.126$	$1.599 \pm 0.077$
MS-54.1	805.44	1609.52	18.37	0.66	$-0.439 \pm 0.187$	$1.710 \pm 0.110$
MS-55.2	1031.73	1639.71	17.87	0.69	$-0.614 \pm 0.149$	$1.660 \pm 0.087$
MS-56.1	917.65	1656.17	18.22	0.66	$-0.603 \pm 0.203$	$1.450 \pm 0.116$
MS-58.1	847.78	1703.65	17.91	0.65	$-0.627 \pm 0.168$	$1.564 \pm 0.100$
MS-59.2	863.07	1730.50	18.25	0.67	$-0.676 \pm 0.211$	$1.493 \pm 0.129$
MS-60.2	859.31	1753.67	18.26	0.69	$-0.387 \pm 0.176$	$1.554 \pm 0.109$
MS-61.2	964.37	1782.24	18.23	0.67	$-0.530 \pm 0.199$	$1.628 \pm 0.119$
MS-62.1	940.44	1795.84	18.54	0.73	$-0.721 \pm 0.171$	$1.658 \pm 0.103$
MS-63.1	829.71	1814.40	17.57	0.60	$-0.430 \pm 0.125$	$1.601 \pm 0.079$
SGB-1.1	929.39	331.90	17.12	0.65	$-0.313 \pm 0.119$	$1.710 \pm 0.065$
SGB-2.1	1053.21	353.35	17.10	0.61	$-0.667 \pm 0.099$	$1.619 \pm 0.060$

*Continued on next page*

Parameters of stars in M22 - *continued*

SGB-6.1	1073.72	464.66	16.93	0.67	$-0.530 \pm 0.101$	$1.807 \pm 0.058$
SGB-7.1	968.37	479.00	17.11	0.61	$-0.570 \pm 0.100$	$1.703 \pm 0.060$
SGB-8.1	1105.85	504.74	17.11	0.66	$-0.512 \pm 0.111$	$1.698 \pm 0.063$
SGB-9.1	1033.27	529.32	16.96	0.73	$-0.195 \pm 0.112$	$1.947 \pm 0.062$
SGB-14.1	992.36	668.45	17.29	0.59	$-0.664 \pm 0.132$	$1.665 \pm 0.072$
SGB-17.1	1103.45	741.89	17.24	0.64	$-0.554 \pm 0.128$	$1.726 \pm 0.071$
SGB-18.2	1032.85	767.74	17.12	0.61	$-0.597 \pm 0.139$	$1.683 \pm 0.075$
SGB-21.1	1112.79	836.01	17.17	0.59	$-0.480 \pm 0.129$	$1.692 \pm 0.073$
SGB-22.1	1057.38	856.27	16.89	0.70	$-0.549 \pm 0.106$	$1.850 \pm 0.061$
SGB-25.1	1059.08	934.83	17.22	0.63	$-0.778 \pm 0.137$	$1.771 \pm 0.077$
SGB-28.1	1077.97	1005.49	16.71	0.70	$-0.377 \pm 0.104$	$1.692 \pm 0.057$
SGB-30.1	956.11	1098.90	17.10	0.63	$-0.630 \pm 0.109$	$1.648 \pm 0.062$
SGB-32.1	840.72	1147.07	16.76	0.72	$-0.548 \pm 0.104$	$1.789 \pm 0.059$
SGB-33.2	1143.10	1180.00	17.11	0.64	$-0.752 \pm 0.128$	$1.559 \pm 0.072$
SGB-34.1	941.86	1198.15	17.28	0.63	$-0.485 \pm 0.129$	$1.738 \pm 0.073$
SGB-35.2	830.83	1216.89	16.97	0.68	$-0.491 \pm 0.104$	$1.662 \pm 0.060$
SGB-36.1	1048.36	1240.95	16.82	0.69	$-0.464 \pm 0.101$	$1.721 \pm 0.057$
SGB-37.2	905.11	1280.86	16.86	0.71	$-0.684 \pm 0.095$	$1.715 \pm 0.056$
SGB-38.1	1006.07	1298.33	16.93	0.76	$-0.191 \pm 0.148$	$2.017 \pm 0.078$
SGB-40.1	1066.30	1339.01	16.97	0.74	$-0.267 \pm 0.126$	$1.799 \pm 0.068$
SGB-42.1	912.15	1387.44	17.39	0.56	$-0.547 \pm 0.126$	$1.635 \pm 0.071$
SGB-43.2	1133.70	1412.69	16.99	0.66	$-0.461 \pm 0.114$	$1.747 \pm 0.065$
SGB-45.1	968.74	1456.15	17.21	0.66	$-0.473 \pm 0.145$	$1.724 \pm 0.077$
SGB-46.1	1316.21	1478.65	16.82	0.74	$-0.496 \pm 0.106$	$1.735 \pm 0.059$
SGB-47.2	814.65	1513.07	17.05	0.75	$-0.395 \pm 0.141$	$1.641 \pm 0.073$
SGB-48.1	1125.50	1538.73	17.06	0.64	$-0.637 \pm 0.115$	$1.698 \pm 0.064$
SGB-49.1	834.05	1560.34	17.23	0.63	$-0.495 \pm 0.125$	$1.555 \pm 0.071$
SGB-52.1	1143.95	1627.66	17.27	0.68	$-0.535 \pm 0.141$	$1.739 \pm 0.077$
SGB-53.1	938.92	1659.36	17.25	0.65	$-0.581 \pm 0.119$	$1.673 \pm 0.067$
SGB-55.1	992.13	1709.57	17.20	0.64	$-0.328 \pm 0.124$	$1.669 \pm 0.068$
SGB-56.1	1058.92	1741.62	17.34	0.64	$-0.476 \pm 0.138$	$1.734 \pm 0.077$
SGB-57.2	880.73	1759.10	17.01	0.63	$-0.615 \pm 0.115$	$1.735 \pm 0.066$
SGB-61.1	967.79	1869.40	17.03	0.68	$-0.560 \pm 0.118$	$1.695 \pm 0.066$
SGB-63.1	831.28	1904.79	16.96	0.71	$-0.453 \pm 0.140$	$1.644 \pm 0.074$
SGB-64.1	844.39	1946.07	17.21	0.66	$-0.535 \pm 0.138$	$1.667 \pm 0.077$
RGB-12.2	1218.48	617.29	16.58	0.76	$-0.636 \pm 0.105$	$1.823 \pm 0.058$
RGB-20.1	966.85	806.14	16.32	0.77	$-0.459 \pm 0.100$	$1.908 \pm 0.054$
RGB-24.1	938.31	909.53	16.33	0.79	$-0.589 \pm 0.099$	$1.961 \pm 0.056$
RGB-26.1	1249.51	955.41	15.28	0.79	$-0.187 \pm 0.066$	$2.316 \pm 0.035$
RGB-27.1	1093.36	982.77	16.20	0.80	$0.096 \pm 0.100$	$1.984 \pm 0.052$
RGB-29.1	1230.59	1083.80	16.79	0.80	$-0.663 \pm 0.095$	$1.697 \pm 0.056$
RGB-31.1	1221.43	1128.13	16.46	0.78	$-0.509 \pm 0.096$	$1.953 \pm 0.053$
RGB-39.1	811.11	1324.31	16.67	0.81	$-0.119 \pm 0.122$	$1.724 \pm 0.063$
RGB-44.1	874.82	1439.70	16.38	0.84	$0.199 \pm 0.098$	$1.949 \pm 0.051$
RGB-50.1	992.96	1581.07	16.38	0.83	$-0.536 \pm 0.100$	$1.888 \pm 0.055$
RGB-51.1	876.86	1603.39	16.49	0.79	$-0.341 \pm 0.114$	$1.803 \pm 0.059$
RGB-54.2	1014.74	1676.61	16.71	0.83	$-0.083 \pm 0.136$	$2.046 \pm 0.070$
RGB-58.1	864.49	1792.23	16.68	0.80	$-0.518 \pm 0.111$	$1.758 \pm 0.061$
RGB-60.1	1167.24	1834.03	16.64	0.80	$-0.780 \pm 0.095$	$1.947 \pm 0.054$
RGB-62.1	1111.04	1890.47	16.82	0.77	$-0.631 \pm 0.113$	$1.855 \pm 0.062$
RGB-65.2	816.71	1968.21	16.68	0.81	$-0.263 \pm 0.133$	$1.838 \pm 0.068$

Table 3.F: Parameters of stars in M55.

Star ID	x-position	y-position	$V$	$(B - V)$	S3839	CH4300
MS-1.1	1123.77	338.80	18.03	0.48	$-0.649 \pm 0.185$	$1.870 \pm 0.131$
MS-2.1	1126.09	342.93	18.70	0.52	$-0.746 \pm 0.123$	$1.599 \pm 0.084$
MS-5.1	1099.34	397.73	18.22	0.53	$-0.672 \pm 0.141$	$1.687 \pm 0.095$
MS-6.1	1244.59	427.10	18.27	0.49	$-0.706 \pm 0.149$	$1.691 \pm 0.100$
MS-7.1	980.85	445.06	18.37	0.45	$-0.709 \pm 0.150$	$1.619 \pm 0.104$
MS-9.1	1094.86	479.07	18.00	0.49	$-0.617 \pm 0.122$	$1.618 \pm 0.082$
MS-10.1	1057.42	506.10	18.16	0.45	$-0.733 \pm 0.137$	$1.619 \pm 0.094$
MS-11.1	1193.68	526.92	18.30	0.49	$-0.711 \pm 0.139$	$1.644 \pm 0.095$
MS-13.1	1006.45	572.20	17.90	0.46	$-0.606 \pm 0.115$	$1.590 \pm 0.077$
MS-14.1	1012.75	583.49	18.28	0.49	$-0.866 \pm 0.144$	$1.595 \pm 0.098$
MS-15.1	1120.31	618.86	17.96	0.45	$-0.555 \pm 0.117$	$1.594 \pm 0.080$
MS-16.1	1345.66	642.88	18.13	0.46	$-0.644 \pm 0.144$	$1.664 \pm 0.094$
MS-17.1	1277.46	679.70	17.98	0.47	$-1.021 \pm 0.126$	$1.625 \pm 0.084$
MS-18.1	1159.05	696.46	17.92	0.47	$-0.589 \pm 0.118$	$1.618 \pm 0.080$
MS-20.1	1058.18	717.72	17.95	0.44	$-0.847 \pm 0.120$	$1.564 \pm 0.078$
MS-22.1	1095.11	765.67	17.84	0.46	$-0.655 \pm 0.117$	$1.572 \pm 0.079$
MS-23.1	917.91	781.70	17.92	0.46	$-0.526 \pm 0.115$	$1.597 \pm 0.078$
MS-24.1	918.00	781.72	17.92	0.46	$-0.353 \pm 0.298$	$1.580 \pm 0.206$
MS-26.1	1080.59	835.85	17.88	0.47	$-0.750 \pm 0.114$	$1.586 \pm 0.076$
MS-27.1	975.85	855.34	18.06	0.49	$-0.638 \pm 0.131$	$1.664 \pm 0.086$
MS-29.1	1171.00	889.30	17.88	0.51	$-0.613 \pm 0.113$	$1.641 \pm 0.076$
MS-31.1	1190.39	927.55	17.88	0.48	$-0.668 \pm 0.111$	$1.625 \pm 0.076$
MS-35.1	1295.84	1008.21	18.05	0.47	$-0.805 \pm 0.124$	$1.646 \pm 0.081$
MS-39.1	794.91	1092.30	18.34	0.51	$-0.815 \pm 0.148$	$1.633 \pm 0.097$
MS-40.1	936.71	1117.78	18.41	0.50	$-0.583 \pm 0.141$	$1.587 \pm 0.094$
MS-41.1	936.24	1139.50	17.98	0.47	$-0.628 \pm 0.122$	$1.658 \pm 0.082$
MS-42.1	1043.07	1180.44	17.82	0.51	$-0.589 \pm 0.112$	$1.540 \pm 0.074$
MS-45.1	948.09	1251.40	17.83	0.49	$-0.623 \pm 0.115$	$1.659 \pm 0.077$
MS-46.1	885.40	1290.09	17.76	0.49	$-0.667 \pm 0.110$	$1.564 \pm 0.072$
MS-47.1	978.83	1308.73	17.97	0.47	$-0.669 \pm 0.116$	$1.618 \pm 0.076$
MS-48.1	909.16	1336.37	18.15	0.46	$-0.657 \pm 0.133$	$1.618 \pm 0.088$
MS-49.1	815.34	1374.79	18.13	0.48	$-0.514 \pm 0.133$	$1.566 \pm 0.089$
MS-50.1	960.86	1396.66	18.19	0.47	$-0.670 \pm 0.135$	$1.567 \pm 0.089$
MS-51.1	1042.34	1428.72	17.76	0.49	$-0.536 \pm 0.112$	$1.567 \pm 0.074$
MS-52.1	826.04	1451.84	18.16	0.47	$-0.569 \pm 0.133$	$1.587 \pm 0.089$
MS-53.1	673.73	1479.79	18.21	0.46	$1.731 \pm 0.181$	$1.603 \pm 0.091$
MS-54.1	791.76	1514.56	18.23	0.47	$-0.559 \pm 0.141$	$1.574 \pm 0.093$
MS-55.1	1092.17	1527.20	17.90	0.47	$-0.672 \pm 0.118$	$1.614 \pm 0.079$
MS-56.1	905.82	1555.93	18.24	0.47	$-0.743 \pm 0.142$	$1.592 \pm 0.096$
MS-57.1	1247.39	1592.92	18.22	0.50	$-0.602 \pm 0.141$	$1.571 \pm 0.092$
MS-58.1	1233.56	1624.61	18.48	0.52	$-0.716 \pm 0.165$	$1.557 \pm 0.108$
MS-60.1	945.43	1678.32	18.13	0.46	$-0.596 \pm 0.132$	$1.586 \pm 0.087$
MS-63.1	1107.78	1733.10	17.96	0.49	$-1.070 \pm 0.118$	$1.635 \pm 0.081$
MS-64.1	774.95	1752.03	18.23	0.46	$-0.560 \pm 0.137$	$1.615 \pm 0.092$
MS-65.1	1181.04	1775.11	18.23	0.47	$-0.796 \pm 0.144$	$1.637 \pm 0.096$
MS-66.1	1329.63	1794.11	17.99	0.47	$-0.675 \pm 0.253$	$1.634 \pm 0.176$
MS-67.1	1329.77	1813.21	17.86	0.49	$-0.760 \pm 0.116$	$1.541 \pm 0.077$
MS-70.1	1348.41	1884.15	18.21	0.47	$-0.620 \pm 0.140$	$1.661 \pm 0.093$
SGB-5.1	1025.34	398.61	17.33	0.52	$-0.850 \pm 0.098$	$1.642 \pm 0.067$
SGB-7.1	1000.31	424.74	17.62	0.44	$-0.758 \pm 0.107$	$1.617 \pm 0.075$
SGB-9.1	1170.40	456.62	17.55	0.52	$-0.740 \pm 0.107$	$1.616 \pm 0.073$
SGB-11.1	973.65	485.85	17.70	0.45	$-0.672 \pm 0.108$	$1.644 \pm 0.076$
SGB-12.1	1190.51	496.09	17.38	0.53	$-0.714 \pm 0.100$	$1.639 \pm 0.068$

Continued on next page

Parameters of stars in M55 - *continued*

SGB-14.1	1254.36	524.60	17.54	0.50	$-0.742 \pm 0.103$	$1.624 \pm 0.070$
SGB-15.1	917.58	559.05	17.30	0.53	$-0.651 \pm 0.097$	$1.612 \pm 0.066$
SGB-16.1	1152.14	577.85	17.56	0.49	$-0.617 \pm 0.099$	$1.588 \pm 0.068$
SGB-18.1	1305.51	628.81	17.51	0.50	$-0.731 \pm 0.095$	$1.683 \pm 0.064$
SGB-19.1	1345.90	670.18	17.71	0.47	$-0.612 \pm 0.109$	$1.663 \pm 0.073$
SGB-20.1	822.33	696.96	17.65	0.47	$-0.680 \pm 0.111$	$1.610 \pm 0.075$
SGB-21.1	1050.29	723.19	17.42	0.49	$-0.764 \pm 0.098$	$1.642 \pm 0.066$
SGB-23.1	1286.97	745.07	17.18	0.60	$-0.898 \pm 0.095$	$1.845 \pm 0.063$
SGB-24.1	1041.73	761.47	17.36	0.53	$-0.759 \pm 0.095$	$1.589 \pm 0.065$
SGB-25.1	1287.89	802.54	17.34	0.56	$-0.793 \pm 0.098$	$1.726 \pm 0.066$
SGB-27.1	742.07	843.09	17.34	0.55	$-0.731 \pm 0.100$	$1.665 \pm 0.070$
SGB-28.1	958.51	878.99	17.67	0.49	$-0.585 \pm 0.109$	$1.589 \pm 0.075$
SGB-29.1	1238.18	905.96	17.31	0.58	$-0.800 \pm 0.100$	$1.732 \pm 0.068$
SGB-30.1	837.25	932.55	17.65	0.47	$-0.629 \pm 0.105$	$1.549 \pm 0.072$
SGB-31.1	861.36	948.39	17.16	0.60	$-0.736 \pm 0.092$	$1.642 \pm 0.062$
SGB-33.1	1063.32	983.28	17.70	0.47	$-0.650 \pm 0.134$	$1.560 \pm 0.091$
SGB-34.1	1227.29	1008.99	17.52	0.48	$-0.731 \pm 0.103$	$1.646 \pm 0.071$
SGB-37.1	1120.50	1114.52	17.67	0.49	$-0.527 \pm 0.110$	$1.655 \pm 0.073$
SGB-38.1	730.03	1145.22	17.51	0.47	$-0.557 \pm 0.110$	$1.591 \pm 0.073$
SGB-39.1	945.67	1171.27	17.49	0.51	$-0.630 \pm 0.111$	$1.657 \pm 0.075$
SGB-41.1	1019.44	1234.13	17.46	0.50	$-0.712 \pm 0.108$	$1.608 \pm 0.072$
SGB-43.1	1116.66	1282.42	17.60	0.51	$-0.621 \pm 0.113$	$1.673 \pm 0.078$
SGB-48.1	869.37	1436.17	17.67	0.49	$-0.548 \pm 0.115$	$1.565 \pm 0.079$
SGB-50.1	809.33	1468.91	17.39	0.51	$-0.592 \pm 0.103$	$1.605 \pm 0.070$
SGB-51.1	811.34	1495.76	17.65	0.48	$-0.543 \pm 0.117$	$1.604 \pm 0.079$
SGB-53.1	986.60	1537.81	17.43	0.51	$-0.667 \pm 0.107$	$1.628 \pm 0.073$
SGB-54.1	714.31	1561.89	17.24	0.56	$-0.770 \pm 0.098$	$1.701 \pm 0.067$
SGB-56.1	1112.84	1623.41	17.51	0.53	$-0.651 \pm 0.102$	$1.679 \pm 0.069$
SGB-57.1	1360.57	1644.03	17.24	0.59	$-0.717 \pm 0.099$	$1.746 \pm 0.067$
SGB-65.1	797.58	1820.41	17.60	0.47	$-0.600 \pm 0.116$	$1.591 \pm 0.080$
RGB-24.1	888.46	875.61	15.39	0.73	$-0.365 \pm 0.063$	$2.091 \pm 0.040$
RGB-29.1	1254.53	999.77	16.59	0.68	$-0.740 \pm 0.141$	$2.066 \pm 0.095$
RGB-30.1	821.21	1067.27	15.44	0.73	$-0.525 \pm 0.092$	$2.048 \pm 0.059$
RGB-31.1	970.28	1081.16	16.70	0.61	$-0.753 \pm 0.136$	$1.788 \pm 0.093$
RGB-35.1	768.25	1194.77	16.41	0.67	$-0.767 \pm 0.158$	$1.815 \pm 0.104$
RGB-37.1	541.83	1265.52	15.40	0.64	$-0.599 \pm 0.080$	$2.195 \pm 0.053$
RGB-44.1	697.73	1409.72	15.79	0.70	$-0.223 \pm 0.105$	$1.959 \pm 0.065$
RGB-51.1	664.25	1592.01	16.32	0.68	$4.739 \pm 0.276$	$1.884 \pm 0.082$
RGB-54.1	671.07	1695.41	16.20	0.69	$3.122 \pm 0.198$	$2.010 \pm 0.079$
RGB-57.1	1514.82	1775.68	15.58	0.75	$-0.712 \pm 0.095$	$2.115 \pm 0.062$
RGB-60.1	1057.87	1860.32	16.87	0.67	$-0.637 \pm 0.157$	$1.916 \pm 0.105$
RGB1-21.1	1057.44	746.52	16.05	0.72	$-0.735 \pm 0.122$	$1.631 \pm 0.083$
RGB1-28.1	974.39	878.05	15.67	0.72	$-0.386 \pm 0.426$	$2.244 \pm 0.259$
RGB1-62.1	1112.12	1718.52	16.94	0.68	$-0.477 \pm 0.332$	$1.837 \pm 0.224$
RGB2-35.1	1203.73	1068.49	17.16	0.64	$-0.679 \pm 0.104$	$1.729 \pm 0.067$
RGB2-60.1	1112.35	1718.53	16.94	0.68	$-0.477 \pm 0.101$	$1.850 \pm 0.067$
RGB2-64.1	923.63	1803.30	16.89	0.65	$-0.627 \pm 0.095$	$1.880 \pm 0.062$

Table 3.G: Parameters of stars in Pal12.

Star ID	x-position	y-position	$V$	$(B - V)$	S3839	CH4300
MS-17.1	1204.54	768.18	20.72	0.36	$-0.846 \pm 0.395$	$1.659 \pm 0.265$
MS-18.1	1407.26	804.76	20.43	0.39	$-0.712 \pm 0.373$	$1.829 \pm 0.234$
SGB-20.1	1466.17	847.26	20.10	0.41	$-0.524 \pm 0.326$	$1.815 \pm 0.211$

*Continued on next page*

Parameters of stars in Pal 12 - *continued*

SGB-58.1	1177.51	1593.49	19.71	0.57	$-0.721 \pm 0.308$	$2.045 \pm 0.197$
RGB-10.1	1322.93	524.64	18.72	0.93	$-0.225 \pm 0.307$	$2.367 \pm 0.146$
RGB-11.1	1176.17	559.57	18.50	0.75	$-0.302 \pm 0.192$	$2.315 \pm 0.117$
RGB-24.1	783.85	928.55	19.00	0.75	$-0.764 \pm 0.279$	$2.357 \pm 0.171$
RGB-27.1	838.42	974.83	16.97	0.74	$-0.567 \pm 0.095$	$2.068 \pm 0.058$
RGB-28.1	1093.16	996.23	19.05	0.72	$-0.467 \pm 0.275$	$2.209 \pm 0.160$
RGB-29.1	1202.39	1075.92	17.15	0.91	$-0.363 \pm 0.125$	$2.383 \pm 0.069$
RGB-30.1	1187.58	1094.28	17.56	0.86	$-0.180 \pm 0.152$	$2.361 \pm 0.086$
RGB-31.1	1258.74	1106.12	17.49	0.87	$-0.461 \pm 0.148$	$2.407 \pm 0.083$
RGB-32.1	943.79	1130.82	16.92	0.75	$-0.442 \pm 0.094$	$2.121 \pm 0.056$
RGB-36.1	1065.65	1194.00	16.21	0.90	$-0.197 \pm 0.100$	$2.273 \pm 0.052$
RGB-40.1	1198.85	1265.86	16.88	0.79	$-0.578 \pm 0.108$	$2.208 \pm 0.062$
RGB-41.1	1253.68	1277.79	17.94	0.83	$-0.655 \pm 0.174$	$2.288 \pm 0.098$
RGB-42.1	1126.87	1303.68	17.01	0.74	$-0.403 \pm 0.101$	$2.121 \pm 0.059$
RGB-44.1	1162.38	1344.42	18.84	0.76	$-0.548 \pm 0.261$	$2.335 \pm 0.158$
RGB-47.1	935.47	1393.46	18.67	0.76	$-0.542 \pm 0.239$	$2.277 \pm 0.142$
RGB-49.1	961.30	1435.74	16.61	0.88	$0.151 \pm 0.105$	$2.509 \pm 0.057$
RGB-50.1	1346.07	1454.23	17.16	0.90	$-0.270 \pm 0.129$	$2.332 \pm 0.070$
RGB-51.1	1181.23	1471.28	17.02	0.75	$-0.540 \pm 0.114$	$2.178 \pm 0.064$
RGB-67.1	1405.60	1788.72	18.23	0.79	$-0.387 \pm 0.185$	$2.398 \pm 0.108$
RGB-70.1	1094.78	1839.93	17.12	0.90	$-0.283 \pm 0.127$	$2.347 \pm 0.069$
RGB-76.1	1178.97	1983.49	18.70	0.75	$-0.708 \pm 0.231$	$2.343 \pm 0.141$

Table 3.H: Parameters of stars in Ter 7.

Star ID	x-position	y-position	V	(B - V)	S3839	CH4300
SGB-7.1	798.20	483.12	20.49	0.52	$-0.930 \pm 0.289$	$2.106 \pm 0.198$
SGB-12.2	1125.57	583.97	20.45	0.55	$-0.699 \pm 0.303$	$1.921 \pm 0.201$
SGB-15.1	1294.95	653.29	20.18	0.80	$-0.597 \pm 0.345$	$2.378 \pm 0.205$
SGB-20.1	988.90	760.74	20.52	0.53	$-0.911 \pm 0.288$	$1.789 \pm 0.191$
SGB-27.1	1344.57	920.23	20.42	0.65	$-0.413 \pm 0.313$	$2.024 \pm 0.202$
SGB-28.1	872.36	935.72	20.55	0.53	$-0.953 \pm 0.311$	$1.747 \pm 0.205$
SGB-29.1	1351.28	954.02	20.42	0.64	$-0.756 \pm 0.297$	$2.055 \pm 0.195$
SGB-30.1	932.99	964.52	20.54	0.55	$-0.903 \pm 0.293$	$1.740 \pm 0.197$
SGB-31.1	1048.99	984.42	20.52	0.56	$-0.626 \pm 0.301$	$1.875 \pm 0.201$
SGB-32.1	959.20	1003.74	20.53	0.54	$-0.834 \pm 0.303$	$1.669 \pm 0.194$
SGB-43.1	1049.54	1203.22	20.45	0.69	$-0.836 \pm 0.323$	$1.991 \pm 0.209$
SGB-46.1	1088.24	1256.38	20.56	0.57	$-0.877 \pm 0.327$	$1.773 \pm 0.217$
SGB-47.1	1020.14	1265.06	20.55	0.55	$-0.944 \pm 0.296$	$1.898 \pm 0.197$
SGB-51.1	1038.97	1333.37	20.57	0.53	$-0.607 \pm 0.293$	$1.812 \pm 0.199$
SGB-52.1	1125.43	1353.52	20.35	0.84	$-0.576 \pm 0.386$	$2.215 \pm 0.236$
SGB-53.1	1021.67	1366.15	20.44	0.69	$-0.707 \pm 0.371$	$2.157 \pm 0.229$
SGB-56.1	808.83	1406.99	20.53	0.48	$-0.606 \pm 0.277$	$1.748 \pm 0.184$
SGB-57.2	1357.67	1438.31	20.49	0.56	$-0.786 \pm 0.279$	$1.887 \pm 0.192$
SGB-58.1	1386.14	1460.03	20.48	0.73	$-0.842 \pm 0.347$	$2.349 \pm 0.221$
SGB-60.1	1092.55	1505.97	20.40	0.76	$-0.536 \pm 0.345$	$2.328 \pm 0.217$
SGB-63.1	1027.72	1561.06	20.52	0.53	$-0.816 \pm 0.282$	$1.918 \pm 0.189$
SGB-64.1	863.30	1577.50	20.46	0.57	$-0.819 \pm 0.278$	$1.806 \pm 0.190$
SGB-65.1	1205.58	1600.50	20.52	0.56	$-0.846 \pm 0.284$	$1.848 \pm 0.185$
SGB-67.1	758.57	1628.00	20.58	0.58	$-0.578 \pm 0.316$	$1.879 \pm 0.201$
SGB-70.1	1377.93	1687.57	20.24	0.83	$-0.714 \pm 0.335$	$2.274 \pm 0.211$
RGB-16.1	950.30	616.91	18.27	0.95	$-0.140 \pm 0.191$	$2.286 \pm 0.096$
RGB-27.1	861.18	796.11	17.88	1.02	$0.051 \pm 0.159$	$2.377 \pm 0.082$
RGB-28.1	1188.82	827.56	17.53	0.98	$-0.265 \pm 0.119$	$2.304 \pm 0.065$

*Continued on next page*



Parameters of stars in Ter 7 - *continued*

RGB-29.1	870.74	845.50	18.34	1.03	$-0.068 \pm 0.187$	$2.301 \pm 0.099$
RGB-31.1	798.28	891.87	17.85	1.07	$-0.024 \pm 0.163$	$2.327 \pm 0.083$
RGB-32.1	1000.41	903.68	16.95	1.19	$0.050 \pm 0.128$	$2.366 \pm 0.057$
RGB-37.1	1207.86	1009.18	18.05	1.05	$-0.198 \pm 0.164$	$2.459 \pm 0.087$
RGB-38.1	1263.39	1070.56	17.81	0.88	$-0.157 \pm 0.126$	$2.265 \pm 0.070$
RGB-39.1	1109.65	1087.18	18.43	0.89	$-0.426 \pm 0.170$	$2.343 \pm 0.095$
RGB-40.1	1223.97	1109.16	19.23	0.88	$-0.435 \pm 0.250$	$2.379 \pm 0.140$
RGB-43.1	1162.81	1146.58	18.06	1.00	$-0.306 \pm 0.163$	$2.391 \pm 0.085$
RGB-45.1	831.70	1178.15	17.42	1.08	$0.179 \pm 0.152$	$2.412 \pm 0.069$
RGB-46.1	1291.67	1198.26	16.82	1.22	$0.350 \pm 0.129$	$2.425 \pm 0.054$
RGB-48.1	864.85	1226.73	18.30	0.97	$-0.119 \pm 0.178$	$2.418 \pm 0.095$
RGB-49.1	1034.86	1246.86	19.34	0.86	$-0.263 \pm 0.243$	$2.293 \pm 0.142$
RGB-50.1	1074.16	1261.24	19.83	0.84	$-0.640 \pm 0.308$	$2.296 \pm 0.184$
RGB-51.1	1223.59	1283.58	18.71	0.95	$-0.275 \pm 0.212$	$2.366 \pm 0.111$
RGB-52.1	862.76	1295.01	17.51	1.10	$0.147 \pm 0.145$	$2.399 \pm 0.070$
RGB-55.1	934.14	1344.94	18.90	0.88	$-0.558 \pm 0.218$	$2.357 \pm 0.119$
RGB-56.1	1013.12	1369.39	18.93	0.93	$-0.135 \pm 0.215$	$2.322 \pm 0.120$
RGB-66.1	1305.23	1546.59	17.81	0.90	$-0.311 \pm 0.121$	$2.279 \pm 0.068$
RGB-76.1	1436.76	1729.53	19.04	0.91	$-0.347 \pm 0.215$	$2.437 \pm 0.126$
RGB-83.1	757.85	1878.77	18.18	0.99	$0.066 \pm 0.168$	$2.366 \pm 0.087$



## Chapter 4

# Structural Parameters of Star Clusters in the Small Magellanic Cloud

### Abstract

We present core radii and heliocentric velocities for twelve populous star clusters in the projected direction of the Small Magellanic Cloud. Using VLT  $V$  band imaging we constructed surface brightness profiles. Core radii for all clusters were determined via fitting models following Elson et al. (1987). The comparison with literature data revealed good agreement with recent studies. From spectra of the near infra-red Calcium II regions of individual stars we were able to derive heliocentric velocities for all twelve star clusters. These were compared with literature values of star clusters and carbon star measurements.

*This project was done in collaboration with Eva K. Grebel and Andreas Koch.*

## 4.1 Introduction

Star clusters are associations of stars tidally bound by gravity. Their compactness makes them robust against dynamical disruption by their host galaxies for a fairly long period of time. Globular clusters, for example, are among the oldest objects in galaxies and give us a lower limit of the age of the Universe. In general we consider star clusters, which are observed to be of single-age and single-metallicity, as fossil remnants of the early environments from which they were formed. The study of star cluster systems in different environments is an important step towards the understanding of cluster evolution, but also the temporal evolution of different stellar systems. Photometric data allow the compilation of surface brightness profiles and therefore enable conclusions on the size, luminosity, and eventually the mass of individual clusters. Abundance and kinematic properties can be best accessed by spectroscopy and reveal information on the motion of the clusters with respect to their host galaxy and eventually of the stars within a cluster itself. Connecting this information with cluster ages one gains insights in the cluster evolution and/or changes in the condition of the formation and the evolution of the host galaxy.

For nearby stellar systems star clusters can be resolved into individual stars, which enables accurate age and metallicity determinations. Although for most extragalactic systems they remain unresolved, star clusters are used to constrain star formation and assembly histories of galaxies (e.g., Kissler-Patig 2000; Brodie & Strader 2006). However, in order to transfer knowledge from resolved to unresolved cluster systems, detailed knowledge of the nearby star clusters and cluster systems is essential.

Located at the Galactocentric distances of  $D \sim 50$  kpc and  $D \sim 63$  kpc, respectively, the Small and Large Magellanic Cloud (SMC and LMC) are two of our closest neighboring galaxies. Both galaxies are known to host a multitude of star clusters. About 4200 star clusters are cataloged for the LMC (Bica et al. 1999) and about 700 for the SMC (Bica & Dutra 2000). Although the star cluster population of the SMC is not as large as that of the LMC, it possesses an important advantage with regard to stellar population studies. For the SMC no gap in the cluster age distribution is observed. That is, the star clusters span a fairly continuous age range of 12 Gyr (Olszewski et al. 1996). In fact, the SMC is the only dwarf galaxy known in the Local Group to have formed and preserved populous star clusters over its entire lifetime. This provides a unique, closely spaced set of single-age, single-metallicity tracers to study the formation and evolution of star clusters and of the SMC itself.

While the photometric, kinematic, and structural properties of the Galactic globular clusters are well studied and cataloged (e.g., Harris 1996, 2003), no such complete listings exist yet, neither for the LMC, nor for the SMC. Nevertheless, a lot of effort in this direction can be noticed from the literature, especially in case of the LMC. Today's most comprehensive catalog is the one by Bica et al. (1999), comprising more than 4000 clusters. Furthermore, structural parameters of many LMC star clusters have been studied by various authors in the past (e.g., Elson et al. 1987; Mateo 1987; Kontizas et al. 1987). A large step towards a more uniform catalog was taken by Mackey & Gilmore (2003b). Using Hubble Space Telescope (HST) archival data they compiled surface brightness profiles and structural parameters, including core radii, luminosity, and mass estimates for 53 LMC clusters.

In case of the SMC until recently, the only published sources of structural parameters of the SMC clusters were the studies by Kontizas et al. (1982); Kontizas & Kontizas (1983); Kontizas et al. (1986). In a follow-up study from their LMC work Mackey & Gilmore (2003a) analyzed HST archival data of 10 SMC clusters. They again compiled surface brightness

profiles and determined core radii, luminosity, and mass estimates of these clusters. A more comprehensive catalog is presented by Hill & Zaritsky (2006), who compiled a new catalog of robust SMC clusters in cross-comparison with the existing databases by Pietrzynski et al. (1998) and Bica & Dutra (2000). They used the Magellanic Cloud Photometric Survey obtained with the Las Campanas Swope (1m) telescope (Zaritsky et al. 2002) to derive core radii and ellipticities for 204 SMC star clusters. Since these are exclusively photometric data, no estimates of radial velocities could be obtained. For the LMC a larger number of radial velocity estimates for its clusters can be found in the literature (e.g., Olszewski et al. 1991; Grocholski et al. 2006). By contrast, for the SMC hardly any radial velocity measurement for the star clusters has been published. In fact we are aware of only two publications of cluster velocities. Zinn & West (1984) measured velocities of two clusters from integrated spectra. Within the framework of their studies of the age-metallicity relation of the SMC Da Costa & Hatzidimitriou (1998) published velocities of seven SMC clusters.

Our work presents results from photometric and spectroscopic data taken at ESO's Very Large Telescope. We determined radii and heliocentric velocities for individual star clusters in the SMC. Our sample comprises a ground-based, homogeneous set of data for twelve star clusters. Nine clusters coincide with Hill & Zaritsky sample whereof six have also been studied by Mackey & Gilmore (2003b). The overlap with the existing kinematic studies is small. Only three clusters have been studied in detail before (Da Costa & Hatzidimitriou 1998). Thus our study can provide a valuable contribution to the existing catalog.

This chapter is structured as follows. In §4.2 we present our data and the standard reductions we performed. The derivation of surface brightness profiles and the subsequent measurement of accurate cluster radii are detailed in §4.3. Section §4.4 is dedicated to the determination of the clusters' radial velocities. Finally, in §4.5 we summarize our findings.

## 4.2 Data and data reduction

We obtained imaging and spectroscopic data for twelve SMC star clusters (Kron 28, Kron 44, Lindsay 11, Lindsay 116, Lindsay 32, Lindsay 38, NGC 152, NGC 339, NGC 361, NGC 411, NGC 416, NGC 419)(see Table 1). For comparison and calibration we also observed three Galactic globular clusters (NGC 104, NGC 362, NGC 7099). The observations were carried out in Service Mode at the Very Large Telescope (VLT) at Cerro Paranal, Chile within the the ESO programs 073.B-0488 and 075.B-0548. The instrument in use was the FORS2 (FOcal Reducer and low dispersion Spectrograph) installed at the Cassegrain focus of the VLT Unit Telescope 1. This setup provides a field of view of  $6'8 \times 6'8$ . The FORS2 detector system consists of two  $2k \times 4k$  MIT CCDs (master and slave) with a pixel scale of  $0'25$ . The CCD mosaic is mounted off-axis to ensure that the target will fall on the upper (master) CCD and that the center of the field of view does not coincide with the gap between the two CCDs. The detector works with a gain factor of  $1.43 \text{ ADU } e^{-1}$  ( $0.7 \text{ e } \text{ADU}^{-1}$ ) and a readout noise of  $2.7$  and  $3.0 \text{ e}^{-1}$  for the two parts of the CCD mosaic, respectively. For spectroscopic observations FORS2 is equipped with the multi-object facility MXU (Mask EXchange Unit). In this mode FORS2 offers the possibility to insert in the focal plane a mask where slits of different length, width, and shape can be cut. A maximum of 120 slits specified by the observer can be distributed over a useful field of view of  $6'8 \times 5'7$ . Up to ten masks can be loaded in MXU during daytime, which are then available for observation during the night.

The imaging run was carried out during six nights in April and May 2004. For each cluster

**Table 4.1:** Observation log of photometry of SMC and MW clusters.

Name	Date	$\alpha$	$\delta$	Filter	Exp. Time	Seeing	Airmass
		(J2000.0)					
Kron 28	2004-06-19	12.9183	-72.0103	<i>I</i> -Bessell	2× 30	0.99	1.54
				<i>V</i> -Bessell	2× 30	0.86	1.54
Kron 44	2004-06-10	15.5156	-73.9454	<i>I</i> -Bessell	2× 30	0.58	1.70
				<i>V</i> -Bessell	2× 30	0.66	1.71
Ln 11	2004-06-11	6.9368	-72.7971	<i>I</i> -Bessell	2× 30	1.07	1.56
				<i>V</i> -Bessell	2× 30	1.12	1.57
Ln 116	2004-06-19	28.8958	-77.6672	<i>I</i> -Bessell	2× 30	1.06	1.82
				<i>V</i> -Bessell	2× 30	1.02	1.83
Ln 32	2004-06-25	11.8538	-68.9413	<i>I</i> -Bessell	2× 10	0.86	1.54
				<i>V</i> -Bessell	2× 10	0.88	1.54
Ln 38	2004-06-25	12.2167	-69.8925	<i>I</i> -Bessell	2× 10	0.64	1.84
				<i>V</i> -Bessell	2× 20	0.61	1.85
NGC 152	2004-06-25	8.2275	-73.1358	<i>I</i> -Bessell	2× 10	0.74	1.87
				<i>V</i> -Bessell	2× 20	0.80	1.88
NGC 339	2004-06-10	14.4396	-74.4926	<i>I</i> -Bessell	2× 30	0.67	1.75
				<i>V</i> -Bessell	2× 30	0.58	1.75
NGC 361	2004-06-25	15.5446	-71.6264	<i>I</i> -Bessell	2× 10	0.73	1.61
				<i>V</i> -Bessell	2× 20	0.85	1.61
NGC 411	2004-06-25	16.9988	-71.7401	<i>I</i> -Bessell	2× 10	0.67	1.60
				<i>V</i> -Bessell	2× 20	0.69	1.61
NGC 416	2004-06-25	16.9925	-72.3741	<i>I</i> -Bessell	2× 10	0.79	1.65
				<i>V</i> -Bessell	2× 20	0.83	1.65
NGC 419	2004-06-25	17.0733	-72.9001	<i>I</i> -Bessell	2× 10	0.64	1.62
				<i>V</i> -Bessell	2× 20	0.69	1.63
NGC 104	2004-06-17	5.6579	-72.0751	<i>B</i> -Bessell	1.00	0.68	1.51
				<i>V</i> -Bessell	0.49	0.68	1.51
NGC 362	2004-06-10	15.6708	-70.8047	<i>B</i> -Bessell	2.50	0.62	1.57
				<i>V</i> -Bessell	0.74	0.57	1.57
NGC 7099	2004-04-20	325.1418	-23.1428	<i>B</i> -Bessell	2.50	0.58	1.45
				<i>V</i> -Bessell	0.74	0.58	1.45

two different frames were observed in the Bessell *V* and *I* filters (Bessell 1990) under good sky conditions. Two short exposures were taken of each object to avoid the saturation of the brightest red giant stars. The exposure times ranged from 10 to 30 s depending on the filter and the cluster. The observation log for our photometric data is given in Table 4.1.

After the standard basic data reduction (bias subtraction and flat-field correction) of the frames, we used the point spread function (PSF) fitting package DAOPHOT under IRAF<sup>1</sup> to derive instrumental magnitudes ( $V_{\text{inst}}$  and  $I_{\text{inst}}$ ) of the stars. The PSF was constructed using typically 10–15 isolated point sources evenly distributed on the image. For very crowded fields

<sup>1</sup>IRAF is distributed by the National Optical Astronomy Observatories, which are operated by the Association of Universities for Research in Astronomy, Inc., under cooperative agreement with the National Science Foundation.

**Table 4.2:** Zero points taken from the ESO quality control program and adopted for the photometric calibration.

Date	$V$ (master)	$V$ (slave)	$B$ (master)	$B$ (slave)	$I$ (master)	$I$ (slave)
2004-04-20	27.548	28.017	27.225	27.58	27.227	27.232
2004-06-10	28.169	28.163	27.686	27.706	27.766	27.772
2004-06-11	28.177	28.171	27.697	27.721	27.769	27.775
2004-06-17	28.136	28.13	27.653	27.684	27.716	27.728
2004-06-19	28.169	28.167	27.673	27.693	27.750	27.752
2004-06-25	28.181	28.168	27.7	27.718	27.766	27.767

**Table 4.3:** Extinction coefficients and Color Terms taken from the ESO quality control program and adopted for the photometric calibration.

	$V$ (master)	$V$ (slave)	$B$ (master)	$B$ (slave)	$I$ (master)	$I$ (slave)
k	0.123	0.162	0.185	0.208	0.031	0.061
CT	0.020	0.034	-0.031	-0.033	-0.005	-0.018

it was not possible to find a sufficient number of isolated stars. In these cases, neighboring stars were removed before the PSF generation.

Since no standard stars were observed within the framework of our project, the color terms (CT), extinction coefficients (k), and zero points (ZP) required in these calibrations were adopted from the ESO quality control program<sup>2</sup>. Like every ESO instrument, FORS2 has a standard calibration plan, which specifies a series of data taken in order to calibrate raw data and to monitor the instrument performance. Part of the quality control process is the tracking of the outer conditions e.g., airmass, fractional lunar illumination, seeing, etc.. Access to the performance of the instrument is gained through instrumental parameters such as photometric zero points, gain values, and bias levels, which are monitored over time to check the stability of the telescope and detect long-term trends. These data are updated regularly, such as during the time of our observations. For most nights quality control values were available on the ESO websites. For those were no quality control values were obtained we interpolated between the nights prior and after our observations. To obtain the final calibrated  $V$  and  $I$ -band magnitudes ( $V_{\text{cal}}$  and  $I_{\text{cal}}$ ), we applied standard photometric calibration equations (e.g., Hilker 2006):

$$V_{\text{cal}} = V_{\text{inst}} + \text{ZP}_V + \text{CT}_V \times (V - I) + k_V \times \text{AM}_V \quad (4.1)$$

$$I_{\text{cal}} = I_{\text{inst}} + \text{ZP}_I + \text{CT}_I \times (V - I) + k_I \times \text{AM}_I. \quad (4.2)$$

A full list of the applied zero-points, color-terms, and extinction coefficients can be found in tables 4.2 and 4.3. The airmass conditions at the time of the observations are listed in the observing log (Tab. 4.1).

The final photometric catalog was obtained by matching  $V$  and  $I$  magnitudes. Detected objects, which exhibit magnitude errors given by DAOPHOT of  $\sigma > 0.15$  mag were culled from the final data set. As an example of the quality of the photometric data Figure 4.1 shows the errors in measured  $V$  band magnitude depending on the  $V$  band magnitude itself. In total we obtained between 700 and 25000 stars per cluster depending on the star richness

<sup>2</sup><http://www.eso.org/observing/dfo/quality/FORS2/qc/qc1.html>

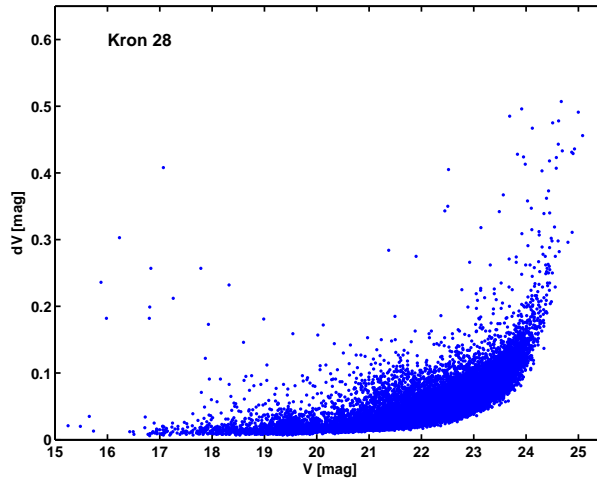


**Figure 4.1:** Errors in measured  $V$  band magnitude depending on the  $V$  band magnitude itself. This illustrates the quality of the photometric data.

of the cluster. A comparison with the Magellanic Clouds Photometric Survey (Zaritsky et al. 2002) (see Fig. 4.2) shows that this method provides a reliable estimation for both the  $V$  and  $I$  magnitudes. The mean differences between both photometries are 0.07 and 0.15 in case of the  $V$  and  $I$  band, respectively.

Candidates for the spectroscopy of both the SMC and the Galactic clusters were selected from their location in the color magnitude diagram. The spectra are ultimately used to measure the equivalent widths of the near-infrared triplet lines of the ionized calcium stage (see Chapter 5). This technique provides a well-established metallicity indicator for red giant stars (Armandroff & Da Costa 1991; Rutledge et al. 1997a,b; Cole et al. 2004; Koch et al. 2006). Since this calibration ideally requires signal to noise ratios of at least 10, we selected primarily targets on the upper red giant branch (RGB). Our data reached down to about 3.5 mag below the tip of the RGB. The magnitude range of the targeted stars is  $15.5 \lesssim V \lesssim 18.5$  mag. For each of the twelve SMC clusters one slit mask was defined containing 40 to 50 stars. The slit length was fixed to  $1''$  whereas the slit width varied between 5 and  $8''$ .

The spectroscopic observations were carried out with FORS2/MXU between September 2004 and July 2006. The grism used carries the ESO denotation 1028z+29 and is used in combination with the OG590+32 order blocking filter. The dispersion of this grism is  $28.5 \text{ \AA/mm}$ . In the  $2 \times 2$  binning mode and the FORS2 pixel size of  $15 \mu\text{m}$  this yields a dispersion of  $0.85 \text{ \AA/pix}$  and a spectral coverage of  $\sim 7730\text{--}9480 \text{ \AA}$  with small variations due to the positions of the slits on the mask. This wavelength region comprises the strong CaII triplet lines at  $\lambda\lambda 8498, 8543, \text{ and } 8661 \text{ \AA}$ . The observations were split into  $4 \times 475$  s to facilitate cosmic ray removal. The seeing during the observing nights was typically of the order of  $1''.6$ . For the spectroscopic observing log see Table 5.1.

The standard daytime calibrations consisted of five bias exposures per night, five lamp flat fields and one HeNeAr lamp exposure for each mask. The data reduction was completed using standard routines within the IRAF packages ONEDSPEC and TWODSPEC. Biases were combined and subtracted from the mask exposures. Individual frames were combined using a sigma clipping algorithm to remove cosmic ray hits. All exposures were corrected for the pixel-to-pixel variation by a normalized flat-field.



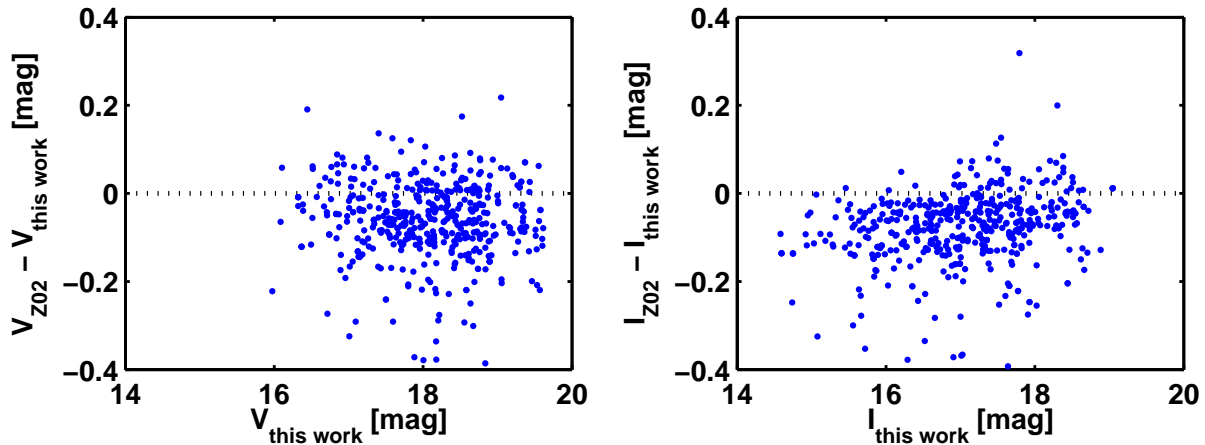


Figure 4.2: Comparison between  $V$  and  $I$  magnitudes derived within the framework of this project and the Magellanic Clouds Photometric Survey (Zaritsky et al. 2002).

The wavelength calibration was performed by fitting the observed day-time arc lamp spectra with template spectra provided by ESO<sup>3</sup>. Typically 20–30 lines, well distributed over the spectral range, were used in the wavelength solution. The root-mean-square errors resulting from these calibrations are of the order of 0.02 Å, corresponding to  $\sim 0.7 \text{ km s}^{-1}$  at the wavelengths of the Ca triplet. One-dimensional spectra were extracted along the slit using the task `apall`. For the background subtraction the sky was extracted from the same slit as the objects. The resulting spectra were continuum-normalized by fitting a low-order spline excluding the strong CaII absorption features.

### 4.3 Cluster core radii

The important characteristic radii of star clusters are the core radius ( $r_c$ ), the half light radius, and the tidal radius. The core radius is defined to be the radius at which the surface brightness has dropped to half of the central value. The latter two, which are not considered in this project, are the radius that contains half the light of the cluster and the radius beyond which the external gravitational field of the galaxy dominates the dynamics.

In order to derive the core radius for each of the twelve SMC clusters, we proceeded in the following way: First we determined the center of each cluster. Next we checked the completeness as a function of distance from the cluster center and magnitude. This allowed us to generate a completeness corrected surface brightness profile. Following Mackey & Gilmore (2003b) we fitted an EFF model (after Elson et al. (1987)) to this distribution, from which we could derive the core radius of the cluster. We chose to work in the more commonly used  $V$  band in order to be comparable with previous studies. Details on this procedures are given in the following subsections.

<sup>3</sup><http://www.eso.org/instruments/fors/inst/grisms.html>

### 4.3.1 Cluster centers

For the study of surface brightness profiles an accurate determination of the cluster centers is necessary in order to avoid the artificial distortion of the profiles. Since by eye we find a mismatch between the cluster center for Kron 28 in our photometry and those in the literature (Welch 1991), we did not rely on the literature values. We rather decided to redetermine the cluster centers in order to be on the safe side.

Our photometric observations suffer from a large contamination of SMC field stars. Although this fraction of field stars is fairly high, the typical star cluster features, such as RGB, red clump, subgiant branch (SGB), and main sequence turn-off (MSTO), are clearly visible for most of the CMDs. In case of Lindsay 116 the RGB is only very sparsely populated.

In order to clean our sample from obvious non-cluster members we primarily selected stars located on the RGB. In addition we added stars of the SGB and the upper main sequence (MS) region, where we still expect a large fraction of cluster members, though it partially overlaps with the SMC field population. As a guide for the selection we selected by eye the inner region of each star cluster and plotted the corresponding CMD. We overlaid Teramo isochrones (Pietrinferni et al. 2004) according to the literature ages and metallicities of each cluster. The values for Kron 28 ( $[\text{Fe}/\text{H}]=-1.2$  dex, age=2.1 Gyr), Kron 44 ( $[\text{Fe}/\text{H}]=-1.1$  dex, age=3.1 Gyr), Lindsay 32 ( $[\text{Fe}/\text{H}]=-1.2$  dex, age=4.8 Gyr), and Lindsay 116 ( $[\text{Fe}/\text{H}]=-1.1$  dex, age=2.8 Gyr) were adopted from Piatti et al. (2001). For Lindsay 38 we chose the metallicity ( $[\text{Fe}/\text{H}]=-1.7$  dex) from Piatti et al. (2001) but took the age (5.6 Gyr) from Glatt et al. (2008). The values for Lindsay 11 ( $[\text{Fe}/\text{H}]=-1.3$  dex, age=3.5 Gyr), NGC 411 ( $[\text{Fe}/\text{H}]=-0.7$  dex, age=1.5 Gyr), and NGC 419 ( $[\text{Fe}/\text{H}]=-0.7$  dex, age=1.2 Gyr) are from Piatti et al. (2005a). For NGC 152 the abundance ( $[\text{Fe}/\text{H}]=-1.4$  dex) and age (1.4 Gyr) are from Crowl et al. (2001). The values for NGC 361 ( $[\text{Fe}/\text{H}]=-1.5$  dex, age=6.8 Gyr) come from Mighell et al. (1998). For NGC 416 de Freitas Pacheco et al. (1998) list  $[\text{Fe}/\text{H}]=-0.8$  dex and Glatt et al. (2008) list an age of 5.6 Gyr. For NGC 339 we adopted the age (6.3 Gyr) from Glatt et al. (2008) and the metallicity ( $[\text{Fe}/\text{H}]=-1.2$  dex) from Da Costa & Hatzidimitriou (1998). Note that only few of these measurements rely on spectroscopic data. Similarly many of the age estimates are based on shallow ground-based photometry. Therefore large uncertainties in the given age and metallicity estimates are expected (see Chapter 5).

An overview of the cluster CMDs and the overlaid isochrones is given in Fig. 4.3. In this figure we distinguish between inner and outer cluster regions. Stars of the inner cluster regions are plotted in red and are more likely cluster member than stars of the outer regions, which are plotted in gray. Note the serious mismatch between the CMDs and the isochrones for the clusters Kron 28 and Lindsay 116. Our data suggest an older age for Kron 28 and a younger value for Lindsay 116. Unfortunately our photometric data are not deep enough to allow for a further quantification of the ages. The ages and metallicities estimates adopted from the literature for both clusters are based on shallow Washington photometry (Piatti et al. 2001). The ages were derived on the magnitude difference between the red clump and the MSTO. New metallicity estimates are presented in Chapter 5. These are in reasonable agreement with the literature values. In order to alleviate uncertainties in the age estimates we strongly recommend the repetition of the age estimations via deep HST photometry and proper isochrone fitting.

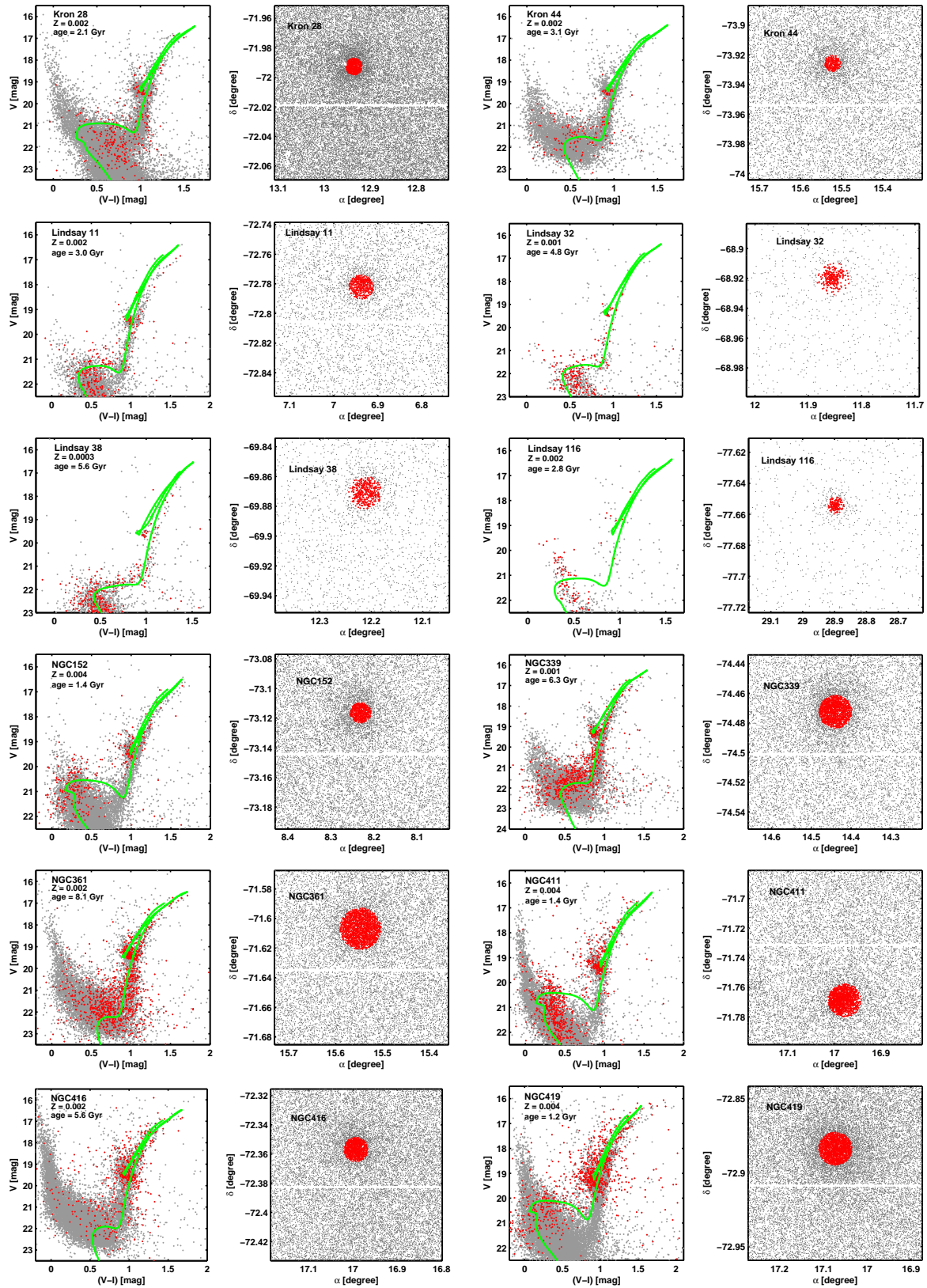
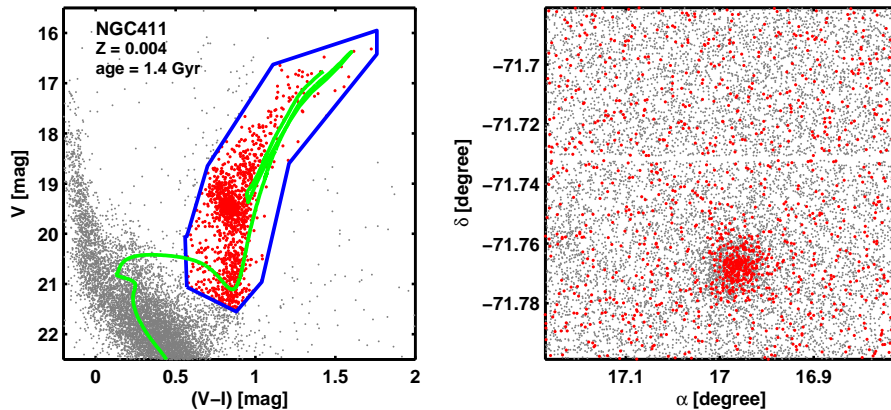


Figure 4.3: Area plots (right) and CMDs (left) of all twelve SMC star clusters in our sample. The selected stars are indicated in red. The remaining stars of the field are plotted in gray. Overplotted as green lines are Teramo isochrones according to the literature values of the clusters.



**Figure 4.4:** Complete CMD of the observed field centered on NGC 411. The Teramo isochrone for  $Z = 0.004$  and 1.3 Gyr according to the literature values of this cluster is overplotted as a green line. Embraced by the blue line are the selected cluster member candidates, which are indicated in red.

For simplicity we ignored the known large depth of the SMC and adopted for all clusters the same distance modulus of  $dm = 18.9$ . Again, we like to emphasize that the isochrones were not fitted in detail to the cluster CMDs, but were rather overplotted in order to guide the eye for the star selection. Possible cluster members were extracted by selecting stars along these lines. In order to select sample sizes large enough for our purposes, i.e., determination of the cluster center and plotting surface brightness profiles, but avoiding a large field star contamination, we focused on the RGB and SGB. Star clusters located in the outer regions of the SMC suffer less from field star contamination. For these clusters we also selected stars of the upper MS. Figure 4.4 shows as an example the complete stellar sample of the observed field centered on the cluster NGC 411. Overplotted is the Teramo isochrone for  $Z = 0.004$  and 1.4 Gyr. In addition, this figure shows the selected stars for the center and radius determinations.

We studied the number of stars of the photometrically cleaned sample as a function of their spatial distribution. The center determinations would also work on the original stellar samples since the clusters clearly stand out from the fields by their higher concentrations. Nevertheless, the restriction to the photometric cleaned sample increases the signal, especially for the sparser clusters in our sample. We generated histograms of right ascension (Ra) and declination (Dec) separately. In order to estimate the center of a cluster, we fitted a Gaussian to both, the Ra and the Dec number distribution. The cluster center coordinates were determined from the peak of a Gaussian fit. This way we achieved an accuracy in the center coordinate determination of about  $3''$ . Figure 4.5 shows the number distributions of stars along the Ra and Dec direction, respectively. The Gaussian fit to both distributions is indicated by the red curve. A full table of our values for the central coordinates is given in Table 4.4, together with previous estimates from the literature published by Welch (1991), Bica & Schmitt (1995), Mackey & Gilmore (2003b), and Hill & Zaritsky (2006). Therefore we processed the values obtained by Welch (1991) to J2000 coordinates. For our study we keep the world coordinate system defined in the fits headers. The comparison with the literature values shows the differences for most clusters are of the order of a few arcsec.

**Table 4.4:** Star cluster centers.

Name	$\alpha$ (J2000.0)	$\delta$ (J2000.0)	$\alpha_{\text{Lit}}$ (J2000.0)	$\delta_{\text{Lit}}$ (J2000.0)	$\Delta$ [ $''$ ]	Ref.
Kron 28	00:51:45	-71:59:29	00:51:39.6	-71:59:57.6	28	c
Kron 44	01:02:06	-73:55:23	01:02:06.3	-73:55:22.7	10	c
Ln 11	00:27:44	-72:46:44	00:27:45.2	-72:46:52.5	8	c
Ln 116	01:55:33	-77:39:09	01:55:34.0	-77:39:16.0	1	d
Ln 32	00:47:25	-68:55:06	00:47:24.8	-68:55:13.0	6	a
Ln 38	00:48:51	-69:52:13	00:48:50.9	-69:52:15.0	2	a
NGC 152	00:32:58	-73:07:04	00:32:55.7	-73:07:01.0	3	b
			00:32:56.3	-73:06:56.6	7	c
NGC 339	00:57:47	-74:28:09	00:57:47.3	-74:28:22.0	12	b
			00:57:48.9	-74:28:00.3	9	c
NGC 361	01:02:10	-71:36:22	01:02:11.6	-71:36:21.0	1	b
			01:02:12.8	-71:36:16.2	6	c
NGC 411	01:07:55	-71:46:07	01:07:56.0	-71:46:03.0	5	b
			01:07:56.0	-71:46:04.5	3	c
NGC 416	01:07:58	-72:21:14	01:07:59.1	-72:21:12.0	3	b
			01:07:54.9	-72:20:50.6	24	c
NGC 419	01:08:16	-72:53:02	01:08:17.5	-72:53:01.0	1	a
			01:08:28.8	-72:53:11.8	9	c

$\Delta$  signifies the difference in the center determination from literature values

<sup>a</sup>Welch (1991), <sup>b</sup>Mackey & Gilmore (2003a),

<sup>c</sup>Hill & Zaritsky (2006), <sup>d</sup>Bica & Schmitt (1995)

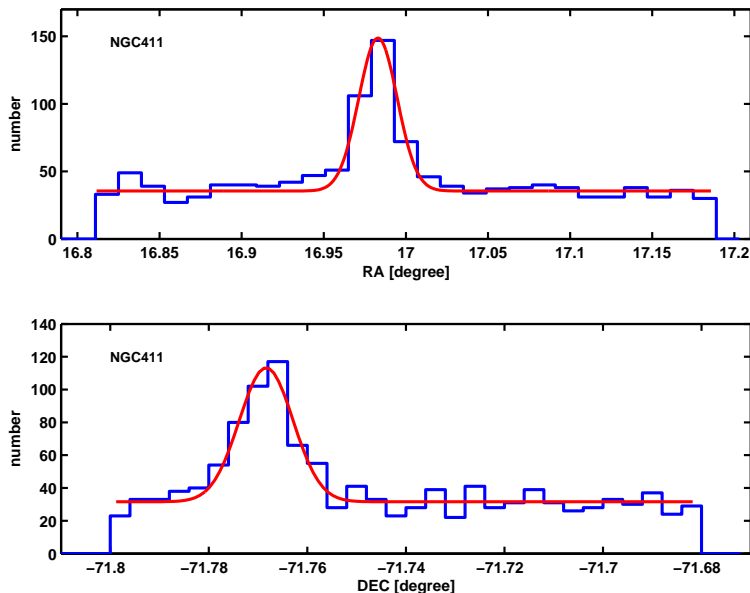


**Figure 4.5:** The determination of the center of NGC 411 from the Gaussian fit (red curve) to the Right Ascension (left) and Declination (right) number distributions.

### Lindsay 116

Lindsay 116 is one of the sparsest clusters in our sample. Furthermore, it is also the one located the furthest apart from the main body of the SMC. This means that we suffer much less from field star contamination than for the more centrally located clusters. During the first rough selection of the cluster member candidates from the CMD of the inner cluster region, we noticed that the Teramo isochrone chosen according to the literature values for this cluster does not represent the observed sequence of the CMD. Referring to Piatti et al. (2005a), who suggested that Lindsay 116 might be in fact located in the foreground of the SMC and actually be a LMC cluster, we adopted as a test the LMC distance modulus of  $dm = 18.5$ . We chose a second isochrone for an age of 1.5 Gyr and  $Z = 0.008$ , which are typical values for the younger group of star clusters in the LMC. Figure 4.6 shows the CMD of the inner region of Lindsay 116 with respect to the two different isochrones. Clearly the CMD sequence is better reproduced by the younger LMC isochrone. Nevertheless, we emphasize that the RGB and SGB of this cluster are very sparsely populated. A more exhaustive photometry, obtained e.g. with the HST is required for an accurate revision of the age of this cluster.

#### 4.3.2 Completeness test

Since we study fairly dense stellar systems we expect problems due to crowding, especially for the central regions of the clusters. Furthermore, we rely on ground-based data, which despite good seeing conditions limits the resolution of the crowded areas. Table 4.1 shows that the seeing was below  $1''$  for most of the exposures.

At small radii the projected density of the stars becomes so large that the light profiles of adjacent stars overlap. Therefore neighboring stars may not be identified as stars or misidentified as single sources by the used photometry package DAOPHOT. The distorting effects are dependent on the position and brightness of the stars. A star located closer to the

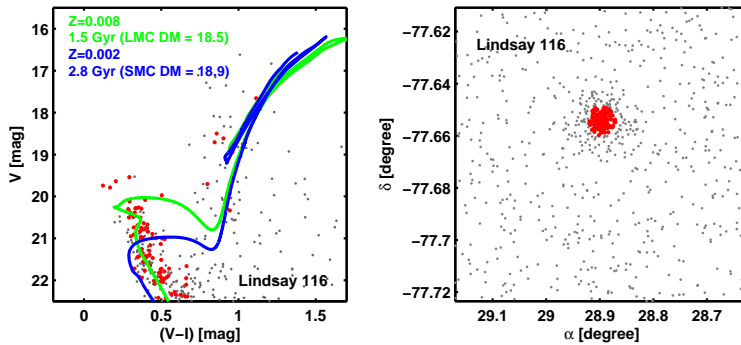


**Figure 4.6:** (left) CMD of the inner region (red points) of the cluster Lindsay 116. Plotted as blue and green lines are two different isochrones adopting SMC and LMC distance moduli and literature ages respectively. Indicated in gray are all detected stars in the observed field. (right) Shown is the observed field.

cluster center is more likely to go undetected than a star in the outer regions. Moreover the probability to detect a central star is higher for brighter stars.

These crowding effects result in a number of missed stars and fluxes depending on position and magnitude of the objects. These missed fluxes can significantly affect the observed surface brightness profiles and therefore the measured radii, which we want to obtain. Since the core radius is defined as the distance from the cluster center at which the central surface density/brightness has dropped by a factor of two, it is important to get a reliable estimate of the amount of crowding effects in each cluster.

We aim to correct for the missed fluxes by applying a standard completeness test. In order to evaluate the number of the missed stars we performed an add-star-experiment, taking into account the brightness and position of the star (e.g., Sosin & King 1997; Bellazzini et al. 2002). For each cluster we added artificial stars onto the original  $V$  image using the IRAF task `addstar` in the DAOPHOT package. These objects were constructed from the PSF for each frame. The positions and magnitudes of the stars were generated at random within magnitude bins of 0.5 mag. For each bin we added 500 point sources divided into 20 runs of 25 objects in order to avoid artificial crowding (e.g., Andreuzzi et al. 2001; Da Rocha et al. 2002). We considered 16 bins covering the magnitude range from 15 to 23 mag in  $V$ . This results in a total of 8000 artificial stars per cluster randomly distributed in position and magnitude. Once the stars were added we recovered them using the same algorithm we used for the detection and photometry on the original frames. The completeness fraction ( $CF$ ) is then defined as the fraction of successfully recovered stars to the total number of added artificial stars as a function of position and magnitude:

$$CF = \frac{\text{number of recovered stars}}{\text{number of added artificial stars}}. \quad (4.3)$$

In order to simplify the correction we adopted radial symmetry of the completeness for a fixed magnitude and considered the radial distance from the cluster center instead of the  $xy$ -position of the stars.

An illustration of the radial dependence of the completeness on the distance from the cluster center is shown in Fig. 4.7 for NGC 416. The left panel shows the resulting completeness fraction as a function of distance for the magnitude bins 15 to 15.5 mag and 18 to 18.4 mag for the cluster NGC 416. One sees that in the innermost 50'' the efficiency to recover fainter

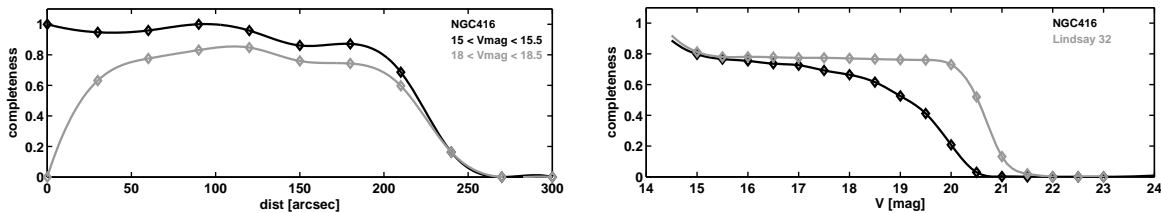


**Figure 4.7:** Completeness deficit due to crowding as a function of brightness of the stars and distance from the cluster center. The probability to recover faint stars located close to the cluster center drops rapidly as one approaches the center. This effect is not visible for brighter stars (left panel). For dense clusters (e.g., NGC 416) the limiting magnitude to which one can recover faint stars is brighter than for sparse clusters (e.g., Lindsay 32).

stars drops rapidly, whereas for the brighter stars we can reach 90 to 100% completeness. The right panel shows the dependency of the completeness fraction on the stellar magnitude for the dense cluster NGC 416 and the sparser cluster Lindsay 32. For the latter a completeness of 60% can be reached for stars about two magnitudes fainter than for the dense cluster. Note that in both cases we included stars at all distances and therefore we do not reach a completeness of 100% in this illustration. For very low magnitudes the estimated completeness corrections are very high and very unreliable. Therefore we excluded all measurements with estimated completenesses lower than 10%. Furthermore, Fig. 4.7 illustrates that even for  $V$  magnitudes of 18 the completeness of the inner regions is less than 10%. Since we can neither efficiently correct for this nor exclude stars with magnitudes up to 18, which would reduce the number of acquired stars too much, we proceed by excluding the innermost region of the cluster from the surface brightness profile fits.

### 4.3.3 Surface brightness profiles and core radii

For the generation of the surface brightness profiles we started with the photometrically selected sample, including the probable members on the RGB, SGB, and for those clusters possible on the region of the MSTO.

In order to further correct for the contribution of SMC field stars, we chose for each cluster a region well separated from the cluster center as a comparison background field. In all cases the cluster itself was located on the master CCD, so that it was possible to select a strip of a width of about  $150''$  on the second CCD for the background inspections. This area was located at a distance of  $225''$  from the cluster center.

Starting from the cluster center specified in Section 3.1, we defined two sets of annuli spaced by  $2''$  and  $3''$  extending out to  $20''$  and  $30''$ , respectively, to sample the inner region of the cluster. For the sampling of the outer cluster region we defined wider-spaced annuli of  $4''$  and  $6''$  extending out to  $100''$ , which is well beyond the expected values of typical cluster core radii. The mean core radius measured by Hill & Zaritsky (2006) is approximately  $15''$ . The use of four different extents of the annuli aims to avoid any bias of the subsequent fits with regard to the chosen bin size (see Mackey & Gilmore (2003b)). For each annulus  $i$  we calculated the surface brightness  $\mu_i$  from the summed flux  $F_j$  of all individual stars in that annulus, corrected for completeness fraction  $CF_i$  and the background contribution  $F_{BG}$ :

$$\mu_i = \frac{F_i - F_{BG}}{A_i}, \quad (4.4)$$



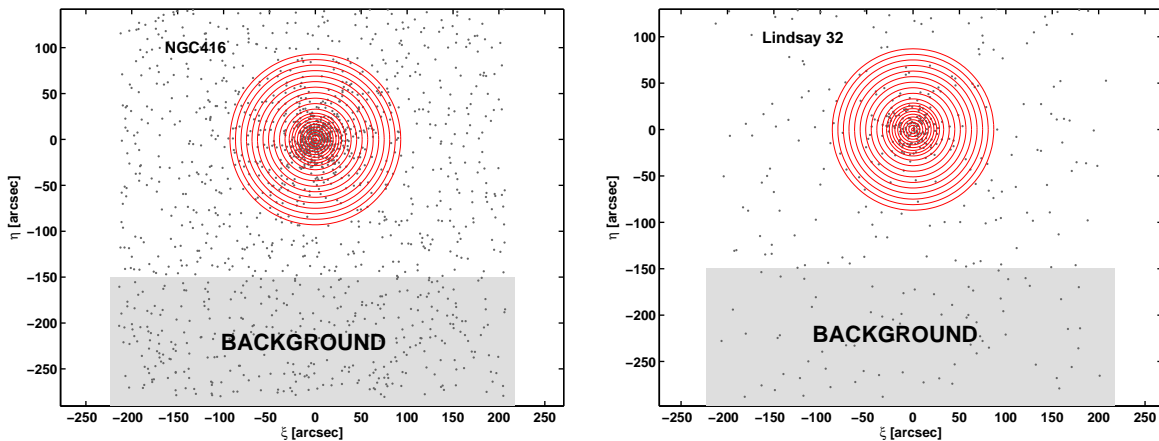


**Figure 4.8:** Location of annuli spaced by  $3''$  and  $6''$  sampling the inner and outer region of the cluster respectively. Shown are the examples of dense cluster NGC 416 (left panel) and sparse cluster Lindsay 32 (right panel). The gray region illustrates the location of the area used for the background subtraction.

where  $A_i$  is the area of the annulus and  $F_i$  and  $F_{\text{BG}}$  are given by:

$$F_i = cc_i \sum_j F_j, \quad (4.5)$$

$$F_{\text{BG}} = \sum_j F_j \frac{A_i}{A_{\text{BG}}}. \quad (4.6)$$

In order not to introduce additional errors by the completeness correction, we considered only stars brighter than a lower magnitude limit at which the completeness drops below 10%. Furthermore, we neglected all annuli with a completeness fraction below 10%, i.e., approximately the innermost  $5''$ , depending on the stellar density of the cluster. This eliminated most of the uncertain measurements in the inner region of the clusters. In spite of our precautions to prevent the inclusion of annuli with large incompleteness, some of the resulting surface brightness profiles show a distinct fall-off towards the central region, which is due to the aforementioned incompleteness effects, and consequently excluded from the fit. This can clearly be seen for the cluster Kron 44. The determined surface brightnesses for all annuli are plotted as functions of radius in Fig. 4.9. In analogy to Mackey & Gilmore (2003b) we used the method of Djorgovski (1988) to estimate the errors of the surface brightnesses in each annulus. We divided each annulus in eight segments of equal area and calculated the surface brightnesses in each segment individually. The standard deviation of the eight sectors then provided an estimate of the initial errors of the surface brightness in each radial bin.

In order to be able to compare the results with other recent studies we followed Mackey & Gilmore (2003a), who again refer to the work by Elson et al. (1987), and fitted the class of Elson-Fall-Freeman (EFF) models to the surface brightness distributions. They argued that clusters in the LMC do not appear to be tidally truncated even at large radii of several hundred arcsec and therefore are better reproduced by the two-dimensional brightness distributions of the form:

$$\mu(r) = \mu_0 \left( 1 + \frac{r^2}{a^2} \right)^{\gamma/2}, \quad (4.7)$$

where  $\mu_0$  is the central surface brightness,  $a$  is a measure of the core radius, and  $\gamma$  is a measure of the steepness of the outer parts of the profile. This model is a generalized form of a Plummer and King profile. For  $\gamma = 4$  it is equal to a Plummer profile (Plummer 1911) and for  $\gamma = 2$  it corresponds to a King profile (King 1962) with a tidal radius much larger than the core radius, i.e., for systems with a high concentration parameter. The value of  $a$  is related to the core radius  $r_c$  of the King (1962) models via

$$r_c = a(2^{2/\gamma} - 1)^{1/2}. \quad (4.8)$$

The errors of the fit parameters were estimated via a bootstrap resampling. We drew (with replacement) 1000 random bootstrap data samples from the original data. Hereby the number of elements in each bootstrap sample equaled the number of elements in the original data set. For each of these resampled data sets we repeated the fitting and obtained new values for the fitting parameters  $\mu_i$ ,  $a$ , and  $\gamma$ . The errors of the fit are then given by the standard deviation of the parameters, from which we derived the uncertainty of the core radius by propagating the above errors through eq. 4.8.

#### 4.3.4 Comparison with previous studies

A complete overview of the determined core radii is given in Tab. 4.5. We furthermore list the results by Kontizas (1984), Mackey & Gilmore (2003a) and Hill & Zaritsky (2006). For the conversion from projected core radius to parsecs we assumed the standard distance modulus of SMC, i.e.,  $dm = 18.9$  mag (cf. Westerlund 1997, and references therein). This is an approximation, since it is known that the SMC has a significant (but somewhat uncertain) depth between 6 and 12 kpc (Crowl et al. 2001).

We confirm that the core radii determined by Kontizas (1984) tend to be systematically smaller. This was already assumed by the authors themselves and mentioned by Mackey & Gilmore (2003a) and Hill & Zaritsky (2006). The deviations are probably a consequence of the spatial resolution of the photographic plates analyzed by Kontizas et al.

Figure 4.10 shows that in comparison with the previous studies we achieve the best agreement with the results by Mackey & Gilmore (2003a). This was expected as we used the same method for the radii determination. Since our data are ground-based the estimated errors are slightly larger than those of the estimates based on HST data (Mackey & Gilmore 2003a). The reason for the small deviations are probably due to remaining crowding effects in the inner regions of the clusters, which we were not able to overcome.

In comparison with Hill & Zaritsky (2006) we also find good agreement within the errors for six out of the eight clusters in common. Nevertheless, Fig. 4.10 indicates that their measured core radii seem to be systematically larger than ours. A slight bias to overestimate the radii with respect to Mackey & Gilmore (2003a) was already noticed by the authors and explained by a lack of resolution in the inner cluster regions. The clusters with the largest discrepancies are Kron 44 and Lindsay 11. By the visual inspection of our surface brightness profiles we find that both profiles show a drop-off towards the central regions. Therefore we suspect that the observed discrepancies result from remaining crowding effects, which we could not correct for.

#### 4.3.5 Cluster evolution

Hill & Zaritsky (2006) found the distribution of core size to be broader in the SMC than in

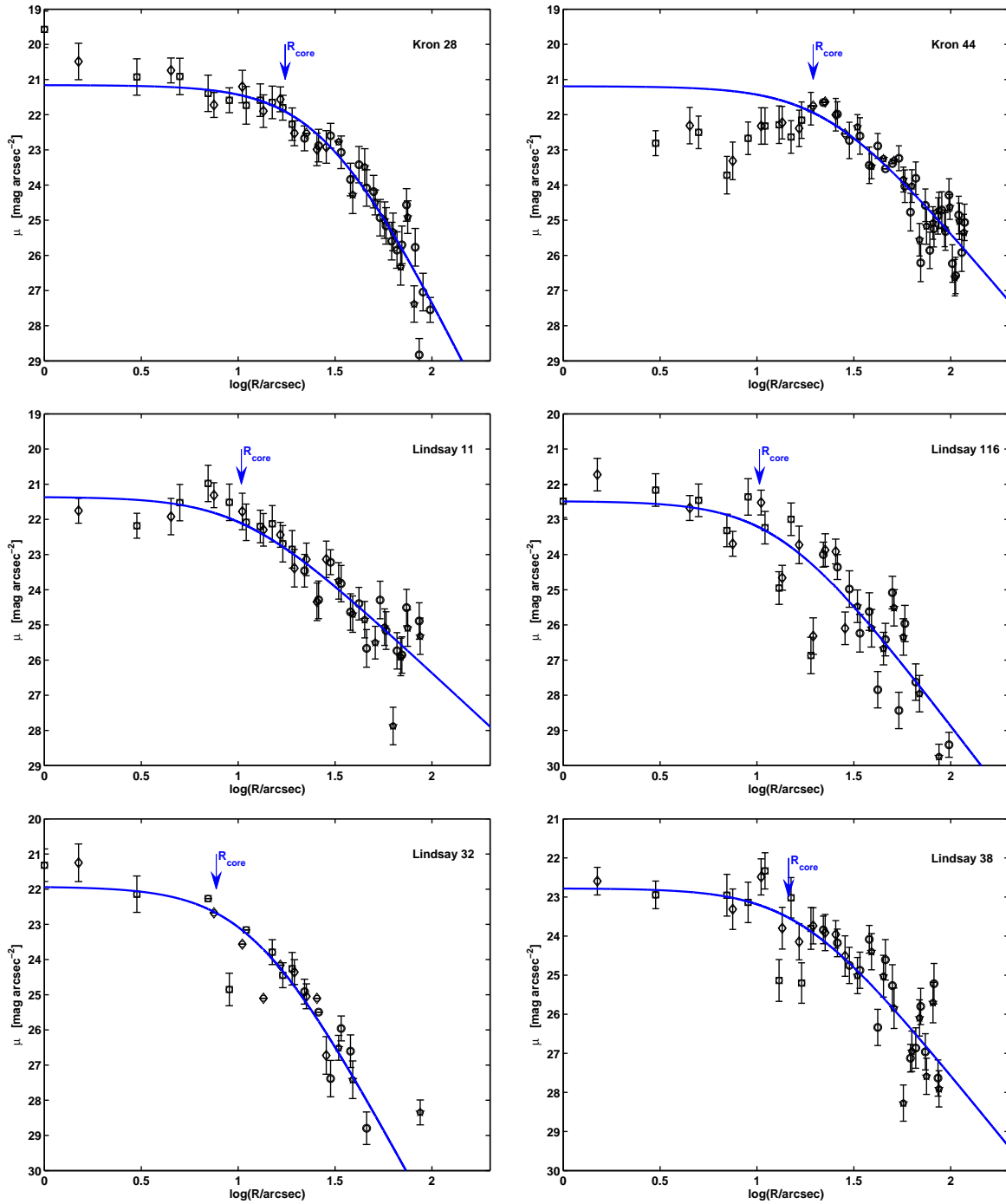
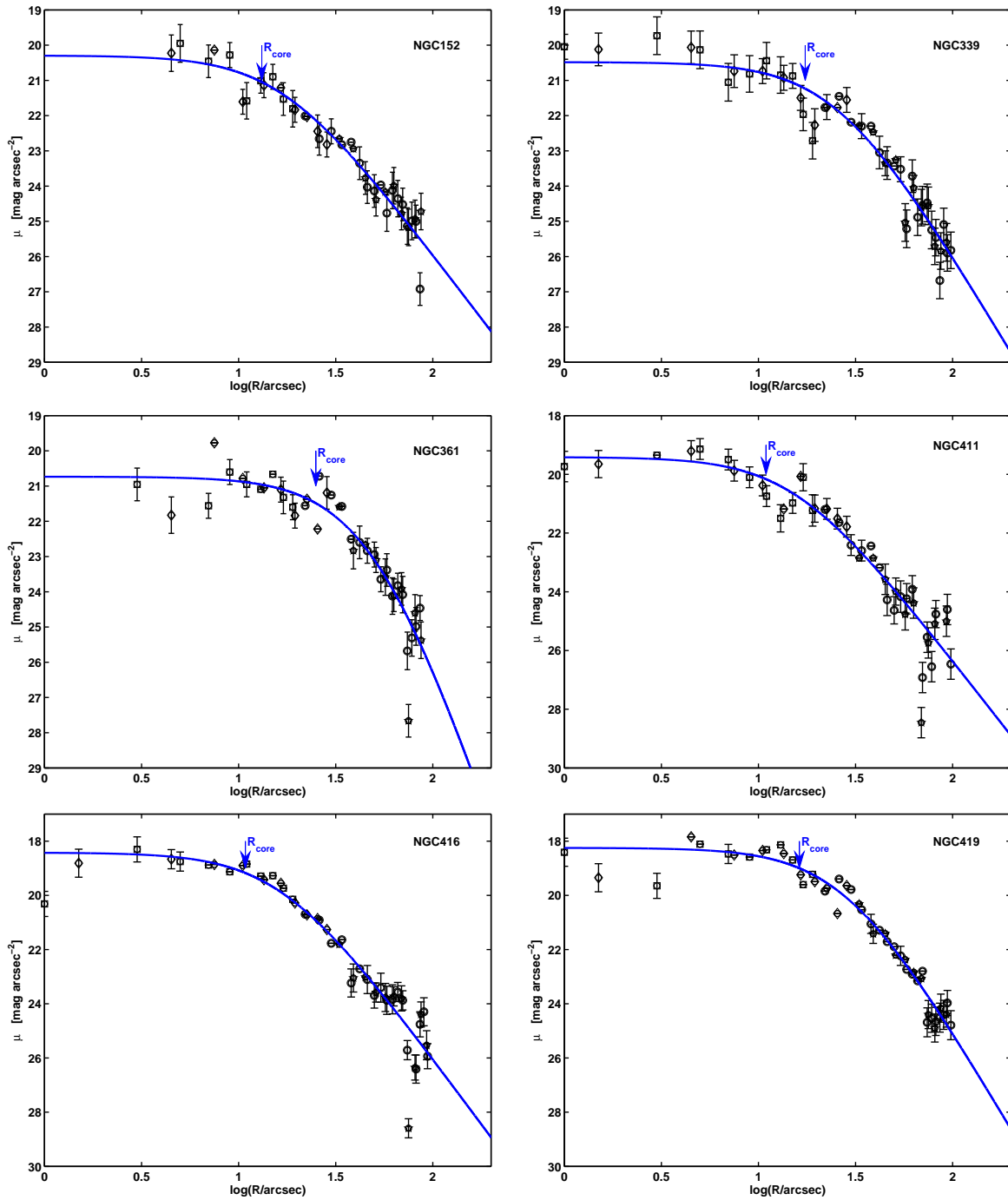
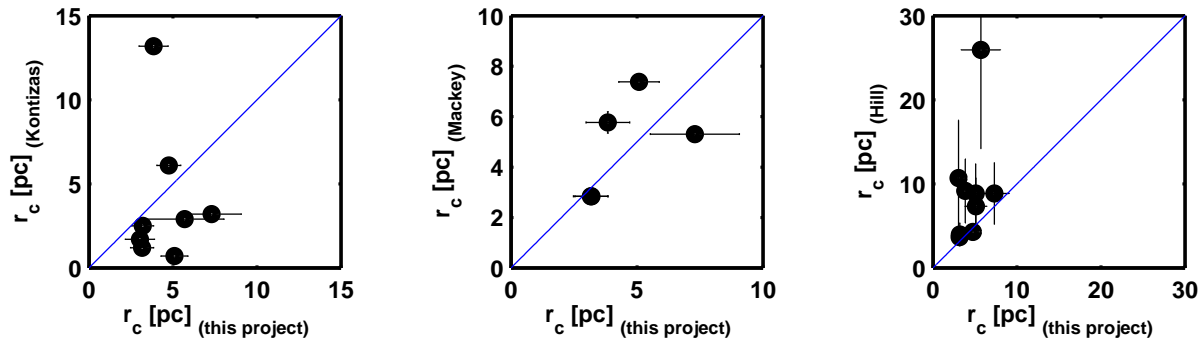


Figure 4.9: Surface brightness profiles of SMC star clusters. Solid lines show the best-fit EFF profiles. The location of the resulting core radius is indicated by arrows.

Figure 4.9: Surface brightness profiles of SMC star clusters - *continued*



**Figure 4.10:** Comparison of core radii derived in previous studies with our results for those clusters in common: Kontizas (1984) (left panel), Mackey & Gilmore (2003a) (middle panel), and Hill & Zaritsky (2006).

the MW (see Fig. 18 in their paper) - which they argue is due to a prevalence of surviving low-concentration clusters in the SMC. Furthermore, they could confirm that the SMC clusters are significantly more elliptical than the MW GCs. In contrast to previous studies (e.g., Frenk & Fall 1982), however, they did not find any clear evidence for a correlation between cluster age and ellipticity. Likewise they do not see any correlation between preferred model and age, i.e., no indication that clusters evolve from EFF (extended wings) to King (tidal cutoff) profile or vice versa.

In her analysis of the LMC star cluster radii Elson (1991) found that for a cluster of a given age there appears to exist an upper limit for its core size. Moreover, this limit was found to increase with age, which was later on confirmed by the analysis of Mackey & Gilmore (2003b). Arguing by a large cluster sample and space-based observations they exclude data reduction and/or selection effects as a possible origin for the observed relation. Mackey & Gilmore (2003b) concluded that the real physical sizes of the clusters are evolving. Young clusters are found to have very compact cores, whereas the cores of older clusters can reach extents of up to 6 pc. Elson (1991) argued that the expansion of the cores with time is caused by mass loss of evolving stars. Indeed the N-body simulations of Goodwin & Bastian (2006) showed that the structural parameters of star clusters change with time. A major driver of these changes is the expulsion of gas, which was not consumed via star formation. Since Lada (1999) suggested that the maximum gas fraction transformed into stars is of the order of 30%, the gas expulsion can induce a significant mass loss.

Kroupa & Boily (2002) suggested that populous star clusters expel their unused gas explosively during their early evolutionary stages due to the presence of numerous O stars. Goodwin & Bastian (2006) also suggested a rapid gas removal caused by stellar winds and supernovae. As a consequence the young clusters are out of virial equilibrium. The stars have too large velocity dispersions for the new potential. In order to restabilize, the cluster expands. The models of Boily & Kroupa (2003) showed that the bound stellar fraction is not only a function of the initial cluster distribution function, but also depends on the star formation efficiency. However, these theoretical studies consider only the early evolution ( $< 100$  Myr) and can therefore only qualitatively explain the larger spread in core radius size observed with increasing cluster age for the very young cluster. The origin of the large scatter and larger radii for older clusters remains unsolved.

Although their sample of the SMC is small and necessarily incomplete, Mackey & Gilmore

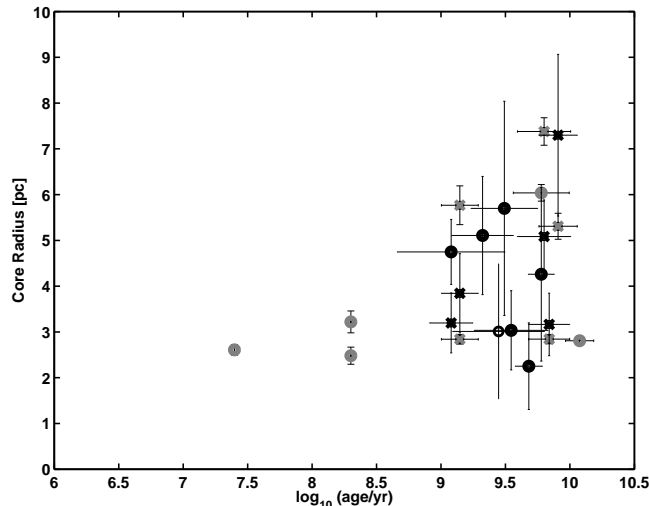


**Figure 4.11:** Age versus core radius diagram for the SMC star clusters. Black symbols indicate our measurements; gray symbols are those of Mackey & Gilmore (2003a). Solid black circles are clusters only measured in our study; solid gray circles are clusters only measured by Mackey & Gilmore (2003a). The crosses indicate clusters with measurements from both studies. The probable LMC cluster Ln 116 is plotted as an open black circle.

(2003a) found evidence of a similar trend like in the LMC. Adding our new data for seven star cluster core radii, (see Fig. 4.11) we confirm the observed relationship between cluster age and spread in core size in the SMC. The combined sample contains 17 clusters. All three younger clusters have compact cores between 2 and 3 pc, while the older clusters ( $\log \text{age} > 9 \text{ yr}$ ) have very different core radii, ranging from 2 to 7.5 pc. Figure 4.11 suggests that among the older clusters some objects may have experienced a significant change in  $r_c$ , while for others  $r_c$  remained almost unchanged.

Since the age-radius correlation has been observed both in the SMC and LMC Mackey & Gilmore (2003a) emphasized the idea of an universal true physical process as the origin. However, this is very speculative and requires a lot of additional observational studies in other galaxies and theoretical models to be worked on.

#### 4.4 Cluster radial velocities and velocity dispersions

In order to determine the radial velocities of the SMC star clusters we used the cross-correlation method, which was developed by Tonry & Davis (1979) and is implemented into the IRAF task `fxcor`. Within this algorithm the object spectrum is cross-correlated against a high signal-to-noise template spectrum of known radial velocity. The position of the correlation peak defines the relative velocity of the object with respect to the template spectrum. We applied this method to all stars in the clusters that were observed spectroscopically. The cross-correlation was performed over the entire spectral range between 8400–8800 Å. In our case we used a well approved synthetic spectrum of the three strong calcium lines with equivalent widths representative of those in K-giants as a template (e.g., Kleyana et al. 2002).

From previous studies we were aware of the possibility that the errors given by `fxcor` underestimate the real uncertainties. To test the impact of this effect in our measurement

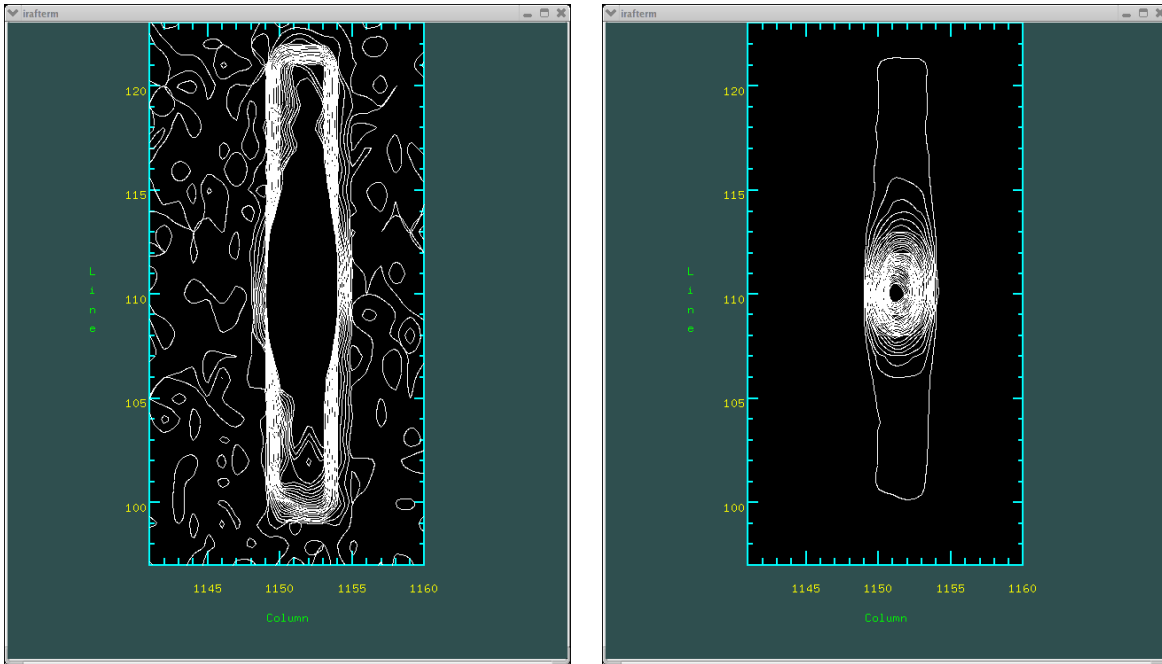


**Figure 4.12:** Two contour plots of the same region in the through slit acquisition image of the cluster NGC 416. In the left figure the contour parameters have been set so that the stellar profile is visible. In the right figure the stellar image is blanked out so that the slit boundaries can be seen.

we followed the method by Kleyna et al. (2002). For each spectrum we cross-correlated each of the three CaT lines against the corresponding template line. This way we obtained three velocity measurements for each star. In the following we treated the SMC and MW spectra independently. The  $\chi^2$  was computed as the sum over the square of the velocity deviations between the measurement of two of the three lines each separate lines divided by their in quadrature added `fxcor` errors:

$$\chi^2 = \sum_{i,j} \frac{(v_i - v_j)^2}{(v_i + v_j)^2}. \quad (4.9)$$

Since we expected the  $\chi^2$  to be equal to three times the number of spectra, the rescaling factor was  $\sqrt{\chi^2/3N}$ . We found that in our case the errors provided by `fxcor` are only slightly too optimistic. We rescaled all errors of the velocity measurements in the SMC and MW by a factor of 1.2 and 1.06, respectively. This results in a median value of 3.5 km/s for the accuracy of the velocity determinations in the SMC and 2.8 km/s in the MW. We added in quadrature the uncertainty of  $0.7 \text{ km s}^{-1}$ , arising from the accuracy of the wavelength solution.

Another effect which we corrected for is a velocity shift due to the position of the star within the slit. Previous studies with the same instrumental setup (e.g., Cole et al. 2005) revealed that the misalignment between the stellar image and the slit can cause velocity shifts up to 30 km/s. In order to correct for this effect we determined the position of the star within the slit. We used the through slit acquisition image taken before each spectroscopic science exposure to verify the proper position of the targets on the slit. These exposures image both, the slit and the star within them. Figure 4.12 shows two contour plots of the same region of the acquisition image for the cluster NGC 411. The contour parameters are set in two different ways to accent the slit and the star, respectively. The centroid of the star was obtained by a

simple Gaussian fit to the stellar profile. For the determination of the slit center we selected in the corresponding contour plot an outer contour of the slit from which we were able to estimate the center. According to the instrument parameters we expected a slit width of four pixel. Due to diffraction effects on the through slit exposures the observed slits were always larger than this value. This can be clearly seen in the right panel of Fig. 4.12. Near the location of the star in the slit the compression of the contours indicates an "overflow" to the left and right. The uncertainties in the determination of the slit center are dominated by this effect. Given the dispersion of the grism 1028z+29 in the  $2 \times 2$  binning mode of  $d = 0.85 \text{ \AA}/\text{pix}$  and the central wavelength of  $8580 \text{ \AA}$  the velocity shift per pixel offset is:

$$\Delta v = c \Delta \lambda / \lambda = c / \lambda d \Delta \text{pix}, \quad (4.10)$$

$$\Delta v / \Delta \text{pix} \approx 29.5 \text{ km/s}. \quad (4.11)$$

The pixel offsets and the resulting velocity shifts were determined for all stars in each cluster individually. For most stars the observed offsets were smaller than 0.5 pix. Nevertheless for few cases the observed offsets were as large as  $0.8 - 1$  pix, so that a fairly large velocity shift was calculated. Finally, the velocities derived via cross-correlation were corrected for the obtained shifts. The overall uncertainties in the velocity measurement are dominated by the uncertainties given by the cross-correlation and the pixel-shift correction.

In order to determine the mean heliocentric radial velocities of the SMC star clusters we considered the velocity distribution as a function of projected distance from the cluster center for each individual cluster (Fig. 5.8). Since stars located closer to the center are more likely to be cluster members, we only consider stars within a maximum distance of seven times the core radius from the cluster center in the velocity determination. In case of a King model this corresponds approximately to the tidal radius for a cluster with a concentration parameter of  $\approx 0.8$ . This concentration parameter is a typical value for star clusters (Binney & Tremaine 1987). For the Galactic globular clusters the concentration parameter varies between 0.5 and 2.5 (Harris 2003). Similar values have been found for the young star clusters in the merging galaxy pair - the Antennae galaxies (Mengel et al. 2002).

We calculated the weighted mean ( $\bar{v}$ ) of the individual velocities and the velocity dispersion ( $\sigma$ ). Stars deviating by more than  $3\sigma$  from the sample mean were assumed to be cluster non-members and were rejected. We applied a maximum likelihood method for a set of velocities with varying uncertainties (Pryor & Meylan 1993) to estimate  $\bar{v}$  and  $\sigma$ . For this purpose the following equations were solved numerically by iteration:

$$\sum_i \frac{v_i}{(\sigma^2 + \delta v_i^2)^2} - \bar{v} \sum_i \frac{1}{(\sigma^2 - \delta v_i^2)} = 0, \quad (4.12)$$

$$\sum_i \frac{(v_i - \bar{v})^2}{(\sigma^2 + \delta v_i^2)^2} - \sum_i \frac{1}{(\sigma^2 - \delta v_i^2)} = 0. \quad (4.13)$$

Typically 5–20 stars (depending on the richness of the cluster) were included in the velocity determinations. We find the cluster velocities to lie within the range between  $\approx 130$  km/s and  $\approx 190$  km/s. For all clusters the estimates for the velocity dispersions are  $< 10$  km/s. However, for many objects our calculated velocity dispersion is larger than the expected value of about 2–3 km/s (e.g., Harris 1996). Responsible are the uncertainties in the velocity determinations mainly resulting from the pixel shift corrections. We therefore disregard the velocity dispersion of the individual clusters in the interpretation of the data.



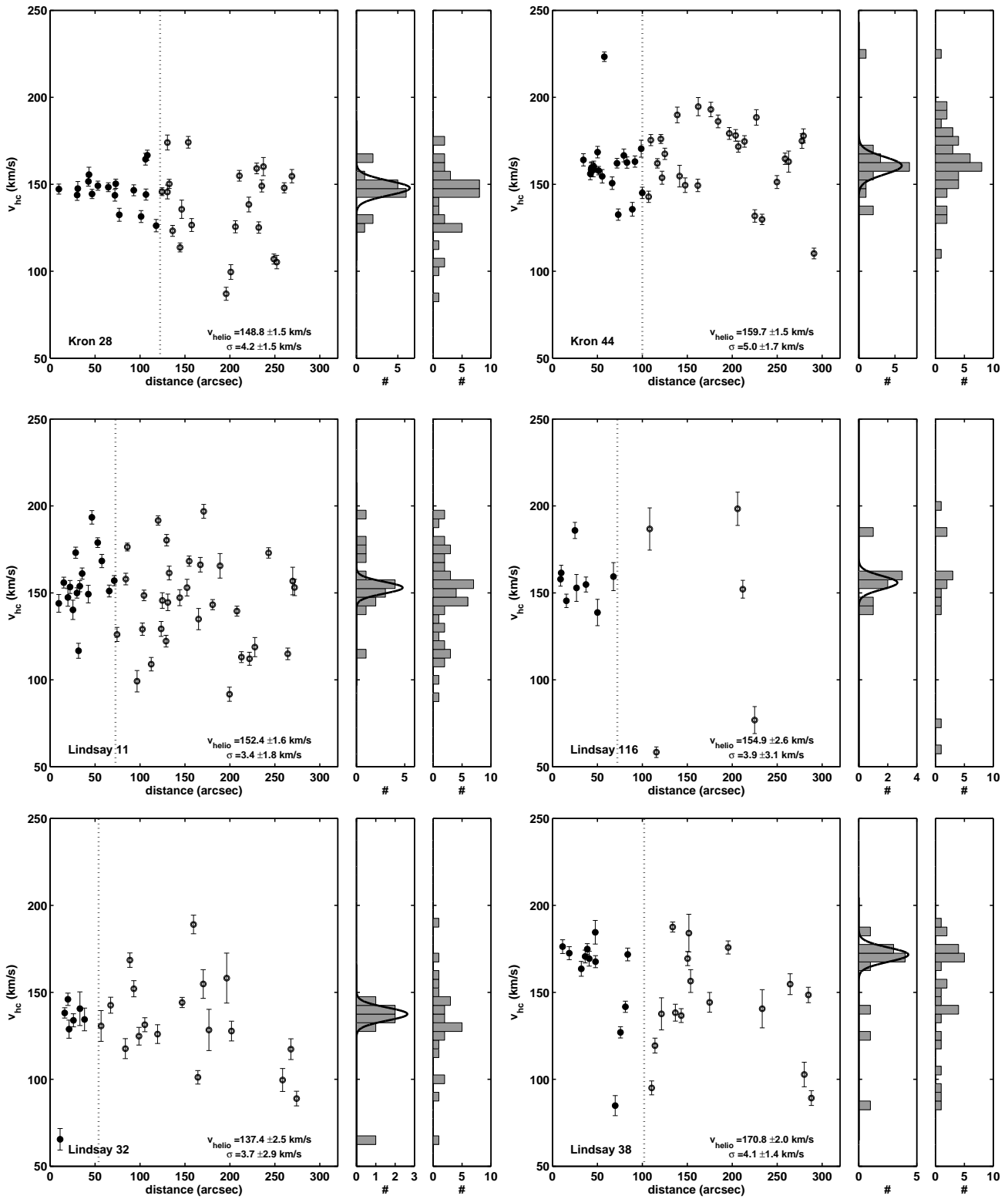


Figure 4.13: Velocity distributions for all observed star clusters. (Left) Measured heliocentric velocity as a function of distance from the corresponding cluster center. The dashed line indicates the distance cut of our velocity measurement. This is seven times the cluster core radii for all except for the sparse cluster Kron 44. For the latter we selected stars within  $100''$ . The open symbols are all spectroscopic targets, the filled symbols are member candidates due to their position in the CMD and distance from the cluster center. (Middle) Velocity distribution of probable members fitted by a Gaussian. (Right) Velocity distribution of all targets.

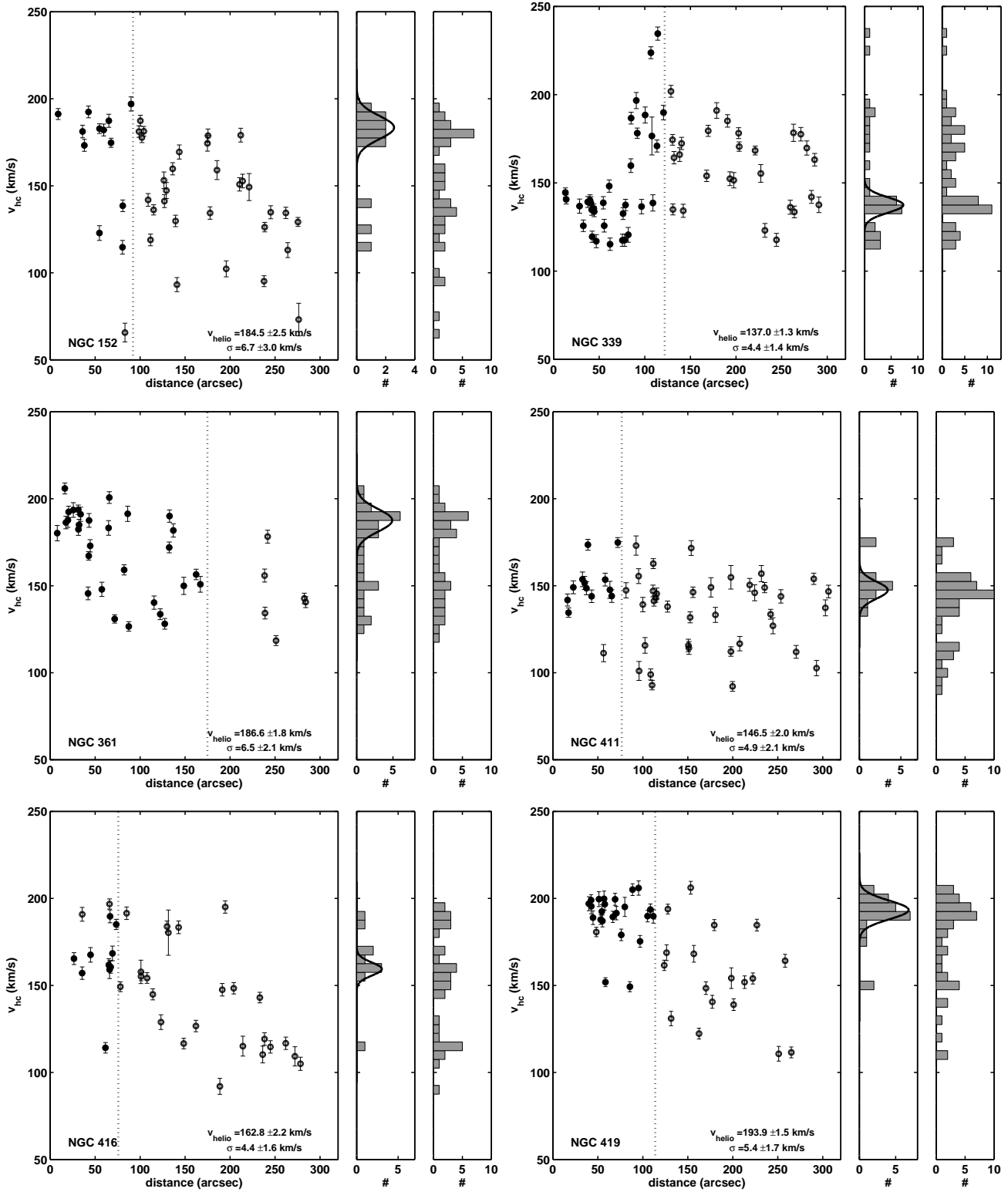
Figure 4.13: Heliocentric velocity vs. distance from the cluster center - *continued*

Figure 5.8 (left panel) shows for each cluster the velocities of the measured stars as a function of distance from the corresponding cluster center. The two histograms to the left show the velocity distributions including only stars within the distance of seven times the core radius from the cluster center (middle panel) and all objects (right panel). An exception was made for Kron 44 for which our estimates for  $r_c$  is enormously high. For this cluster we restricted the measurement to stars within a projected distance of maximal  $100''$  from the clusters center. For all histograms was the bin size chosen to be 5 km/s, which is slightly larger than the mean uncertainty of the velocity measurements. Overplotted are Gaussians with the computed dispersions, fitted to the mean velocities.

The velocity histograms comprising not only the inner region of a certain cluster but the whole sample of observed stars show that some clusters exhibit multiple peaks in the velocity distribution (e.g., NGC 339). The investigation of the spatial distribution of the stars of these secondary peaks revealed a uniform distribution. We could not find any evidence of a group of associated stars belonging to a background cluster or the like. Most likely these stars are SMC field stars.

To check the reliability of this method we also determined the velocities of the Galactic globular clusters in our sample in the same way. For MW clusters accurate heliocentric velocity measurements can be found in the literature (Harris 1996). For all three clusters our velocity estimates agree very well with the literature values within the error ranges (see Table 4.5). We are therefore confident that we obtained reliable measurements for the SMC clusters. A full list of the derived velocities and velocity dispersions is given in Table 4.5.

#### 4.4.1 Comparison with previous studies

In case of the SMC only for very few of the clusters velocity measurements have been published before. An overview of our velocity measurements as well as the literature values is given in Tab. 4.5. Zinn & West (1984) published radial velocities based on integrated spectra of the clusters NGC 416 and NGC 419. Their values of  $158 \pm 20$  km/s and  $181 \pm 20$  km/s are found to be in agreement with our results computed from individual stars. Da Costa & Hatzidimitriou (1998) measured velocities of red giant stars in seven SMC clusters. Unfortunately these estimates are only based on measurements of three to six stellar spectra. For the three clusters in common these literature values do not agree within the uncertainties with our results. The observed discrepancies are 20.4 km/s for Lindsay 11, 20.0 km/s for NGC 339, and 22.6 km/s for NGC 361. In all cases our values exceed the values of Da Costa & Hatzidimitriou (1998). The systematic difference of  $\approx 20$  km/s is larger than the observed errors. Nevertheless, we are confident that our estimates are the more trustable as they comprise a much larger sample of spectra. Furthermore, it is worth mentioning that Kunkel et al. (2000) also consulted the data of Da Costa & Hatzidimitriou (1998) in their project dedicated to Carbon star velocities in the SMC field. They detected an offset of 18 km/s, which is of the same order of magnitude as the discrepancies we observed.

It might be important to mention that the values for NGC 339 from Da Costa & Hatzidimitriou (1998) coincides fairly good with the position of the secondary peak in this distribution (see Fig. 4.14 ). Possibly Da Costa & Hatzidimitriou (1998) have measured stars from the secondary peak, which does not belong to the main population.

Interestingly, Lindsay 116, which was considered as a candidate of a LMC cluster, has a heliocentric velocity of  $v_{\text{helio}} = 154.9 \pm 2.6$ , which is consistent with the SMC kinematics. Since the LMC has a much higher systemic velocity of 257 km/s (Cole et al. 2005) the velocity

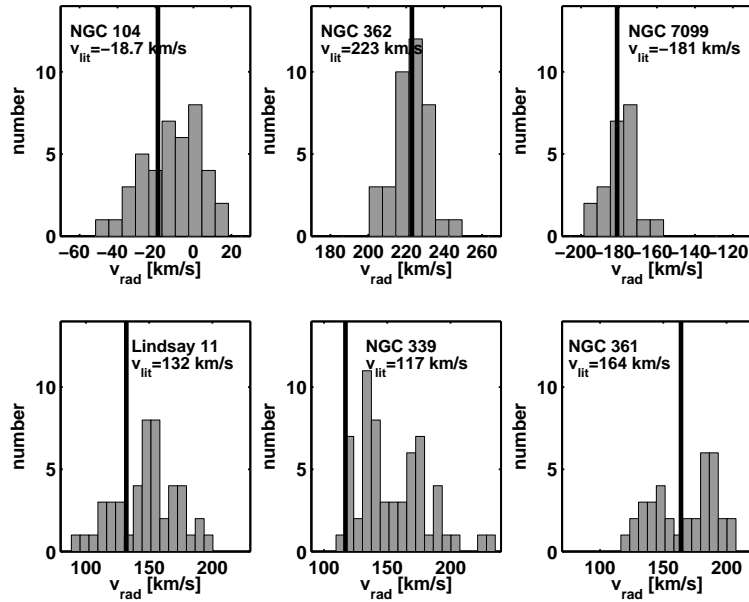


**Figure 4.14:** Top panels: The derived velocity distributions from our measurements for the three MW globular clusters in our sample. The black lines indicate the location of the clusters heliocentric velocities found in the literature. For NGC 362 and NGC 7099 we find good agreement with the peaks in our distribution. Our sample for NGC 104 suffers from a large contamination of SMC field stars but is also fairly consistent with the literature. Bottom panel: Comparison of our velocity distributions with the values by Da Costa & Hatzidimitriou (1998) for the three SMC clusters in common. We find a systematic offset of the order of 20 km/s between our measurements and the velocities measured by Da Costa & Hatzidimitriou (1998). Note that in these diagrams we show the complete sample of measured velocities.

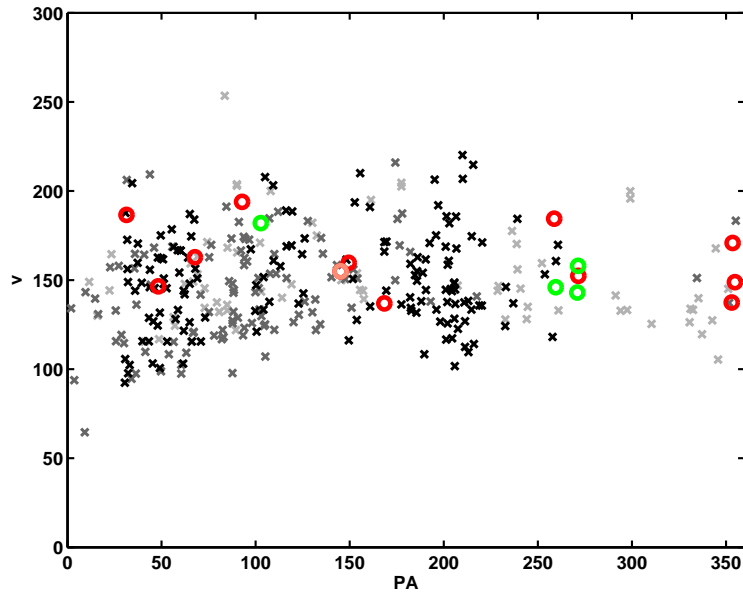


**Figure 4.15:** Measured heliocentric velocities of the star clusters as a function of the position angle. The star clusters of our project are plotted as red circles, those of the Da Costa & Hatzidimitriou (1998) sample by green circles. Lindsay 116 is plotted in light red. Indicated by crosses are results from Carbon star measurements by Hardy et al. (1989) (black), Hatzidimitriou et al. (1997) (light gray), and Kunkel et al. (2000) (gray).

measurement is in conflict with the LMC membership and rather favors an affiliation with the SMC. We included Lindsay 116 in the following discussion, however in Fig. 4.15 and Fig. 4.16 we marked this clusters by a different color.

In Figure 4.15 we plotted the heliocentric velocities versus position angle for the star cluster and Carbon star measurements taken from the literature. We see good agreement between these tracers of intermediate age and old stellar populations. The different projects dedicated to Carbon stars by Hardy et al. (1989), Hatzidimitriou et al. (1997), and Kunkel et al. (2000) found no clear sign of rotation. The complete sample of stars studied in these velocity surveys comprised more than 350 stars in various regions in the SMC and extended to a radius of  $12^\circ$  from the photocenter. The observed velocity distribution was interpreted by the inclination of this galaxy. Since our data follow nicely the determined Carbon star velocities, we find no in situ argument for any, up to now, undetected rotation of the intermediate age population in the SMC. However, a sophisticated conclusion on the rotation of the star cluster population in the SMC requires a more detailed analysis, which is foreseen in a subsequent project. Furthermore, our sample of 16 clusters is still very small.

In contrast, observations of neutral hydrogen by Stanimirović et al. (2004) showed a large velocity gradient extending from the southwest to the northeast of the SMC. From the symmetry of this velocity field the authors suggested the present of a differential rotation among the younger population in the SMC, which is traced by HI.

Interestingly, differences between the young and old population in the SMC can also be seen in their morphologies (e.g., Cioni et al. 2000; Zaritsky et al. 2000). The young star in the SMC were found to show an irregular distribution while the stars older than 1 Gyr are regularly, almost spherically distributed.

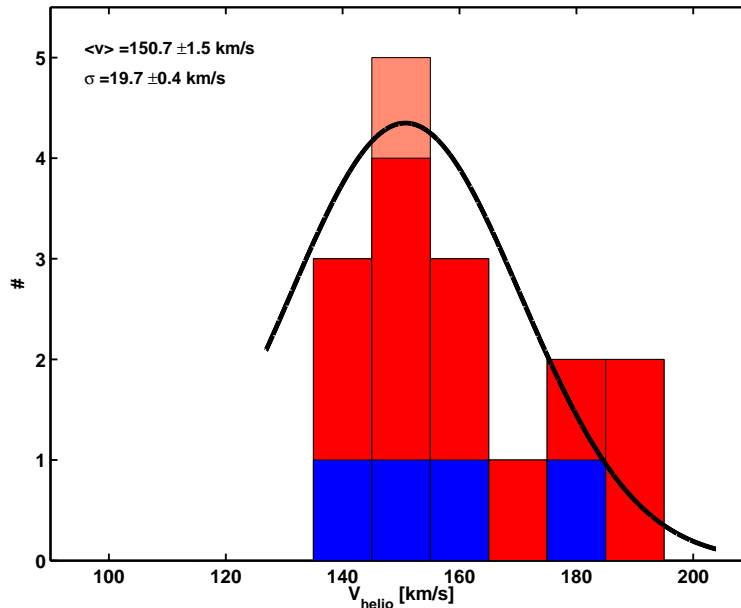


**Figure 4.16:** Velocity distribution frequency of the star cluster in the SMC and the resulting mean heliocentric velocity and the velocity dispersion of the star cluster system. In the histogram the measurements by Da Costa & Hatzidimitriou (1998) are indicated in blue, our measurements in red. The probable LMC cluster Lindsay 116 is indicated in light red. The solid line indicates a Gaussian fitted to the data.

Focusing on the main peak in the velocity distribution (see Fig. 4.16) we estimated the mean systemic velocities of the SMC star cluster including all cluster velocities available and only the clusters in our sample to be  $\bar{v} = 150.7 \pm 1.5$  km/s and  $\bar{v} = 151.2 \pm 1.3$  km/s, respectively. These are in good agreement with the results from Carbon star measurements ( $v = 149.3 \pm 3$  km/s, Hatzidimitriou et al. (1997)) and also agree with the systemic velocity of  $v_{sys} = 158 \pm 4$  km/s listed in the catalog of neighboring galaxies by Karachentsev et al. (2004). Furthermore, the values are of similar order of magnitude as the systematic velocity of the apparent kinematic center derived from the velocity field based on radio observations, 160 km/s (Stanimirović et al. 2004). Due to the asymmetry of the velocity distribution, we derived an estimate of the velocity dispersion from the calculation of separate values, left and right of the main peak of the distribution. The resulting rms- velocity dispersions are found to be  $\sigma = 19.7 \pm 0.4$  km/s and  $\sigma = 20.7 \pm 0.4$  km/s for all available data and only our sample, respectively (see Figure 4.16). The error were estimated from Monte Carlo resampling. These values are slightly higher than the results by Da Costa & Hatzidimitriou (1998), who derived a velocity dispersion of  $16 \pm 4$  km/s from seven star clusters. However, our outcome better coincides with the findings by Hatzidimitriou et al. (1997) and Dopita et al. (1985) on Carbon stars ( $21 \pm 2$  km/s) and planetary nebulae ( $25 \pm 3$  km/s). The progenitors of these objects are presumed to have similar ages as the star clusters. Da Costa & Hatzidimitriou (1998) pointed out that regardless of age and therewith connected morphological and rotational differences, all populations in the SMC show heliocentric velocities and velocity dispersions of the same order of magnitude. Our study more than triples the existing sample of SMC star cluster velocities. It confirms the remark made by Da Costa & Hatzidimitriou (1998) that the old and intermediate star cluster population in the SMC follows the overall observed kinematics.

**Table 4.5:** Derived properties of SMC clusters and literature values.

Name	$r_c$ [ $''$ ]	$r_{c(Lit)}$ [ $''$ ]	$rmr_c$ [pc]	$r_{c(Lit)}$ [pc]	$v_{helio}$ [km s $^{-1}$ ]	$v_{helio(Lit)}$ [km s $^{-1}$ ]	Ref.
Kron 28	$16.08 \pm 3.99$		$4.39 \pm 1.03$	$7.33 \pm 3.36$	$148.8 \pm 1.5$		b
				2.9			c
Kron 44	$28.49 \pm 8.92$		$7.35 \pm 1.43$	$25.96 \pm 11.76$	$158.2 \pm 1.5$		b
Ln 11	$10.39 \pm 2.96$		$2.56 \pm 0.61$	$10.69 \pm 8.88$	$152.4 \pm 1.6$	$132 \pm 5$	b,d
				1.7			c
Ln 116	$10.31 \pm 5.05$		$0.77 \pm 1.22$		$154.9 \pm 3.9$		
Ln 32	$7.71 \pm 3.24$		$3.32 \pm 2.23$		$137.4 \pm 2.5$		
Ln 38	$14.58 \pm 6.49$		$5.13 \pm 1.90$		$170.0 \pm 2.0$		
NGC 152	$13.16 \pm 2.96$	$19.74 \pm 1.45$	$5.63 \pm 1.60$	$5.77 \pm 0.42$	$184.5 \pm 2.5$		a
				$9.16 \pm 3.82$			b
				13.2			c
NGC 339	$17.40 \pm 2.74$	$25.26 \pm 1.03$	$5.69 \pm 1.36$	$7.38 \pm 0.30$	$136.9 \pm 1.4$	$117 \pm 8$	a,d
				$8.86 \pm 3.51$			b
				0.7			c
NGC 361	$24.98 \pm 6.05$	$18.17 \pm 0.97$	$7.27 \pm 2.48$	$5.31 \pm 0.28$	$186.6 \pm 1.8$	$164 \pm 6$	a,d
				$8.86 \pm 3.67$			b
				3.2			c
NGC 411	$10.94 \pm 2.24$	$9.72 \pm 0.36$	$3.25 \pm 0.62$	$2.84 \pm 0.11$	$146.5 \pm 2.0$		a,d
				$3.97 \pm 1.38$			b
				5.72			c
NGC 416	$10.83 \pm 2.34$	$9.73 \pm 0.35$	$3.58 \pm 0.56$	$2.84 \pm 0.10$	$162.8 \pm 2.2$	$158 \pm 20$	a,e
				3.67			b
				1.2			c
NGC 419	$16.25 \pm 2.43$		$4.91 \pm 0.98$	4.28	$193.9 \pm 1.5$	$181 \pm 20$	b,e
				6.1			c

<sup>a</sup>Mackey & Gilmore (2003a), <sup>b</sup>Hill & Zaritsky (2006), <sup>c</sup>Kontizas (1984),

<sup>d</sup>Da Costa & Hatzidimitriou (1998), <sup>e</sup>Zinn & West (1984)

## 4.5 Summary

From the analysis of VLT/FORS2 imaging data we obtained surface brightness profiles for twelve populous star clusters in the SMC. Following Mackey & Gilmore (2003b) we measured core radii for all clusters in our sample. The comparison with previous measurements showed good agreement with the recent studies (Mackey & Gilmore 2003a). In comparison with the data by Hill & Zaritsky (2006) we also found good agreement within the errors for six out of the eight clusters in common. Nevertheless, their measured core radii seem to be systematically larger than ours. A slight bias to overestimate the radii with respect to Mackey & Gilmore (2003a) was already noticed by the authors and explained by a lack of resolution in the inner cluster regions. Older values (Kontizas et al. 1987) tend to be systematically smaller.

We could further strengthen the existence of an age-radius relation in the SMC suggested by Mackey & Gilmore (2003a). At a given age there seems to exist an upper limit for the core size of star clusters, which is larger for older ages. Since Mackey & Gilmore (2003a) observed a similar relation for the LMC, this strengthens the idea of a universal physical effect changing the cluster parameters with time.

Furthermore, we studied near infra-red CaII triplet spectra of individual red giant stars in these twelve SMC star clusters. We determined heliocentric velocities and velocity dispersions from a distance-selected sub-sample of the spectra. This increased the presently known sample by a four-fold in size. We found a systematic offset in measured velocities between our results and those by Da Costa & Hatzidimitriou (1998) of 20 km/s for the three clusters in common. Combining our sample with four additional clusters by Da Costa & Hatzidimitriou (1998) we obtained a systemic velocity  $v_{sys} = 150.7 \pm 1.5$  km/s and a velocity dispersion of  $\sigma = 19.7 \pm 0.4$  km/s, which is in excellent agreement to measurements from Carbon stars and planetary nebulae. Those measurement did not show any sign of rotation. From the consistency between the results we speculate that probably the star clusters system is not rotating either. However, a larger clusters sample and a more sophisticated investigation is necessary in order drawn draw better conclusions on the kinematics of the star cluster system.



## Chapter 5

# The Age-Metallicity Relation and Star Formation History of the Small Magellanic Cloud

### Abstract

This chapter presents accurate spectroscopic metallicities for 12 populous star clusters associated with the Small Magellanic Cloud (SMC). We obtained more than 300 spectra of the near infra-red Ca II triplet region of individual red giant stars in these clusters and their surrounding fields. Our metallicity estimates are based on five to 16 stars per cluster, carefully selected by velocity, position in the CMD, distance from the clusters center, and metallicity itself. The Ca triplet provides a well calibrated, reddening independent metallicity indicator, yielding accuracies of the order of  $\sim 0.1$  dex in  $[\text{Fe}/\text{H}]$ . Combing these newly derived spectroscopic metallicities with the most recent age measurements taken from the literature, we present for the first time an age-metallicity relation for the SMC that is exclusively based on spectroscopic metallicity estimates. Since the SMC is the only dwarf galaxy in the Local Group with a seemingly continuous cluster formation over the past 12 Gyr, our measurements provide a closely spaced set of single-age and single-metallicity tracers. Our results clearly show a large scatter of up to 0.45 dex in metallicity at a given age, indicating that the SMC was not perfectly mixed during its lifetime. There is a mild trend of more metal-poor clusters at larger distances from the central regions of the SMC at a given age. For the more recent past we detect an increase in metallicity accompanied by a decrease of the observed scatter. The comparison with different chemical evolution models suggests that our age-metallicity relation is best represented by a bursting model of star formation history.

*This project was done in collaboration with Eva K. Grebel, Andreas Koch, Jay S. Gallagher, Daniel Harbeck, Andrew A. Cole, Katharina Glatt, and Gary S. Da Costa.*

## 5.1 Introduction

The desire to understand the formation and evolution of galaxies requires in particular an improvement of our knowledge of their chemical enrichment histories. This deserves the study of the evolution of metallicity with time and its dependence on galaxy mass and type fundamental questions of galactic studies.

Important tools towards an answer to these questions are star clusters. Considered to be fossil remnants of the environment out of which they formed, star clusters trace the chemical evolution of their host galaxies and thus provide clues to the evolutionary histories of different types of galaxies. Star clusters are relatively simple single stellar populations. They are generally regarded as single-age and single-metallicity objects, which makes them a unique and powerful diagnostic tool in the study of galactic star formation histories. Nevertheless, the disadvantage of using star clusters as tracers of galaxy evolution is that the number of these objects observable in a galaxy varies from galaxy to galaxy (e.g., Grebel 2000; Brodie & Strader 2006). Moreover, their properties may not necessarily be representative of the field star population in the host galaxy.

Most studies of unresolved cluster populations suffer from a degeneracy between age and metallicity. This means that it is impossible by photometric observations to measure both properties simultaneously. One important means to break this degeneracy is the spectroscopy, ideally of individual stars. Up to date star clusters can only be resolved within our own Galaxy and in our closest neighbors, e.g., the Magellanic Clouds. Therefore, the star clusters in the Magellanic Clouds (MCs) play a key role for understanding properties of unresolved star clusters. They allow a detailed view on the chemical evolution of irregular galaxies.

The MCs are two of our nearest Galactic neighbors and provide a very important laboratory for the study of galaxy evolution. Their proximity enables us to resolve stellar populations well below the oldest main sequence turn offs and thus permits reliable age dating. In contrast to the studies of Galactic globular clusters, which are often plagued by dust and gas obscuring much of the Galactic disk and bulge, the MCs suffer only little from foreground extinction. Although the Small Magellanic Cloud (SMC) is, at a distance of  $D \approx 63$  kpc (Olszewski et al. 1996), 20% farther away than the Large Magellanic Cloud (LMC;  $D \approx 50$  kpc), the system can still be resolved into individual stars, which allows for accurate age dating of the star clusters via isochrone fits.

The LMC hosts a multitude of star clusters, which have been cataloged by Bica et al. (1999). There is a large number of both old and metal-poor and young and metal-rich clusters, but apparently only one cluster of intermediate age in the range from approximately 4 to 9 Gyr (Mateo et al. 1986). Previous studies showed that the LMC has experienced a complex star formation history. The age distribution of the LMC indicates a bursty star formation history (Olszewski et al. 1996; Geisler et al. 1997). The reason for the onset and cessation of star cluster formation remains yet unknown and is not seen in the field star population (Cole et al. 2005).

Despite the close interaction with the LMC, the SMC seems to have undergone a different formation history. In particular, its cluster population does not show any sign of a substantial age gap. In fact, the SMC is the only dwarf galaxy in the Local Group known to have formed and preserved massive ( $M > 10^4 M_{\odot}$ ) star clusters continuously over the past 12 Gyr (Olszewski et al. 1996). Nevertheless, various research groups (e.g., Rich et al. 2000; Piatti et al. 2001) suggest that also the SMC has experienced episodes of stronger and weaker star cluster formation. This episodic cluster formation is not as pronounced as in the LMC.



**Figure 5.1:** Optical image of the SMC.

source: <http://www.astrooptik.com/Bildergalerie/Deltagraph/Wallner/smc.jpg>

Generally the SMC seems to be the simpler one of the two clouds, with a more continuous star formation history. Although the star cluster population of the SMC is not as populous as that of the LMC, the presence of star clusters of all ages is a big advantage in the study of the chemical evolution of the MCs. The fact that its cluster population covers the full range of all ages makes the SMC ideally suited for the derivation of a well-defined age-metallicity relation.

However, to the present time, spectroscopically based metallicity estimates exist only for a small number of seven clusters. Six of them were studied by Da Costa & Hatzidimitriou (1998) and the seventh, the brightest and very young SMC cluster NGC 330, by various groups (e.g., Meliani et al. 1995; Hill 1999; Gonzalez & Wallerstein 1999). All abundance estimates of the other clusters are purely based on photometric observations, obtained through a medley of heterogeneous methods. Examples of the applied methods are the simultaneous reddening and metallicity method by Sarajedini (1994) or the comparison of the color of the cluster RGB with standard RGBs by Geisler & Sarajedini (1999). All these methods suffer severely from the age-metallicity degeneracy.

The age determinations suffer from a similar difficulty. Deep high-resolution data obtained with the Hubble Space Telescope (HST) are currently available only for a subset of the SMC clusters. The remaining age estimates arise from a variety of ground-based observations (e.g., Mighell et al. 1998; de Freitas Pacheco et al. 1998; Piatti et al. 2001) of variable quality and often of insufficient depth to fully gain access to the age-sensitive regions of the main-sequence turn-off (MSTO) and subgiant branch (SGB). This means that no large uniform data set exists at present, neither for metallicities nor for ages.

In order to alleviate many of these uncertainties we requested for spectroscopy and deep photometry with the Very Large Telescope (VLT) and HST for a statistically significant sample of SMC clusters. The photometry with the Advanced Camera for Surveys (ACS) on HST allows us to accurately and self-consistently date the clusters via simultaneous fitting of signature populations such as MSTO, SGB, and red clump/horizontal branch stars (see Glatt et al. 2008). This part of the project includes seven star clusters. In the spectroscopic part of our project we aim to more than double the available spectroscopic data set by the observation of ten additional clusters (Kayser et al. 2008b). In this work we determine the metallicity of each cluster via Ca II triplet measurements in individual cluster red giants. Selecting a closely spaced set of clusters by their ages, we obtain a well sampled age-metallicity relation for the SMC that is fully based on spectroscopic metallicity measurements. The resulting relation allows new implications for the chemical evolution of the SMC.

The present chapter of this thesis focuses on the spectroscopic part of the project and is structured as follows: § 5.2 introduces the target selection, data collection, and data reduction. The method used to measure metallicities is explained in § 5.3. In § 5.4 this method is applied to determine the metallicities of the individual red giants within the clusters. In § 5.5 we carefully select the cluster members and calculate the cluster metallicities. The results and conclusions on the star formation history of the SMC are presented in § 5.6. After a detailed discussion of the outcomes we give a summary of this work in § 5.7.

## 5.2 Data

### 5.2.1 Target selection

In order to obtain a homogeneous sampling of the SMC's star formation history (SFH), we sought for a set of spectroscopic and deep photometric data for a statistically significant sample of star clusters in the SMC. To tie our observations to the previous study by Da Costa & Hatzidimitriou (1998) we observed spectra of the near-infrared (IR) Ca II triplet (CaT) region of individual red giants in twelve different clusters. We selected primarily those clusters that have only been observed photometrically so far, namely Lindsay 116, Lindsay 32, Lindsay 38, Kron 28, Kron 44, NGC 152, NGC 361, NGC 411, NGC 416, and NGC 419. In order to be able to assess the consistency of our measurements with those by Da Costa & Hatzidimitriou (1998), we selected two clusters to coincide with their sample (Lindsay 11 and NGC 339). The cluster sample was selected to cover a large spatial area of the SMC in order to search for potential metallicity gradients. Our targets are located across the main body of the SMC, from the central bar (at R.A.(J2000)=  $00^h52^m45^s$ , DEC.(J2000)=  $-72^\circ49'43''$ ) (Crowl et al. 2001) out to a projected distance of 7 kpc. Thereby we sample a range of (diverse) environments within the galaxy, from the dense central regions to low density regions in the outskirts. Furthermore, in combination with the seven (five additional) previously spectroscopically studied clusters of Da Costa & Hatzidimitriou (1998) we now cover the largest possible range in age (12 Gyr). The expected range in metallicity, based on previous spectroscopic and photometric estimates, is approximately  $-0.6$  to  $-1.6$  dex. For calibration purposes we also obtained spectra of red giants in three Galactic globular clusters (NGC 104, NGC 362 and NGC 7099). An overview of the spatial distribution of the selected target clusters in the direction of the SMC with respect to the photometric catalog by Zaritsky et al. (2002) is shown in Fig. 5.2.

The first part of the observations consisted of short imaging exposures in the Bessell  $V$

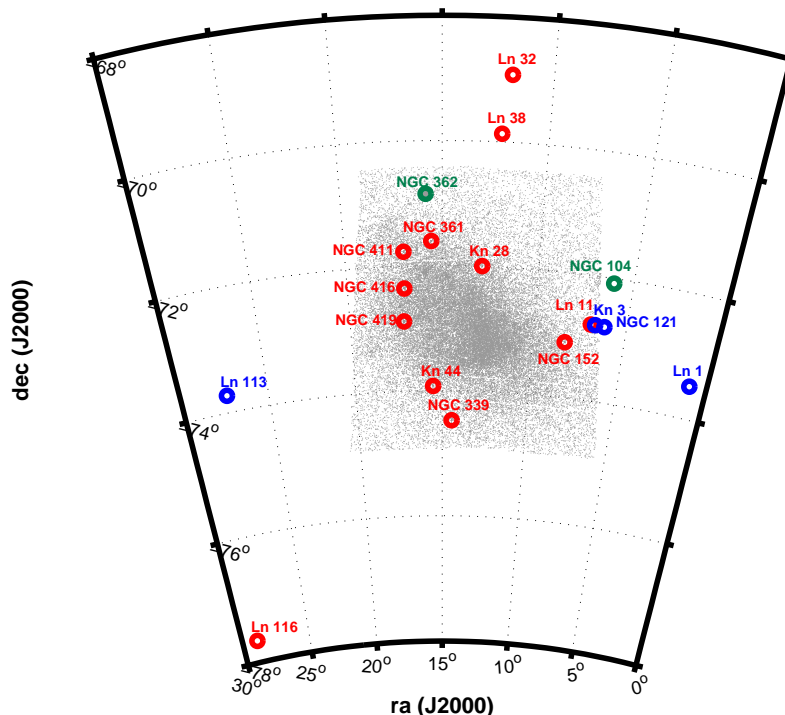


**Figure 5.2:** Position of the targeted SMC star clusters (red circles) and two of our calibrating MW globular clusters (green circles) with respect to the Zaritzky et al. catalog (Zaritzky et al. 2002) (small gray dots). The location of the four additional clusters studied by Da Costa & Hatzidimitriou (1998) are indicated in blue.

and  $I$  filters for the three MW clusters and  $V$  and  $B$  filters for the twelve SMC clusters. These so-called Pre-Images were taken during seven nights in April and June 2004 at the Very Large Telescope (VLT) of the European South Observatory (ESO) at Cerro Paranal, Chile. The instrument in use was the FORS2 (FOcal Reducer and low dispersion Spectrograph) installed on the Cassegrain focus of the VLT Unit Telescope 4. The Pre-Images were obtained in order to select suitable target stars for the subsequent spectroscopic observations. Since the CaT method is only well calibrated for (bright) red giants, we targeted stars on the upper RGB in the SMC clusters with  $15.5 \lesssim V \lesssim 18.5$  mag, i.e., from the tip of the RGB to  $\approx 3$  mag below. To avoid saturation, typical exposure times were about 10 s in  $I$  and 20 s in  $V$ . For the more luminous Galactic GCs exposure times of 1–3 seconds in both filters ( $V$  and  $B$ ) were sufficient. These short exposure images were provided pipeline-reduced by ESO.

Follow-up PSF-photometry was used for the target selection for the later spectroscopy. For a more detailed description see Chapter 4. We restricted our spectroscopic observations to stars on the upper RGB. Down to approximately 2 mag below the tip of the RGB ( $V \sim 16.5$  mag) stars were selected as first priority candidates. Adopting a  $V$  band distance modulus for the SMC of 18.9 mag (Westerlund 1997) this corresponds to an absolute visual magnitude of  $M_V \sim -2.4$  mag. Stars with magnitudes of the order of the red clump brightness at  $\approx 17$  mag and brighter were selected as second priority candidates for the spectroscopy. Using the color-magnitude diagrams these selection criteria were adopted for each cluster individually by eye according to their stellar content. Thus, the actual magnitude ranges vary from cluster to cluster. This classification in two priority classes was made since for

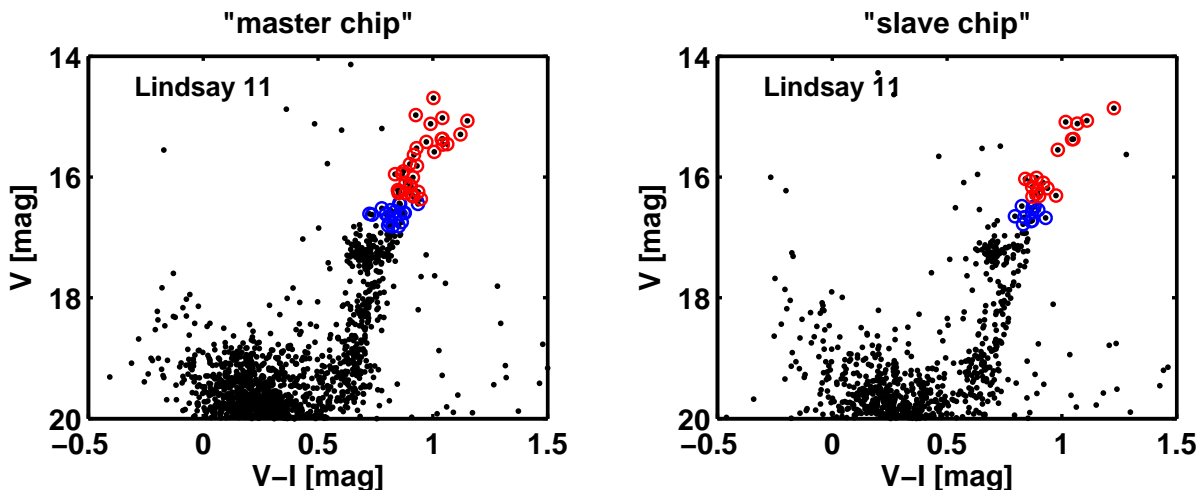


**Figure 5.3:** Selection of our spectroscopic targets from the Pre-Imaging photometry for the SMC cluster Lindsay 11 from the two FORS CCDs (master and slave). First priority candidates for the spectroscopy are marked by red circles, second priority candidates by blue circles.

the brighter objects we expected to receive spectra with higher signal-to-noise ratios. Fig. 5.3 shows the high and low priority targets for the cluster Lindsay 11 in red and blue, respectively.

For each cluster we designed a slit mask using ESO's FORS Instrumental Mask Simulator (FIMS). Typically 20 to 30 high priority candidates and additional 10 to 15 low priority stars were selected for each mask. Only isolated stars were chosen to avoid the blending of light from close/adjacent stars. We used a fixed slit width of  $1''$  according to the subarcsecond seeing conditions on Paranal. The slit length varied between  $5\text{--}8''$ . This allowed us to observe the local sky background within the same slit for each object.

### 5.2.2 Observations

All spectroscopic observations were carried out in service mode at the VLT during eleven nights between September 2004 and July 2006. For the spectroscopic observations we used again the FORS2 instrument at the VLT Unit Telescope 1, which was already used to obtain the Pre-Images. This setup provides a field of view (FoV) of  $6'.8 \times 6'.8$ . FORS2 is equipped with a mosaic of two  $2k \times 4k$  MIT CCDs (pixel size of  $15 \times 15 \mu\text{m}$ ) with a pixel scale of  $0''.25/\text{pixel}$ , using the default readout mode (2 by 2 binning) and the standard resolution collimator. The two parts of the CCD mosaics are mounted with an offset perpendicular to the optical axis to ensure that the center of the FoV does not coincide with the gap between the two CCDs. The CCD containing the center of the FoV is called *master* while the CCD recording the smaller portion of the FoV is called *slave*. The detector system works with a gain factor of  $1.43 \text{ ADU } e^{-1}$  ( $0.7 \text{ e ADU}^{-1}$ ) and readout noise of 2.7 and  $3.0 \text{ e}^{-1}$  for master and slave, respectively. For spectroscopic observations FORS2 is equipped with the multi-object facility MXU (Mask EXchange Unit). MXU can be loaded during the day with up to ten slit masks which are then available for the observation during the night.

The grism best suited for CaT observations with FORS2 carries the ESO denotation 1028x+29 and is used in combination with the OG590+32 order blocking filter. This results in a resolving power of  $R \sim 3400$ . In the  $2 \times 2$  binning mode this setup yields a dispersion

of  $0.85 \text{ \AA}/\text{pixel}$  and a spectral coverage of  $\approx 7730\text{--}9480 \text{ \AA}$  for a slit located in the field center. The actual covered wavelength range of individual spectra depends on the position in dispersion direction of the according slit on the mask.

Each mask was observed for 1900 s split into four exposures of 475 s each in order to facilitate cosmic ray removal. This yields a S/N of  $> 30$  /pixel for the SMC star clusters. For the Galactic GCs the observing blocks consisted of five exposures of 20 s each. The observing nights were clear, resulting in a typical seeing of  $0.6''\text{--}1.0''$ . The observing log is given in Table 5.1.

Additional standard calibration exposures were taken according to the ESO daytime calibration plan. These consist of bias frames, internal screen flat fields, and arc spectra from a He-Ne-Ar lamp.

### 5.2.3 Data reduction

The data were processed using standard routines in IRAF<sup>1</sup>. For each night the bias exposures were combined and subtracted from the corresponding flat field, science, and arclamp exposures. Afterwards the sets of flatfields and science exposures were combined. A careful choice of sigma clipping parameters eliminates cosmic ray hits.

Before the extraction of the spectra all science and lamp exposures were corrected for the pixel-to-pixel variation of the sensitivity of the CCD by flat-field correction. Depending on the spatial position (y-position) on the CCD, through-slit exposures (i.e., science, flat-field, and lamp images) are geometrically distorted by the instrument. The distortion effect is minimized near the center of the field of view and increases towards the edges. We mapped the distortion

<sup>1</sup>IRAF is distributed by the National Optical Astronomy Observatories, which are operated by the Association of Universities for Research in Astronomy, Inc., under cooperative agreement with the National Science Foundation.

**Table 5.1:** Observation log of spectroscopic observations.

Name	Date	$\alpha$ (J2000)	$\delta$ (J2000)	Exposure Time [s]	Seeing [arcsec]	Airmass
Kron 28	2005-07-09	00:51:24	-72:01:02	4× 475	0.66	1.576
Kron 44	2005-08-06	01:02:03	-73:56:43	4× 475	0.60	1.656
Lindsay 11	2005-07-09	00:27:45	-72:47:55	4× 475	0.83	1.641
Lindsay 116	2005-09-12	01:55:27	-77:40:01	4× 475	0.93	1.72
Lindsay 32	2005-07-10	00:47:20	-68:56:29	4× 475	0.68	1.739
Lindsay 38	2005-12-22	00:48:53	-69:53:40	4× 475	0.78	1.514
NGC 152	2005-06-10	00:33:03	-73:08:08	4× 475	0.62	1.746
NGC 339	2005-08-08	00:57:48	-74:29:33	4× 475	0.65	1.666
NGC 361	2004-09-25	01:02:10	-71:37:32	4× 475	0.44	1.472
NGC 411	2006-07-03	01:07:49	-71:44:25	4× 475	1.01	1.605
NGC 416	2005-08-08	01:07:58	-72:22:25	4× 475	0.82	1.724
NGC 419	2005-07-09	01:08:17	-72:54:03	4× 475	0.76	1.529
NGC 104	2005-06-08	00:22:46	-72:04:27	5× 20	0.63	1.585
NGC 362	2005-08-08	01:03:00	-70:48:17	5× 20	0.61	1.751
NGC 7099	2004-05-23	21:40:27	-23:09:30	5× 20	0.63	1.009

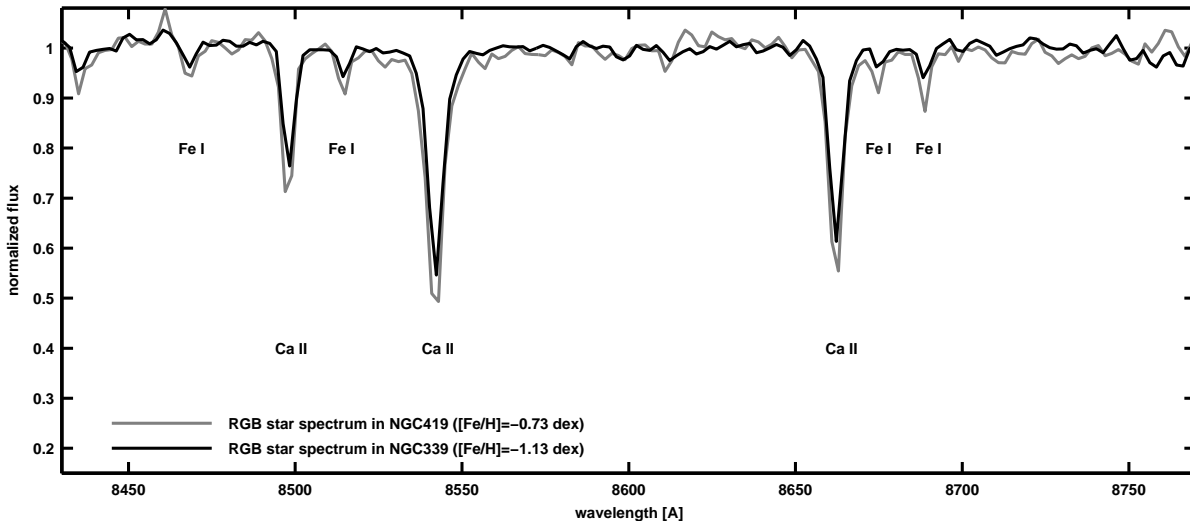


**Figure 5.4:** Observed spectra of RGB stars in two different SMC star clusters centered on the near IR CaT region. Stars with approximately the same  $V$  magnitude were chosen. The spectra have been sky-subtracted, continuum normalized, and corrected for Doppler-shifts.

for each slit individually. For each slit we defined the aperture on the flatfield and traced it over the full extent of the image. The tracing parameters were then transferred to the science and lamp exposures. For each aperture the response function was fitted in dispersion direction on the flatfields using a low order cubic spline. The IRAF task `response` creates a normalized pixel-to-pixel flatfield, which was applied for the correction of the illumination response to the corresponding science and lamp exposures.

For the dispersion correction the strong emission lines in the He-Ne-Ar lamp spectra were used to determine the wavelength solution for the science spectra. Since the individual wavelength coverage depends on the position of the slit on the mask, each slit had to be considered separately. Typically 15 to 20 arc lines well distributed over the wavelength range were included. Overall, the r.m.s. scatter for the wavelength calibration was found to be of the order of  $0.02 \text{ \AA}$ , which is equivalent to an uncertainty of  $0.7 \text{ km/s}$  at the wavelength of the CaT ( $8500 \text{ \AA}$ ).

One-dimensional spectra were extracted for each slit using the tasks `apall` and `apextract`. For each spectrum the local sky background was selected and extracted from the same slit. Therefore each profile was examined along the spatial axis in order to identify satisfactory intervals to fit the sky level. The sky was modeled in wavelength direction and subtracted from the spectrum. For the further analysis all spectra were continuum normalized by a low-order spline excluding the regions of the strong Ca II absorption features.

The resulting mean S/N is about  $70 \text{ pixel}^{-1}$ , exceeding  $100 \text{ pixel}^{-1}$  for the brightest stars. Sample spectra of two RGB stars showing the prominent near IR Ca II triplet absorption lines at  $\lambda\lambda 8498, 8542, \text{ and } 8662 \text{ \AA}$  are presented in Fig. 5.4. These spectra were selected such that the stars have approximately the same  $V$  magnitude. Thus, the visible difference in line strengths between the two spectra is entirely caused by metallicity differences rather than by effects of temperature or surface gravity.



### 5.3 Calcium triplet metallicities

The near-IR CaT technique is an ideal tool for studying the metal content in resolved, low-surface-brightness objects like dwarf spheroidal galaxies and high-surface-brightness objects like globular clusters. It is particularly useful for the investigation of old and intermediate age stellar populations. The method has been devised for evolved red giant stars, which are among the brightest objects these stellar populations. In these stars, the CaT provides the strongest lines in the 8500 Å region, making them easy to identify. The lines arise from an excited state of Ca, which means that no correction for interstellar Ca absorption is necessary (Cole et al. 2004). Furthermore, the CaT technique focuses on the examination of RGB stars in a spectral regime where their energy distribution is close to its maximum. An additional benefit is that the sensitivity of most of the detectors is significantly higher in the near IR than in the blue. This allows the integration times to be kept reasonably short. Using an 8 m class telescope they are of the order of a few minutes for Galactic objects and few hours for stars in Milky Way companions. Moreover with today's multi-object spectrographs it is possible to obtain a large amount of spectra within one go.

Despite all these advantages it seems at first sight not very trustable to use Ca as a metallicity indicator, since Ca and Fe are produced in different nucleosynthesis processes and returned to the interstellar medium via different mechanisms (supernovae type II and type I, respectively). However Armandroff & Zinn (1988) demonstrated that the strength of the CaT lines is strongly correlated with metallicity. In a more detailed analysis Diaz et al. (1989) investigated the dependence of the CaT on stellar atmospheric parameters in 106 late type stars and 3 globular clusters. They found a biparametrical behavior with 98% of the variance resulting from a linear combination of  $\log g$  and metallicity. It is well known that the ratio of  $\alpha$  to iron-peak elements varies between different environments (Shetrone et al. 2001; Pritzl et al. 2005). Nevertheless, various detailed abundance studies have revealed that although Ca is an  $\alpha$ -element it correlates well with overall metal abundance of intermediate age and old populations in nearby galaxies (e.g., Koch et al. 2006; Battaglia et al. 2007). The low resolution CaT spectroscopic estimates of the overall metallicities agree well (to  $\pm 0.1 - 0.2$  dex) with high resolution spectroscopic determinations from the same stars.

The use of the near IR CaT lines as a measure of the metallicity of simple-stellar population was developed by Armandroff & Zinn (1988) for integrated spectra of Galactic globular clusters. The basis of this method is the measurement of the line-strength of the individual Ca II lines with respect to a pseudo-continuum. Therefore the definition of two or three bandpasses per line is necessary, one covering the line to be measured and ideally two line free regions on either side for the continuum. (For spectral regions with a flat continuum one neighboring bandpass is sufficient.) The continuum above the absorption line is defined by the linear interpolation of the average intensities in the neighboring windows. This continuum is lower than the true continuum since it is estimated by an average including small absorption lines. Thus it is referred to as a pseudo-continuum. Fortunately the spectrum is fairly flat in the Ca triplet region, allowing the clear definition of the pseudo-continuum. Accordingly, the measured equivalent width with respect to the pseudo-continuum is referred to as the pseudo-equivalent width. Armandroff & Zinn (1988) calculated the sum of the pseudo-equivalent widths ( $\Sigma W$ ) of the three lines.  $\Sigma W$  was found to be well correlated with various previously used metallicity indicators such as photometric metallicities, other line indices, and metallicities from integrated light measurements by Zinn & West (1984) (hereafter ZW84).

Later Armandroff & Da Costa (1991) investigated the suitability of this method as a metallicity indicator for individual red giants in Galactic globular clusters. Apart from metallicity itself, the strength of the Ca absorption lines is strongly dependent on the surface gravity of the star ( $\log g$ ) and to a lesser degree on its effective temperature ( $T_{\text{eff}}$ ). In order to remove the dependence on  $\log g$  and  $T_{\text{eff}}$  Armandroff & Da Costa (1991) suggested to use the CaT index ( $\Sigma W$ ) in terms of the  $V$  magnitude difference from the horizontal branch (HB). They found a simple linear relation between  $\Sigma W$  and the  $V$  magnitude such that stars further up the RGB have lower  $\log g$ , resulting in a larger  $\Sigma W$ . They introduced the term *reduced equivalent width*

$$W' = \Sigma W + \beta(V - V_{\text{HB}}), \quad (5.1)$$

as a parameter purely dependent on metallicity.

It could be shown empirically that the value of  $\beta$  is nearly independent of the cluster metallicity (Armandroff & Da Costa 1991). The use of only relative luminosities furthermore avoids uncertainties due to cluster distance measurements and reddening determinations. On the ZW84-scale Armandroff & Da Costa (1991) found a linear abundance sensitivity for metallicities lower than  $[\text{Fe}/\text{H}]_{\text{ZW84}} = -1.2$  dex. For higher metallicities up to  $[\text{Fe}/\text{H}]_{\text{ZW84}} = -0.7$  dex they approximated the relation between  $W'$  and  $[\text{Fe}/\text{H}]$  by a cubic fit.

Rutledge et al. (1997a,b) were able to extend this calibration to  $-2.1 < [\text{Fe}/\text{H}]_{\text{ZW84}} < -0.6$  dex and  $9 < \text{age} < 13$  Gyr. Furthermore, they compared the correlation of  $\Sigma W$  with metallicity on different scales. In contrast to the ZW84-scale, which causes a curvature in the metallicity calibration, they found a linear relation of  $\Sigma W$  with the results from the high dispersion spectroscopy of Galactic globular clusters by Carretta & Gratton (1997) (hereafter CG97) over the whole metallicity range. However, due to the calibration via Galactic GCs, this method was still restricted to predominantly low metallicities and old ages.

Including younger open clusters in the Milky Way from the compilation of Friel et al. (2002), Cole et al. (2004) could extend this linear correlation to higher metallicities and younger ages. They confirmed the applicability of the CaT calibration method for a metallicity range of  $-2.1 < [\text{Fe}/\text{H}]_{\text{GC97}}^{\text{F02}} < -0.2$  dex and an age range of  $2.5 < \text{age} < 13$  Gyr. Their study indicated no influence of the age across the range of ages investigated.

Recently Kraft & Ivans (2003) established a new metallicity scale for globular clusters based on the equivalent widths of FeII lines measured from high-resolution spectra in red giants. This scale is also linearly correlated with the reduced equivalent width. Carrera et al. (2007) investigated CaT observations of RGB stars in 29 Galactic open and globular clusters and considered all three common metallicity scales. Their resulting relationships between  $\Sigma W$  and the various scales cover the largest range in age ( $0.25 < \text{age} < 13$  Gyr) and metallicity  $-2.2 < [\text{Fe}/\text{H}] < +0.47$  dex so far.

The recent extension of the CaT calibration to higher metallicities and younger ages now covers the complete parameter range into which the SMC clusters are expected to fall. Therefore this method is the ideal means to determine accurate metallicities in these clusters. It provides the best compromise between precise but time-consuming high resolution spectroscopy and faster but inaccurate photometric metallicity measurements. It is faster than high-resolution spectroscopy, which requires much longer integration times and would include fewer stars per exposure. It is more accurate than photometric estimates, which suffer from the age-metallicity degeneracy.

Nowadays the CaT method is one of the most widely applied techniques for to derive the metallicity of individual RGs. Originally calibrated using Galactic star clusters this method

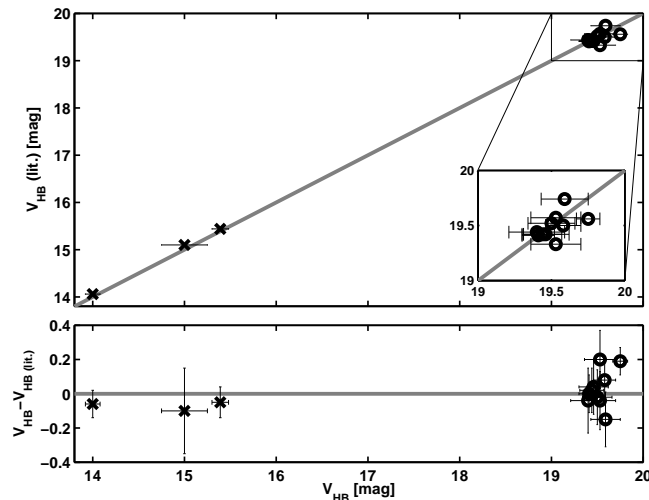


**Figure 5.5:** Comparison of the measured horizontal branch/red clump magnitudes with literature data. The solid line indicates identity. The MW globular clusters are marked as crosses, the SMC star clusters are marked as open circles.

is now applied in many studies on nearby extragalactic objects like dwarf spheroidal galaxies (e.g., Pont et al. 2004; Koch et al. 2006), the Magellanic Clouds (SMC: Da Costa & Hatzidimitriou (1998) and LMC: e.g., Olszewski et al. (1991); Cole et al. (2000); Grocholski et al. (2006)), and M31 (e.g., Reitzel & Guhathakurta 2002; Chapman et al. 2006). Nevertheless, no standardized use has been established yet. Depending on the quality of the data some groups consider only the two strongest or all three Ca lines. Furthermore, the use of both, a weighted and unweighted mean to calculate  $\Sigma W$  can be found in the literature. Hence the derived steepness of the slope  $\beta$  varies between 0.64 (Rutledge et al. 1997a), 0.73 (Cole et al. 2004) and 0.55 (Koch et al. 2006). For the metallicity calibration, in most recent studies the metallicity scale defined by CG97 scale was preferred over the ZW84-scale, because the former does not cause any curvature in the metallicity calibration. However, there is no a priori reason to prefer the one or the other scale.

## 5.4 Metallicity determination

### 5.4.1 ( $V - V_{HB}$ )

In order to calculate the reduced equivalent width  $W'$  for each stellar spectrum, it is essential to know the star's magnitude difference from the apparent magnitude of the HB. This requires the knowledge of  $V_{HB}$  for all clusters in our sample. Since these young and relatively metal-rich clusters do not have HB stars, we instead rely on the luminosity of the red clump (RC) of core He-burning stars. It is important to point out that although we consider the RC we keep the standard nomenclature  $V_{HB}$ . Following Grocholski et al. (2006) we consider  $V_{HB}$  as equivalent to  $V_{RC}$ .

Unfortunately, RC luminosity estimates can be found in the literature only for few of our sample clusters. Therefore we (re)derived the median  $V$  magnitude of data points of the RC in the CMD of each cluster to get an estimate for the  $V_{HB}$  values. To avoid a large contamination by SMC field stars we considered only those stars within a projected distance

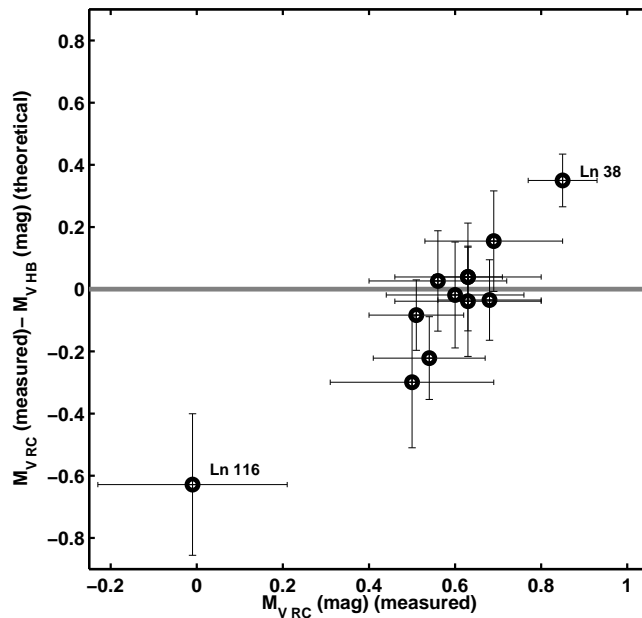


**Figure 5.6:** Comparison of measured red clump magnitudes with theoretical horizontal branch magnitudes. The solid line indicates identity. The two deviating clusters are labeled with their names.

of less than five times the core radius (known from Kayser et al. (2008a), see Chapter 4) from the cluster center. For the very sparse cluster Lindsay 116 this resulted in too few stars and we had to include all stars in the sample in order to obtain an estimate for the RC magnitude. The errors on the resulting metallicities, introduced by the RC determinations, were taken as the standard error of the median and are of the order of 0.15 mag. Tests of randomly assigning HB levels to stars in star clusters showed that variations of the luminosity of the cluster HB levels of the order of 0.4 mag in  $V$  can produce changes in the metallicity estimates the order of 0.05 to 0.1 dex (see, Cole et al. 2004; Koch et al. 2007). Our uncertainties in the RC determination are much smaller than the adopted HB magnitude variations in these test and are therefore negligible within in the metallicity errors.

For those clusters, for which values for the RC/HB magnitudes exist in the literature, we find good agreement with our newly derived apparent magnitudes. The r.m.s. scatter around unity is 0.11 mag. The comparison between the literature values and our measurements for the three MW globular clusters and ten SMC clusters is shown in Fig. 5.5. Adopting the RC magnitude as reference we achieved an estimate for  $(V - V_{HB})$  for each star.

For an additional test we adopted the standard distance modulus of the SMC of  $dm = 18.9$  (Westerlund 1997) and for simplification assume that all clusters lie at the same distance. Thus, we can estimate the absolute magnitude of the RCs of the clusters ( $M_{VRC}$ ). Furthermore, the relation of the absolute  $V$  magnitude of the zero age horizontal branch (i.e., the level of the RR Lyae stars) with metallicity allows to calculate a theoretical value of the HB magnitude ( $M_{VHB}$ ) (see Sandage & Tammann 2006):

$$M_{VHB} = 1.109 + 0.600 ([Fe/H]) + 0.140 ([Fe/H])^2. \quad (5.2)$$

Fig. 5.6 shows a comparison between the measured and theoretical absolute magnitudes. The values scatter around identity with a standard deviation of 0.24 mag, which is expected

due to neglected depth of the SMC. The two clusters deviating most are Lindsay 116 and Lindsay 38. This is also not surprising, since previous studies showed that Lindsay 38 is located in the rear part of the SMC and Lindsay 116 is likely to be an LMC cluster, i.e., located in the foreground of the SMC (Crowl et al. 2001; Piatti et al. 2001). Under consideration of these caveats we find the measured and theoretical values to be in good agreement.

### 5.4.2 Velocities

The radial velocities are important for two reasons. First, they are necessary to correct for the Doppler-shift of the spectrum. This is essential for a correct measurements of the EW because the individual relative velocity of a star shifts the position of the spectrum with respect to the bandpasses. This can cause changes in the continuum and thus in the measured EWs. Second, the velocities are an important criterion for the SMC cluster membership of a star. Due to the systemic velocity of  $\approx 158$  km/s (Karachentsev et al. 2004), SMC stars can be easily separated from Galactic foreground stars. We also expect the cluster members to stand out in the velocity against the underlying SMC field stars (see 5.5.1).

The velocity of each star was measured by cross-correlating the star spectrum with a zero-velocity template spectrum. We used a well established synthetic spectrum of the three near IR CaT lines with equivalent widths representative of those in K-giants (Kleyna et al. 2002) as a template spectrum. In practice, this method was applied within IRAF’s task `fxcor` and allowed for an accuracy of  $\approx 5$  km/s. All velocities were corrected for heliocentric motion. For a more detailed description see Chapter 4.

### 5.4.3 [Fe/H] for individual RBs

In order to measure the equivalent widths in individual stars we used a heavily modified version of Da Costa’s EWPROG-code modified and kindly provided by A. Cole. This program is based on the original idea of Armandroff & Zinn (1988) of the use of three bandpasses. Cole et al. (2004) suggested that a profile consisting of a combination of a Gaussian core with Lorentzian wings with a common line center provides a better fit to the CaT. Especially for higher metallicities sensitivity was lost before, since pure Gaussian profiles failed to take care of the extremely broad wings of the lines. Furthermore, the present method is an improvement compared to estimating the line strengths via numerical integration, because it ensures metallicity sensitivity in the high metallicity range where the contribution of the wings increases (e.g., Koch et al. 2007). Prior to the fitting of the lines, the positions of the bandpasses are adjusted according to the shifts due to the radial velocity of each star. The windows chosen in a zero-velocity spectrum are given in Table 5.2. These bandpass definitions are identical to the original bandpasses from Armandroff & Zinn (1988). Errors of the pseudo EW arise from the residuals of the fit (Cole et al. 2004).

**Table 5.2:** Bandpass definition.

Feature	Line Bandpass [Å]	Blue Continuum [Å]	Red Continuum [Å]
Ca II $\lambda$ 8498	8490 – 8506	8474 – 8489	8521 – 8531
Ca II $\lambda$ 8542	8532 – 8552	8521 – 8531	8555 – 8595
Ca II $\lambda$ 8662	8653 – 8671	8626 – 8650	8695 – 8725

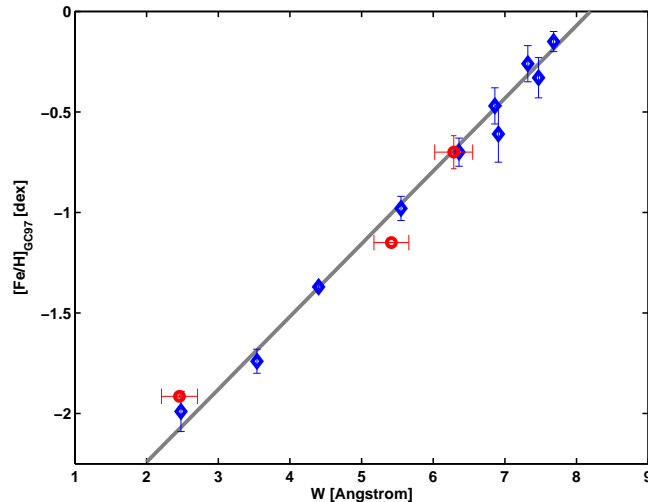


**Figure 5.7:** Measured  $W'$  for the three MW clusters (red open circles) from our project vs. their according metallicities on the GC97 scale. The Galactic globular clusters and open star clusters used by Cole et al. (2004) to define the calibration are plotted as blue open diamonds. The derived metallicity calibration of  $W'$  is indicated by the solid line.

Since our observations are of good spectral quality i.e., high S/N ratios and since they were performed with the same telescope and instrumental setup as those of Grocholski et al. (2006) and Cole et al. (2004), we followed their prescription and defined  $\Sigma W$  as the unweighted linear combination of all three lines:

$$\Sigma W = W_{8498} + W_{8542} + W_{8662}. \quad (5.3)$$

As mentioned above, a variety of estimates for the steepness of the slope ( $\beta$ ) exist in the literature, which are mostly based on studies of the globular clusters in the Milky Way. Since the SMC clusters are known to be fairly young compared to Galactic globular clusters we decided to adopt the value derived by Cole et al. (2004) because they include young open clusters in the MW into their calibration:

$$W' = \Sigma W + (0.73 \pm 0.04)(V - V_{\text{HB}}). \quad (5.4)$$

We checked for consistency with the Cole et al. (2004) calibration by calculating the  $W'$  for the three Galactic globular clusters in our sample (NGC 104, NGC 362, and NGC 7099) following the procedure described above. We adopted metallicities for these clusters from Rutledge et al. (1997b) on the Carretta & Gratton-scale. In Fig. 5.7 we compare the positions of these three data points from our Galactic clusters to the measurement of Galactic globular clusters and open star clusters used by Cole et al. (2004) to derive the calibration; (see Figure 4 in their paper). We find good agreement for all three data-points. The largest discrepancies are observed for the cluster NGC 7099, which is near the very low metallicity calibration limit of the CaT method. However, the SMC clusters do not reach this limit. We are therefore confident that we can adopt the CaT calibration of Cole et al. (2004) for our purposes. In Table 5.3 we list the parameters for the Galactic globular clusters used to check the consistency of the calibration.

**Table 5.3:** Parameters of Calibrating Galactic Globular Clusters.

cluster	$W'$ (this work) Å	$W'$ (Lit.) Å	$[\text{Fe}/\text{H}]_{\text{CG97}}^a$ [dex]	$V_{\text{HB}}^b$ [mag]
NGC 104	$6.67 \pm 0.10$	6.36	$-0.69 \pm 0.05$	14.06
NGC 362	$6.39 \pm 0.06$		$-1.09 \pm 0.03$	15.44
NGC 7099	$3.51 \pm 0.06$		$-1.92 \pm 0.04$	15.10

<sup>a</sup>Rutledge et al. (1997b) <sup>b</sup>Harris (1996)

The reduced equivalent widths were converted to metallicity estimates following Cole et al. (2004) who used the metallicity scales of Carretta & Gratton (1997) and Friel et al. (2002) for Galactic globular clusters and open clusters, respectively. Their empirical linear relation is:

$$[\text{Fe}/\text{H}] = (-2.966 \pm 0.032) + (0.362 \pm 0.014)W'. \quad (5.5)$$

Note that they did not find any indication for an age effect in this calibration.

## 5.5 Analysis of the star clusters

### 5.5.1 Membership

Given the SMC's high Galactic latitude of  $l \sim 45$  (Karachentsev et al. 2004), we expect to suffer only marginally from stellar Milky Way foreground contamination. The table of Milky Way field star densities by Ratnatunga & Bahcall (1985) predicts in the direction towards the SMC in the color range of  $0.8 < (B - V) < 1.3$  and for apparent visual magnitudes of  $17 < V < 19$  mag  $9.3 \cdot 10^{-2}$  Galactic field stars per square arcmin. This yields a total of only four stars for the field of view of the VLT/FORS2.

A much larger problem is the contamination of our cluster star sample by SMC field stars. This varies to a large extent throughout our sample of star clusters. For star clusters located close to the main body of the SMC (e.g., Kron 28) this effect is more severe than for the clusters at larger distances from the SMC center (e.g., Lindsay 116). It is therefore essential to carefully select the probable cluster member candidates. In order to assess the cluster members and minimize the effects by outliers in our results we used the four different selection criteria described below. For reference a complete list of the targeted stars listing their positions,  $V$  and  $I$  luminosities,  $V - V_{\text{HB}}$ , measured  $\Sigma W$ , derived metallicities and a flag indicating if their passed the various membership criteria is given by the tables in the appendix to this chapter. The flag is coded as follows: 1 means that the star passed the corresponding membership criterion, 0 means it did not pass the criterion. The transformation from the pixel coordinate system to the R.A. and DEC. positions is performed using the `wcsctran` tool within IRAF.

### Velocities

With a systemic heliocentric velocity of  $\approx 158$  km/s (Karachentsev et al. 2004) and a velocity dispersion of 28 km/s of the red giant population (Harris & Zaritsky 2006), the SMC clearly

stands out against the Milky Way foreground stars. We are therefore confident to successfully identify and sort out the foreground stars by their velocities.

Within the SMC the observed heliocentric velocities range from  $\approx 40$  to 240 km/s (Harris & Zaritsky 2006). The fields analyzed in this study are, however, dominated by the populous star clusters. Since star clusters are known to have fairly small velocity dispersions of the order of 5 km/s (Harris 1996), they were expected to stand out in the velocity distribution of the observed fields. Comparing the velocity distributions of the inner- and outermost clusters Kron 28 and Lindsay 116 the impact of the cluster position on the field star contamination becomes strikingly clear. For Lindsay 116, the cluster stars clearly stand out against the underlying distribution, whereas for Kron 28 it is difficult to determine the cluster members when only the velocities are considered.

In order to distinguish between cluster members and non-members we assumed the velocity distribution of the clusters to be Gaussian. The uncertainties in our velocity measurements are of the order of  $\sim 5$  km/s. Only stars within the velocity range of  $\pm 2\sigma$  ( $\sim 10$  km/s) of the mean radial velocity of the cluster were considered member candidates.

### CMD position

Since the near IR CaII triplet method is only calibrated for bright RGB stars we restricted our sample to stars located on the RGB above the red clump.

In the CMDs of the observed fields the RGBs are the most outstanding features of the star clusters as compared to the SMC field populations. Thus, the restriction to RGB stars furthermore minimizes the contribution of non-cluster members to the analyzed stars.

Note that our photometry did not allow the clear distinction between asymptotic giant branch (AGB) and RGB stars. We excluded the strong outliers but cannot exclude that some AGB stars might fall into our selected stellar sample.

### Distance from the cluster center

The further away a certain star is located from the cluster center, the higher is the probability that it is not bound to that particular star cluster, but is rather a field or foreground star.

We use the previously determined cluster centers and core radii (Kayser et al. 2008a) in order to define a selection criterion taking into account the distance of a star from the clusters center. Considering the King model the concentration parameter is given as  $c = \log(r_t/r_c)$  (King 1962), where  $r_c$  is the core radius and  $r_t$  denotes the nominal tidal radius. Typical values for  $c$  range between  $c = 0.75$  to 1.75 for star clusters (Binney & Tremaine 1987) corresponding to tidal radii of 5.6 to 56 times larger than the core radii. We adopt a conservative value and consider only stars within a distance less than 7 times the core radius of the cluster as probable member candidates.

### Metallicity

The spectroscopy of stars in Galactic globular clusters revealed that, with the exception of  $\omega$  Centauri, these objects exhibit no significant abundance variations with respect to iron peak elements (see review from Gratton et al. (2004)). Grocholski et al. (2006) showed that this statement also holds for LMC star clusters. They found typical metallicity dispersions of the order of 0.15 dex in LMC star clusters.



Obviously, there is no reason to suspect any substantial abundance spread in Fe and Ca within the SMC clusters. Thus, we consider the star clusters in our sample to be single metallicity objects. This assumption is confirmed since the majority of the data points follow the slope of the iso-metallicity lines in Fig. 5.10 and show a narrow distribution in  $[\text{Fe}/\text{H}]$  in Fig. 5.11. Therefore, we assume that, under consideration of the uncertainties, the very few outliers whose measured CaT index lies significantly away from the majority of data points in these diagrams are most likely non-cluster-members.

We calculated the scatter around mean cluster metallicity as the standard deviation for each star cluster. In the further analysis data points that deviate by more than  $2\sigma$  were ignored.

### 5.5.2 Considering outliers

One star that was located closely to the cluster center of NGC 152 passed both, the velocity and CMD membership criteria but differed from the remaining clusters member candidates by its metallicity. This star is more metal-poor by more than 0.4 dex, which exceeds the errors in metallicity by approximately a threefold. The re-identification of this star in the star cluster CMD showed that it is the faintest of the selected probable cluster members and is located near the RC region. In order to test whether it is likely that this star is a SMC field star we considered the distribution of RGB stars in the observed field. We selected all RGB stars from the CMD of the field centered on NGC 152. We counted the number of RGB stars in a  $150'' \times 330''$  stripe located beyond  $150''$  from the cluster center to achieve an estimate of the RGB field star density. This region was assumed to be populated purely by SMC field stars. We found 42 stars in this area corresponding to a stellar density of  $8.36 \cdot 10^{-4}$  stars/arcsec<sup>2</sup>. Thus, we expected about 6 and 26 field RGB stars within the innermost  $50''$  and  $100''$  of the cluster, respectively. We concluded that it is quite reasonable to find a field RGB star in the inner region of the cluster that subsequently was selected for spectroscopy.

Similarly we detected two stars with lower metallicities for the cluster NGC 411, which passed all other selection criteria. Like NGC 152 this cluster is located in projection closely to the main body of the SMC. In analogy we assume these two low metallicity stars to be field stars. We therefore neglected them for the further considerations.

For Lindsay 11 we observed two stars in the outer region with much lower metallicities than the more centrally located stars. We assumed that these stars are probably field stars and therefore excluded these stars from the metallicity determination. In fact, most of the metallicity outliers were found to be located in the outer regions of the corresponding cluster and were therefore considered as SMC field stars.

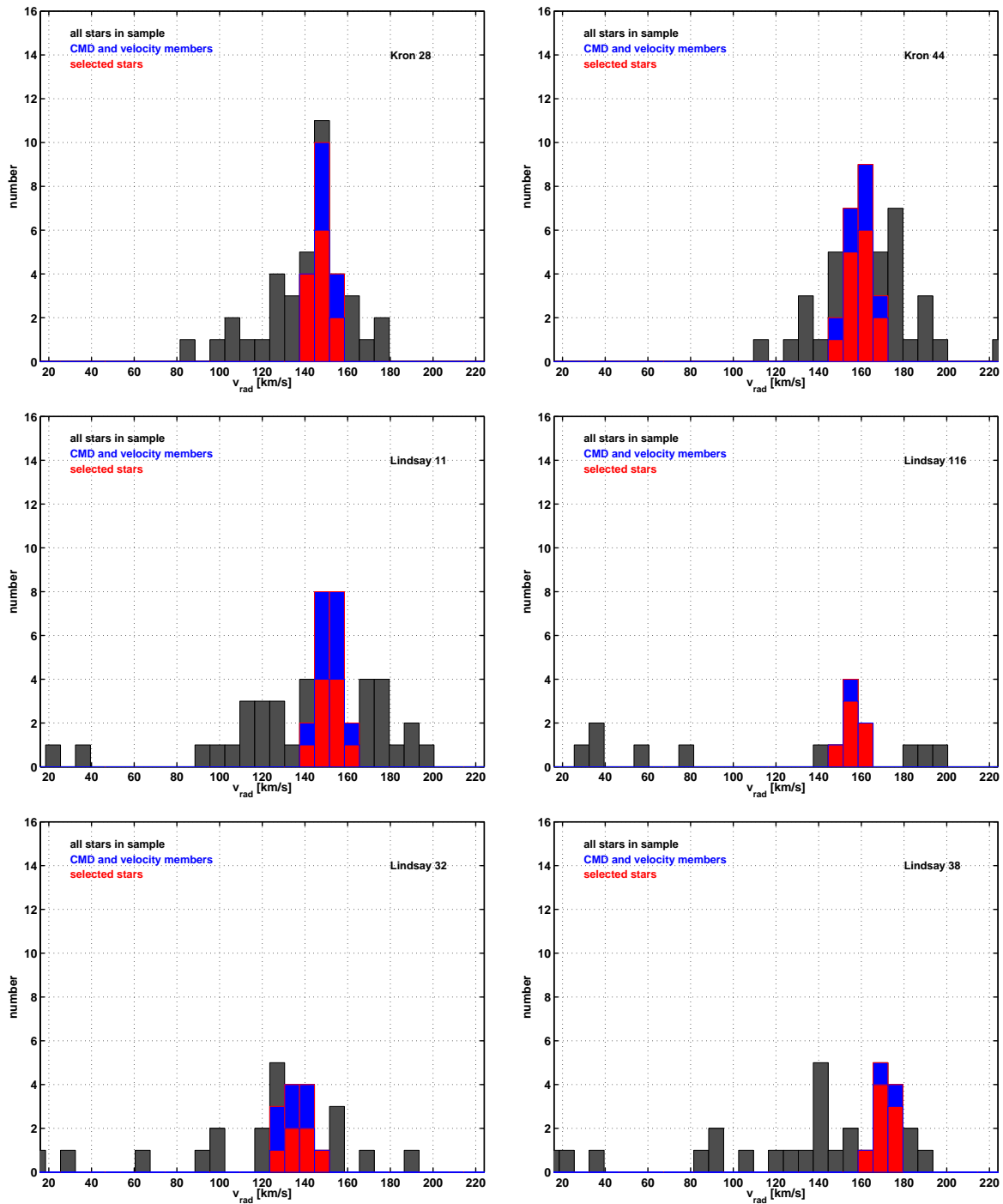
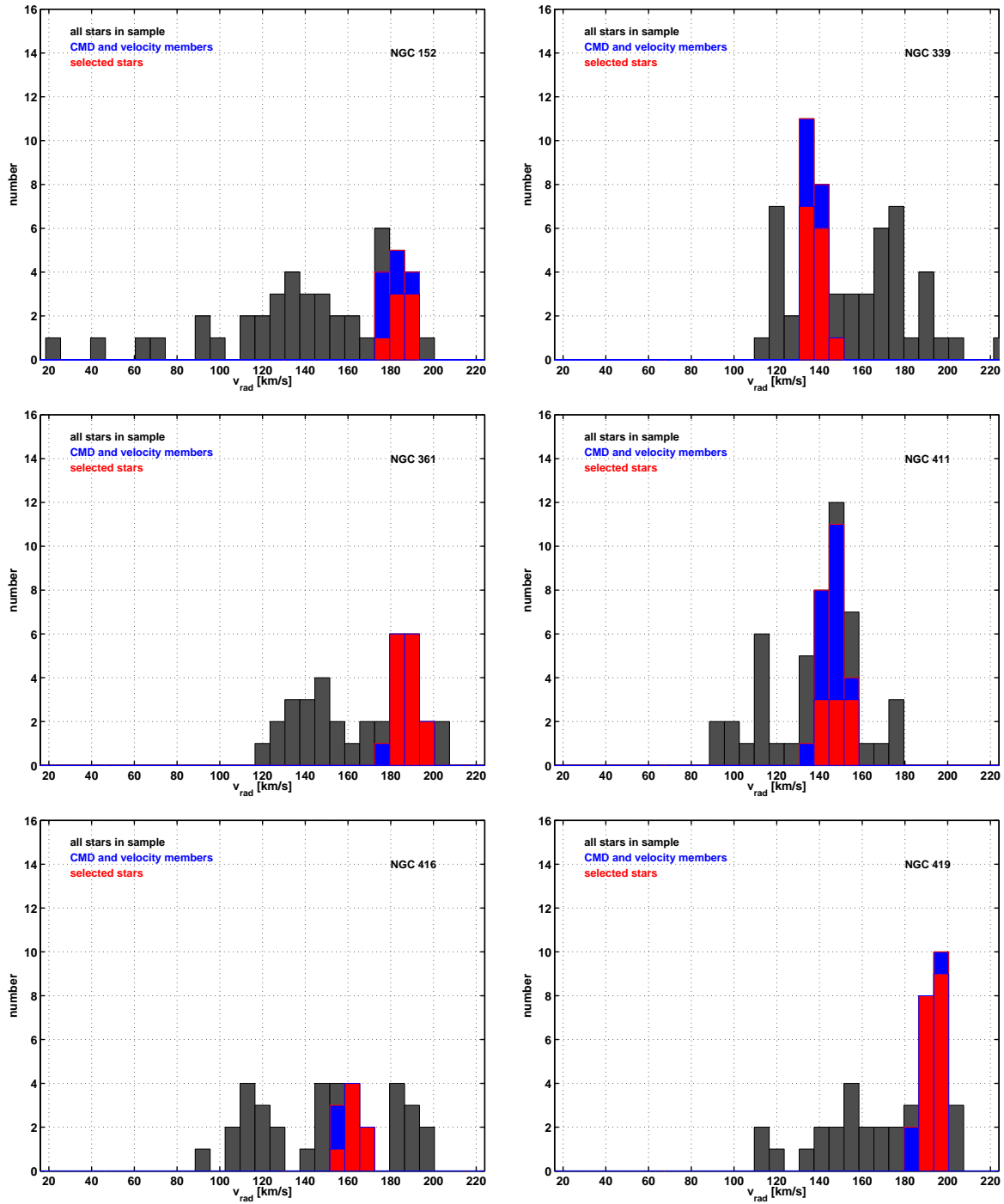
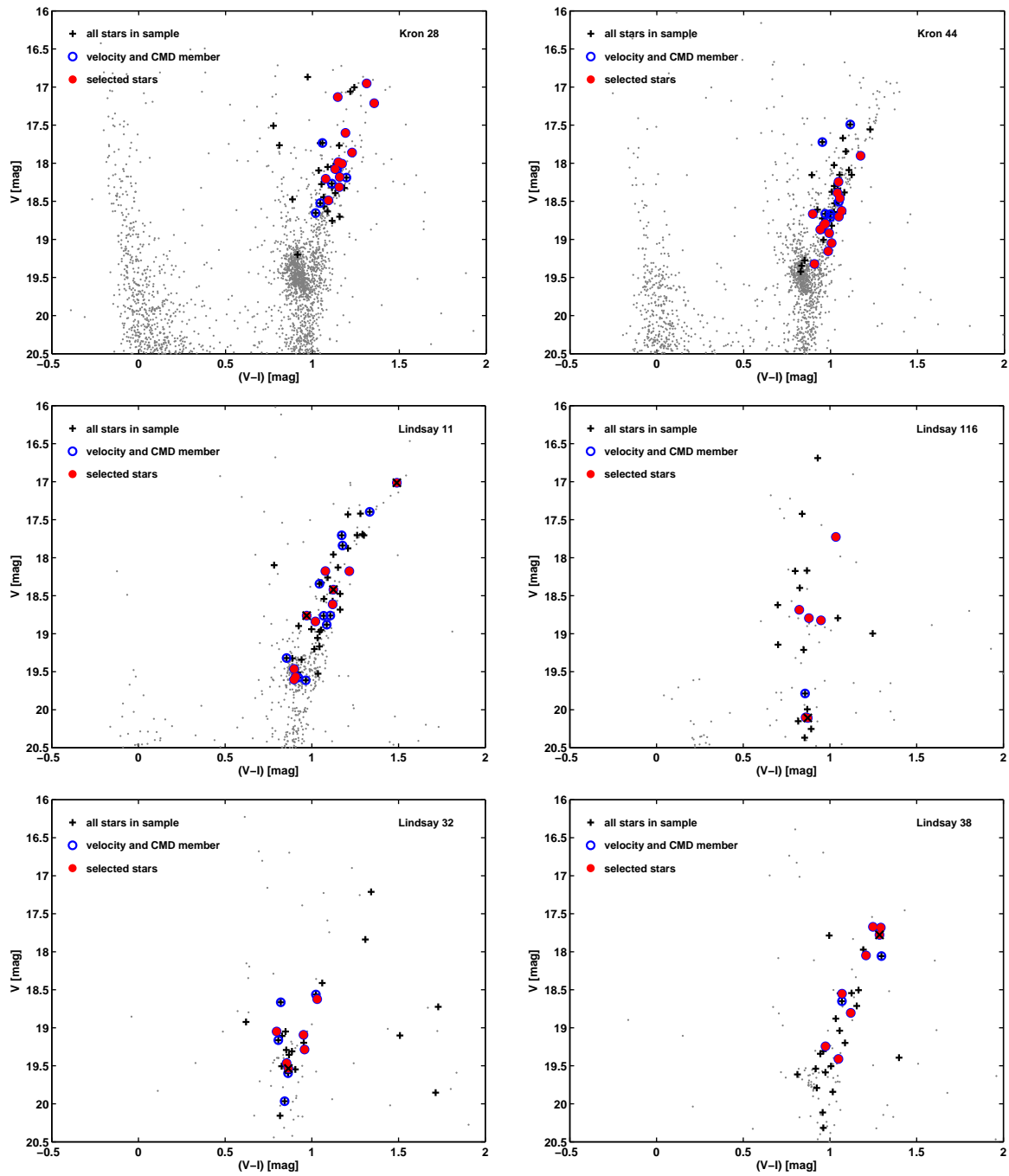
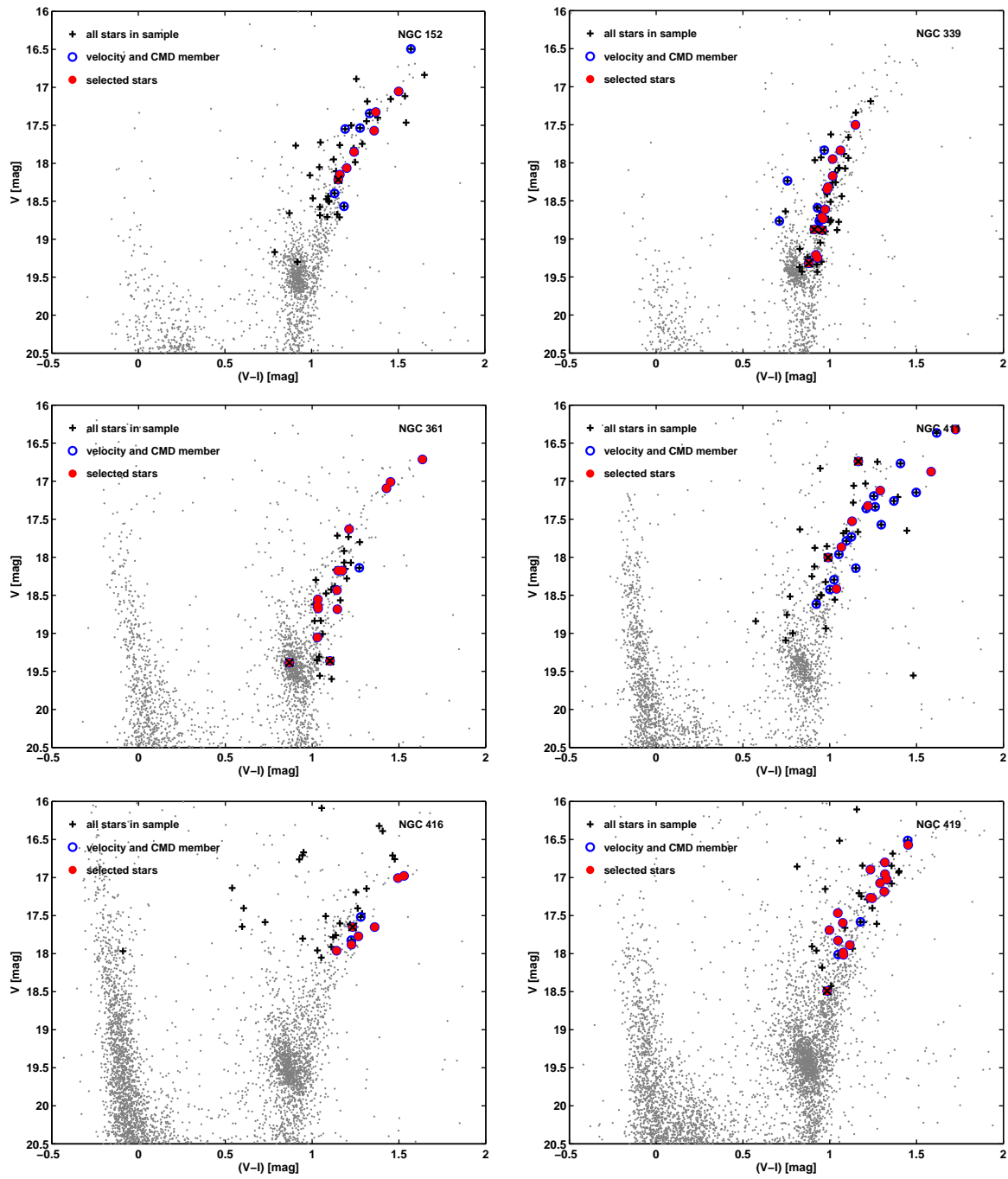


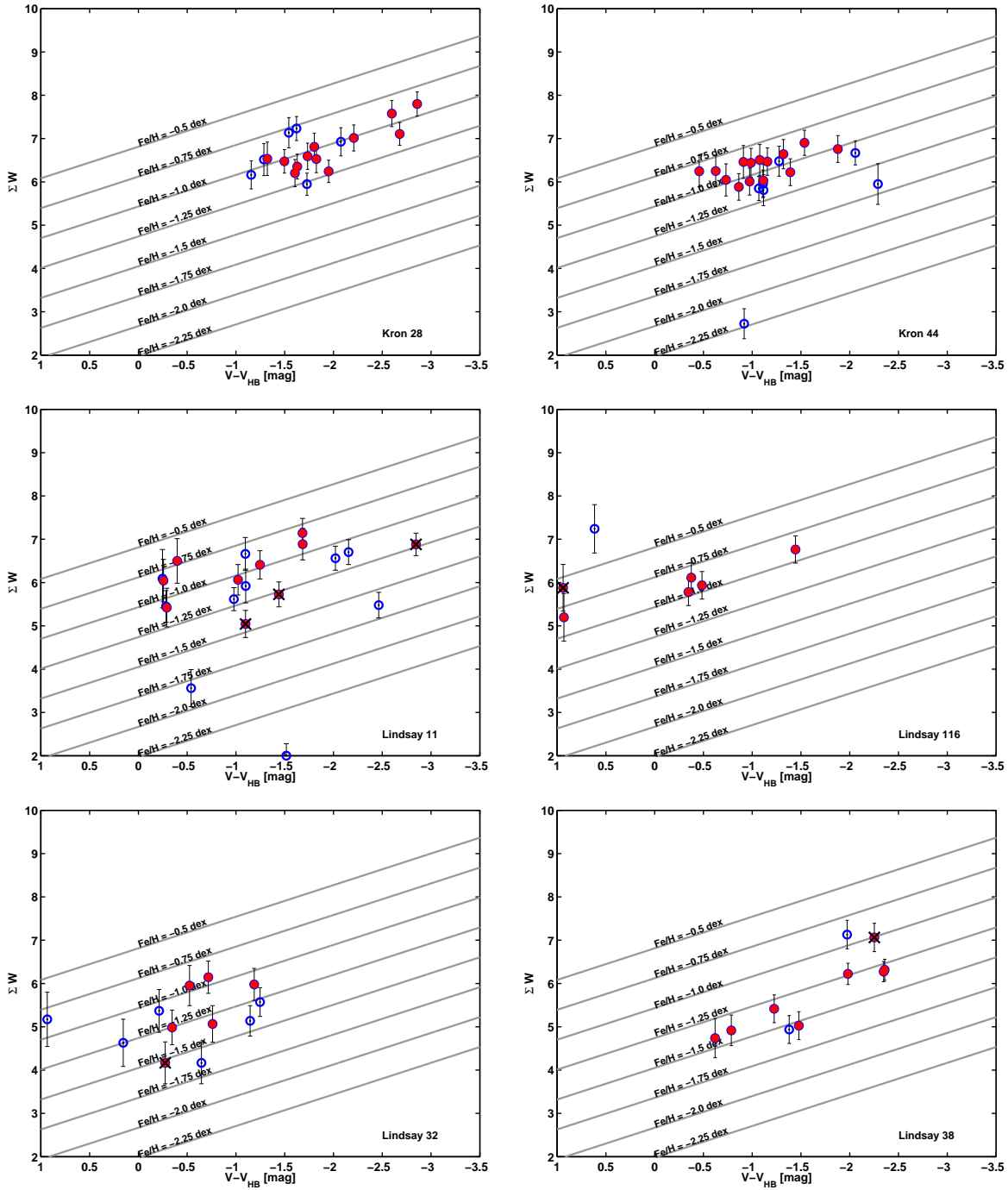
Figure 5.8: Velocity distributions for stars in and around the SMC star clusters. Indicated in black are stars observed spectroscopically but that did not pass the membership criteria. Stars identified as CMD and velocity members of the corresponding clusters are marked in blue. Stars that furthermore passed the distance and metallicity criteria are shown in red.

Figure 5.8: Velocity distributions for stars in and around SMC star clusters - *continued*



**Figure 5.9:** CMDs for SMC star clusters and their surrounding fields. Indicated in black are stars observed spectroscopically but that did not pass the membership criteria. Stars identified as CMD and velocity members of the corresponding clusters are marked in blue. Stars that furthermore passed the distance and metallicity criteria are shown in red.

Figure 5.9: CMDs for SMC star clusters and their surrounding fields - *continued*



**Figure 5.10:** Summed equivalent width,  $\Sigma W$ , vs.  $V - V_{HB}$ . Selected cluster members in the original calibration-plane. For reference the iso-metallicity lines by Cole et al. (2004) are plotted in gray. Stars deviating are considered as non-cluster members and are crossed out. Stars identified as CMD and velocity members of the corresponding clusters are marked in blue. Stars that furthermore passed the distance and metallicity criteria are shown in red.

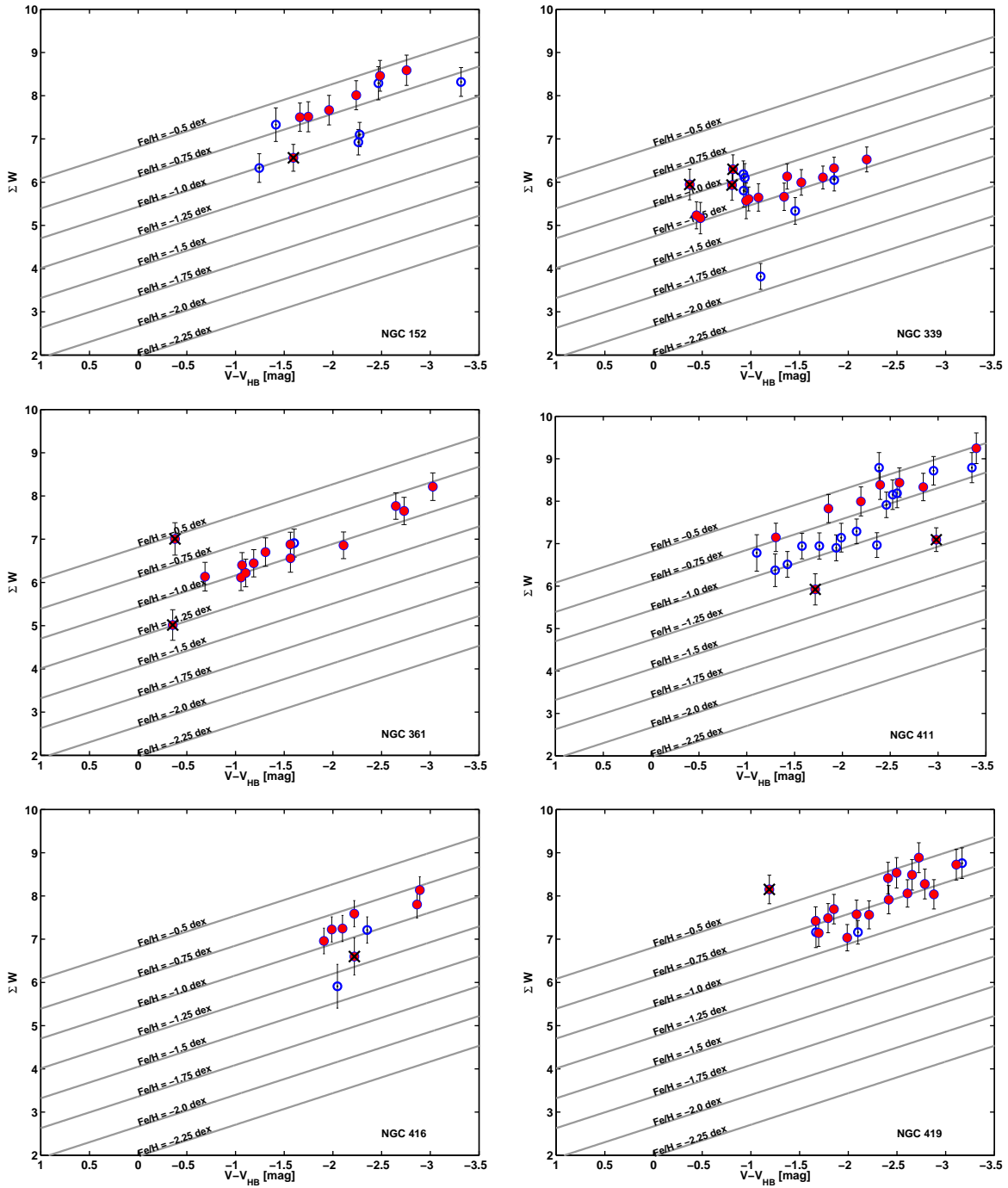
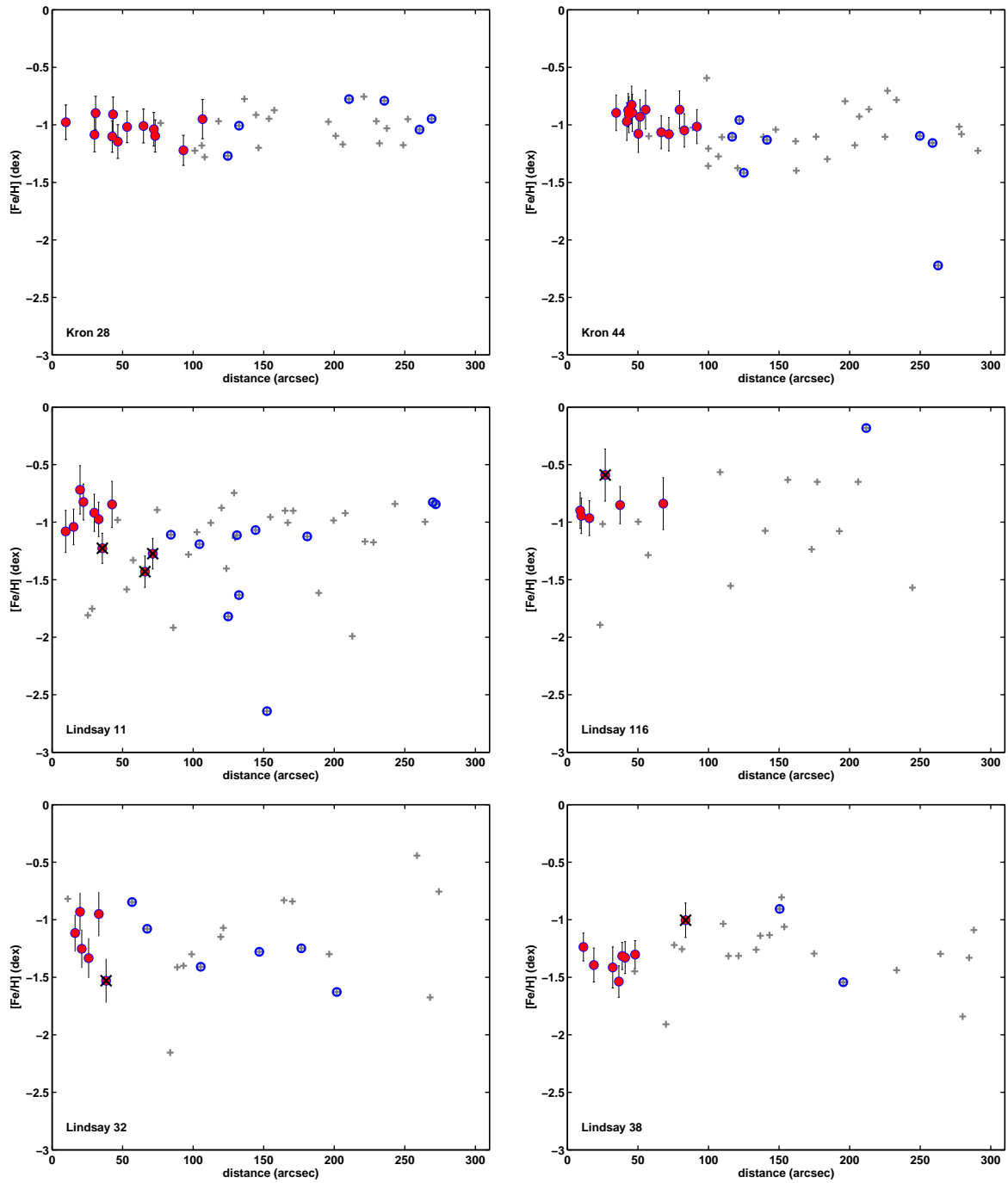
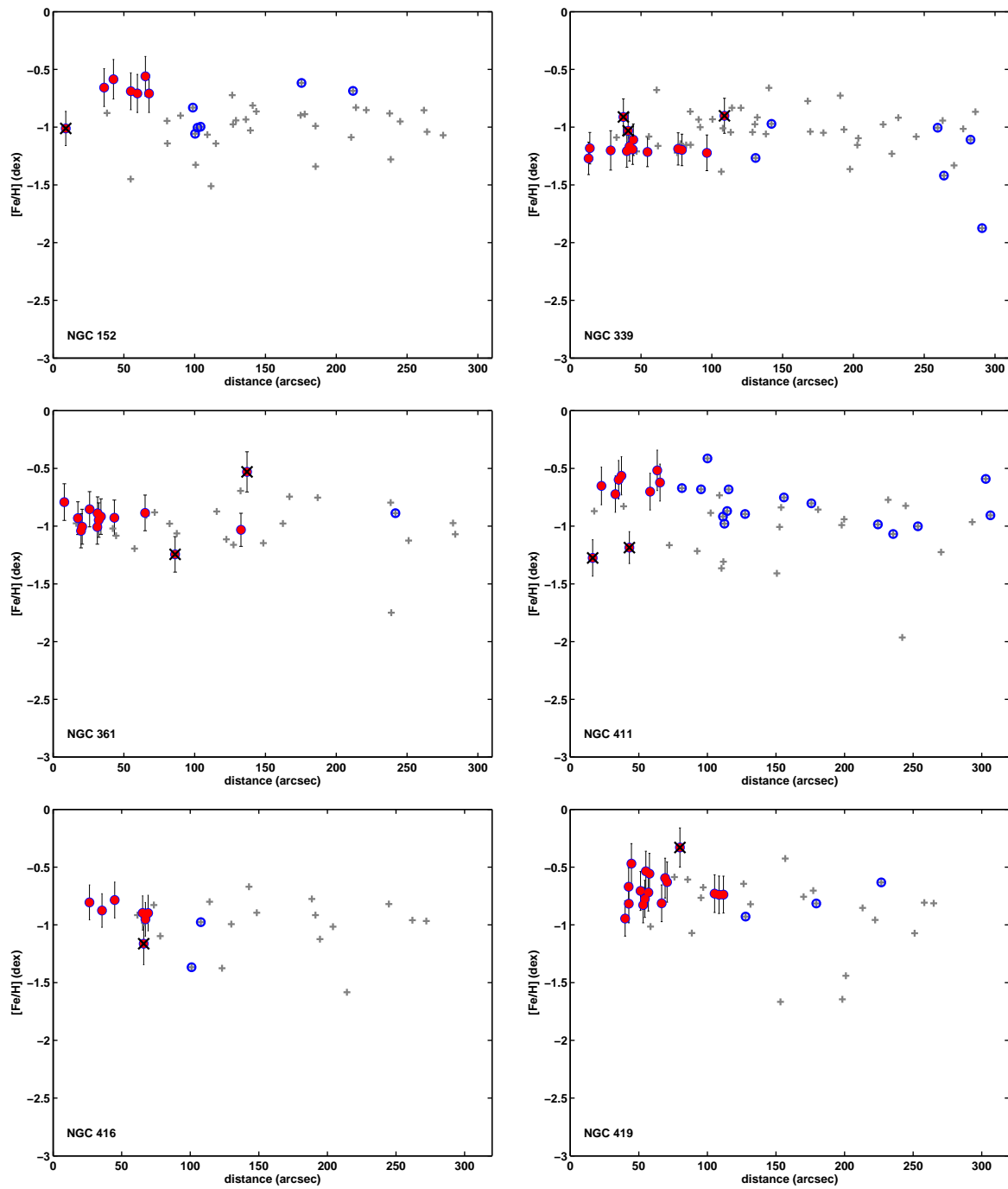


Figure 5.10: Summed equivalent width vs.  $V - V_{HB}$  - continued



**Figure 5.11:** Stellar metallicity distributions as a function of distance from the cluster center. The whole stellar sample of each cluster is indicated in gray. Stars identified as CMD and velocity members of the corresponding clusters are marked in blue. Stars that furthermore passed the distance and metallicity criteria are shown in red. Stars that fulfill the other cluster membership criteria but deviate in metallicity are crossed out.



Figure 5.11: Stellar metallicity as a function of distance from the cluster center - *continued*

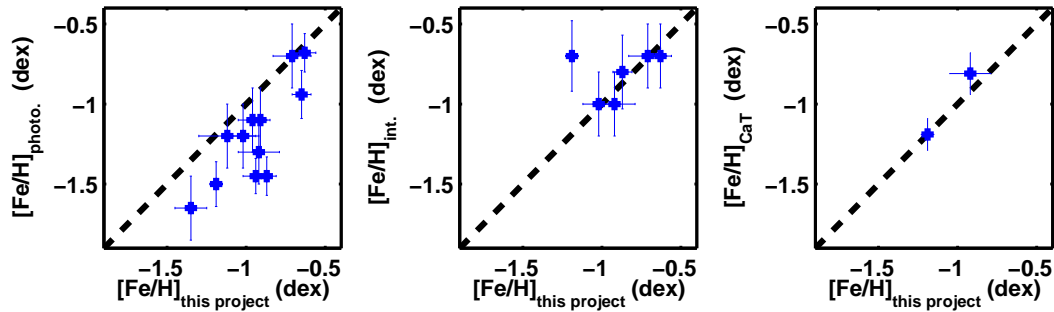


**Figure 5.12:** Comparison of the newly derived spectroscopic metallicities with literature values measured via different methods. The left panel shows a comparison with photometric metallicity estimates. The middle panel shows a comparison with results from integrated spectroscopy. In the right panel we compare our results with those of the spectroscopic study by Da Costa & Hatzidimitriou (1998) for the two stars clusters in common. The dashed line indicates the 1:1 correlation.

### 5.5.3 Metallicities

For each star cluster in our sample we calculated the mean of the  $[\text{Fe}/\text{H}]$  values determined via the CaT method. Only those stars that passed our selection criteria were included. The resulting new metallicity estimates of twelve SMC clusters nearly triple the existent sample of spectroscopically derived  $[\text{Fe}/\text{H}]$  values based on the observations of individual stars. The mean accuracy achieved in the determination of the cluster metallicities is 0.09 dex. The results are listed in Table 5.4. Apart from the determined metallicity we also list the number of member candidates on which this estimate is based. For each cluster we considered at least five and up to 16 *bona fide* member stars.

We found our clusters to cover the metallicity range of  $[\text{Fe}/\text{H}] \approx -1.4$  to  $-0.6$  dex. This is in good agreement with previous photometric metallicity estimates. For example Mighell et al. (1998) and Piatti et al. (2001) found the metallicities of their sample of clusters to vary between  $[\text{Fe}/\text{H}] \approx -1.65$  to  $-1.1$  dex and  $[\text{Fe}/\text{H}] \approx -1.71$  to  $-1.16$  dex, respectively. In the study of additional ten star clusters Piatti et al. (2005b) determined metallicities between  $[\text{Fe}/\text{H}] \approx -1.3$  to  $-0.6$  dex.

Considering the individual SMC star clusters our work provides an important step towards a more certain assessment of their metallicities. Although for some clusters multiple measurements exist, the metallicities suffer from large uncertainties, reflected by the large discrepancies between the results of different groups for the same cluster (see Table 5.5). An example for this is NGC 416. The published estimates range from  $-1.45$  dex (Mighell et al. 1998) to  $-0.80$  dex (de Freitas Pacheco et al. 1998). Note that both values were published in the same year. The first value is based on photometric measurements and the latter on measurement of line indices on integrated spectra. Our spectroscopic measurements confirm the higher metallicity and suggest  $[\text{Fe}/\text{H}] = -0.87$  dex. Similarly, for NGC 339, metallicities between  $-1.5$  dex and  $-0.70$  dex can be found in the literature. Again, the first value is based on photometry and the latter on integrated spectra. Our estimated value of  $-1.19$  dex lies in between both values and confirms the value of Da Costa & Hatzidimitriou (1998), who applied the same method as we do. For NGC 152, like for the majority of the clusters, only photometric metallicities can be found in the literature. These vary between  $-1.25$  dex (Bica et al. 1986) and  $-0.80$  dex (Mould & Da Costa 1988). Our findings now suggest an even higher value of  $-0.65$  dex. For the very metal-poor cluster Lindsay 38 only one photometric

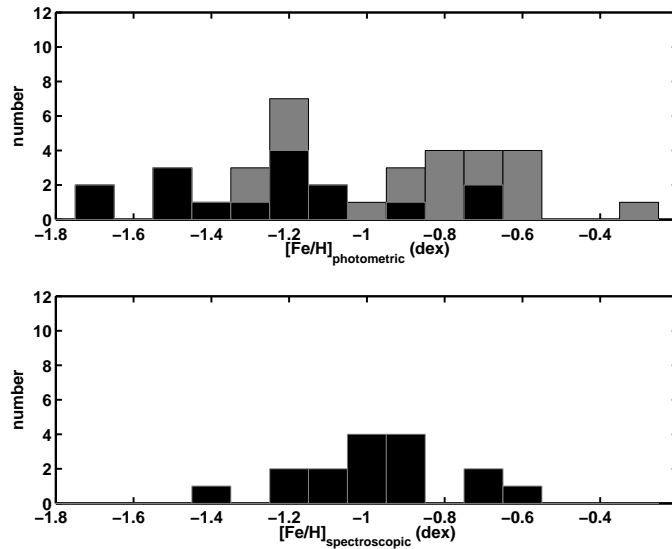


**Figure 5.13:** Distribution of cluster metallicities based on photometric measurements from the literature (top panel) and spectroscopic measurements from this project and Da Costa & Hatzidimitriou (1998) (bottom panel). Those clusters for which both, photometric and CaT measurements exist, are indicated in black. All additional photometric cluster metallicities found in the literature are plotted in gray.

metallicity estimate has been published so far,  $-1.65$  dex (Piatti et al. 2001). Although our result suggests a much higher value of  $-1.35$  dex, it is still the most metal-poor cluster in the sample.

Fig. 5.12 shows a comparison of our metallicity estimates with values taken from the literature. We distinguished between results based on photometry, line index measurements on integrated spectra, and the CaT method (panels left, middle, and right, respectively). In the case of multiple published values we adopted the most recent ones. Obviously, our study tends to predict higher metallicities than the previous photometric studies. This discrepancy is largest for the lowest metallicities. The comparison with integrated spectroscopy reveals in general a good consistency. The only clusters deviating is NGC 339. However, we are confident that our estimate is more reliable since it is in agreement with the CaT measurements by Da Costa & Hatzidimitriou (1998).

Only two clusters have been observed with the CaT method before: Lindsay 11 and NGC 339 (Da Costa & Hatzidimitriou 1998). Within the errors we find good agreement in their estimated metallicities. As mentioned above there is excellent agreement with the results for NGC 339. The difference for Lindsay 11 is slightly larger ( $\approx 0.1$  dex), but likewise are the uncertainties in the determination. Fig. 5.12 shows the good agreement between our results and those of Da Costa & Hatzidimitriou (1998). However, one has to keep in mind that the Da Costa & Hatzidimitriou (1998) data are based on only very few 4–6 stars per cluster. Due to these small sample sizes, no detailed membership selection was possible. The authors only rejected outliers from the calculation of the mean metallicity. Since we observed about 20 stars in the direction of each cluster and carefully selected 5–10 stars as member candidates we are confident that our results are more reliable.

In Fig. 5.13 we present the distribution of the SMC cluster metallicities based on photometric (top panel) and spectroscopic studies (bottom panel). As mentioned above, for most

of the star clusters only photometric metallicity estimates exist. One can clearly see a shift towards higher metallicities when comparing the metallicity distribution of spectroscopic with photometric measurements. Considering only the lower panel of spectroscopic abundances we see a broad distribution of metallicities with no clear evidence for a bimodality as suggested by Piatti et al. (2001). Nevertheless, we advise to take this results with caution since the cluster samples are highly incomplete with respect to the total number of  $\approx 700$  clusters associated with the SMC (Bica & Dutra 2000). This incompleteness is largest for very young objects. Ages derived from integrated colors by Rafelski & Zaritsky (2005) suggest that the age distribution of SMC star clusters is strongly peaked to ages  $< 1$  Gyr. Nevertheless, Rafelski & Zaritsky (2005) found up to 48 clusters with ages greater than 5 Gyr, depending on the applied model.

The more detailed comparison of the individual cluster measurements shows that the metallicities determined via the CaT method, both from our study and Da Costa & Hatzidimitriou (1998), are systematically higher by 0.26 dex than the photometric ones. A possible reason for this are the different metallicity scales used in these studies. For our project we adopt the scale of Carretta & Gratton (1997), which is obtained from the homogeneous analysis of high resolution spectra in 160 cluster red giants in 24 Galactic GCs. They reanalyzed the available data using a common set of FeI  $gf$ -values, model atmospheres, etc. The majority of the photometric measurements rely on the ZW84 scale, obtained from low resolution data of integrated light in 60 GCs. In order to increase the sample size to 121 MW GCs they compiled various measurements of metallicity indices. The third and most recent scale by Kraft & Ivans (2003) is not adopted to any measurements on the SMC so far and neglected in this context.

Most authors, who recently derived metallicities for the SMC star clusters from photometry, rely on two methods. The first one is the simultaneous reddening and metallicity method by Sarajedini (1994). This method is calibrated on Galactic globular clusters and uses the shape of the RGB, the  $V$  magnitude of the HB, and the apparent ( $V - I$ ) color of the RGB at the level of the HB as references. It yields metallicities on the scale introduced by Zinn & West (1984) with uncertainties of the order of  $\pm 0.2$  dex. The second widely applied method is the comparison with standard giant branches in the Washington photometric system (Geisler & Sarajedini 1999). It yields a sensitivity in metallicity three times higher than that from the  $V, I$  technique. This methods provide metallicity estimates on various scales; in case of the SMC mostly the ZW84-scale has been adopted. Since both methods are calibrated on MW GCs, systematic differences can not be excluded when applying them to the younger SMC star clusters. (Sarajedini & Layden 1997) found the simultaneous reddening and metallicity method to be mostly insensitive to age effects for red HB clusters older than  $\sim 5$  Gyr. For younger clusters the authors used the formalism derived from Galactic open clusters (e.g., Alves & Sarajedini 1999; Crowl et al. 2001). In case of Washington photometry the more recently derived metallicities were corrected for age effects via the prescription given in Geisler et al. (2003).

Fig. 5.14 shows the comparison between our derived metallicities and the photometric values found in the literature. The left panel shows the original data on the ZW84 scale. In the right panel we have transformed the most recent photometric values to the metallicity scale by Carretta & Gratton (1997) via the nonlinear transformation given in their paper. This comparison shows that possible effects caused by different scales have to be considered when comparing results originating from different studies. After the transformation we find our results to be consistent with the transformed photometric results. The remaining scatter

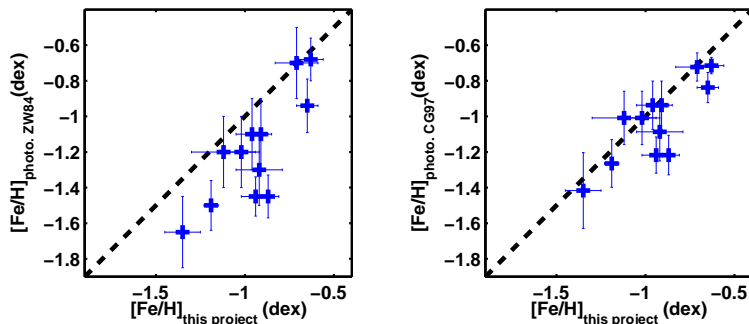


**Figure 5.14:** Comparison of the newly derived spectroscopic metallicities with photometric values from various sources. The dashed line indicates the 1:1 correlation. The left panel shows the photometric metallicities on the original ZW84 scale. In the right panel these metallicities have been transformed to the CG97 scale.

has a standard deviation of 0.13 dex, which is even smaller than the combined error of the photometric and spectroscopic uncertainties ( $\sqrt{\sigma_{phot}^2 + \sigma_{spec}^2} = 0.15$ ). The reduced  $\chi^2$  has a value of 1.45, which means that the spectroscopic and photometric metallicities are consistent within the 2 sigma level.

Although, compared to spectroscopy, photometric measurements suffer from many uncertainties, the good agreement affirms that the applied photometric methods introduced by Sarajedini (1994) and (Geisler & Sarajedini 1999) provide satisfying metallicities. When detailed spectroscopy is not possible due to telescope facilities, sample size etc., photometric methods are an adequate alternative in order to get estimates of the metallicities of stellar populations. However, one has to keep in mind the disadvantage that many methods of photometric metallicity measurements do not consider reddening and metallicity independently. Furthermore, in order to reliably apply these methods one very carefully has to correct for age effects, which induces additional uncertainties. In order to obtain accurate metallicity estimates with the lowest possible uncertainties, spectroscopic data are indispensable.

## 5.6 Results

### 5.6.1 Spatial distribution

For a better understanding of the formation, evolutionary, and enrichment history of SMC it is important to study the abundance trends with the spatial distribution of star clusters within this galaxy. We adopted the value provided by Crowl et al. (2001) ( $\alpha : 00^h 52^m 44.8^s$ ,  $\delta : -72^\circ 49' 43''$  (J2000)) for the optical center of the SMC. From this we determined the distances of the clusters to the galaxy's center. Since we lack absolute distances to the MW for the majority of the clusters, we considered only *projected* distances. Note that due to the depth extent of the SMC of 6–12 kpc (Crowl et al. 2001) this is not an ideal approach. Figure 5.15 gives a two and a three-dimensional overview of the position of the star cluster with respect to the photometric survey by Zaritsky et al. (2002), color-coded by their spectroscopic metallicities. In the three-dimensional plot we include only those 12 out of 16 star clusters for which distances are provided in the literature by Crowl et al. (2001).

In the two-dimensional illustration regions seem to exist with preferably more metal-rich clusters. Particularly the metal-rich (and young) clusters NGC 411 (age =  $1.2 \pm 0.5$  Gyr)

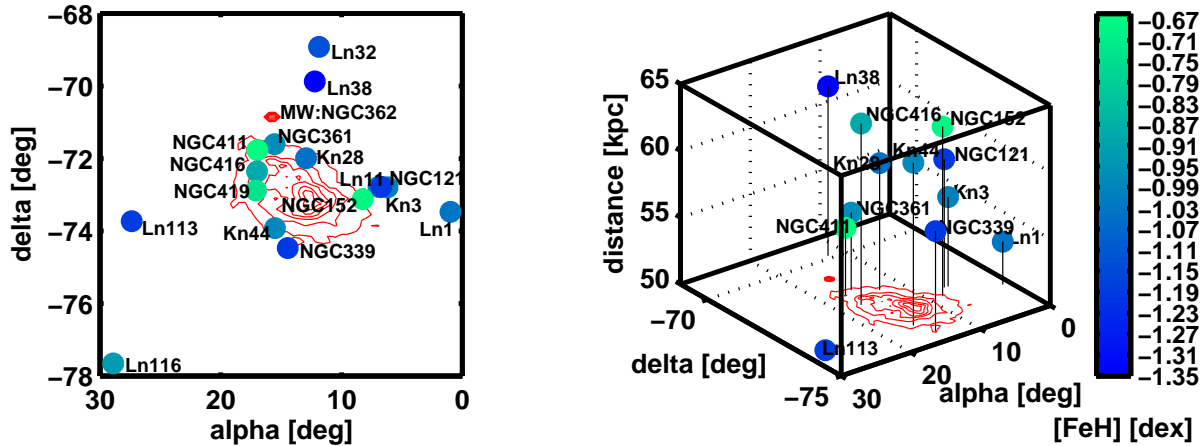


**Figure 5.15:** Two-dimensional (left panel) and three-dimensional (right) distributions of the SMC clusters, color-coded by their metallicities. The red contour lines are isopleths based on the stellar photometric survey of Zaritsky et al. (2002).

and NGC 419 (age=  $1.2 \pm 0.2$  Gyr) are located in the same region at the north-western part of the main body of the SMC. The present-day appearance of the interstellar medium of the SMC shows structures of clouds and shells. From the study of HI maps, Chiosi et al. (2006) found for very young clusters (age  $< 1$  Gyr) a close relation between young clusters and HI intensities, suggesting that cluster formation in the SMC is somehow connected to the formation of the gaseous shells. Our findings now allow the speculation that possibly such regions of local, very intense cluster formation also existed in the past of the SMC. Nevertheless, these statements have to be taken with care due to the depth of the SMC. The three-dimensional illustration shows that the clusters NGC 411 and the older cluster NGC 416 (age=  $5.6 \pm 0.3$  Gyr), which are close to each other in the projected image, are actually located at different distances within the SMC. Unfortunately, NGC 419 was not part of the project of Crowl et al. (2001). In order to trace the spatial distribution in detail and search for locally enhanced star cluster formation, a much larger sample of cluster is required.

In Fig. 5.16 we plot the cluster ages and metallicities as functions of the projected distances from the SMC center. We find that the clusters more metal rich than  $\sim -1$  dex are preferentially located within the inner 1.6 degrees from the SMC center. The mean metallicity of these intermediate star clusters of the inner SMC clusters is  $-0.83 \pm 0.16$  dex whereas the mean metallicity of the outer clusters is  $-1.11 \pm 0.14$  dex. Adopting the most recent cluster ages (see Table 5.4), we find that the clusters younger than  $\sim 5$  Gyr are preferably located within the central 2 degrees of the SMC. By contrast, the older and more metal-rich star clusters are more uniformly distributed throughout the SMC.

The SMC star cluster deviating most from these observed trends is Lindsay 116. Interestingly, Piatti et al. (2001) suggested from its absolute distance modulus that this cluster may be in the foreground of the SMC and rather be associated with the LMC. With our measured metallicity estimate of  $-0.91 \pm 0.06$  dex and the adopted age of  $2.8 \pm 1.0$  Gyr (Piatti et al. 2001), Lindsay 116 falls in the age and metallicity regime of the LMC cluster NGC 1783, which has a metallicity of  $-0.75 \pm 0.23$  and an age of  $3.0 \pm 1.3$  (de Freitas Pacheco et al. 1998). The

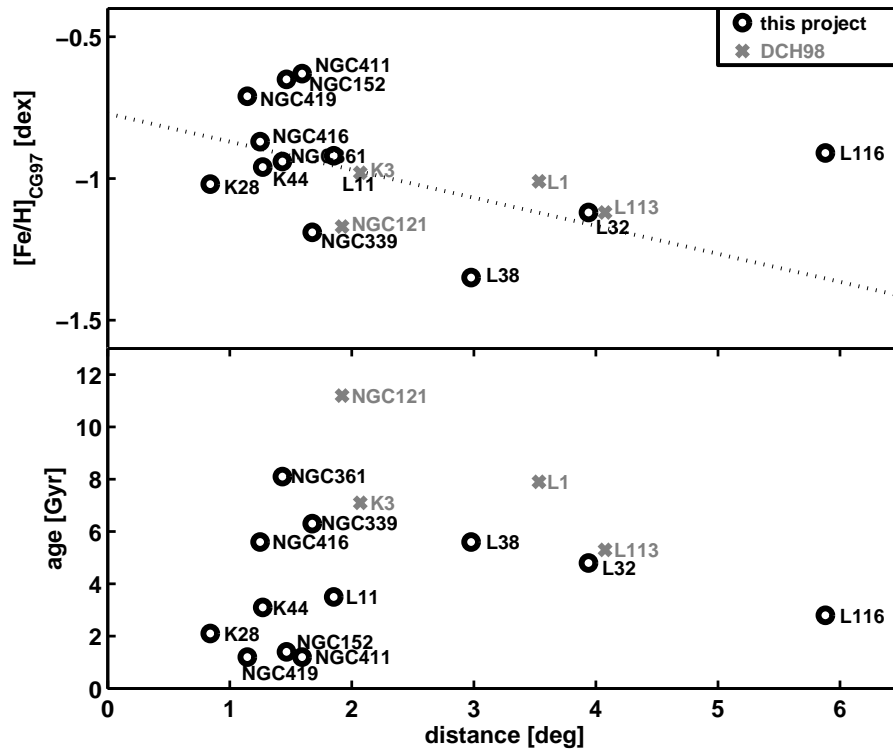


**Figure 5.16:** Metallicities (top) and ages (bottom) of the clusters as a function of distance from the SMC center. The black open circles indicate the clusters of this work, the gray crosses indicate the four additional clusters by Da Costa & Hatzidimitriou (1998).

good agreement strengthens the suggestion by Piatti et al. (2001). We therefore neglected this cluster in this diagram. A linear fit to the observed weak metallicity gradient reveals a decline in  $[Fe/H]$  towards the outer regions of the galaxy of  $\approx -1 \text{ dex/deg}$ . However, the scatter around this fit is large ( $\sigma = 0.17 \text{ dex}$ ). Considering clusters of similar ages no such decline of metallicity with distance is detectable. Therefore we conclude that the observed metallicity gradient may be primarily caused by ages. In the LMC for clusters of similar ages also no metallicity gradient is present (Olszewski et al. 1991; Grocholski et al. 2006). The authors argued that the existence of an extended bar could be a reason for the dilution of the metallicity gradient.

Our results support the findings from Piatti et al. (2007), who combined photometric data from various works dedicated to the study of the spatial distribution of SMC star clusters. They suggested that clusters with  $[Fe/H] > -1.2 \text{ dex}$  in the inner disk formed during the last 4 Gyr whereas older, more metal-poor clusters are more spread out. This is also in agreement with the results from observations of field stars (Piatti et al. 2001). In the inner regions of the SMC, the intermediate-age stellar population is mixed with a younger component that is not present in the outer parts. All in all, photometric and spectroscopic evidence in the star clusters and the SMC field suggest that star and star cluster formation must have lasted longer in the inner regions than in the outskirts and is still ongoing closer to the center of the SMC.

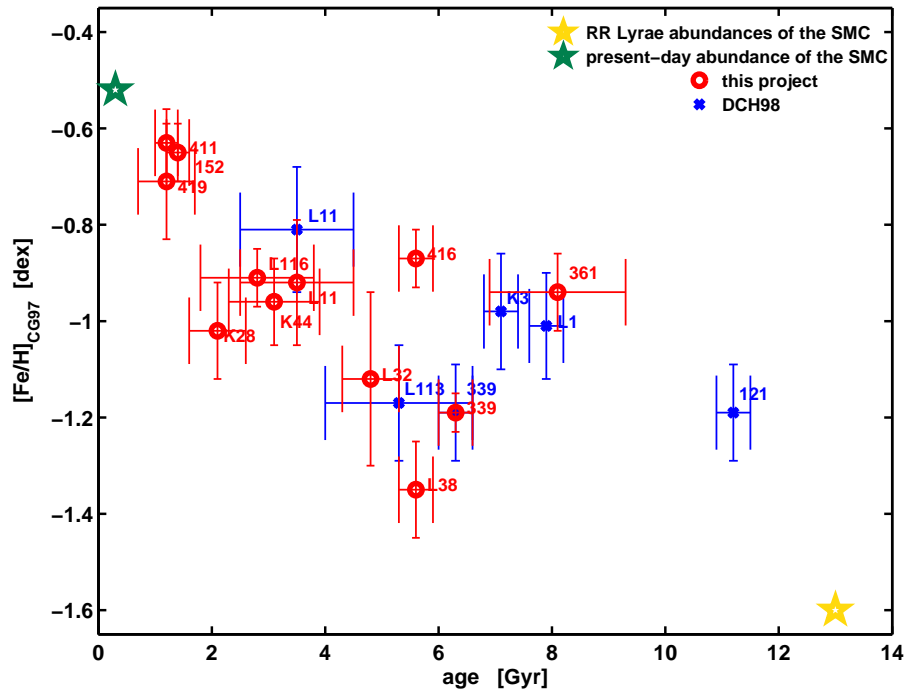


**Figure 5.17:** Metallicities for of SMC derived from star clusters. Indicated in red are clusters of this project. Indicated in blue are clusters from Da Costa & Hatzidimitriou (1998). Additionally we plot the present-day metallicity determined by Rolleston et al. (2003) and an estimate for the ancient metallicity derived from RR Lyrae stars by Smith et al. (1992).

### 5.6.2 Age-metallicity relation

Previous studies addressing the star and cluster formation history of the SMC suggest different interpretations of the observed data. Da Costa & Hatzidimitriou (1998) found that, if the two deviating clusters Lindsay 113 and NGC 339 were ignored, the SFH implied by their data was consistent with a closed-box model of chemical enrichment. Rich et al. (2000) obtained deep HST photometry of seven bright star clusters older than 1 Gyr and reported to find two age groups of clusters. They suggested that the clusters in the SMC formed in two distinct episodes of star formation. This result was confirmed by Piatti et al. (2001) and Piatti et al. (2005a) by a larger, ground-based sample of 26 star clusters observed with Washington photometry. It is important to mention, that since their data were not deep enough to cover the age-sensitive region of the MSTO and SGB sufficiently detailed for isochrone fitting, they had to rely on age estimates based on the magnitude differences between RC and MSTO. Both results indicated two peaks in the cluster formation 6 and 3 Gyr ago and 6.5 and 2.5 Gyr ago for the latter. In a more recent study of a statistically more complete sample Rafelski & Zaritsky (2005) presented ages based on integrated colors for 204 star clusters. They observed an initial, older population of clusters and another, more recent epoch of cluster formation, starting about 3 Gyr ago, with a relatively quiescent phase in between. However, since the position of the peak strongly varied with the adopted metallicities in their models, no statement could be made if the observed peaks were real. Nevertheless, despite the existence of the younger cluster population they concluded that the dominant epoch of clusters formation was the initial one. From HST/ACS Glatt et al. (2008) obtained



**Table 5.4:** Derived Metallicities and adopted ages for SMC Clusters.

Cluster	[Fe/H] <sub>CG97</sub> [dex]	Nr. of member stars	Adopted age [Gyr]	Reference
Kron 28	$-1.02 \pm 0.10$	12	$2.1 \pm 0.5$	Piatti et al. (2001)
Kron 44	$-0.96 \pm 0.09$	14	$3.1 \pm 0.8$	Piatti et al. (2001)
Lindsay 11	$-0.92 \pm 0.13$	7	$3.5 \pm 1.0$	Mould et al. (1992)
Lindsay 116	$-0.91 \pm 0.06$	5	$2.8 \pm 1.0$	Piatti et al. (2001)
Lindsay 32	$-1.12 \pm 0.18$	5	$4.8 \pm 0.5$	Piatti et al. (2001)
Lindsay 38	$-1.35 \pm 0.10$	7	$5.6 \pm 0.3$	Glatt et al. (2008)
NGC 152	$-0.65 \pm 0.06$	6	$1.4 \pm 0.2$	Crowl et al. (2001)
NGC 339	$-1.19 \pm 0.04$	11	$6.3 \pm 0.3$	Glatt et al. (2008)
NGC 361	$-0.94 \pm 0.08$	12	$8.1 \pm 1.2$	Mighell et al. (1998)
NGC 411	$-0.63 \pm 0.07$	7	$1.2 \pm 0.2$	Alves & Sarajedini (1999)
NGC 416	$-0.87 \pm 0.06$	6	$5.6 \pm 0.3$	Glatt et al. (2008)
NGC 419	$-0.71 \pm 0.12$	16	$1.2 \pm 0.5$	Glatt et al. (2008)

well-populated CMDs of five star cluster covering the RGB, SGB, and MS, reaching at least 3 mag below the MSTO. By fitting isochrones to the observed ridge lines and comparing various models (Padova, Teramo, and Dartmouth) they could carry out the most accurate age measurements so far. They conclude that the SMC has continuously formed star clusters between 6 and 8.3 Gyr, which makes the SMC the only dwarf galaxy containing star clusters in this age range. In summary the majority of recent data seem to suggest that the SMC has formed clusters during its entire lifetime with some epochs of more intense star cluster formation activity.

The age-metallicity relation (AMR) is one of the most important diagnostics through which we can learn about the governing chemical enrichment processes of a particular stellar system. Combining the newly derived metallicities with age estimates adopted from different sources in the literature (de Freitas Pacheco et al. 1998; Mighell et al. 1998; Piatti et al. 2001; Glatt et al. 2008) we can for the first time derive a well-sampled age-metallicity relation for the SMC, which is fully based on spectroscopic metallicity estimates. An overview of the adopted ages is given in Table 5.4. We also include the data obtained by Da Costa & Hatzidimitriou (1998). Since they observed six star clusters, out of which two are in common with our sample, with the same method as employed in this work, this is an ideal supplement to our new data. The authors provide abundance estimates on both, the ZW84 and the CG97 scale. Adopting the CG97 metallicities no inhomogeneities caused by different scales are expected. Nevertheless, one has to keep in mind that the data of Da Costa & Hatzidimitriou (1998) are based on only very few 4–6 stars per cluster.

Fig. 5.17 shows our newly derived age-metallicity relation. For reference, we also plot the present-day metallicity ( $-0.5$  dex) of the SMC determined from the spectroscopy of a B-type main sequence star by Rolleston et al. (2003). This value is slightly higher than the results from supergiant spectroscopy (e.g., Hill (1999):  $[\text{Fe}/\text{H}] = -0.69$  and Venn (1999):  $[\text{Fe}/\text{H}] = -0.7$  dex). Tracing the earliest times in the history of the SMC is quite difficult. Unfortunately, this galaxy host only one known very old Galactic GC-like star cluster, NGC 121. Photometric and spectroscopic studies suggested an age of 11.2 Gyr (Glatt et al. 2008) and a metallicity of  $-1.19$  dex (Da Costa & Hatzidimitriou 1998) for this cluster. Thus, additional

tracers of the early evolution are required. One possibility is the investigation of RR Lyrae stars. These evolved low mass stars are excellent tracers of the oldest stellar populations in galaxies and therefore of the early epochs of galaxy formation. In the Milky Way these short periodic variable stars are very common in globular clusters and in the old field population (Vivas et al. 2004). In order to illustrate the SMC's metallicity at about 13 Gyr ago we plot in Fig. 5.17 the result from the period-amplitude relationship of 42 RR Lyrae stars in a 1.3 square degree field surrounding NGC 361 (Smith et al. 1992). This study suggests an mean metallicity of  $[\text{Fe}/\text{H}] = -1.6$  dex.

In the following we point out four major features in the new AMR:

- Initial increase of metallicity:

We confirm the fairly high metallicity of  $[\text{Fe}/\text{H}] \approx -1$  dex at an age of approximately 8 Gyr. Indications for this were already observed by Da Costa & Hatzidimitriou (1998). The metallicity for NGC 361 is of the order of those of K 3 and L 1, the two clusters of approximately the same age of the Da Costa & Hatzidimitriou (1998) sample. Taking into consideration the results of the RR Lyrae study by Smith et al. (1992) and the measurements for NGC 121 (Da Costa & Hatzidimitriou 1998; Glatt et al. 2008) we agree with the statement of Da Costa & Hatzidimitriou (1998) that the SMC has experienced a relative rapid increase in abundance in its early history. The initial metallicity was raised to  $\approx -1$  dex within about 6 Gyr. Since the SMC hosts only one cluster older than 10 Gyr we can not draw any conclusion how uniformly this early enrichment took place and whether the galaxy was well mixed during that time.

- Constant mean metallicity for several Gyr:

After the initial enrichment the mean  $[\text{Fe}/\text{H}]$  seems to stay fairly constant at about  $-1.14$  dex for several Gyr ( $\approx 4$  Gyr). Note that this mean value of  $\approx 0.16$  dex is slightly below the observed metallicity for the star cluster with an age around 8 Gyr, which have a mean metallicity of  $\approx -0.98$  dex. We find this decrease in mean metallicity significant since it exceed the uncertainties in our metallicity estimates (0.90 dex). Da Costa & Hatzidimitriou (1998) noticed in the regime between 10 and 3 Gyr ago a modest rise of the abundances.

- Scatter in metallicity at certain age:

Apart from the fairly flat slope of the mean  $[\text{Fe}/\text{H}]$ , our derived AMR clearly shows the presence of a significant abundance dispersion. At all ages a weak scatter within the errors seems to be omnipresent. However, given an age of  $\approx 6$  Gyr the spread of about 0.45 dex exceeds the errors in  $[\text{Fe}/\text{H}]$  by about a factor of four. The two clusters constituting most to the scatter are Lindsay 38 and NGC 416. They have the same age of about 5.6 Gyr, but differ in metallicity by 0.64 dex. Therefore, this scatter appears to be real and not to be caused by the uncertainties in the metallicity determination. Lindsay 38 is about 0.37 dex more metal-poor than the mean and located in the outer regions of the SMC, whereas NGC 416 is 0.27 dex more metal-rich and located close to the main body. Obviously, there is no direct correlation between age and metallicity at that time. Evidently the SMC was not well mixed during its entire past, which is at first sight surprising, as one expects the contrary for dwarf galaxies like this (Roy & Kunth 1995). Expanding gas shells driven by evolving massive stars are expected to thoroughly mix the interstellar medium on time-scales considerably less than a Hubble time.

- Increase in metallicity in the more recent past:

For the more recent past from 2 to 3 Gyr ago to the present day we observe an increased enrichment, which raises the abundance to the present day value of  $[\text{Fe}/\text{H}] = -0.5$  dex (Rolleston et al. 2003). In fact none of our younger clusters has a metallicity below  $\approx -1$  dex, suggesting the lack of young, metal-poor clusters. Furthermore, for this age range we find a very narrow age-abundance correlation. The observed scatter of around 0.1 dex is close to the observational errors. This decrease in relative scatter suggests that the SMC was again, or for the first time well mixed. Likewise, the estimates of the present-day abundance of the SMC from various stellar sources in the field are consistent with each other. Metallicities based on supergiant spectroscopy by Hill (1999) and Venn (1999) are reported as  $[\text{Fe}/\text{H}] = -0.69$  and  $-0.7$  dex, respectively. No evidence for any substantial abundance gradient or large scatter was found so far from supergiant observations. Moreover, Cepheid observations by Luck et al. (1998) stated a mean value of  $-0.68$  dex. Their dispersion in  $[\text{Fe}/\text{H}]$  in the SMC is comparable with a standard deviation of 0.15 dex. As pointed out before, the more recent results by Rolleston et al. (2003) from high resolution spectroscopy of a B-type main sequence star suggested a slightly higher metallicity of  $[\text{Fe}/\text{H}] = -0.5 \pm 0.19$  dex. However, it is important to mention that the abundance for the young cluster NGC 330 (age  $\sim 2.5$  Myr) is controversial discussed with indications for a lower overall metallicity of the order of  $-0.9$  dex (e.g., Hill 1999; Gonzalez & Wallerstein 1999).

### 5.6.3 Comparison with theoretical models of chemical evolution

For a better understanding of the chemical evolution history of the SMC we compare our newly derived age-metallicity relation with standard theoretical models from the literature.

#### Da Costa & Hatzidimitriou 1998

The model, kindly provided by G. S. Da Costa, is based on the Simple closed-box model. It adopts the fundamental equations for the chemical evolution and the abundance changes of the interstellar medium and the resulting abundance distributions of stars (e.g., Tinsley 1980). The SMC is considered as a self-contained system with no infall or outflow of gas. Consequently the gas of the initial cloud is used up with time, since more and more material is locked up in low-mass, long-lived stars. The enrichment in heavy elements proceeds by the supernova ejecta of the short-lived, massive stars of each generation into the interstellar medium. We modified the original model by Da Costa & Hatzidimitriou (1998) by adopting the most recent measurement of the present-day abundance of the SMC ( $[\text{Fe}/\text{H}] = -0.5$  dex, Rolleston et al. (2003)) and the estimated age of the universe by WMAP ( $\approx 14$  Gyr (Spergel et al. 2003)). Figure 5.18 shows the evolution of metallicity with time predicted by this model overplotted to our star cluster measurements. One sees that this model does not very well reproduce the observed cluster formation history. The constraints necessary to fit the present-day abundance of the SMC result in the overestimation of the metallicity of most of the star clusters older than 2 Gyr.

The fact that the Simple closed-box model does not reproduce the observed age-metallicity relation is neither surprising nor alarming, since it is well known that the galaxies in the universe are in interaction with their surroundings and neighboring objects. In fact the SMC together with the LMC and MW is an example of a very intensive galaxy interaction (see

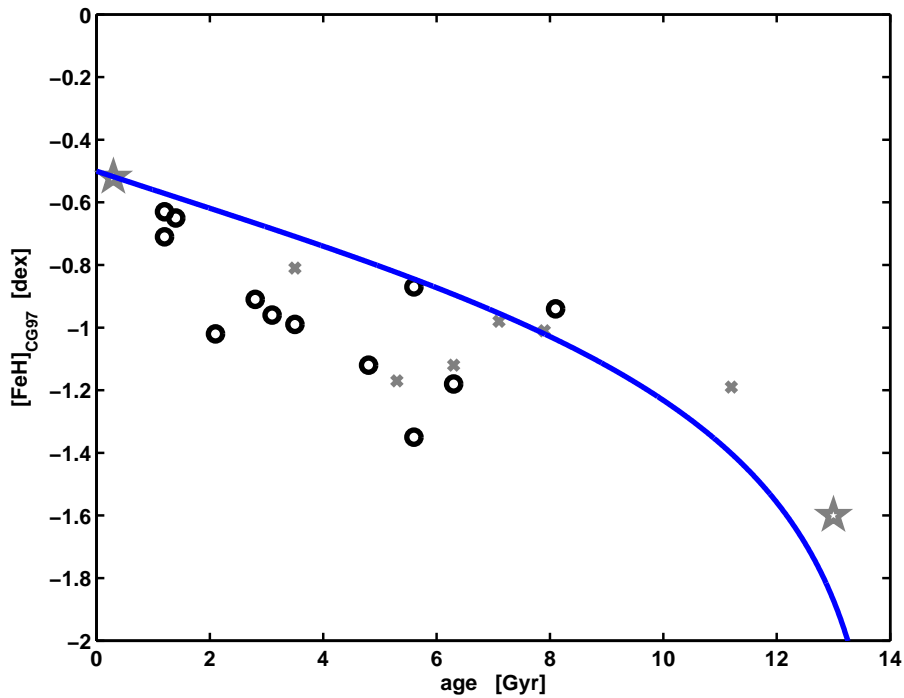


**Figure 5.18:** Age-metallicity relation of the SMC in comparison with the chemical evolution model by Da Costa & Hatzidimitriou (1998). The black circles and gray crosses indicate the metallicity results from this project and by Da Costa & Hatzidimitriou (1998), respectively. The ancient and present day metallicity of the SMC are indicated by large gray stars.

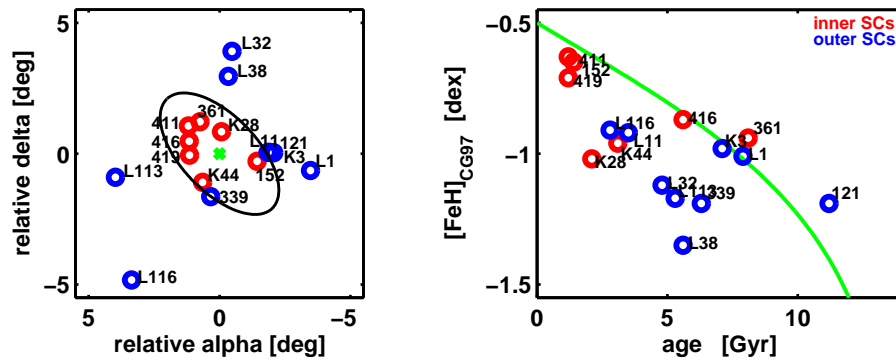


**Figure 5.19:** Differentiation between inner (red symbols) and outer (blue symbols) star clusters. These were selected by an ellipse (black line) orientated along the main body of the SMC. The adapted center of the SMC is marked by the green cross. The green line indicates the Simple closed-box model by Da Costa & Hatzidimitriou (1998).

e.g., Bekki & Chiba 2005).

Even though the overall age-metallicity relation does not follow the predictions of the Simple close-box model, it is conceivable that the clusters located closer to the center of the SMC experienced a different chemical evolution than the outer clusters. To differentiate between inner and outer star clusters we approximated the main body of the SMC by an ellipse with the axial ratio of 2:1. In order mark the location of the main body (bar) of

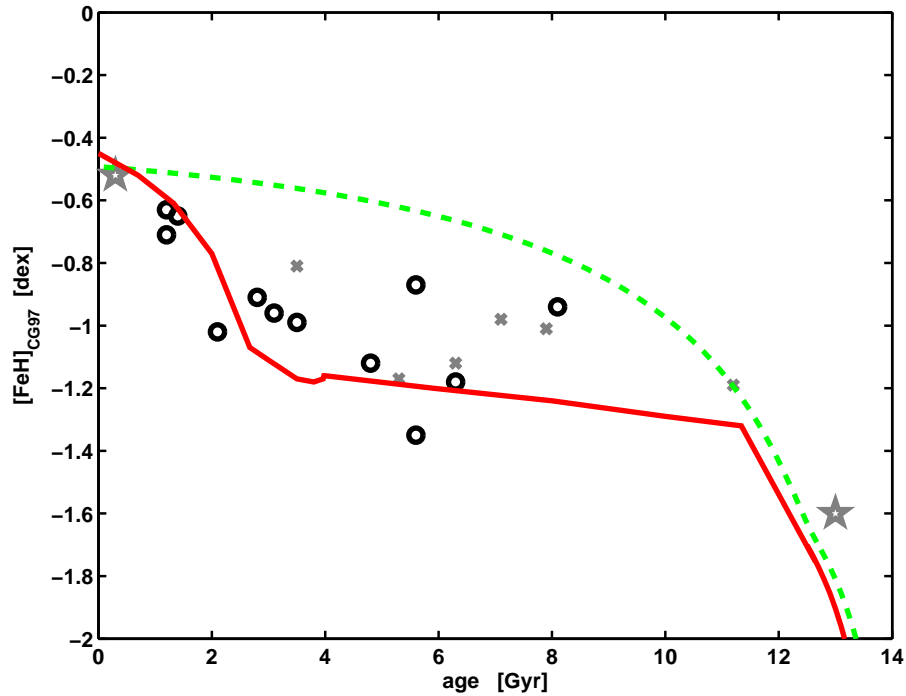


**Figure 5.20:** Age-metallicity relation of the SMC in comparison with chemical evolution models by Pagel & Tautvaišienė (1998). The continuous model is plotted as the green dashed line. The red solid line shows the bursting models with three major phases of different star formation efficiencies. The black circles and gray crosses indicate the metallicity results from this project and by Da Costa & Hatzidimitriou (1998), respectively. The ancient and pre-set day metallicity of the SMC are indicated by large gray stars.

the SMC we used the photometric survey by Zaritsky et al. (2002) as a guide. We re-identified both, the inner and outer clusters in the age-metallicity plot. Figure 5.19 confirms the previously mentioned metallicity gradient (see Chapter 5.6.1). Most of the metal-poor clusters are located in the outer part of the SMC, whereas the metal-rich clusters tend to be located more centrally. We compared both selected groups with the slope of the Simple closed-box model. It turns out that neither follows the theoretical predictions of the model.

### Pagel & Tautvaišienė 1998

More sophisticated models were presented by Pagel & Tautvaišienė (1998). They distinguished between a simple continuous model and a bursting model of star formation. A well known problem of simple theoretical evolution models is that a closed-box model predicts a too large number of very metal-poor stars (G-dwarfs) (see Tinsley (1980) for a review). In order to alleviate this G-dwarf problem many previous models either assumed a steepened initial mass function (IMF), selective galactic winds (e.g., Pilyugin 1996; Russell & Dopita 1992), or star formation from pre-enriched gas. In contrast, Pagel & Tautvaišienė (1998) intended to reproduce the age-metallicity relation without any of these modifications. They assumed that the SMC was built up by gradual infall of unprocessed material. Furthermore, for both models they included a time delay approximation, accounting for the delayed ejection of elements after the time of star formation. The mass loss from the galaxy is still assumed to take place instantaneously.

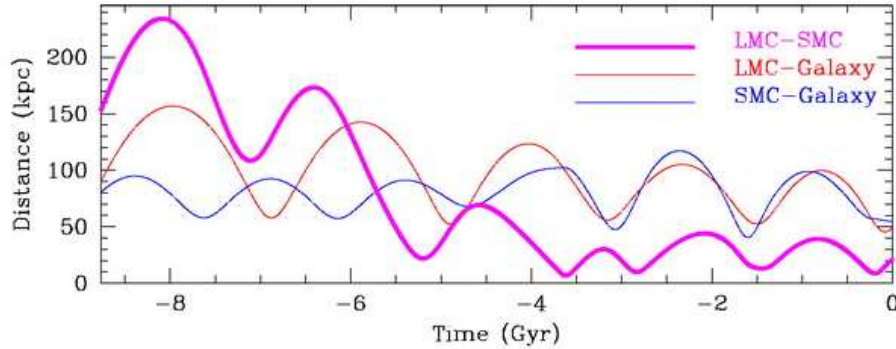


**Figure 5.21:** Schematic view of the orbital evolution of the Clouds. The plot is taken from Bekki et al. (2004). The distances are given as a function of time for the LMC-SMC (thick magenta line), LMC-MW (red line) and SMC-MW (blue line) individually. Negative values of time represent the past. Note that the LMC-SMC distance remains very small ( $< 40$  kpc) over the last 4 Gyr.

For the continuous model Pagel & Tautvaišienė (1998) assumed a constant star formation rate over the entire time period. The bursting model includes three intervals of constant star formation rates with abrupt changes of star formation efficiencies in between. This model starts with an initial star burst, which is followed by a quiescent phase during the time from 1.3 to 10 Gyr. After 10 Gyr the model assumes a second stronger starburst.

The resulting AMRs are shown in Fig. 5.20 in comparison with our data. Neither the continuous nor the bursting model provide a perfect reproduction of the observed relation. Nevertheless, we find the observed age-metallicity relation based on our star cluster analysis to be better reproduced by the model with temporal changes in the star formation history. Due to the lack of very old, globular cluster like star clusters in the SMC we cannot make any comment on the earliest evolution of this galaxy. The flat regime between 1.3 and 10 Gyr in the bursting model is qualitatively in agreement with the observed mean metallicity of the star clusters during that epoch. The large scatter in metallicity cannot be reproduced. This is not alarming since the model only reproduces the overall chemical evolution of this system. Local abundance variations are not implemented. For the most recent past we observe an increase in metallicity which is also reasonably well fitted by the second model of Pagel & Tautvaišienė (1998).

Given these caveats, the bursting model is by far the best fit to the observed age-metallicity relation. The comparison between model and data suggests that small modifications of the model may improve the fit, e.g., a small extension of the first initial enrichment period may better reproduce the metallicity of the oldest star cluster NGC 121 and the flat regime.

### Dynamical models

It is known that the SMC is strongly interacting with its neighboring galaxies, the LMC and the MW. Though a recent re-determination of the proper motions has cast doubts on that picture (Besla et al. 2007). Evidence for the tidal distortion is clearly visible in the form of the Magellanic Stream and Magellanic Bridge. Therefore, it is self-evident to study their mutual dynamical evolution in order to draw conclusions on impacts on the star and cluster formation histories of the individual objects. Various numerical models of the orbital evolution the Magellanic Clouds around the Galaxy exist in the literature (e.g., Gardiner

et al. 1994; Girardi et al. 1995; Gardiner & Noguchi 1996; Bekki & Chiba 2005). In these models the Magellanic Stream and the Magellanic Bridge are generally modeled as products of the tidal interaction between the component the triple-system.

Grebel (2000) pointed out that the pronounced peak in the cluster formation history of the LMC 1–2 Gyr ago coincides with the second last close encounter with the Milky Way from the Girardi et al. (1995) model. Furthermore, the peaks in the LMC and SMC cluster distributions at 100–200 Myr lookback time fall in the same epoch as the last close encounter between the two Clouds predicted by Gardiner et al. (1994). Thus, the probably enhanced cluster formation at those times may have been triggered by these events.

The recent theoretical models by Bekki et al. (2004) predict a close encounter between the SMC and LMC 3.6 Gyr ago, with an apocentric distance of less than 10 kpc. Figure 5.21 gives a schematic view of the orbital evolution of the Clouds. From  $N$ -body simulations they found that due to dynamical coupling the distance of the two clouds remained very small ( $< 40$  pc) at all times after this first encounter. The initial idea of this theoretical work was to model the observed cluster age distribution of the LMC. The interaction between LMC and the MW was considered as a potential cause for the prominent gap in the star cluster age distribution and of the enhanced star formation at a lookback time of 3 Gyr.

More recently this concept has been picked up to interpret the observed age distribution function of the SMC star clusters (e.g., Piatti et al. 2005b). The simulated close encounter may have given rise to an enhanced cluster formation, although these peaks in the age distribution are not as pronounced as in the LMC. The comparison with our age-metallicity relation shows that the time of the close encounter 3.6 Gyr ago is also the time regime at which we observe the strong increase in metallicity. Furthermore, the most recent perigalactic encounter with the MW ( $\approx 1.5$  Gyr) (Gardiner & Noguchi 1996) approximately falls in the epoch of enhanced star formation observed by Harris & Zaritsky (2004). This indicates that interaction between the three galaxies may have strongly influenced the star cluster formation efficiency and the mixing in the SMC.

However, the "traditional" orbital models of the Magellanic Clouds have recently been challenged. New proper motion measurements and new detailed Milky Way models allowed a revised modeling of the orbital history of the two Galactic companions. Besla et al. (2007) suggested from their model that the Magellanic Clouds have completed only one passage about the MW with in 10 Gyr. Hence the timescale over which the triplesystem has interacted was much shorter. However, the time of the first encounter still supports a significant increase in the star formation rate of the Magellanic Clouds 1–2 Gyr ago.

#### 5.6.4 Discussion

The comparison of our age-metallicity relation with the theoretical models favors a bursting model as described by Pagel & Tautvaisiene (1998). This model implies a variable star formation rate with a quiescent phase of the SMC between 12 and 4 Gyr ago. Low star formation means on the other hand a slow increase of abundances due to the decreased injection of SNeII ejecta into the ISM. Therefore, the existence of a less active period of star formation (SF) could be a possible explanation of the observed constant  $[\text{Fe}/\text{H}]$  over several Gyr. Recent photometric studies (e.g., Rafelski & Zaritsky 2005; Piatti et al. 2005a) also suggested the existence of at least two bursts of star/cluster formation activity. This was also confirmed by the field star analysis by Harris & Zaritsky (2004) of the Magellanic Cloud Photometric Survey (Zaritsky et al. 2002). The bursting model of Pagel & Tautvaisiene

(1998) also assumes the SMC to have been built up by gradual infall of unprocessed material. An inhomogeneous episodic gas accretion could furthermore drive the variations in  $[\text{Fe}/\text{H}]$  observed at that time. A question often addressed in this context is: If the SFR was really that low, why did the SMC form so many clusters during that early time? An answer to this question might be that the SMC was not completely quiescent but in a low SF mode and might have continued forming a low number of star clusters. Furthermore the gap in the age distribution of the star clusters in the LMC, which is not seen for field stars, shows that the star cluster formation is not necessarily closely related to overall star formation.

Such a bursting model could naturally explain the underabundance of  $\alpha$ -elements relative to iron compared to Galactic stars found in the MCs (Gilmore & Wyse 1991). If star formation occurs in an initial burst and is followed by a period of low star formation, then Type Ia supernovae will contribute extra iron during this phase. Consequently, stars forming afterwards are underabundant in  $\alpha$ -elements. The model of star formation activities by Hirashita (2000) showed that intermitting star formation histories are expected for dIrr galaxies. The small size (i.e., short propagation time-scales) and the low metallicity (i.e., short cooling time-scales) are responsible for the intermittences. Furthermore, their model exhibits a relation between mixing efficiency and star formation history. Efficient interstellar mixing shortens the cooling time and therefore may prevent intermittence. The mixing of the ISM with primordial material would dilute the abundances locally. In such a scenario we expect the stars in the surrounding fields of the clusters to have experienced the same chemical history as the clusters themselves. Open questions that still remain are: Where did the gas come from? Could metal-poor intergalactic HI clouds be possible sources of the infalling gas? What are the drivers of SF? What is the relation to the Magellanic Stream?

Besides this locally varying gas infall, another possible explanation of the scatter in  $[\text{Fe}/\text{H}]$  could be temporal variations in overall gas content of the SMC. We could hypothesize that if the overall amount of gas varied with time this would have had consequences for the enrichment efficiency in the galaxy. A high gas content involves a strong dilution of the metal-enriched ejecta by supernovae and evolving stars. A lower gas content in the past means that the cloud material could be enriched more efficiently. The resulting local abundance pattern in the SMC would then be strongly dependent on the structure of the cloud - which is not understood so far. Complex shell structures have been found in the neutral Hydrogen map (HI), which are all apparently very young (Staveley-Smith et al. 1997). It is conceivable that similar structures might have also existed in the past. However, for a local enrichment these shell structures would need to be smaller than the ones observed today. In smaller regions shorter time scales are needed to enrich/dilute the material. Again the open question of the origin of the primordial gas remains.

Another idea could be that the cloud enriched itself locally on timescales of a few megayears by supernova type II -explosions (SN II) (see e.g., Lanfranchi & Matteucci 2003). We find this scenario very unlikely, since in order to enrich the entire pre-cluster cloud an unrealistically large number of SNe would be needed. To enrich material of the mass of a typical SMC star cluster ( $M_i = 10\,000 M_\odot$ ) by  $Z = 0.005$ , a mass of metals in the initial pre-cluster gas of  $ZM_i = 50 M_\odot$  is required. Therefore about 10 to 20 SN II are needed. As only  $\approx 10\%$  of the initial material is locked into the star cluster, whereas the majority of 85% remains in a gaseous phase, one would need 100 to 200 SNe II in order to enrich the whole cloud. According to the standard IMF this is a very high and therefore unlikely amount. Thus, the major problem of this scenario is: How could the first generation of stars in the pre-clusters produce enough metals to account for the enrichment that we observe today? Furthermore,



at that time, when the large scatter is present, clusters are found with metallicities lower than those observed after the initial enrichment of the SMC. This favors a scenario of infall of low metallicity gas and local dilution instead of the local enrichment scenario.

Another possibility to explain the observed scatter in the SMC at a given age could be a spatial gradient of metallicity in the SMC when it was young. For the majority of Local Group dwarf spheroidal galaxies Harbeck et al. (2001) found the younger, more metal rich stars to be more centrally concentrated than their old and metal poor counterparts. Although we only see a weak gradient in  $[\text{Fe}/\text{H}]$  in the SMC star clusters system for the intermediate age clusters today, this does not mean that it could not have been strongly present in the past. Due to the evolution of the system we do not know where these clusters were located in the SMC at the time of their formation. But why don't we see a clear spatial gradient today?

A possible explanation of the observed sudden increase in  $[\text{Fe}/\text{H}]$  starting about 3 Gyr ago can be drawn from the dynamical model by e.g., Bekki et al. (2004) or more recently Besla et al. (2007). Although the models deviate significantly in the proposed orbital histories, they both suggest a recent close encounter of the SMC/LMC/MW system. Thus, they both support the theory that the significant increase in the star cluster formation rates of the Magellanic Clouds during the last  $\sim 3$  Gyr may be caused by the interaction of the MCs and/or the interaction with the MW. The theoretical model by Pagel & Tautvaišienė (1998) showed that this leads to a strong increase in metallicity. Since the expanding shells from high mass stars are considered to be responsible for the mixing of the interstellar material (Roy & Kunth 1995), the recent strong starburst a few Gyr ago and the corresponding larger number of high mass stars could have produced in a more uniformly mixed SMC. Heating effects (e.g., tidal heating) may have supported the present-day SMC to be mixed again. This is in agreement with the observed decrease of the relative scatter in metallicity at later epochs. An example for such a mechanism of heating effects by Galactic tides, which can also trigger dynamical instabilities and reshape small galaxies, was described by Mayer et al. (2001). They referred to it as "tidal shirring". A question that might arise in this context is: Why are the cluster formation histories of the LMC and SMC so different? An answer to this was proposed in Bekki et al. (2004). They argued that the difference results from the different initial masses and places of formation of the two clouds within the Local Group.

Strong evidence for chemical inhomogeneities in another dIrr galaxy was given by Kniazev et al. (2005). They observed high-quality spectra of HII regions in the two dIrr galaxies Sextans A and Sextans B. In the latter they found considerable inhomogeneities in the present-day metallicity distribution. Thus, we believe that, although dIrr galaxies are usually believed to be chemically well mixed, some of these objects can exhibit local deviations from the average galactic metallicity at a given age. It might be interesting to mention that despite star formation histories are substantially different for various kinds of galaxies, some of the observed feature of the age-metallicity relation of the SMC can also be found in other near-by galaxies. For example, Koch et al. (2007) found that the age-metallicity relation of the Leo II dSph is essentially flat over a long time interval, with evidence for an enrichment during the last 2–4 Gyr. Furthermore, investigations of field stars in the LMC (Cole et al. 2005) and in the solar neighborhood (e.g., Feltzing et al. 2001; Nordström et al. 2004) revealed a large scatter in metallicity at a given age in the age-metallicity relations of both galaxies.

A brief overview of our findings as well as the possible explanations and open questions are given in Table 5.6.

**Table 5.5:** Compilation of available SMC cluster data. Listed are only those cluster for which metallicity estimates exist.

Cluster	Instrument	Age [Gyr]	[Fe/H] <sub>photo</sub> [dex]	[Fe/H] <sub>int</sub> [dex]	[Fe/H] <sub>spec</sub> [dex]	Reference
L 1			-1.0±			Gascoigne et al. (1981)
	CTIO <sup>f</sup>	9 ± 1	-1.3 ± 0.2			Olszewski et al. (1987)
	HST/WFP2 <sup>b</sup>	7.7 ± 0.4	-1.35 ± 0.08			Mighell et al. (1998)
		9.0 ± 1.0				
	AAT <sup>c</sup>	9 – 10	-1.05 ± 0.14		-1.01 ± 0.11	Da Costa & Hatzidimitriou (1998)
	HST/WFP2 <sup>b</sup>	7.9 ± 0.3			Alcaino et al. (2003)	
L 4, K 1		3.1 ± 0.9	-0.9 ± 0.2			Glatt et al. (2008)
L 5		4 ± 0.9	-1.2 ± 0.2			Piatti et al. (2005b)
		3.0 ± 1.5		-1.1 ± 0.2		Piatti et al. (2005a)
L 6, K 4		3.3 ± 0.9	-0.9 ± 0.2			Piatti et al. (2005b)
L 7, K 5		3.2 ± 0.3	-1.1 ± 0.2			Bica et al. (1986)
		1.2 ± 0.5		-0.5 ± 0.2		Piatti et al. (2005a)
		2.0 ± 0.2	-0.6 ± 0.2			Piatti et al. (2005b)
L 8, K 3	CTIO <sup>f</sup>	6 ± 2	-1.3±			Rich et al. (1984)
		> 10	-1.5 ± 0.2			Bica et al. (1986)
	MPIT <sup>e</sup>	9.0 ± 2.0	-1.26 ± 0.11			Alcaino et al. (1996)
	HST/WFP2 <sup>b</sup>	4.7 ± 0.6	-1.16 ± 0.09			Mighell et al. (1998)
		6.0 ± 1.3				
	AAT <sup>c</sup>				-0.98 ± 0.12	Da Costa & Hatzidimitriou (1998)
	LNA <sup>d</sup>	3.5 ± 2.0		-1.00 ± 0.28		de Freitas Pacheco et al. (1998)
	7.0 ± 1.0		-1.2 ± 0.2		Piatti et al. (2005a)	
	HST/WFP2 <sup>b</sup>	7.1 ± 0.3			Glatt et al. (2008)	
L 9, K 6		1.6 ± 0.4		-0.7 ± 0.2		Piatti et al. (2005b)
L 10, K 2, NGC 121	HST/WFP2 <sup>b</sup>	10.6 ± 0.7	-1.71 ± 0.10			Mighell et al. (1998)
		11.9 ± 1.3				
	AAT <sup>c</sup>				-1.19 ± 0.12	Da Costa & Hatzidimitriou (1998)
	CTIO <sup>f</sup>	12.0 ± 2.0	-1.4±			Stryker et al. (1985)
		> 10	-1.3 ± 0.2			Bica et al. (1986)
	LNA <sup>d</sup>	12.0 ± 5.0		-1.20 ± 0.32		de Freitas Pacheco et al. (1998)
	HST/WFP2 <sup>b</sup>	11.2 ± 0.3				Glatt et al. (2008)
L 11	CTIO <sup>f</sup>	3.5 ± 1.0	-1.3 ± 0.2			Mould et al. (1992)
	AAT <sup>c</sup>				-0.81 ± 0.13	Da Costa & Hatzidimitriou (1998)

Continued on next page

Compilation of available SMC cluster data - <i>continued</i>						
		$3.5 \pm 0.5$		$-1.0 \pm 0.2$		Piatti et al. (2005a)
					$-0.92 \pm 0.13$	Kayser et al. (2008b)
L 15, NGC 152	HST/WFP2 <sup>b</sup>	$3.2 \pm 0.3$	$-1.25 \pm 0.25$			Bica et al. (1986)
	CTIO <sup>f</sup>	$1.4 \pm 0.2$	$-0.94 \pm 0.15$			Crowl et al. (2001)
		$1.9 \pm 0.5$	$-0.8 \pm 0.3$			Hodge (1981); Mould & Da Costa (1988)
					$-0.65 \pm 0.06$	Kayser et al. (2008b)
L 16, K 12, NGC 176	HST/WFP2 <sup>b</sup>	$0.2 \pm 0.2$	$-0.6$			Mackey & Gilmore (2003a)
L 19		$2.1 \pm 0.2$	$-0.75 \pm 0.2$			Piatti et al. (2005b)
L 27, K 21		$2.1 \pm 0.2$	$-1.3 \pm 0.3$			Piatti et al. (2005b)
L 32	CTIO <sup>a</sup>	$4.8 \pm 0.5$	$-1.2 \pm 0.2$			Piatti et al. (2001)
					$-1.12 \pm 0.18$	Kayser et al. (2008b)
L 34, K 24, NGC 265		$0.32$	$-0.62$			Chiosi & Vallenari (2007)
L 38	CTIO <sup>a</sup>	$6.0 \pm 0.6$	$-1.65 \pm 0.2$			Piatti et al. (2001)
					$-1.35 \pm 0.10$	Kayser et al. (2008b)
	HST/WFP2 <sup>b</sup>	$5.6 \pm 0.3$				Glatt et al. (2008)
L 42, NGC 290		$0.06$	$-0.75$			Chiosi & Vallenari (2007)
L 43, K 28	CTIO <sup>a</sup>	$2.1 \pm 0.5$	$-1.2 \pm 0.2$			Piatti et al. (2001)
	CTIO <sup>h</sup> , CASLEO <sup>i</sup>	$1.5 \pm 0.6$		$-1.0 \pm 0.2$		Piatti et al. (2005a)
					$-1.02 \pm 0.10$	Kayser et al. (2008b)
L 44, K 29		$0.16$	$-0.75$			Chiosi & Vallenari (2007)
L 54, K 35, NGC 330			$-1.0 \pm$			Spite et al. (1991)
			$-1.26 \pm$			Grebel & Richtler (1992)
		$0.025 \pm 0.015$				Chiosi et al. (1995)
					$-0.82 \pm 0.1$	Hill (1999)
					$-0.94 \pm 0.02$	Gonzalez & Wallerstein (1999)
L 59, K 36, NGC 339		$> 10$	$-1.5 \pm 0.2$			Bica et al. (1986)
	HST/WFP2 <sup>b</sup>	$5.0 \pm 0.6$	$-1.50 \pm 0.14$			Mighell et al. (1998)
		$6.3 \pm 1.3$				
	AAT <sup>c</sup>	$4.0 \pm 1.5$			$-1.19 \pm 0.10$	Da Costa & Hatzidimitriou (1998)
	LNA <sup>d</sup>	$2.0 \pm 0.7$		$-0.70 \pm 0.22$		de Freitas Pacheco et al. (1998)
					$-1.19 \pm 0.04$	Kayser et al. (2008b)
	HST/WFP2 <sup>b</sup>	$6.3 \pm 0.3$				Glatt et al. (2008)
L 67, K 46, NGC 361		$8 \pm 1.5$	$-1.25 \pm 0.2$			Bica et al. (1986)
	HST/WFP2 <sup>b</sup>	$6.8 \pm 0.5$	$-1.45 \pm 0.11$			Mighell et al. (1998)
		$8.1 \pm 1.2$				
					$-0.94 \pm 0.08$	Kayser et al. (2008b)
L 68, K 44	CTIO <sup>a</sup>	$3.1 \pm 0.8$	$-1.1 \pm 0.2$			Piatti et al. (2001)

*Continued on next page*

Compilation of available SMC cluster data - *continued*

				$-0.96 \pm 0.09$	Kayser et al. (2008b)
L 82 K 60, NGC 411	CTIO <sup>f</sup>	$1.8 \pm 0.3$	$-0.9 \pm 0.3$		Da Costa & Mould (1986)
		$3.4 \pm 0.3$	$-1.3 \pm 0.2$		Bica et al. (1986)
	HST/WFP2 <sup>b</sup>	$1.4 \pm 0.2$	$-0.68 \pm 0.12$		Alves & Sarajedini (1999)
	LNA <sup>d</sup>	$1.3 \pm 0.7$		$-0.70 \pm 0.22$	de Freitas Pacheco et al. (1998)
	CTIO <sup>h</sup> ,CASLEO <sup>i</sup>	$1.5 \pm 0.3$		$-0.7 \pm 0.2$	Piatti et al. (2005a)
	CTIO <sup>h</sup>	$1.2 \pm 0.2$	$-0.43 \pm 0.14$		Leonardi & Rose (2003)
				$-0.63 \pm 0.07$	Kayser et al. (2008b)
L 83, K 83, NGC 416	DPT <sup>g</sup>	$2.5 \pm 0.7$			Durand et al. (1984)
		$8 \pm 1.5$	$-1.25 \pm 0.2$		Bica et al. (1986)
	HST/WFP2 <sup>b</sup>	$5.6 \pm 0.3$	$-1.45 \pm 0.12$		Mighell et al. (1998)
		$6.9 \pm 1.1$			
	LNA <sup>d</sup>	$4.0 \pm 1.5$		$-0.80 \pm 0.23$	de Freitas Pacheco et al. (1998)
				$-0.87 \pm 0.06$	Kayser et al. (2008b)
					Glatt et al. (2008)
L 85, K 58, NGC 419	DPT <sup>g</sup>	$1.2 \pm 0.7$	$-0.7 \pm 0.3$		Durand et al. (1984)
		$3.5 \pm 0.3$	$-1.2 \pm 0.2$		Bica et al. (1986)
	LNA <sup>d</sup>	$1.2 \pm 0.5$		$-0.60 \pm 0.21$	de Freitas Pacheco et al. (1998)
	HST/WFP2 <sup>b</sup>	$2.0 \pm 0.2$			Rich et al. (2000)
	CTIO <sup>h</sup> ,CASLEO <sup>i</sup>	$1.2 \pm 0.4$		$-0.7 \pm 0.2$	Piatti et al. (2005a)
				$-0.71 \pm 0.12$	Kayser et al. (2008b)
L 96, K 69, NGC 458		$0.3 \pm 0.2$	$-0.3$		Papenhausen & Schommer (1988)
		$0.13 \pm 0.06$		$-0.23 \pm 0.2$	Piatti et al. (2005a)
L 111, NGC 643		$1.5 \pm 0.3$	$-0.6 \pm 0.25$		Bica et al. (1986)
L 113	HST/WFP2 <sup>b</sup>	$4.0 \pm 0.7$	$-1.24 \pm 0.11$		Mighell et al. (1998)
		$5.3 \pm 1.3$			
	CTIO <sup>f</sup>	$6.0 \pm 1.0$	$-1.4 \pm$		Mould et al. (1984); Seidel et al. (1987)
				$-1.17 \pm 0.12$	Da Costa & Hatzidimitriou (1998)
L 116	AAT <sup>c</sup>				
	CTIO <sup>a</sup>	$2.8 \pm 1.0$	$-1.1 \pm 0.2$		Piatti et al. (2001)
				$-0.91 \pm 0.06$	Kayser et al. (2008b)
BS 90, NGC 346		$4.5 \pm 0.1$	$-0.84 \pm$		Sabbi et al. (2007)
		$4.5 \pm 0.5$	$-0.71 \pm$		Rochau et al. (2007)
BS 121		$2.3 \pm 0.2$	$-1.2 \pm 0.4$		Piatti et al. (2005b)
HW 47		$2.8 \pm 0.9$	$-1.0 \pm 0.4$		Piatti et al. (2005b)
HW 84		$2.4 \pm 0.2$	$-1.2 \pm 0.4$		Piatti et al. (2005b)
HW 86		$1.6 \pm 0.2$	$-0.75 \pm 0.4$		Piatti et al. (2005b)

*Continued on next page*

Compilation of available SMC cluster data - *continued*

---

<sup>a</sup>Cerro Tololo Inter-American Observatory (0.9 m), <sup>b</sup>Hubble Space Telescope/Wide Field Planetary Camera2, <sup>c</sup>Anglo-Australian Telescope,  
<sup>d</sup>Laboratório Nacional de Astrofísica, Brazil (1.6 m), <sup>e</sup>Max-Planck-Institute Telescope ESO/La Silla, Chile (2.2 m),  
<sup>f</sup>Cerro Tololo Inter-American Observatory (4 m), <sup>g</sup>Du Pont Telescope, Las Campanas (2.5 m),  
<sup>h</sup>Cerro Tololo Inter-American Observatory (1.5 m), <sup>i</sup>Complejo Astronómico El Leoncito San Juan/Argentina (2.15 m)

**Table 5.6:** Overview of our findings, possible explanations, and open questions.

Detection	Possible Explanation	Problems
Scatter in $[\text{Fe}/\text{H}]$ at a certain age	SMC was not well mixed in the past <ul style="list-style-type: none"> <li>• Spatial: Spatial gradient when young</li> <li>• Easier metal loss in outskirts areas</li> <li>• Time: Overall gas content varies with time <math>\Rightarrow</math> Variations in dilution</li> <li>• Spatial &amp; Time: Small regions <math>\Rightarrow</math> Short timescales <math>\Rightarrow</math> Local enrichment</li> <li>• Self enrichment via SN II</li> </ul>	<ul style="list-style-type: none"> <li>• Where does the gas come from?</li> <li>• What is the driver of SF?</li> <li>• How does this make enough metals that are retained?</li> </ul>
Mean $[\text{Fe}/\text{H}]$ fairly constant for several Gyr	Less active phase in SMC <ul style="list-style-type: none"> <li>• PT98 model: gas infall and variable SFR</li> </ul> $\Rightarrow$ Can probably also drive $[\text{Fe}/\text{H}]$ variations via dilution $\Rightarrow$ Field stars $\sim$ star clusters	<ul style="list-style-type: none"> <li>• Where does the gas come from?</li> <li>• Why so many star clusters in this period?</li> </ul>
Increase of $[\text{Fe}/\text{H}]$ and decrease of relative scatter in recent past (3 Gyr ago)	Interaction of LMC/SMC <ul style="list-style-type: none"> <li>• Heating <math>\Rightarrow</math> SMC well mixed again</li> <li>• BC04 model <math>\Rightarrow</math> enhanced star formation rates</li> </ul>	<ul style="list-style-type: none"> <li>• Why are the clusters formation histories of LMC and SMC different?</li> </ul>

## 5.7 Summary and Conclusions

The SMC is the only dwarf galaxy on the Local Group known to have formed and preserved stars clusters throughout its entire lifetime. Despite its proximity and rich cluster population its has only been sparsely studied.

Our study allows an improvement of the knowledge of the overall chemical evolution of the SMC. We provide an important step towards the understanding of the history of the SMC. We present the results from our VLT multi-object spectroscopy of individual red giant stars in twelve star clusters in the SMC. The targeted clusters span a large spatial area within the SMC, ranging from the central body to the outskirts, out to about 6 kpc in projected distance from the center. In combination with the preceding study by Da Costa & Hatzidimitriou (1998) we cover the largest possible age range.

We observed about 40–50 stars in the direction of each cluster. Member candidates for each cluster were carefully selected by their positions in the CMD, their radial velocities, their distances from the cluster centers, and their metallicities. Absolute  $[\text{Fe}/\text{H}]$  values were derived for all twelve clusters using the CaT technique. We achieved a mean accuracy of 0.09 dex. Our metallicity results were found to be in good agreement with previous metallicity estimates, both photometric and spectroscopic.

The consideration of the star clusters' spatial distribution revealed a slight indication for a radial metallicity gradient, where the more metal-rich clusters are located closer to the center of the galaxy. The linear fit yields the small decline of 1 dex/°. In contrast the more metal-poor clusters are more widely spread over the entire galaxy. This gradient disappears when only clusters of similar ages are considered, meaning, that the observed gradient is probably primarily caused by age effects. This suggests that star formation could proceed for longer times in the inner regions of the SMC.

The combination with age estimates from various sources in the literature provides for the first time a well-sampled age-metallicity relation for the SMC, which is fully based on spectroscopic metallicity estimates. We find a weak scatter in metallicity within the errors to be present at almost all ages. However, at an age of  $\approx 6$  Gyr we detect a pronounced metallicity spread of more than 0.4 dex, much larger than the mean uncertainty in  $[\text{Fe}/\text{H}]$  of 0.09 dex. Obviously the SMC was not well mixed in the past. Furthermore, we confirm a strong increase in metallicity, starting 2–3 Gyr ago. This increase is accompanied by a decrease of the scatter in metallicity of clusters of approximately the same age.

The comparison with theoretical models suggests that the chemical enrichment did not occur continuously in the SMC. We find that our observed age-metallicity relation cannot be reproduced by a Simple closed-box model. In fact, our relation favors the bursting model by Pagel & Tautvaisiene (1998). Nevertheless, there is a clear need for more sophisticated models, ideally exclusively tailored for the MCs. Both the theoretical model, as well as the observed scatter at a given age strongly suggest that infall of unprocessed material has probably played an important role in the history of the SMC.

The comparison with the dynamical models (e.g., Bekki et al. 2004; Besla et al. 2007) suggests that the interaction between LMC-SMC-MW needs to be carefully considered. The detected increase in metallicity coincides in time with a recent close encounter of the SMC and LMC (or MW) that occurred  $\sim 3$  Gyr ago. We conclude that this interaction and associated mechanism, such as tidal heating, may be a significant driver for an enhanced star and star cluster formation activity and mixing effects within the SMC.

In order to further constrain our results, especially the scatter in  $[\text{Fe}/\text{H}]$  at 6 Gyr it is nec-

essary to further complete the existing sample of spectroscopic metallicity estimates of SMC star clusters. Moreover, still only for a minority of star clusters accurate age estimates based on HST observation are existent. Better age determinations for most clusters are absolutely essential in order to alleviate remaining uncertainties due to inaccurate age estimates.

For comparison, the observation of the age-metallicity relation based on the SMC field star population would be very interesting. This will further constrain the chemical evolution history of the SMC but also will shed light on how well star cluster investigations trace the overall chemical evolution of a galaxy.



## Appendix 5.A

### Target stars in SMC star clusters

Table 5.A: Parameters of stars in Kron28.

Star	alpha	delta	$I$	$V$	$(V - I)$	$V - V_{\text{HB}}$	$\Sigma W$	$[\text{Fe}/\text{H}]$	CMD	membership criteria		
	(J2000)	(J2000)	[mag]	[mag]	[mag]	[mag]	Å	dex		velocity	distance	metallicity
2.1	0 : 51 : 40	-72 : 3 : 57	17.48	18.52	1.04	-1.29	6.52 ± 0.08	-0.95 ± 0.10	1	1	0	0
4.1	0 : 51 : 35	-72 : 3 : 45	17.64	18.65	1.02	-1.16	6.16 ± 0.06	-1.04 ± 0.10	1	1	0	0
5.1	0 : 51 : 49	-72 : 3 : 40	17.38	18.45	1.06	-1.36	6.56 ± 0.06	-0.95 ± 0.10	1	0	0	0
6.1	0 : 51 : 34	-72 : 3 : 33	17.55	18.63	1.09	-1.18	5.80 ± 0.06	-1.18 ± 0.09	1	0	0	0
7.1	0 : 51 : 47	-72 : 3 : 24	17.16	18.27	1.11	-1.54	7.13 ± 0.07	-0.79 ± 0.11	1	1	0	0
8.1	0 : 51 : 40	-72 : 3 : 20	17.50	18.57	1.07	-1.24	5.89 ± 0.07	-1.16 ± 0.09	1	0	0	0
10.1	0 : 51 : 23	-72 : 3 : 4	17.64	18.75	1.11	-1.06	6.12 ± 0.07	-1.03 ± 0.10	1	0	0	0
11.1	0 : 51 : 41	-72 : 2 : 54	15.76	17.00	1.24	-2.81	7.01 ± 0.04	-1.17 ± 0.10	1	0	0	0
12.1	0 : 52 : 4	-72 : 2 : 38	16.99	18.19	1.20	-1.62	7.23 ± 0.05	-0.78 ± 0.11	1	1	0	0
13.1	0 : 51 : 18	-72 : 2 : 33	15.84	17.06	1.22	-2.75	8.12 ± 0.05	-0.75 ± 0.11	1	0	0	0
14.1	0 : 51 : 12	-72 : 2 : 24	17.59	18.47	0.89	-1.34	6.49 ± 0.07	-0.97 ± 0.10	1	0	0	0
15.1	0 : 51 : 21	-72 : 2 : 18	17.14	18.33	1.18	-1.48	6.25 ± 0.05	-1.10 ± 0.10	1	0	0	0
17.1	0 : 51 : 18	-72 : 2 : 1	16.92	18.04	1.12	-1.77	6.80 ± 0.05	-0.97 ± 0.10	1	0	0	0
18.1	0 : 51 : 32	-72 : 1 : 55	17.06	18.10	1.04	-1.71	7.04 ± 0.06	-0.87 ± 0.10	1	0	0	0
20.1	0 : 51 : 54	-72 : 1 : 37	17.55	18.70	1.16	-1.11	6.86 ± 0.08	-0.78 ± 0.11	1	0	0	0
21.1	0 : 51 : 28	-72 : 1 : 33	18.29	19.20	0.91	-0.61	5.33 ± 0.08	-1.20 ± 0.09	1	0	0	0
21.2	0 : 51 : 28	-72 : 1 : 31	16.96	18.05	1.09	-1.76	6.96 ± 0.05	-0.91 ± 0.10	1	0	0	0
23.1	0 : 51 : 45	-72 : 1 : 15	17.40	18.49	1.09	-1.32	6.53 ± 0.09	-0.95 ± 0.10	1	1	1	1
24.1	0 : 51 : 59	-72 : 0 : 52	17.22	18.28	1.05	-1.53	5.78 ± 0.05	-1.28 ± 0.09	1	0	0	0
25.1	0 : 51 : 55	-72 : 0 : 46	16.63	17.86	1.23	-1.95	6.24 ± 0.04	-1.22 ± 0.09	1	1	1	0
27.1	0 : 51 : 53	-72 : 0 : 34	17.26	18.39	1.13	-1.42	6.51 ± 0.05	-0.98 ± 0.10	1	0	0	0
29.1	0 : 51 : 34	-72 : 0 : 23	17.02	18.18	1.16	-1.63	6.35 ± 0.05	-1.10 ± 0.10	1	1	1	1
30.1	0 : 51 : 25	-72 : 0 : 12	16.69	17.74	1.04	-2.07	6.33 ± 0.04	-1.22 ± 0.09	1	0	0	0
31.1	0 : 51 : 57	-72 : 0 : 8	16.95	18.08	1.13	-1.73	6.59 ± 0.05	-1.04 ± 0.10	1	1	1	1
32.1	0 : 51 : 17	-71 : 59 : 59	16.95	17.76	0.81	-2.05	5.77 ± 0.05	-1.42 ± 0.09	0	1	0	0
33.1	0 : 51 : 48	-71 : 59 : 52	16.84	17.99	1.15	-1.82	6.53 ± 0.06	-1.09 ± 0.10	1	1	1	1
35.2	0 : 51 : 44	-71 : 59 : 38	16.84	18.01	1.17	-1.80	6.81 ± 0.06	-0.98 ± 0.10	1	1	1	1
37.1	0 : 51 : 51	-71 : 59 : 20	15.64	16.95	1.31	-2.86	7.80 ± 0.05	-0.90 ± 0.11	1	1	1	1
39.1	0 : 51 : 53	-71 : 59 : 6	17.13	18.20	1.08	-1.61	6.20 ± 0.06	-1.15 ± 0.09	1	1	1	1
40.1	0 : 51 : 16	-71 : 59 : 0	16.68	17.73	1.06	-2.08	6.93 ± 0.06	-1.01 ± 0.10	1	1	0	0
41.1	0 : 51 : 49	-71 : 58 : 53	15.99	17.13	1.15	-2.68	7.11 ± 0.04	-1.10 ± 0.10	1	1	1	1
42.1	0 : 51 : 44	-71 : 58 : 45	15.86	17.21	1.35	-2.60	7.58 ± 0.05	-0.91 ± 0.11	1	1	1	1
43.1	0 : 51 : 47	-71 : 58 : 37	17.16	18.31	1.15	-1.50	6.47 ± 0.04	-1.02 ± 0.10	1	1	1	1
45.1	0 : 51 : 46	-71 : 58 : 24	16.41	17.60	1.19	-2.21	7.02 ± 0.05	-1.01 ± 0.10	1	1	1	1

Continued on next page

Parameters of stars in Kron 28 - *continued*

47.1	0 : 52 : 0	-71 : 57 : 57	16.61	17.77	1.15	-2.04	$7.01 \pm 0.04$	$-0.97 \pm 0.10$	1	0	0	0
48.1	0 : 51 : 17	-71 : 57 : 50	16.73	17.51	0.78	-2.30	$4.34 \pm 0.04$	$-2.00 \pm 0.08$	0	0	0	0
49.1	0 : 51 : 42	-71 : 57 : 43	17.03	18.18	1.15	-1.63	$6.12 \pm 0.04$	$-1.18 \pm 0.09$	1	0	0	0
50.1	0 : 51 : 33	-71 : 57 : 35	16.94	18.08	1.14	-1.73	$5.95 \pm 0.04$	$-1.27 \pm 0.09$	1	1	0	0
51.1	0 : 51 : 25	-71 : 57 : 23	17.20	18.32	1.11	-1.49	$6.67 \pm 0.06$	$-0.95 \pm 0.10$	1	0	0	0
52.1	0 : 51 : 47	-71 : 57 : 19	15.90	16.87	0.97	-2.94	$8.08 \pm 0.06$	$-0.82 \pm 0.11$	0	0	0	0

Table 5.B: Parameters of stars in Kron 44.

Star	alpha	delta	$I$	$V$	$(V - I)$	$V - V_{\text{HB}}$	$\Sigma W$	$[\text{Fe}/\text{H}]$	CMD	membership criteria		
	(J2000)	(J2000)	[mag]	[mag]	[mag]	[mag]	Å	dex		velocity	distance	metallicity
1.1	1 : 2 : 16	-74 : 0 : 6	17.28	18.30	1.02	-1.48	$5.89 \pm 0.06$	$-1.22 \pm 0.09$	1	0	0	0
2.1	1 : 2 : 9	-73 : 59 : 56	18.51	19.34	0.83	-0.44	$5.70 \pm 0.10$	$-1.02 \pm 0.10$	1	0	0	0
3.1	1 : 1 : 46	-73 : 59 : 49	17.10	18.15	1.05	-1.63	$6.40 \pm 0.05$	$-1.08 \pm 0.09$	1	0	0	0
4.1	1 : 2 : 8	-73 : 59 : 42	17.91	18.86	0.95	-0.92	$2.72 \pm 0.07$	$-2.22 \pm 0.07$	1	1	0	0
5.1	1 : 1 : 49	-73 : 59 : 31	17.69	18.66	0.97	-1.12	$5.81 \pm 0.08$	$-1.16 \pm 0.09$	1	1	0	0
6.1	1 : 1 : 48	-73 : 59 : 22	16.77	17.72	0.95	-2.06	$6.67 \pm 0.05$	$-1.10 \pm 0.10$	1	1	0	0
7.1	1 : 2 : 15	-73 : 59 : 8	17.91	18.85	0.94	-0.93	$6.71 \pm 0.08$	$-0.78 \pm 0.10$	1	0	0	0
8.1	1 : 1 : 54	-73 : 59 : 2	16.60	17.67	1.07	-2.11	$6.68 \pm 0.06$	$-1.10 \pm 0.10$	1	0	0	0
9.1	1 : 2 : 24	-73 : 58 : 50	18.59	19.42	0.83	-0.36	$6.51 \pm 0.11$	$-0.70 \pm 0.11$	1	0	0	0
10.1	1 : 1 : 57	-73 : 58 : 42	17.50	18.53	1.02	-1.25	$5.86 \pm 0.07$	$-1.18 \pm 0.09$	1	0	0	0
11.1	1 : 2 : 23	-73 : 58 : 37	16.33	17.56	1.23	-2.22	$7.43 \pm 0.06$	$-0.86 \pm 0.10$	1	0	0	0
12.1	1 : 1 : 42	-73 : 58 : 26	17.30	18.38	1.08	-1.40	$6.65 \pm 0.06$	$-0.93 \pm 0.10$	1	0	0	0
13.1	1 : 2 : 25	-73 : 58 : 14	17.62	18.64	1.02	-1.14	$6.83 \pm 0.06$	$-0.79 \pm 0.10$	1	0	0	0
15.1	1 : 1 : 56	-73 : 57 : 59	17.81	18.82	1.01	-0.96	$5.03 \pm 0.06$	$-1.40 \pm 0.09$	1	0	0	0
16.1	1 : 2 : 28	-73 : 57 : 54	17.37	18.38	1.01	-1.40	$5.63 \pm 0.05$	$-1.30 \pm 0.09$	1	0	0	0
17.1	1 : 2 : 4	-73 : 57 : 47	17.59	18.66	1.07	-1.12	$6.14 \pm 0.07$	$-1.04 \pm 0.10$	1	0	0	0
18.1	1 : 2 : 29	-73 : 57 : 39	17.78	18.76	0.98	-1.02	$5.89 \pm 0.07$	$-1.10 \pm 0.09$	1	0	0	0
19.1	1 : 1 : 51	-73 : 57 : 32	17.71	18.71	1.00	-1.07	$5.85 \pm 0.04$	$-1.13 \pm 0.09$	1	1	0	0
20.1	1 : 1 : 59	-73 : 57 : 24	16.38	17.49	1.11	-2.29	$5.95 \pm 0.17$	$-1.42 \pm 0.11$	1	1	0	0
21.1	1 : 2 : 4	-73 : 57 : 0	17.86	18.83	0.97	-0.95	$5.14 \pm 0.08$	$-1.36 \pm 0.09$	1	0	0	0
22.1	1 : 1 : 59	-73 : 56 : 50	16.73	17.90	1.17	-1.88	$6.76 \pm 0.06$	$-1.02 \pm 0.10$	1	1	1	1
23.1	1 : 2 : 2	-73 : 56 : 39	18.17	19.15	0.99	-0.63	$6.25 \pm 0.08$	$-0.87 \pm 0.10$	1	1	1	1
24.1	1 : 2 : 2	-73 : 56 : 31	17.35	18.39	1.04	-1.39	$6.22 \pm 0.06$	$-1.08 \pm 0.09$	1	1	1	1
25.1	1 : 1 : 45	-73 : 56 : 26	17.00	18.02	1.02	-1.76	$6.14 \pm 0.05$	$-1.21 \pm 0.09$	1	0	0	0
26.1	1 : 2 : 12	-73 : 56 : 15	17.93	18.92	0.99	-0.86	$5.88 \pm 0.06$	$-1.06 \pm 0.09$	1	1	1	1

Continued on next page

Parameters of stars in Kron 44 - *continued*

27.1	1 : 2 : 30	-73 : 56 : 9	16.76	17.85	1.09	-1.93	5.80 ± 0.04	-1.38 ± 0.09	1	0	0	0
28.1	1 : 2 : 3	-73 : 56 : 2	18.04	19.05	1.01	-0.73	6.05 ± 0.08	-0.97 ± 0.10	1	1	1	1
29.1	1 : 2 : 5	-73 : 55 : 54	17.82	18.79	0.97	-0.99	6.44 ± 0.07	-0.90 ± 0.10	1	1	1	1
30.1	1 : 1 : 55	-73 : 55 : 46	17.41	18.46	1.05	-1.32	6.64 ± 0.07	-0.91 ± 0.10	1	1	1	1
31.1	1 : 2 : 21	-73 : 55 : 36	18.43	19.28	0.85	-0.50	5.58 ± 0.08	-1.08 ± 0.10	1	0	0	0
32.1	1 : 1 : 53	-73 : 55 : 30	17.20	18.24	1.05	-1.54	6.90 ± 0.05	-0.87 ± 0.10	1	1	1	1
33.1	1 : 2 : 16	-73 : 55 : 20	17.56	18.62	1.06	-1.16	6.47 ± 0.06	-0.93 ± 0.10	1	1	1	1
34.1	1 : 1 : 50	-73 : 55 : 10	17.68	18.61	0.92	-1.17	6.01 ± 0.08	-1.10 ± 0.10	1	0	0	0
36.1	1 : 2 : 16	-73 : 55 : 0	17.93	18.87	0.94	-0.91	6.46 ± 0.08	-0.87 ± 0.10	1	1	1	1
38.1	1 : 2 : 11	-73 : 54 : 45	17.65	18.70	1.05	-1.08	6.51 ± 0.07	-0.90 ± 0.10	1	1	1	1
39.1	1 : 2 : 8	-73 : 54 : 38	18.42	19.32	0.91	-0.46	6.25 ± 0.07	-0.83 ± 0.10	1	1	1	1
40.1	1 : 1 : 59	-73 : 54 : 33	17.77	18.67	0.90	-1.11	6.03 ± 0.08	-1.08 ± 0.10	1	1	1	1
41.1	1 : 1 : 49	-73 : 54 : 22	17.84	18.81	0.96	-0.97	6.01 ± 0.06	-1.05 ± 0.09	1	1	1	1
42.1	1 : 2 : 27	-73 : 54 : 15	17.67	18.67	1.00	-1.11	5.96 ± 0.06	-1.10 ± 0.09	1	1	0	0
43.1	1 : 2 : 32	-73 : 54 : 9	17.77	18.72	0.95	-1.06	5.91 ± 0.07	-1.10 ± 0.09	1	0	0	0
44.1	1 : 2 : 14	-73 : 54 : 2	16.98	18.09	1.11	-1.69	6.60 ± 0.05	-1.02 ± 0.10	1	0	0	0
45.1	1 : 1 : 52	-73 : 53 : 53	18.05	19.01	0.96	-0.77	7.12 ± 0.10	-0.59 ± 0.11	1	0	0	0
46.1	1 : 2 : 23	-73 : 53 : 48	17.46	18.50	1.05	-1.28	6.48 ± 0.07	-0.96 ± 0.10	1	1	0	0
47.1	1 : 2 : 13	-73 : 53 : 37	17.26	18.16	0.89	-1.62	6.32 ± 0.05	-1.11 ± 0.09	1	0	0	0
48.1	1 : 2 : 2	-73 : 53 : 33	17.29	18.33	1.04	-1.45	5.73 ± 0.06	-1.27 ± 0.09	1	0	0	0
49.1	1 : 1 : 36	-73 : 53 : 23	17.03	18.15	1.12	-1.63	6.22 ± 0.06	-1.14 ± 0.09	1	0	0	0

Table 5.C: Parameters of stars in Lindsay 11.

Star	alpha	delta	$I$	$V$	$(V - I)$	$V - V_{\text{HB}}$	$\Sigma W$	[Fe/H]	CMD	membership criteria		
	(J2000)	(J2000)	[mag]	[mag]	[mag]	[mag]	Å	dex		velocity	distance	metallicity
1.1	0 : 27 : 54	-72 : 51 : 14	18.65	19.61	0.96	-0.25	6.09 ± 0.28	-0.83 ± 0.14	1	1	0	0
2.1	0 : 27 : 30	-72 : 51 : 6	17.31	18.48	1.16	-1.38	6.45 ± 0.06	-1.00 ± 0.09	1	0	0	0
3.1	0 : 28 : 8	-72 : 50 : 58	17.70	18.76	1.07	-1.10	6.66 ± 0.08	-0.84 ± 0.10	1	1	0	0
4.1	0 : 27 : 28	-72 : 50 : 41	17.45	18.57	1.12	-1.29	6.81 ± 0.08	-0.84 ± 0.10	1	0	0	0
5.1	0 : 27 : 46	-72 : 50 : 35	16.14	17.42	1.28	-2.44	6.73 ± 0.12	-1.18 ± 0.10	1	0	0	0
6.1	0 : 27 : 36	-72 : 50 : 27	18.40	19.34	0.94	-0.52	5.35 ± 0.12	-1.17 ± 0.09	1	0	0	0
7.1	0 : 27 : 44	-72 : 50 : 21	17.27	18.33	1.06	-1.53	3.81 ± 0.04	-1.99 ± 0.06	1	0	0	0
8.1	0 : 27 : 32	-72 : 50 : 9	16.40	17.69	1.29	-2.17	7.23 ± 0.06	-0.92 ± 0.10	1	0	0	0
10.1	0 : 27 : 27	-72 : 49 : 54	18.12	19.17	1.04	-0.69	5.98 ± 0.08	-0.99 ± 0.09	1	0	0	0
11.1	0 : 27 : 29	-72 : 49 : 45	18.49	19.53	1.04	-0.33	3.98 ± 0.09	-1.62 ± 0.08	1	0	0	0

*Continued on next page*

Parameters of stars in Lindsay 11 - *continued*

12.1	0 : 27 : 51	-72 : 49 : 35	17.48	18.60	1.12	-1.26	6.62 ± 0.06	-0.90 ± 0.10	1	0	0	0
13.1	0 : 27 : 40	-72 : 49 : 27	16.30	18.44	2.13	-1.42	4.48 ± 0.04	-1.72 ± 0.07	0	0	0	0
14.1	0 : 27 : 28	-72 : 49 : 20	17.93	18.97	1.04	-0.89	6.06 ± 0.06	-1.01 ± 0.09	1	0	0	0
15.1	0 : 27 : 34	-72 : 49 : 16	16.44	17.70	1.26	-2.16	7.13 ± 0.06	-0.96 ± 0.10	1	0	0	0
16.1	0 : 28 : 10	-72 : 49 : 5	16.66	17.84	1.18	-2.02	6.56 ± 0.05	-1.12 ± 0.09	1	1	0	0
17.1	0 : 27 : 43	-72 : 49 : 0	16.06	17.40	1.33	-2.46	5.48 ± 0.05	-1.63 ± 0.08	1	1	0	0
18.1	0 : 27 : 35	-72 : 48 : 52	17.94	18.94	1.00	-0.92	5.73 ± 0.07	-1.14 ± 0.09	1	0	0	0
19.1	0 : 27 : 21	-72 : 48 : 44	17.30	18.34	1.04	-1.52	2.00 ± 0.05	-2.64 ± 0.05	1	1	0	0
20.1	0 : 27 : 41	-72 : 48 : 40	18.19	19.20	1.01	-0.66	5.89 ± 0.08	-1.01 ± 0.09	1	0	0	0
21.1	0 : 27 : 49	-72 : 48 : 29	17.79	18.88	1.09	-0.98	5.62 ± 0.04	-1.19 ± 0.08	1	1	0	0
22.1	0 : 27 : 51	-72 : 48 : 5	16.53	17.71	1.17	-2.15	6.70 ± 0.05	-1.11 ± 0.09	1	1	0	0
23.1	0 : 27 : 50	-72 : 47 : 57	16.67	17.88	1.21	-1.98	7.17 ± 0.05	-0.89 ± 0.10	1	0	0	0
24.1	0 : 27 : 46	-72 : 47 : 52	17.79	18.76	0.97	-1.10	5.04 ± 0.06	-1.43 ± 0.08	1	1	1	0
25.1	0 : 27 : 25	-72 : 47 : 42	18.59	19.51	0.92	-0.35	4.91 ± 0.13	-1.28 ± 0.09	1	0	0	0
26.1	0 : 27 : 43	-72 : 47 : 34	17.97	18.90	0.92	-0.96	6.19 ± 0.08	-0.98 ± 0.10	1	0	0	0
27.1	0 : 27 : 41	-72 : 47 : 29	18.71	19.60	0.90	-0.26	6.04 ± 0.15	-0.85 ± 0.11	1	1	1	1
28.1	0 : 27 : 45	-72 : 47 : 22	15.52	17.01	1.49	-2.85	6.88 ± 0.04	-1.23 ± 0.09	1	1	1	1
29.1	0 : 27 : 47	-72 : 47 : 14	18.62	19.53	0.91	-0.33	5.83 ± 0.10	-0.94 ± 0.10	1	0	0	0
30.1	0 : 27 : 39	-72 : 47 : 8	16.98	18.13	1.15	-1.73	4.61 ± 0.03	-1.75 ± 0.07	1	0	0	0
31.1	0 : 27 : 48	-72 : 47 : 2	18.02	19.06	1.03	-0.80	3.78 ± 0.09	-1.81 ± 0.07	1	0	0	0
32.1	0 : 27 : 45	-72 : 46 : 55	18.66	19.57	0.91	-0.29	5.42 ± 0.12	-1.08 ± 0.10	1	1	1	1
33.1	0 : 27 : 40	-72 : 46 : 48	17.82	18.84	1.02	-1.02	6.06 ± 0.07	-1.04 ± 0.09	1	1	1	1
34.1	0 : 27 : 51	-72 : 46 : 39	17.49	18.61	1.12	-1.25	6.41 ± 0.06	-0.98 ± 0.09	1	1	1	1
35.1	0 : 27 : 44	-72 : 46 : 28	18.56	19.46	0.90	-0.40	6.50 ± 0.15	-0.72 ± 0.11	1	1	1	1
35.2	0 : 27 : 44	-72 : 46 : 26	16.96	18.18	1.22	-1.68	7.14 ± 0.07	-0.82 ± 0.10	1	1	1	1
36.1	0 : 27 : 45	-72 : 46 : 19	17.10	18.18	1.08	-1.68	6.89 ± 0.08	-0.92 ± 0.10	1	1	1	1
37.1	0 : 27 : 22	-72 : 46 : 10	16.83	17.96	1.12	-1.90	6.58 ± 0.05	-1.09 ± 0.09	1	0	0	0
38.1	0 : 27 : 52	-72 : 46 : 4	17.47	18.54	1.07	-1.32	5.48 ± 0.05	-1.33 ± 0.08	1	0	0	0
39.1	0 : 27 : 45	-72 : 45 : 56	17.17	18.26	1.09	-1.60	4.99 ± 0.04	-1.58 ± 0.08	1	0	0	0
40.1	0 : 27 : 20	-72 : 45 : 48	17.52	18.68	1.16	-1.18	6.63 ± 0.07	-0.88 ± 0.10	1	0	0	0
41.1	0 : 27 : 50	-72 : 45 : 44	17.30	18.42	1.12	-1.44	5.73 ± 0.05	-1.27 ± 0.08	1	1	1	0
42.1	0 : 27 : 33	-72 : 45 : 36	16.22	17.43	1.21	-2.43	4.67 ± 0.03	-1.92 ± 0.07	1	0	0	0
44.1	0 : 28 : 2	-72 : 45 : 13	18.46	19.32	0.85	-0.54	3.56 ± 0.11	-1.82 ± 0.07	1	1	0	0
45.1	0 : 28 : 0	-72 : 45 : 10	17.90	18.95	1.05	-0.91	4.98 ± 0.07	-1.40 ± 0.08	1	0	0	0
46.1	0 : 27 : 58	-72 : 44 : 55	17.65	18.76	1.11	-1.10	5.92 ± 0.09	-1.11 ± 0.09	1	1	0	0
47.1	0 : 27 : 55	-72 : 44 : 49	16.40	17.71	1.30	-2.15	7.70 ± 0.07	-0.75 ± 0.11	1	0	0	0
48.1	0 : 27 : 24	-72 : 44 : 39	17.32	18.10	0.78	-1.76	4.63 ± 0.05	-1.76 ± 0.07	0	0	0	0
49.1	0 : 27 : 36	-72 : 44 : 27	18.65	19.58	0.92	-0.28	5.45 ± 0.08	-1.07 ± 0.09	1	1	0	0

*Continued on next page*

Parameters of stars in Lindsay 11 - *continued*

50.1	0 : 27 : 26	-72 : 44 : 23	18.44	19.32	0.89	-0.54	$6.10 \pm 0.10$	$-0.90 \pm 0.10$	1	0	0	0
------	-------------	---------------	-------	-------	------	-------	-----------------	------------------	---	---	---	---

Table 5.D: Parameters of stars in Lindsay 32.

Star	alpha	delta	$I$	$V$	$(V - I)$	$V - V_{\text{HB}}$	$\Sigma W$	[Fe/H]	CMD	membership criteria		
	(J2000)	(J2000)	[mag]	[mag]	[mag]	[mag]	Å	dex		velocity	distance	metallicity
2.1	0 : 47 : 0	-68 : 59 : 39	16.53	18.64	2.11	-1.17	$5.00 \pm 0.05$	$-1.47 \pm 0.07$	0	0	0	0
4.1	0 : 47 : 4	-68 : 59 : 19	18.24	19.20	0.95	-0.61	$6.55 \pm 0.12$	$-0.76 \pm 0.10$	1	0	0	0
5.1	0 : 47 : 7	-68 : 59 : 8	19.69	20.50	0.82	0.69	$6.46 \pm 0.19$	$-0.44 \pm 0.13$	1	0	0	0
7.1	0 : 46 : 58	-68 : 58 : 54	18.20	19.05	0.85	-0.76	$4.12 \pm 0.10$	$-1.68 \pm 0.07$	1	0	0	0
10.1	0 : 47 : 31	-68 : 58 : 28	18.36	19.16	0.81	-0.65	$4.17 \pm 0.14$	$-1.63 \pm 0.08$	1	1	0	0
11.1	0 : 47 : 23	-68 : 58 : 5	19.12	19.97	0.84	0.16	$4.63 \pm 0.19$	$-1.25 \pm 0.10$	1	1	0	0
12.1	0 : 46 : 59	-68 : 57 : 56	17.00	18.72	1.73	-1.09	$6.00 \pm 0.06$	$-1.08 \pm 0.09$	0	0	0	0
13.1	0 : 47 : 20	-68 : 57 : 46	18.30	18.92	0.62	-0.89	$4.37 \pm 0.10$	$-1.62 \pm 0.08$	0	0	0	0
14.1	0 : 47 : 8	-68 : 57 : 33	18.49	19.36	0.87	-0.45	$6.20 \pm 0.13$	$-0.84 \pm 0.10$	1	0	0	0
15.1	0 : 47 : 15	-68 : 57 : 26	17.54	18.56	1.02	-1.25	$5.57 \pm 0.06$	$-1.28 \pm 0.08$	1	1	0	0
16.1	0 : 46 : 57	-68 : 57 : 13	19.34	20.16	0.82	0.35	$4.35 \pm 0.33$	$-1.30 \pm 0.14$	1	0	0	0
17.1	0 : 47 : 20	-68 : 57 : 5	18.28	19.11	0.83	-0.70	$5.53 \pm 0.10$	$-1.15 \pm 0.09$	1	0	0	0
18.1	0 : 47 : 31	-68 : 56 : 49	17.84	18.66	0.82	-1.15	$5.14 \pm 0.07$	$-1.41 \pm 0.08$	1	1	0	0
19.1	0 : 47 : 35	-68 : 56 : 31	18.68	19.51	0.83	-0.30	$4.82 \pm 0.11$	$-1.30 \pm 0.09$	1	0	0	0
20.1	0 : 47 : 11	-68 : 56 : 23	19.28	20.70	1.42	0.89	$6.52 \pm 0.14$	$-0.37 \pm 0.12$	0	0	0	0
21.1	0 : 46 : 57	-68 : 56 : 16	15.87	17.21	1.34	-2.60	$7.79 \pm 0.07$	$-0.83 \pm 0.10$	1	0	0	0
22.1	0 : 47 : 38	-68 : 56 : 9	15.95	18.31	2.36	-1.50	$3.97 \pm 0.04$	$-1.92 \pm 0.06$	0	0	0	0
24.1	0 : 47 : 12	-68 : 55 : 52	18.64	19.55	0.90	-0.26	$2.43 \pm 0.09$	$-2.16 \pm 0.06$	1	0	0	0
25.1	0 : 47 : 17	-68 : 55 : 44	19.83	20.74	0.92	0.93	$5.17 \pm 0.25$	$-0.85 \pm 0.13$	1	1	0	0
26.1	0 : 47 : 25	-68 : 55 : 35	18.25	19.05	0.80	-0.76	$5.07 \pm 0.10$	$-1.33 \pm 0.08$	1	1	1	1
28.1	0 : 47 : 22	-68 : 55 : 22	18.14	19.09	0.95	-0.72	$6.14 \pm 0.08$	$-0.93 \pm 0.09$	1	1	1	1
29.1	0 : 47 : 27	-68 : 55 : 12	18.42	19.31	0.89	-0.50	$6.30 \pm 0.15$	$-0.82 \pm 0.11$	1	0	0	0
30.1	0 : 47 : 19	-68 : 55 : 4	18.33	19.29	0.96	-0.52	$5.95 \pm 0.13$	$-0.95 \pm 0.10$	1	1	1	1
31.1	0 : 47 : 23	-68 : 54 : 57	17.59	18.62	1.03	-1.19	$5.98 \pm 0.08$	$-1.12 \pm 0.09$	1	1	1	1
32.1	0 : 47 : 26	-68 : 54 : 49	18.61	19.46	0.85	-0.35	$4.99 \pm 0.10$	$-1.25 \pm 0.08$	1	1	1	1
34.1	0 : 47 : 21	-68 : 54 : 38	18.67	19.54	0.86	-0.27	$4.17 \pm 0.14$	$-1.53 \pm 0.08$	1	1	1	0
36.1	0 : 47 : 11	-68 : 54 : 18	17.35	18.41	1.06	-1.40	$5.31 \pm 0.06$	$-1.41 \pm 0.08$	1	0	0	0
37.1	0 : 47 : 32	-68 : 54 : 9	18.44	20.67	2.23	0.86	$4.35 \pm 0.12$	$-1.16 \pm 0.09$	0	0	0	0
38.1	0 : 47 : 23	-68 : 54 : 2	18.73	19.60	0.86	-0.21	$5.37 \pm 0.15$	$-1.08 \pm 0.10$	1	1	0	0
39.1	0 : 47 : 38	-68 : 53 : 48	18.14	19.85	1.71	0.04	$5.32 \pm 0.13$	$-1.03 \pm 0.10$	0	0	0	0

Continued on next page

Parameters of stars in Lindsay 32 - *continued*

40.1	0 : 47 : 20	-68 : 53 : 40	18.44	19.29	0.85	-0.52	$4.70 \pm 0.10$	$-1.40 \pm 0.08$	1	0	0	0
41.1	0 : 47 : 37	-68 : 53 : 23	17.59	19.10	1.51	-0.71	$5.38 \pm 0.08$	$-1.20 \pm 0.08$	0	0	0	0
42.1	0 : 47 : 28	-68 : 53 : 9	16.53	17.84	1.31	-1.97	$6.67 \pm 0.09$	$-1.07 \pm 0.09$	1	0	0	0

Table 5.E: Parameters of stars in Lindsay 38.

Star	alpha	delta	$I$	$V$	$(V - I)$	$V - V_{\text{HB}}$	$\Sigma W$	$[\text{Fe}/\text{H}]$	CMD	membership criteria		
	(J2000)	(J2000)	[mag]	[mag]	[mag]	[mag]	$\text{\AA}$	dex		velocity	distance	metallicity
1.1	0 : 48 : 55	-69 : 57 : 0	16.78	17.97	1.19	-2.06	$6.69 \pm 0.05$	$-1.09 \pm 0.09$	1	0	0	0
2.1	0 : 48 : 43	-69 : 56 : 54	17.34	18.51	1.16	-1.52	$5.63 \pm 0.06$	$-1.33 \pm 0.08$	1	0	0	0
3.1	0 : 49 : 3	-69 : 56 : 37	15.09	17.31	2.21	-2.72	$4.47 \pm 0.03$	$-2.07 \pm 0.07$	0	0	0	0
4.1	0 : 49 : 4	-69 : 56 : 28	18.83	19.84	1.02	-0.19	$4.75 \pm 0.10$	$-1.30 \pm 0.08$	1	0	0	0
5.1	0 : 49 : 16	-69 : 56 : 21	18.80	19.61	0.81	-0.42	$3.41 \pm 0.21$	$-1.84 \pm 0.10$	1	0	0	0
6.1	0 : 48 : 58	-69 : 56 : 6	18.00	19.39	1.40	-0.64	$5.68 \pm 0.09$	$-1.08 \pm 0.09$	0	0	0	0
7.1	0 : 48 : 38	-69 : 55 : 57	19.16	20.11	0.96	0.08	$4.16 \pm 0.21$	$-1.44 \pm 0.10$	1	0	0	0
8.1	0 : 49 : 2	-69 : 55 : 20	17.58	18.65	1.07	-1.38	$4.94 \pm 0.06$	$-1.54 \pm 0.07$	1	1	0	0
9.1	0 : 49 : 7	-69 : 55 : 13	16.97	19.86	2.89	-0.17	$2.59 \pm 0.06$	$-2.07 \pm 0.06$	0	0	0	0
10.1	0 : 48 : 35	-69 : 54 : 48	18.40	19.34	0.94	-0.69	$5.12 \pm 0.12$	$-1.29 \pm 0.09$	1	0	0	0
11.1	0 : 48 : 58	-69 : 54 : 39	16.76	18.06	1.30	-1.97	$7.13 \pm 0.06$	$-0.91 \pm 0.10$	1	1	0	0
12.1	0 : 48 : 38	-69 : 54 : 33	18.61	19.59	0.97	-0.44	$5.58 \pm 0.16$	$-1.06 \pm 0.10$	1	0	0	0
13.1	0 : 49 : 0	-69 : 54 : 21	18.11	19.20	1.09	-0.83	$5.65 \pm 0.10$	$-1.14 \pm 0.09$	1	0	0	0
14.1	0 : 49 : 2	-69 : 54 : 1	17.42	18.54	1.12	-1.49	$5.65 \pm 0.34$	$-1.31 \pm 0.15$	1	0	0	0
15.1	0 : 48 : 32	-69 : 53 : 46	17.85	18.88	1.03	-1.15	$5.55 \pm 0.07$	$-1.26 \pm 0.08$	1	0	0	0
16.1	0 : 48 : 56	-69 : 53 : 30	17.49	18.55	1.06	-1.48	$5.81 \pm 0.05$	$-1.26 \pm 0.08$	1	0	0	0
17.1	0 : 48 : 51	-69 : 53 : 23	19.35	20.32	0.96	0.29	$2.71 \pm 0.14$	$-1.91 \pm 0.08$	1	0	0	0
18.1	0 : 49 : 3	-69 : 53 : 8	16.97	19.19	2.22	-0.84	$4.35 \pm 0.04$	$-1.61 \pm 0.07$	0	0	0	0
19.1	0 : 48 : 48	-69 : 52 : 59	16.42	17.67	1.25	-2.36	$6.32 \pm 0.04$	$-1.30 \pm 0.08$	1	1	1	1
20.1	0 : 48 : 30	-69 : 52 : 53	18.34	19.31	0.96	-0.72	$5.09 \pm 0.10$	$-1.32 \pm 0.08$	1	0	0	0
21.1	0 : 48 : 44	-69 : 52 : 47	18.87	19.79	0.92	-0.24	$4.37 \pm 0.12$	$-1.45 \pm 0.08$	1	0	0	0
23.1	0 : 48 : 51	-69 : 52 : 32	18.27	19.24	0.97	-0.79	$4.92 \pm 0.07$	$-1.39 \pm 0.08$	1	1	1	1
24.1	0 : 48 : 58	-69 : 52 : 24	17.48	18.55	1.07	-1.48	$5.03 \pm 0.06$	$-1.54 \pm 0.07$	1	1	1	1
25.1	0 : 49 : 7	-69 : 52 : 19	16.49	17.78	1.29	-2.25	$7.06 \pm 0.06$	$-1.00 \pm 0.09$	1	1	1	0
26.1	0 : 48 : 53	-69 : 52 : 12	16.84	18.05	1.21	-1.98	$6.22 \pm 0.04$	$-1.24 \pm 0.08$	1	1	1	1
28.1	0 : 48 : 45	-69 : 51 : 59	18.36	19.41	1.05	-0.62	$4.74 \pm 0.12$	$-1.41 \pm 0.08$	1	1	1	1
29.1	0 : 48 : 44	-69 : 51 : 51	17.68	18.80	1.12	-1.23	$5.42 \pm 0.06$	$-1.33 \pm 0.08$	1	1	1	1
30.1	0 : 48 : 54	-69 : 51 : 46	16.79	17.79	1.00	-2.24	$5.93 \pm 0.07$	$-1.41 \pm 0.08$	0	0	0	0

Continued on next page

Parameters of stars in Lindsay 38 - *continued*

31.1	0 : 48 : 53	-69 : 51 : 37	16.39	17.68	1.29	-2.35	$6.27 \pm 0.03$	$-1.32 \pm 0.08$	1	1	1	1
32.1	0 : 49 : 3	-69 : 51 : 30	17.98	19.04	1.06	-0.99	$5.55 \pm 0.07$	$-1.22 \pm 0.08$	1	0	0	0
34.1	0 : 48 : 33	-69 : 51 : 11	17.56	18.71	1.15	-1.32	$6.30 \pm 0.08$	$-1.04 \pm 0.09$	1	0	0	0
35.1	0 : 49 : 17	-69 : 50 : 59	18.62	19.54	0.92	-0.49	$6.33 \pm 0.53$	$-0.81 \pm 0.21$	1	0	0	0
36.1	0 : 49 : 10	-69 : 50 : 28	18.50	19.51	1.01	-0.52	$5.45 \pm 0.10$	$-1.13 \pm 0.09$	1	0	0	0
37.1	0 : 48 : 51	-69 : 50 : 13	17.61	19.82	2.21	-0.21	$4.41 \pm 0.05$	$-1.42 \pm 0.07$	0	0	0	0

Table 5.F: Parameters of stars in Lindsay 116.

Star	alpha	delta	$I$	$V$	$(V - I)$	$V - V_{\text{HB}}$	$\Sigma W$	$[\text{Fe}/\text{H}]$	CMD	membership criteria		
	(J2000)	(J2000)	[mag]	[mag]	[mag]	[mag]	$\text{\AA}$	dex		velocity	distance	metallicity
3.1	1 : 55 : 54	-77 : 43 : 9	18.36	19.21	0.85	0.04	$3.83 \pm 0.12$	$-1.57 \pm 0.10$	1	0	0	0
5.1	1 : 55 : 19	-77 : 42 : 51	19.28	21.21	1.93	2.04	$4.25 \pm 0.14$	$-0.89 \pm 0.12$	0	0	0	0
6.1	1 : 55 : 37	-77 : 42 : 38	19.33	20.15	0.82	0.98	$5.68 \pm 0.19$	$-0.65 \pm 0.13$	1	0	0	0
8.1	1 : 55 : 30	-77 : 42 : 4	17.30	18.17	0.87	-1.00	$5.51 \pm 0.06$	$-1.24 \pm 0.10$	1	0	0	0
9.1	1 : 55 : 31	-77 : 41 : 48	19.51	20.37	0.85	1.20	$5.57 \pm 0.29$	$-0.63 \pm 0.15$	1	0	0	0
10.1	1 : 54 : 48	-77 : 41 : 40	18.93	19.79	0.86	0.62	$7.24 \pm 0.19$	$-0.18 \pm 0.14$	1	1	0	0
14.1	1 : 55 : 27	-77 : 41 : 4	15.76	16.69	0.93	-2.48	$5.71 \pm 0.05$	$-1.55 \pm 0.10$	1	0	0	0
15.1	1 : 54 : 48	-77 : 40 : 43	17.75	18.79	1.05	-0.38	$6.67 \pm 0.07$	$-0.65 \pm 0.11$	1	0	0	0
18.1	1 : 55 : 18	-77 : 39 : 50	18.08	20.34	2.26	1.17	$4.05 \pm 0.07$	$-1.19 \pm 0.10$	0	0	0	0
19.1	1 : 55 : 39	-77 : 39 : 37	19.24	20.11	0.87	0.94	$5.88 \pm 0.17$	$-0.59 \pm 0.13$	1	1	1	0
21.1	1 : 55 : 36	-77 : 39 : 21	16.69	17.73	1.03	-1.44	$6.76 \pm 0.06$	$-0.90 \pm 0.11$	1	1	1	1
22.1	1 : 55 : 20	-77 : 39 : 16	19.12	19.99	0.87	0.82	$4.84 \pm 0.18$	$-1.00 \pm 0.12$	1	0	0	0
23.1	1 : 55 : 32	-77 : 39 : 12	17.86	18.69	0.82	-0.48	$5.94 \pm 0.06$	$-0.94 \pm 0.11$	1	1	1	1
24.1	1 : 55 : 31	-77 : 39 : 5	17.88	18.82	0.95	-0.35	$5.78 \pm 0.06$	$-0.97 \pm 0.10$	1	1	1	1
25.1	1 : 55 : 41	-77 : 38 : 56	17.92	18.62	0.70	-0.55	$3.36 \pm 0.07$	$-1.89 \pm 0.08$	1	0	0	0
26.1	1 : 55 : 31	-77 : 38 : 52	18.44	19.14	0.70	-0.03	$5.41 \pm 0.11$	$-1.02 \pm 0.11$	1	0	0	0
28.1	1 : 55 : 34	-77 : 38 : 35	17.92	18.79	0.88	-0.38	$6.12 \pm 0.07$	$-0.85 \pm 0.11$	1	1	1	1
29.1	1 : 55 : 52	-77 : 38 : 28	19.24	20.10	0.86	0.93	$5.20 \pm 0.18$	$-0.84 \pm 0.12$	1	1	1	1
30.1	1 : 55 : 42	-77 : 38 : 18	17.38	18.17	0.80	-1.00	$5.37 \pm 0.07$	$-1.29 \pm 0.10$	1	0	0	0
35.1	1 : 55 : 24	-77 : 37 : 31	17.75	19.00	1.25	-0.17	$6.69 \pm 0.09$	$-0.59 \pm 0.12$	0	0	0	0
36.1	1 : 55 : 29	-77 : 37 : 26	19.36	20.25	0.89	1.08	$5.84 \pm 0.29$	$-0.57 \pm 0.16$	1	0	0	0
37.1	1 : 55 : 13	-77 : 37 : 13	17.57	18.40	0.83	-0.77	$5.79 \pm 0.08$	$-1.07 \pm 0.10$	1	0	0	0
40.1	1 : 54 : 59	-77 : 36 : 39	16.58	17.42	0.84	-1.75	$6.49 \pm 0.08$	$-1.08 \pm 0.11$	1	0	0	0



Table 5.G: Parameters of stars in NGC 152.

Star	alpha	delta	$I$	$V$	$(V - I)$	$V - V_{\text{HB}}$	$\Sigma W$	$[\text{Fe}/\text{H}]$	CMD	membership criteria		
	(J2000)	(J2000)	[mag]	[mag]	[mag]	[mag]	Å	dex		velocity	distance	metallicity
1.1	0 : 33 : 2	-73 : 11 : 32	18.38	19.17	0.79	-0.64	4.28 ± 0.11	-1.58 ± 0.09	0	0	0	0
2.1	0 : 32 : 39	-73 : 11 : 21	16.60	17.76	1.16	-2.05	6.73 ± 0.06	-1.07 ± 0.10	1	0	0	0
3.1	0 : 32 : 43	-73 : 11 : 13	17.17	18.16	0.99	-1.65	6.52 ± 0.07	-1.04 ± 0.10	1	0	0	0
4.1	0 : 33 : 15	-73 : 11 : 6	17.53	18.67	1.15	-1.14	6.66 ± 0.08	-0.85 ± 0.10	1	0	0	0
5.1	0 : 32 : 52	-73 : 10 : 53	15.58	17.12	1.54	-2.69	7.72 ± 0.06	-0.88 ± 0.11	1	0	0	0
6.1	0 : 32 : 42	-73 : 10 : 46	15.86	17.19	1.32	-2.62	6.57 ± 0.05	-1.28 ± 0.10	1	0	0	0
7.1	0 : 32 : 52	-73 : 10 : 36	17.45	18.46	1.01	-1.35	6.82 ± 0.10	-0.85 ± 0.11	1	0	0	0
8.1	0 : 33 : 1	-73 : 10 : 29	15.70	17.16	1.46	-2.65	7.84 ± 0.05	-0.83 ± 0.11	1	0	0	0
9.1	0 : 33 : 29	-73 : 10 : 19	16.02	17.40	1.38	-2.41	7.33 ± 0.06	-0.95 ± 0.10	1	0	0	0
10.1	0 : 32 : 51	-73 : 10 : 10	18.38	19.30	0.92	-0.51	6.19 ± 0.15	-0.86 ± 0.11	0	0	0	0
11.1	0 : 33 : 20	-73 : 10 : 3	16.27	17.50	1.23	-2.31	6.87 ± 0.05	-1.09 ± 0.10	1	0	0	0
12.1	0 : 33 : 23	-73 : 9 : 56	17.26	18.40	1.13	-1.41	7.33 ± 0.09	-0.69 ± 0.11	1	1	0	0
13.1	0 : 33 : 3	-73 : 9 : 50	16.01	17.34	1.34	-2.47	8.29 ± 0.09	-0.62 ± 0.12	1	1	0	0
14.1	0 : 33 : 12	-73 : 9 : 38	17.39	18.49	1.10	-1.32	6.68 ± 0.13	-0.90 ± 0.11	1	0	0	0
15.1	0 : 33 : 18	-73 : 9 : 29	16.82	17.95	1.13	-1.86	7.10 ± 0.07	-0.89 ± 0.10	1	0	0	0
16.1	0 : 33 : 3	-73 : 9 : 18	17.64	18.69	1.05	-1.12	6.63 ± 0.07	-0.86 ± 0.10	1	0	0	0
17.1	0 : 32 : 49	-73 : 9 : 11	16.73	17.99	1.25	-1.82	6.68 ± 0.05	-1.03 ± 0.10	1	0	0	0
18.1	0 : 32 : 55	-73 : 9 : 3	16.13	17.45	1.32	-2.36	7.22 ± 0.06	-0.98 ± 0.10	1	0	0	0
19.1	0 : 32 : 39	-73 : 8 : 54	17.34	18.44	1.10	-1.37	6.95 ± 0.08	-0.81 ± 0.11	1	0	0	0
20.1	0 : 32 : 53	-73 : 8 : 47	16.96	18.10	1.14	-1.71	5.27 ± 0.04	-1.51 ± 0.08	1	0	0	0
21.1	0 : 33 : 8	-73 : 8 : 25	16.35	17.55	1.19	-2.26	6.92 ± 0.05	-1.06 ± 0.10	1	1	0	0
22.1	0 : 33 : 9	-73 : 8 : 18	15.63	16.89	1.26	-2.92	6.83 ± 0.08	-1.27 ± 0.10	0	0	0	0
23.1	0 : 33 : 6	-73 : 8 : 9	16.53	18.76	2.23	-1.05	4.07 ± 0.04	-1.77 ± 0.08	0	0	0	0
24.1	0 : 33 : 15	-73 : 8 : 1	16.67	17.72	1.05	-2.09	6.05 ± 0.07	-1.33 ± 0.09	1	0	0	0
26.1	0 : 33 : 21	-73 : 7 : 45	16.45	17.74	1.29	-2.07	6.55 ± 0.06	-1.14 ± 0.10	1	0	0	0
27.1	0 : 33 : 13	-73 : 7 : 39	17.01	18.05	1.05	-1.76	6.33 ± 0.05	-1.14 ± 0.09	1	0	0	0
28.1	0 : 33 : 0	-73 : 7 : 29	16.21	17.57	1.36	-2.24	8.01 ± 0.07	-0.66 ± 0.11	1	1	1	1
29.1	0 : 32 : 51	-73 : 7 : 24	17.62	18.71	1.09	-1.10	6.57 ± 0.10	-0.88 ± 0.11	1	0	0	0
30.1	0 : 33 : 21	-73 : 7 : 16	17.41	18.51	1.10	-1.30	6.20 ± 0.08	-1.07 ± 0.10	1	0	0	0
31.1	0 : 32 : 36	-73 : 7 : 11	16.86	17.77	0.91	-2.04	5.87 ± 0.07	-1.38 ± 0.09	0	0	0	0
32.1	0 : 33 : 10	-73 : 7 : 5	16.86	18.06	1.20	-1.75	7.51 ± 0.07	-0.71 ± 0.11	1	1	1	1
33.1	0 : 32 : 59	-73 : 6 : 53	17.06	18.22	1.15	-1.59	6.56 ± 0.06	-1.01 ± 0.10	1	1	1	0
34.1	0 : 32 : 34	-73 : 6 : 44	14.92	16.49	1.57	-3.32	8.32 ± 0.07	-0.83 ± 0.11	1	1	0	0
35.1	0 : 32 : 45	-73 : 6 : 36	16.99	18.15	1.16	-1.66	7.50 ± 0.06	-0.69 ± 0.11	1	1	1	1

Continued on next page

Parameters of stars in NGC 152 - *continued*

37.1	0 : 33 : 9	-73 : 6 : 21	15.96	17.33	1.37	-2.48	8.46 ± 0.07	-0.56 ± 0.12	1	1	1	1
38.1	0 : 32 : 58	-73 : 6 : 14	15.55	17.05	1.50	-2.76	8.59 ± 0.07	-0.59 ± 0.12	1	1	1	1
39.1	0 : 32 : 52	-73 : 6 : 6	17.53	18.58	1.05	-1.23	5.09 ± 0.06	-1.45 ± 0.09	1	0	0	0
40.1	0 : 33 : 2	-73 : 5 : 53	16.60	17.85	1.25	-1.96	7.67 ± 0.07	-0.71 ± 0.11	1	1	1	1
41.1	0 : 32 : 44	-73 : 5 : 45	17.55	18.71	1.16	-1.10	6.51 ± 0.07	-0.90 ± 0.10	1	0	0	0
42.1	0 : 32 : 52	-73 : 5 : 38	15.18	16.84	1.65	-2.97	7.75 ± 0.05	-0.95 ± 0.11	1	0	0	0
43.1	0 : 33 : 8	-73 : 5 : 27	17.38	18.57	1.19	-1.24	6.33 ± 0.06	-1.00 ± 0.10	1	1	0	0
44.1	0 : 32 : 37	-73 : 5 : 21	16.56	17.80	1.24	-2.01	7.06 ± 0.07	-0.94 ± 0.10	1	0	0	0
45.1	0 : 33 : 0	-73 : 5 : 13	16.26	17.54	1.28	-2.27	7.10 ± 0.05	-1.00 ± 0.10	1	1	0	0
46.1	0 : 33 : 31	-73 : 5 : 4	15.92	17.46	1.55	-2.35	7.17 ± 0.08	-0.99 ± 0.10	1	0	0	0
47.1	0 : 33 : 13	-73 : 4 : 59	16.61	17.86	1.24	-1.95	7.04 ± 0.05	-0.93 ± 0.10	1	0	0	0
48.1	0 : 32 : 51	-73 : 4 : 53	17.39	18.47	1.09	-1.34	7.17 ± 0.09	-0.72 ± 0.11	1	0	0	0
49.1	0 : 33 : 26	-73 : 4 : 41	17.78	18.66	0.87	-1.15	5.33 ± 0.13	-1.34 ± 0.10	1	0	0	0

Table 5.H: Parameters of stars in NGC 339.

Star	alpha	delta	<i>I</i>	<i>V</i>	( <i>V</i> - <i>I</i> )	<i>V</i> - <i>V</i> <sub>HB</sub>	$\Sigma W$	[Fe/H]	CMD	membership criteria		
	(J2000)	(J2000)	[mag]	[mag]	[mag]	[mag]	Å	dex		velocity	distance	metallicity
1.1	0 : 57 : 46	-74 : 33 : 1	17.66	18.59	0.93	-1.10	3.82 ± 0.05	-1.87 ± 0.07	1	1	0	0
2.1	0 : 57 : 45	-74 : 32 : 53	18.06	18.76	0.71	-0.93	5.81 ± 0.08	-1.11 ± 0.09	1	1	0	0
3.1	0 : 57 : 28	-74 : 32 : 47	17.42	18.41	0.99	-1.28	6.73 ± 0.05	-0.87 ± 0.10	1	0	0	0
4.1	0 : 57 : 50	-74 : 32 : 41	16.98	17.93	0.95	-1.76	5.80 ± 0.04	-1.33 ± 0.08	1	0	0	0
5.1	0 : 57 : 48	-74 : 32 : 34	17.48	18.24	0.76	-1.45	5.33 ± 0.06	-1.42 ± 0.08	1	1	0	0
6.1	0 : 57 : 31	-74 : 32 : 26	18.50	19.43	0.93	-0.26	5.78 ± 0.10	-0.94 ± 0.10	1	0	0	0
7.1	0 : 58 : 17	-74 : 32 : 19	18.30	19.13	0.83	-0.56	5.80 ± 0.09	-1.01 ± 0.09	1	0	0	0
8.1	0 : 57 : 22	-74 : 32 : 10	17.81	18.75	0.94	-0.94	6.10 ± 0.06	-1.01 ± 0.09	1	1	0	0
9.1	0 : 57 : 27	-74 : 32 : 2	16.19	17.34	1.15	-2.35	6.92 ± 0.04	-1.08 ± 0.09	1	0	0	0
10.1	0 : 58 : 2	-74 : 31 : 54	17.84	18.88	1.04	-0.81	6.25 ± 0.07	-0.92 ± 0.09	1	0	0	0
11.1	0 : 58 : 3	-74 : 31 : 47	17.93	18.90	0.98	-0.79	5.37 ± 0.08	-1.23 ± 0.09	1	0	0	0
12.1	0 : 58 : 3	-74 : 31 : 41	17.37	18.44	1.07	-1.25	6.41 ± 0.05	-0.98 ± 0.09	1	0	0	0
13.1	0 : 57 : 48	-74 : 31 : 33	15.95	17.19	1.24	-2.50	6.83 ± 0.05	-1.15 ± 0.09	1	0	0	0
14.1	0 : 57 : 35	-74 : 31 : 29	17.05	17.97	0.91	-1.72	6.43 ± 0.06	-1.10 ± 0.09	1	0	0	0
15.1	0 : 57 : 47	-74 : 31 : 23	17.22	18.26	1.03	-1.43	6.42 ± 0.05	-1.02 ± 0.09	1	0	0	0
16.1	0 : 58 : 2	-74 : 31 : 17	17.89	18.64	0.75	-1.05	5.20 ± 0.07	-1.36 ± 0.08	1	0	0	0
17.1	0 : 57 : 39	-74 : 31 : 6	18.10	19.05	0.95	-0.64	5.76 ± 0.07	-1.05 ± 0.09	1	0	0	0
18.1	0 : 57 : 47	-74 : 31 : 0	17.01	18.07	1.06	-1.62	6.51 ± 0.04	-1.04 ± 0.09	1	0	0	0

*Continued on next page*

Parameters of stars in NGC 339 - *continued*

19.1	0 : 57 : 39	-74 : 30 : 55	17.77	18.77	1.00	-0.92	6.72 ± 0.06	-0.77 ± 0.10	1	0	0	0
20.1	0 : 57 : 18	-74 : 30 : 43	17.51	18.51	1.00	-1.18	7.05 ± 0.08	-0.73 ± 0.10	1	0	0	0
21.1	0 : 57 : 51	-74 : 30 : 31	17.83	18.77	0.94	-0.92	6.18 ± 0.06	-0.97 ± 0.09	1	1	0	0
22.1	0 : 57 : 42	-74 : 30 : 27	16.56	17.66	1.11	-2.03	6.75 ± 0.05	-1.06 ± 0.09	1	0	0	0
23.1	0 : 57 : 43	-74 : 30 : 20	16.87	17.83	0.97	-1.86	6.05 ± 0.04	-1.27 ± 0.08	1	1	0	0
24.1	0 : 58 : 5	-74 : 30 : 10	18.38	19.27	0.89	-0.42	6.68 ± 0.08	-0.66 ± 0.10	1	0	0	0
25.1	0 : 57 : 55	-74 : 29 : 52	18.59	19.43	0.84	-0.26	5.59 ± 0.08	-1.01 ± 0.09	1	0	0	0
26.1	0 : 58 : 3	-74 : 29 : 42	18.35	19.30	0.95	-0.39	5.59 ± 0.08	-1.04 ± 0.09	1	0	0	0
27.1	0 : 57 : 59	-74 : 29 : 38	18.41	19.33	0.92	-0.36	5.88 ± 0.07	-0.93 ± 0.09	1	0	0	0
28.1	0 : 57 : 48	-74 : 29 : 28	17.02	18.07	1.05	-1.62	6.21 ± 0.04	-1.14 ± 0.09	1	0	0	0
29.1	0 : 57 : 52	-74 : 29 : 22	17.42	18.40	0.98	-1.29	5.76 ± 0.05	-1.22 ± 0.08	1	0	0	0
30.1	0 : 57 : 34	-74 : 29 : 18	17.38	18.35	0.97	-1.34	5.98 ± 0.05	-1.15 ± 0.09	1	0	0	0
31.1	0 : 57 : 42	-74 : 29 : 10	17.10	18.13	1.03	-1.56	6.12 ± 0.04	-1.16 ± 0.09	1	0	0	0
32.1	0 : 57 : 42	-74 : 29 : 3	18.37	19.24	0.87	-0.45	5.53 ± 0.08	-1.08 ± 0.09	1	0	0	0
33.1	0 : 57 : 47	-74 : 28 : 57	17.69	18.63	0.95	-1.06	5.62 ± 0.05	-1.21 ± 0.08	1	0	0	0
34.1	0 : 58 : 4	-74 : 28 : 48	17.24	18.26	1.02	-1.43	6.05 ± 0.04	-1.15 ± 0.09	1	0	0	0
35.1	0 : 57 : 40	-74 : 28 : 43	16.80	17.88	1.08	-1.81	6.45 ± 0.05	-1.11 ± 0.09	1	0	0	0
36.1	0 : 57 : 33	-74 : 28 : 36	16.99	18.07	1.09	-1.62	7.50 ± 0.07	-0.68 ± 0.10	1	0	0	0
37.1	0 : 57 : 55	-74 : 28 : 31	17.64	18.61	0.97	-1.08	5.65 ± 0.06	-1.21 ± 0.08	1	1	1	1
38.1	0 : 57 : 56	-74 : 28 : 21	16.77	17.84	1.06	-1.85	6.32 ± 0.04	-1.17 ± 0.09	1	1	1	1
39.1	0 : 57 : 56	-74 : 28 : 16	18.44	19.32	0.88	-0.37	5.95 ± 0.07	-0.91 ± 0.09	1	1	1	0
40.1	0 : 57 : 57	-74 : 28 : 11	17.33	18.32	0.99	-1.37	6.13 ± 0.05	-1.11 ± 0.09	1	1	1	1
41.1	0 : 57 : 44	-74 : 28 : 3	17.36	18.35	0.99	-1.34	5.66 ± 0.06	-1.27 ± 0.08	1	1	1	1
41.2	0 : 57 : 44	-74 : 28 : 1	16.35	17.50	1.15	-2.19	6.52 ± 0.05	-1.18 ± 0.09	1	1	1	1
42.1	0 : 57 : 37	-74 : 27 : 54	17.93	18.88	0.96	-0.81	5.93 ± 0.07	-1.03 ± 0.09	1	1	1	1
43.1	0 : 57 : 34	-74 : 27 : 48	16.93	17.95	1.02	-1.74	6.11 ± 0.04	-1.21 ± 0.09	1	1	1	1
44.1	0 : 57 : 44	-74 : 27 : 43	17.77	18.74	0.96	-0.95	5.57 ± 0.10	-1.20 ± 0.09	1	1	1	1
45.1	0 : 57 : 44	-74 : 27 : 39	17.66	18.58	0.93	-1.11	5.99 ± 0.05	-1.09 ± 0.09	1	0	0	0
46.1	0 : 58 : 17	-74 : 27 : 31	17.75	18.69	0.94	-1.00	6.23 ± 0.06	-0.98 ± 0.09	1	0	0	0
47.1	0 : 57 : 45	-74 : 27 : 26	17.76	18.71	0.95	-0.98	5.61 ± 0.04	-1.19 ± 0.08	1	1	1	1
48.1	0 : 57 : 30	-74 : 27 : 18	17.72	18.78	1.05	-0.91	6.47 ± 0.05	-0.87 ± 0.09	1	0	0	0
49.1	0 : 57 : 24	-74 : 27 : 14	16.62	17.63	1.01	-2.06	5.87 ± 0.04	-1.39 ± 0.08	1	0	0	0
50.1	0 : 57 : 58	-74 : 27 : 7	17.16	18.17	1.02	-1.52	5.99 ± 0.05	-1.20 ± 0.09	1	1	1	1
51.1	0 : 58 : 8	-74 : 27 : 2	17.96	18.87	0.91	-0.82	6.30 ± 0.07	-0.90 ± 0.09	1	1	1	0
52.1	0 : 57 : 50	-74 : 26 : 56	18.32	19.25	0.93	-0.44	5.23 ± 0.06	-1.19 ± 0.08	1	1	1	1
53.1	0 : 57 : 56	-74 : 26 : 47	17.75	18.74	0.99	-0.95	6.30 ± 0.05	-0.93 ± 0.09	1	0	0	0
54.1	0 : 57 : 45	-74 : 26 : 39	17.32	18.32	1.01	-1.37	6.43 ± 0.06	-1.00 ± 0.09	1	0	0	0
55.1	0 : 57 : 49	-74 : 26 : 34	18.29	19.21	0.92	-0.48	5.17 ± 0.08	-1.22 ± 0.09	1	1	1	1

*Continued on next page*

Parameters of stars in NGC 339 - *continued*

56.1	0 : 58 : 2	-74 : 26 : 26	18.54	19.37	0.83	-0.32	$6.13 \pm 0.11$	$-0.83 \pm 0.10$	1	0	0	0
57.1	0 : 57 : 39	-74 : 26 : 20	17.74	18.75	1.01	-0.94	$6.58 \pm 0.06$	$-0.83 \pm 0.10$	1	0	0	0
58.1	0 : 57 : 30	-74 : 26 : 16	16.83	17.94	1.11	-1.75	$6.94 \pm 0.05$	$-0.92 \pm 0.10$	1	0	0	0
59.1	0 : 57 : 57	-74 : 26 : 8	17.76	18.74	0.98	-0.95	$6.00 \pm 0.05$	$-1.04 \pm 0.09$	1	0	0	0

Table 5.I: Parameters of stars in NGC 361.

Star	alpha	delta	$I$	$V$	$(V - I)$	$V - V_{\text{HB}}$	$\Sigma W$	$[\text{Fe}/\text{H}]$	CMD	membership criteria		
	(J2000)	(J2000)	[mag]	[mag]	[mag]	[mag]	Å	dex		velocity	distance	metallicity
1.1	1 : 2 : 5	-71 : 41 : 4	17.61	18.62	1.01	-1.12	$6.05 \pm 0.08$	$-1.07 \pm 0.10$	1	0	0	0
2.1	1 : 1 : 55	-71 : 40 : 54	16.52	17.73	1.21	-2.01	$6.97 \pm 0.04$	$-0.97 \pm 0.10$	1	0	0	0
5.1	1 : 2 : 7	-71 : 40 : 23	16.87	18.14	1.27	-1.60	$6.91 \pm 0.06$	$-0.89 \pm 0.10$	1	1	0	0
6.1	1 : 2 : 2	-71 : 40 : 17	16.73	17.92	1.18	-1.82	$4.69 \pm 0.03$	$-1.75 \pm 0.08$	1	0	0	0
7.1	1 : 1 : 48	-71 : 40 : 8	17.28	18.30	1.02	-1.44	$6.14 \pm 0.05$	$-1.12 \pm 0.09$	1	0	0	0
8.1	1 : 1 : 48	-71 : 39 : 55	17.95	19.01	1.06	-0.73	$6.53 \pm 0.09$	$-0.80 \pm 0.11$	1	0	0	0
10.1	1 : 2 : 15	-71 : 39 : 28	18.33	19.35	1.03	-0.39	$6.39 \pm 0.08$	$-0.75 \pm 0.10$	1	0	0	0
11.1	1 : 2 : 16	-71 : 39 : 7	18.27	19.31	1.04	-0.43	$6.45 \pm 0.07$	$-0.74 \pm 0.10$	1	0	0	0
12.1	1 : 2 : 6	-71 : 39 : 2	17.08	18.28	1.20	-1.46	$6.56 \pm 0.05$	$-0.98 \pm 0.10$	1	0	0	0
13.1	1 : 2 : 2	-71 : 38 : 44	18.51	19.56	1.04	-0.18	$5.16 \pm 0.10$	$-1.15 \pm 0.10$	1	0	0	0
14.1	1 : 2 : 15	-71 : 38 : 38	18.26	19.36	1.10	-0.38	$7.01 \pm 0.08$	$-0.53 \pm 0.11$	1	1	1	0
15.1	1 : 2 : 1	-71 : 38 : 25	18.49	19.60	1.11	-0.14	$6.38 \pm 0.08$	$-0.69 \pm 0.11$	1	0	0	0
16.1	1 : 2 : 5	-71 : 38 : 13	17.25	18.38	1.13	-1.36	$6.77 \pm 0.06$	$-0.87 \pm 0.10$	1	0	0	0
17.1	1 : 2 : 17	-71 : 37 : 45	17.39	18.48	1.08	-1.26	$6.18 \pm 0.05$	$-1.06 \pm 0.09$	1	0	0	0
19.1	1 : 2 : 13	-71 : 37 : 33	16.85	18.07	1.22	-1.67	$6.98 \pm 0.06$	$-0.88 \pm 0.10$	1	0	0	0
23.1	1 : 2 : 8	-71 : 37 : 4	17.03	18.17	1.13	-1.57	$6.35 \pm 0.05$	$-1.08 \pm 0.09$	1	0	0	0
24.1	1 : 2 : 6	-71 : 36 : 57	16.53	17.80	1.27	-1.94	$6.79 \pm 0.05$	$-1.02 \pm 0.10$	1	0	0	0
25.1	1 : 2 : 9	-71 : 36 : 51	17.03	18.18	1.15	-1.56	$6.88 \pm 0.05$	$-0.89 \pm 0.10$	1	1	1	1
26.1	1 : 1 : 58	-71 : 36 : 45	17.29	18.43	1.14	-1.31	$6.70 \pm 0.06$	$-0.89 \pm 0.10$	1	1	1	1
27.1	1 : 2 : 10	-71 : 36 : 41	16.42	17.63	1.21	-2.11	$6.86 \pm 0.06$	$-1.04 \pm 0.10$	1	1	1	1
28.1	1 : 2 : 2	-71 : 36 : 36	18.02	19.05	1.03	-0.69	$6.13 \pm 0.06$	$-0.93 \pm 0.10$	1	1	1	1
29.1	1 : 2 : 11	-71 : 36 : 30	15.08	16.71	1.64	-3.03	$8.21 \pm 0.06$	$-0.79 \pm 0.11$	1	1	1	1
31.1	1 : 2 : 15	-71 : 36 : 21	17.64	18.67	1.03	-1.07	$6.40 \pm 0.05$	$-0.93 \pm 0.10$	1	1	1	1
32.1	1 : 2 : 18	-71 : 36 : 15	15.56	17.01	1.45	-2.73	$7.65 \pm 0.06$	$-0.92 \pm 0.11$	1	1	1	1
33.1	1 : 2 : 5	-71 : 36 : 11	17.52	18.55	1.03	-1.19	$6.44 \pm 0.06$	$-0.95 \pm 0.10$	1	1	1	1
34.1	1 : 2 : 12	-71 : 36 : 6	17.82	18.84	1.01	-0.90	$6.16 \pm 0.06$	$-0.98 \pm 0.10$	1	0	0	0
35.1	1 : 2 : 10	-71 : 36 : 2	17.00	18.18	1.17	-1.56	$6.56 \pm 0.06$	$-1.00 \pm 0.10$	1	1	1	1

Continued on next page

Parameters of stars in NGC 361 - *continued*

36.1	1 : 2 : 12	-71 : 35 : 56	15.67	17.09	1.43	-2.65	7.77 ± 0.06	-0.85 ± 0.11	1	1	1	1
37.1	1 : 2 : 9	-71 : 35 : 52	17.60	18.64	1.03	-1.10	6.22 ± 0.06	-1.01 ± 0.10	1	1	1	1
39.1	1 : 2 : 11	-71 : 35 : 39	16.89	18.07	1.18	-1.67	6.84 ± 0.06	-0.93 ± 0.10	1	0	0	0
40.1	1 : 2 : 13	-71 : 35 : 25	16.96	18.15	1.19	-1.59	6.05 ± 0.05	-1.19 ± 0.09	1	0	0	0
41.1	1 : 2 : 15	-71 : 35 : 19	17.32	18.43	1.11	-1.31	6.65 ± 0.05	-0.91 ± 0.10	1	0	0	0
43.1	1 : 2 : 4	-71 : 35 : 7	17.40	18.57	1.16	-1.17	6.35 ± 0.04	-0.98 ± 0.10	1	0	0	0
44.1	1 : 2 : 10	-71 : 34 : 56	18.52	19.38	0.87	-0.36	5.01 ± 0.07	-1.24 ± 0.09	1	1	1	0
47.1	1 : 2 : 0	-71 : 34 : 31	16.57	17.72	1.15	-2.02	6.59 ± 0.04	-1.11 ± 0.09	1	0	0	0
48.1	1 : 2 : 22	-71 : 34 : 26	17.79	18.84	1.05	-0.90	5.64 ± 0.05	-1.16 ± 0.09	1	0	0	0
49.1	1 : 2 : 3	-71 : 34 : 14	17.54	18.68	1.14	-1.06	6.11 ± 0.05	-1.03 ± 0.09	1	1	1	1

Table 5.J: Parameters of stars in NGC 411.

Star	alpha	delta	$I$	$V$	$(V - I)$	$V - V_{\text{HB}}$	$\Sigma W$	$[\text{Fe}/\text{H}]$	CMD	membership criteria		
	(J2000)	(J2000)	[mag]	[mag]	[mag]	[mag]	Å	dex		velocity	distance	metallicity
1.1	1 : 8 : 1	-71 : 40 : 58	16.61	17.73	1.12	-1.99	7.14 ± 0.07	-0.91 ± 0.10	1	1	0	0
2.1	1 : 8 : 7	-71 : 41 : 6	15.36	16.77	1.41	-2.95	8.72 ± 0.06	-0.59 ± 0.11	1	1	0	0
3.1	1 : 7 : 53	-71 : 41 : 14	16.81	17.63	0.83	-2.09	6.47 ± 0.05	-1.17 ± 0.09	0	1	0	0
4.1	1 : 7 : 36	-71 : 41 : 25	17.21	18.12	0.91	-1.60	6.70 ± 0.10	-0.96 ± 0.10	1	0	0	0
5.1	1 : 7 : 33	-71 : 41 : 30	16.21	17.65	1.44	-2.07	6.53 ± 0.06	-1.15 ± 0.09	0	0	0	0
6.1	1 : 7 : 56	-71 : 41 : 33	17.55	18.50	0.95	-1.22	5.70 ± 0.07	-1.23 ± 0.09	1	0	0	0
7.1	1 : 7 : 29	-71 : 41 : 42	18.07	19.55	1.48	-0.17	6.12 ± 0.15	-0.80 ± 0.11	0	0	0	0
9.1	1 : 8 : 5	-71 : 41 : 54	17.42	18.42	1.00	-1.30	6.37 ± 0.09	-1.00 ± 0.10	1	1	0	0
10.1	1 : 8 : 0	-71 : 42 : 0	17.55	18.50	0.95	-1.22	6.81 ± 0.09	-0.82 ± 0.10	1	0	0	0
12.1	1 : 7 : 51	-71 : 42 : 13	17.53	18.56	1.03	-1.16	6.91 ± 0.11	-0.77 ± 0.11	1	0	0	0
13.1	1 : 7 : 37	-71 : 42 : 17	15.83	17.03	1.21	-2.69	4.73 ± 0.03	-1.96 ± 0.07	1	0	0	0
16.1	1 : 7 : 33	-71 : 42 : 33	16.15	17.36	1.21	-2.36	6.97 ± 0.05	-1.07 ± 0.10	1	1	0	0
17.1	1 : 7 : 34	-71 : 42 : 42	17.27	18.30	1.02	-1.42	6.51 ± 0.06	-0.99 ± 0.09	1	1	0	0
18.1	1 : 7 : 47	-71 : 42 : 50	16.15	17.28	1.14	-2.44	7.24 ± 0.06	-0.99 ± 0.10	1	0	0	0
19.1	1 : 7 : 32	-71 : 42 : 55	18.00	18.76	0.75	-0.96	6.50 ± 0.09	-0.87 ± 0.10	0	1	0	0
20.1	1 : 7 : 39	-71 : 43 : 2	18.21	19.00	0.79	-0.72	5.12 ± 0.14	-1.30 ± 0.09	0	1	0	0
21.1	1 : 7 : 31	-71 : 43 : 9	17.74	18.52	0.77	-1.20	5.60 ± 0.09	-1.26 ± 0.09	0	0	0	0
23.1	1 : 8 : 12	-71 : 43 : 22	17.96	18.94	0.98	-0.78	6.40 ± 0.10	-0.86 ± 0.10	1	0	0	0
24.1	1 : 7 : 29	-71 : 43 : 27	17.35	18.33	0.98	-1.39	6.62 ± 0.07	-0.94 ± 0.10	1	0	0	0
25.1	1 : 7 : 57	-71 : 43 : 33	16.87	17.86	0.98	-1.86	5.66 ± 0.04	-1.41 ± 0.08	1	0	0	0
27.1	1 : 7 : 33	-71 : 43 : 43	17.69	18.62	0.92	-1.10	6.78 ± 0.12	-0.80 ± 0.11	1	1	0	0

Continued on next page

Parameters of stars in NGC 411 - *continued*

28.1	1 : 7 : 37	-71 : 43 : 57	17.62	18.55	0.93	-1.17	6.73 ± 0.07	-0.84 ± 0.10	1	0	0	0
31.1	1 : 7 : 48	-71 : 44 : 18	16.91	17.96	1.05	-1.76	6.95 ± 0.06	-0.92 ± 0.10	1	1	0	0
32.1	1 : 7 : 30	-71 : 44 : 26	15.89	17.26	1.37	-2.46	7.91 ± 0.05	-0.75 ± 0.11	1	1	0	0
33.1	1 : 7 : 59	-71 : 44 : 29	18.35	19.09	0.75	-0.63	5.82 ± 0.13	-1.02 ± 0.10	0	0	0	0
36.1	1 : 7 : 43	-71 : 44 : 48	15.65	17.15	1.50	-2.57	8.19 ± 0.07	-0.68 ± 0.11	1	1	0	0
37.1	1 : 7 : 37	-71 : 44 : 51	15.47	16.75	1.27	-2.97	6.75 ± 0.04	-1.31 ± 0.09	1	0	0	0
38.1	1 : 7 : 36	-71 : 44 : 59	16.69	17.78	1.10	-1.94	6.90 ± 0.06	-0.98 ± 0.10	1	1	0	0
39.1	1 : 8 : 2	-71 : 45 : 5	16.80	17.87	1.07	-1.85	7.83 ± 0.06	-0.62 ± 0.11	1	1	1	1
40.1	1 : 7 : 35	-71 : 45 : 12	16.50	17.67	1.16	-2.05	7.67 ± 0.07	-0.73 ± 0.11	1	0	0	0
41.1	1 : 8 : 2	-71 : 45 : 16	18.27	18.84	0.57	-0.88	5.63 ± 0.13	-1.16 ± 0.10	0	0	0	0
42.1	1 : 7 : 47	-71 : 45 : 21	15.29	16.87	1.58	-2.85	8.33 ± 0.06	-0.70 ± 0.11	1	1	1	1
43.1	1 : 7 : 54	-71 : 45 : 26	16.11	17.33	1.22	-2.39	8.38 ± 0.07	-0.56 ± 0.11	1	1	1	1
45.1	1 : 7 : 41	-71 : 45 : 35	16.42	17.54	1.12	-2.18	6.57 ± 0.04	-1.16 ± 0.09	1	0	0	0
46.1	1 : 7 : 53	-71 : 45 : 43	16.40	17.53	1.13	-2.19	8.00 ± 0.07	-0.65 ± 0.11	1	1	1	1
47.1	1 : 8 : 1	-71 : 45 : 48	17.38	18.42	1.04	-1.30	7.15 ± 0.07	-0.72 ± 0.10	1	1	1	1
48.1	1 : 7 : 47	-71 : 45 : 53	15.82	17.21	1.39	-2.51	7.74 ± 0.05	-0.83 ± 0.10	1	0	0	0
49.1	1 : 7 : 52	-71 : 46 : 1	17.01	18.00	0.99	-1.72	5.92 ± 0.08	-1.28 ± 0.09	1	1	1	0
50.1	1 : 7 : 23	-71 : 46 : 5	16.56	17.66	1.10	-2.06	6.92 ± 0.05	-1.01 ± 0.10	1	0	0	0
52.1	1 : 7 : 36	-71 : 46 : 14	16.61	17.68	1.08	-2.04	6.32 ± 0.13	-1.22 ± 0.10	1	0	0	0
53.1	1 : 7 : 54	-71 : 46 : 20	16.96	17.88	0.91	-1.84	7.14 ± 0.06	-0.87 ± 0.10	1	0	0	0
54.1	1 : 7 : 32	-71 : 46 : 28	15.92	17.06	1.14	-2.66	6.37 ± 0.04	-1.36 ± 0.09	1	0	0	0
56.1	1 : 7 : 55	-71 : 46 : 39	15.83	17.12	1.29	-2.60	8.44 ± 0.07	-0.60 ± 0.11	1	1	1	1
57.1	1 : 7 : 52	-71 : 46 : 44	15.57	16.74	1.16	-2.98	7.09 ± 0.05	-1.19 ± 0.10	1	1	1	0
58.1	1 : 8 : 15	-71 : 46 : 49	17.35	18.25	0.90	-1.47	6.82 ± 0.09	-0.89 ± 0.10	1	0	0	0
60.1	1 : 7 : 34	-71 : 46 : 58	15.94	17.20	1.25	-2.53	8.15 ± 0.07	-0.68 ± 0.11	1	1	0	0
61.1	1 : 7 : 56	-71 : 47 : 7	14.60	16.32	1.72	-3.40	9.25 ± 0.08	-0.52 ± 0.12	1	1	1	1
63.1	1 : 7 : 27	-71 : 47 : 18	15.89	16.83	0.95	-2.89	7.35 ± 0.05	-1.07 ± 0.10	0	0	0	0
64.1	1 : 7 : 55	-71 : 47 : 25	14.75	16.37	1.62	-3.35	8.79 ± 0.07	-0.67 ± 0.11	1	1	0	0
65.1	1 : 8 : 5	-71 : 47 : 33	16.08	17.34	1.26	-2.38	8.79 ± 0.07	-0.41 ± 0.12	1	1	0	0
66.1	1 : 7 : 37	-71 : 47 : 39	16.27	17.57	1.30	-2.15	7.29 ± 0.05	-0.90 ± 0.10	1	1	0	0
68.1	1 : 7 : 46	-71 : 47 : 50	16.99	18.14	1.15	-1.58	6.94 ± 0.06	-0.87 ± 0.10	1	1	0	0

Table 5.K: Parameters of stars in NGC 416.

Star	alpha	delta	$I$	$V$	$(V - I)$	$V - V_{\text{HB}}$	$\Sigma W$	$[\text{Fe}/\text{H}]$	CMD	membership criteria		
	(J2000)	(J2000)	[mag]	[mag]	[mag]	[mag]	Å	dex		velocity	distance	metallicity

*Continued on next page*

Parameters of stars in NGC 416 - *continued*

1.1	1 : 7 : 52	-72 : 25 : 49	16.93	17.96	1.03	-1.91	6.92 ± 0.06	-0.97 ± 0.10	1	0	0	0
2.1	1 : 7 : 38	-72 : 25 : 40	14.94	16.32	1.39	-3.55	8.32 ± 0.07	-0.89 ± 0.11	0	0	0	0
3.1	1 : 8 : 12	-72 : 25 : 32	16.66	17.78	1.12	-2.09	7.07 ± 0.06	-0.96 ± 0.10	1	0	0	0
4.1	1 : 7 : 58	-72 : 25 : 23	16.80	17.91	1.11	-1.96	7.36 ± 0.05	-0.82 ± 0.10	1	0	0	0
5.1	1 : 7 : 48	-72 : 25 : 11	14.98	16.39	1.41	-3.48	8.39 ± 0.07	-0.85 ± 0.11	0	0	0	0
6.1	1 : 8 : 14	-72 : 25 : 4	16.86	17.59	0.73	-2.28	5.98 ± 0.05	-1.40 ± 0.09	0	0	0	0
7.1	1 : 8 : 16	-72 : 24 : 56	15.84	16.76	0.93	-3.11	6.80 ± 0.05	-1.33 ± 0.10	0	0	0	0
9.1	1 : 7 : 55	-72 : 24 : 41	15.28	16.76	1.48	-3.11	7.66 ± 0.05	-1.02 ± 0.10	1	0	0	0
10.1	1 : 8 : 18	-72 : 24 : 32	15.83	17.15	1.31	-2.72	5.81 ± 0.12	-1.58 ± 0.10	1	0	0	0
11.1	1 : 7 : 49	-72 : 24 : 24	15.94	17.19	1.25	-2.68	7.62 ± 0.05	-0.92 ± 0.10	1	0	0	0
12.1	1 : 8 : 15	-72 : 24 : 18	16.19	17.47	1.29	-2.40	6.84 ± 0.05	-1.12 ± 0.10	1	0	0	0
13.1	1 : 7 : 42	-72 : 24 : 10	17.00	18.05	1.05	-1.82	7.38 ± 0.07	-0.78 ± 0.11	1	0	0	0
16.1	1 : 7 : 56	-72 : 23 : 41	17.05	17.65	0.60	-2.22	3.00 ± 0.03	-2.47 ± 0.07	0	0	0	0
18.1	1 : 7 : 59	-72 : 23 : 21	16.86	17.80	0.95	-2.07	5.90 ± 0.04	-1.38 ± 0.09	1	0	0	0
19.1	1 : 7 : 33	-72 : 23 : 13	15.76	16.71	0.94	-3.16	7.54 ± 0.06	-1.07 ± 0.10	0	0	0	0
20.1	1 : 7 : 41	-72 : 23 : 4	16.80	17.40	0.61	-2.47	8.48 ± 0.10	-0.55 ± 0.12	0	0	0	0
21.1	1 : 8 : 9	-72 : 22 : 47	16.60	17.82	1.23	-2.05	5.91 ± 0.15	-1.37 ± 0.10	1	1	0	0
22.1	1 : 8 : 15	-72 : 22 : 37	16.24	17.52	1.28	-2.35	7.21 ± 0.05	-0.98 ± 0.10	1	1	0	0
23.1	1 : 7 : 51	-72 : 22 : 27	16.62	17.76	1.14	-2.11	6.70 ± 0.04	-1.10 ± 0.10	1	0	0	0
24.1	1 : 7 : 55	-72 : 22 : 21	16.51	17.77	1.27	-2.10	7.25 ± 0.05	-0.90 ± 0.10	1	1	1	1
25.1	1 : 7 : 50	-72 : 22 : 13	16.82	17.96	1.14	-1.91	6.96 ± 0.05	-0.95 ± 0.10	1	1	1	1
27.1	1 : 8 : 0	-72 : 21 : 53	14.74	15.98	1.23	-3.89	8.49 ± 0.07	-0.92 ± 0.11	0	0	0	0
28.1	1 : 8 : 0	-72 : 21 : 43	16.29	17.65	1.36	-2.22	7.59 ± 0.05	-0.81 ± 0.11	1	1	1	1
29.1	1 : 8 : 6	-72 : 21 : 33	16.66	17.88	1.23	-1.99	7.23 ± 0.05	-0.88 ± 0.10	1	1	1	1
30.1	1 : 7 : 49	-72 : 21 : 24	15.45	16.98	1.53	-2.89	8.14 ± 0.06	-0.78 ± 0.11	1	1	1	1
31.1	1 : 7 : 42	-72 : 21 : 14	16.14	17.40	1.26	-2.47	7.71 ± 0.06	-0.83 ± 0.11	1	0	0	0
32.1	1 : 7 : 44	-72 : 21 : 2	15.72	16.67	0.95	-3.20	7.97 ± 0.05	-0.93 ± 0.11	0	0	0	0
33.1	1 : 7 : 45	-72 : 20 : 52	16.44	17.60	1.16	-2.27	7.13 ± 0.06	-0.98 ± 0.10	1	0	0	0
34.1	1 : 8 : 16	-72 : 20 : 43	15.03	16.09	1.06	-3.78	8.15 ± 0.07	-1.02 ± 0.11	0	0	0	0
35.1	1 : 7 : 48	-72 : 20 : 38	16.41	17.64	1.22	-2.23	7.30 ± 0.05	-0.92 ± 0.10	1	0	0	0
36.1	1 : 7 : 48	-72 : 20 : 30	16.42	17.65	1.23	-2.22	6.60 ± 0.11	-1.16 ± 0.10	1	1	1	0
38.1	1 : 8 : 5	-72 : 20 : 15	15.51	17.01	1.49	-2.86	7.80 ± 0.06	-0.90 ± 0.11	1	1	1	1
40.1	1 : 8 : 17	-72 : 20 : 2	16.60	17.14	0.54	-2.73	3.91 ± 0.05	-2.27 ± 0.07	0	0	0	0
41.1	1 : 8 : 15	-72 : 19 : 51	16.61	17.85	1.23	-2.02	7.46 ± 0.07	-0.80 ± 0.11	1	0	0	0
43.1	1 : 7 : 57	-72 : 19 : 37	18.06	17.97	-0.09	-1.90	7.14 ± 0.05	-0.88 ± 0.10	0	1	0	0
44.1	1 : 7 : 38	-72 : 19 : 31	16.43	17.51	1.08	-2.36	8.07 ± 0.06	-0.67 ± 0.11	1	0	0	0
46.1	1 : 8 : 18	-72 : 19 : 18	15.25	16.71	1.46	-3.16	8.03 ± 0.05	-0.89 ± 0.11	1	0	0	0
47.1	1 : 8 : 1	-72 : 19 : 9	16.40	17.62	1.22	-2.25	7.10 ± 0.04	-0.99 ± 0.10	1	0	0	0

*Continued on next page*

**Table 5.L:** Parameters of stars in NGC 419.

Star	alpha (J2000)	delta (J2000)	$I$ [mag]	$V$ [mag]	$(V - I)$ [mag]	$V - V_{\text{HB}}$ [mag]	$\Sigma W$ Å	[Fe/H] dex	CMD	membership criteria		
										velocity	distance	metallicity
1.1	1 : 8 : 25	-72 : 57 : 25	15.72	17.08	1.36	-2.60	7.85 ± 0.06	-0.81 ± 0.11	1	0	0	0
2.1	1 : 8 : 18	-72 : 57 : 14	15.66	16.84	1.19	-2.84	7.30 ± 0.09	-1.07 ± 0.11	1	0	0	0
3.1	1 : 8 : 36	-72 : 57 : 6	16.07	17.25	1.18	-2.43	7.74 ± 0.07	-0.81 ± 0.11	1	0	0	0
5.1	1 : 8 : 9	-72 : 56 : 47	15.06	16.51	1.45	-3.17	8.76 ± 0.07	-0.63 ± 0.12	1	1	0	0
6.1	1 : 8 : 10	-72 : 56 : 34	15.54	16.93	1.40	-2.75	7.84 ± 0.06	-0.85 ± 0.11	1	0	0	0
7.1	1 : 8 : 38	-72 : 56 : 24	15.32	16.69	1.36	-2.99	7.73 ± 0.05	-0.96 ± 0.11	1	0	0	0
8.1	1 : 8 : 28	-72 : 56 : 17	17.42	18.43	1.01	-1.25	5.13 ± 0.09	-1.44 ± 0.09	1	0	0	0
9.1	1 : 8 : 31	-72 : 56 : 10	17.23	18.18	0.96	-1.50	4.74 ± 0.11	-1.64 ± 0.09	1	0	0	0
10.1	1 : 8 : 13	-72 : 56 : 2	16.96	18.01	1.05	-1.67	7.16 ± 0.07	-0.81 ± 0.11	1	1	0	0
11.1	1 : 8 : 12	-72 : 55 : 52	15.49	16.84	1.36	-2.84	8.17 ± 0.07	-0.76 ± 0.11	1	0	0	0
12.1	1 : 8 : 14	-72 : 55 : 45	14.95	16.10	1.16	-3.58	7.02 ± 0.04	-1.37 ± 0.10	0	0	0	0
13.1	1 : 8 : 36	-72 : 55 : 37	16.39	17.59	1.19	-2.09	7.78 ± 0.06	-0.70 ± 0.11	1	0	0	0
14.1	1 : 8 : 6	-72 : 55 : 28	17.01	17.91	0.90	-1.77	4.88 ± 0.05	-1.67 ± 0.08	1	0	0	0
15.1	1 : 8 : 1	-72 : 55 : 19	15.46	16.52	1.06	-3.16	8.15 ± 0.06	-0.85 ± 0.11	0	0	0	0
16.1	1 : 8 : 19	-72 : 55 : 14	15.52	16.92	1.40	-2.76	7.94 ± 0.06	-0.82 ± 0.11	1	0	0	0
18.1	1 : 8 : 39	-72 : 55 : 3	16.34	17.61	1.27	-2.07	8.53 ± 0.08	-0.43 ± 0.12	1	0	0	0
19.1	1 : 8 : 4	-72 : 54 : 56	16.04	17.21	1.17	-2.47	8.22 ± 0.06	-0.64 ± 0.12	1	0	0	0
20.1	1 : 8 : 22	-72 : 54 : 48	16.03	17.27	1.23	-2.41	7.91 ± 0.06	-0.74 ± 0.11	1	1	1	1
21.1	1 : 8 : 8	-72 : 54 : 42	16.77	17.89	1.12	-1.79	7.49 ± 0.07	-0.73 ± 0.11	1	1	1	1
22.1	1 : 8 : 17	-72 : 54 : 23	17.51	18.49	0.98	-1.19	8.15 ± 0.06	-0.33 ± 0.12	1	1	1	0
23.1	1 : 8 : 17	-72 : 54 : 12	15.70	17.03	1.33	-2.65	8.49 ± 0.07	-0.59 ± 0.12	1	1	1	1
24.1	1 : 8 : 27	-72 : 54 : 4	15.73	17.03	1.30	-2.65	8.51 ± 0.08	-0.59 ± 0.12	1	0	0	0
25.1	1 : 8 : 17	-72 : 53 : 58	15.87	17.18	1.31	-2.50	8.54 ± 0.07	-0.54 ± 0.12	1	1	1	1
26.1	1 : 8 : 18	-72 : 53 : 50	16.18	17.15	0.97	-2.53	7.26 ± 0.06	-1.01 ± 0.11	0	0	0	0
27.1	1 : 8 : 7	-72 : 53 : 44	17.04	17.96	0.92	-1.72	6.65 ± 0.05	-1.01 ± 0.10	1	0	0	0
29.1	1 : 8 : 30	-72 : 53 : 30	16.42	17.47	1.05	-2.21	7.56 ± 0.06	-0.81 ± 0.11	1	1	1	1
30.1	1 : 8 : 6	-72 : 53 : 24	15.66	16.89	1.23	-2.79	8.28 ± 0.07	-0.71 ± 0.12	1	1	1	1
31.1	1 : 8 : 26	-72 : 53 : 16	15.48	16.80	1.32	-2.88	8.04 ± 0.07	-0.82 ± 0.11	1	1	1	1
32.1	1 : 8 : 3	-72 : 53 : 9	16.03	17.27	1.24	-2.41	8.41 ± 0.08	-0.56 ± 0.12	1	1	1	1
33.1	1 : 7 : 54	-72 : 53 : 3	16.80	17.93	1.13	-1.75	7.60 ± 0.07	-0.68 ± 0.11	1	0	0	0
34.1	1 : 8 : 28	-72 : 52 : 57	16.91	17.98	1.08	-1.70	7.14 ± 0.06	-0.83 ± 0.11	1	1	1	1

*Continued on next page*



Parameters of stars in NGC 419 - *continued*

35.1	1 : 8 : 7	-72 : 52 : 49	16.78	17.83	1.05	-1.85	$7.70 \pm 0.07$	$-0.67 \pm 0.11$	1	1	1	1
36.1	1 : 8 : 8	-72 : 52 : 38	15.64	16.96	1.32	-2.72	$8.88 \pm 0.07$	$-0.47 \pm 0.12$	1	1	1	1
38.1	1 : 8 : 17	-72 : 52 : 23	16.69	17.69	1.00	-1.99	$7.04 \pm 0.05$	$-0.94 \pm 0.11$	1	1	1	1
39.1	1 : 8 : 9	-72 : 52 : 16	16.94	18.02	1.08	-1.66	$7.42 \pm 0.06$	$-0.72 \pm 0.11$	1	1	1	1
40.1	1 : 8 : 15	-72 : 52 : 9	16.52	17.60	1.08	-2.08	$7.57 \pm 0.06$	$-0.77 \pm 0.11$	1	1	1	1
41.1	1 : 8 : 29	-72 : 51 : 58	16.16	17.40	1.25	-2.28	$8.18 \pm 0.08$	$-0.61 \pm 0.12$	1	0	0	0
42.1	1 : 8 : 17	-72 : 51 : 52	15.12	16.57	1.45	-3.11	$8.72 \pm 0.07$	$-0.63 \pm 0.12$	1	1	1	1
43.1	1 : 8 : 38	-72 : 51 : 45	16.04	16.86	0.81	-2.82	$6.47 \pm 0.04$	$-1.37 \pm 0.10$	0	0	0	0
44.1	1 : 8 : 22	-72 : 51 : 37	16.07	17.29	1.22	-2.39	$6.98 \pm 0.04$	$-1.07 \pm 0.10$	1	0	0	0
45.1	1 : 8 : 12	-72 : 51 : 29	16.57	17.66	1.09	-2.02	$7.55 \pm 0.07$	$-0.77 \pm 0.11$	1	0	0	0
46.1	1 : 8 : 25	-72 : 51 : 17	15.78	17.07	1.29	-2.61	$8.06 \pm 0.06$	$-0.74 \pm 0.11$	1	1	1	1
48.1	1 : 8 : 24	-72 : 50 : 59	16.40	17.58	1.18	-2.10	$7.16 \pm 0.04$	$-0.93 \pm 0.10$	1	1	0	0



## Chapter 6

# Summary, Conclusions, and Outlook

### Milky Way globular clusters

We present for the first time a homogeneous data sample comprising eight Galactic globular clusters, whereof two are associated with the accreted Sagittarius dwarf galaxy. Our data set consists of more than 500 medium resolution spectra of stars in different evolutionary stages, ranging from the upper main sequence (MS), sub-giant branch (SGB) to the lower red giant branch (RGB). We concentrate on the investigation of the CN and CH molecule absorption bands. Line index measurements reveal strong CN and CH abundance variations for nearly all clusters studied. For two clusters in our sample (NGC 288 and NGC 362) we detect a clear bimodal distribution in CN for RGB stars.

Interestingly, the two clusters that show no CN strong stars are the two accreted clusters (Pal 12 and Ter 7). These are fairly metal-rich objects. Hence, CN-strong stars, if present, should be easily detectable. We conclude that these stars are actually lacking in Pal 12 and Ter 7. This suggests that environmental conditions during the formation scarcely influence the chemical composition of the clusters.

Considering the CN and CH absorption bands we find that for the clusters with a strong CN-bimodality an anticorrelation between CN and CH. This anticorrelation also seems to be present for the less evolved stars. Since all our measurements are focused on stars fainter than the RGB bump, the point where deep mixing is believed to set in, we conclude that pure evolutionary effects within the stellar interior cannot be the main driver of the observed patterns. The CN and CH variations most likely originate from pollution by ejecta of evolved stars as described in the so-called self-enrichment scenario.

In order to search for the drivers of these anomalies we compute for each globular cluster the number ratio of CN-strong to CN-weak stars and compare this parameter with various cluster properties. Although we hardly see any correlations, our data suggest a dependency on total cluster luminosity in such a way that only the brightest clusters were able to form many CN strong stars. These findings support the idea that CN was formed in the pre-cluster environment and that the more massive, i.e., brighter, objects were able to retain the enriched material more efficiently.

The results of this study clearly confirm the emerging general consensus that globular clusters can only to first order be considered as simple stellar populations. In fact, their formation and evolution seem to be quite complex. Our results favor a scenario of a prolonged

star formation within globular clusters. A first generation of stars contaminated the intra-cluster gas from which a second generation of stars formed. Possible candidates discussed in the literature are asymptotic giant branch stars and fast rotation massive stars. Both types of stars eject their material via a slow wind. The stars we observe today are only the long-lived stars of the first and the second generation. The amount of CN-strong stars formed seems to depend on quantities such as the mass and the environmental conditions of the cluster.

Unfortunately, our cluster sample is still small. To further strengthen our findings a larger sample of globular cluster measurements is required. In order to investigate the external influences on the cluster chemistry, observations of additional accreted, young halo clusters are desired.

For the further search for correlations between the number ratio of CN-strong stars and cluster parameters we plan in a subsequent project a comparable study using parameters adopted from other literature sources (e.g., McLaughlin & van der Marel 2005). Although these compilations do not comprise as many parameters as the catalog by Harris (2003), they have the advantage that they provide a more homogeneous set of structural parameters of globular clusters.

During the analysis of our data it turned out that the stars on SGB and upper MS are not the ideal candidates for molecule absorption measurements. Due to higher effective temperatures the investigated features are fairly weak. Ideally we would like to observe stars on the lower MS for an adequate sample of star clusters. These stars are unevolved and can shed light on the origin of the observed bimodality in CN.

### Small Magellanic Cloud

The Small Magellanic Cloud (SMC) is one of our closest galactic neighbors and hosts a large system of about 700 star clusters. However, despite its proximity the SMC star cluster system is still sparsely studied. Our work provides an important step towards a complete catalog of SMC star clusters. We estimate new core radii for twelve SMC star clusters. For the clusters in common we find good agreement between our ground-based estimates and the most recent high-resolution HST observations by Mackey & Gilmore (2003a). Furthermore, we determine the heliocentric velocities of the twelve clusters in our sample. Only three of them have previous kinematic measurements based on single star observations (Da Costa & Hatzidimitriou 1998). The comparison reveals a systematic offset of about 20 km/s. Since our measurements are based on a much larger spectroscopic sample, we are confident that our results are more trustable. Our determined heliocentric velocities of the star clusters and the velocity dispersion of the system follow nicely the kinematic studies of Carbon stars (e.g., Kunkel et al. 2000), which are also tracers of intermediate age and old stellar populations. Since those studies did not find any sign for rotation inside the SMC, we speculate that also the star clusters system is probably not rotating.

In collaboration with Dr. Niranjan Sambhus we plan a more sophisticated investigation of the rotation of the intermediate age stellar population in the SMC. Herein we shall include the velocities of the star clusters and field stars determined in the framework of this thesis. Moreover, we plan to revise the existing data on Carbon stars from Hardy et al. (1989), Hatzidimitriou et al. (1997), and Kunkel et al. (2000). For this dynamical investigation we will apply the running average method (e.g., Sambhus et al. 2006). In order to carefully correct for galactic rotation we will perform a transformation of the heliocentric velocities into the Galactocentric system.

During this project we detected for two clusters in our sample (Kron 28 and Lindsay 116) a significant mismatch between the CMDs based on our Pre-Image photometry and the theoretical isochrones chosen according to the literature age and metallicity values. Since our spectroscopic metallicity estimates are in acceptable agreement with the photometric measurements, we suspect that the observed deviations are mainly caused by erroneous age estimates. Both age values were derived from shallow photometry from the magnitude difference between the red giant clump and the main-sequence turn-off (Piatti et al. 2001). We strongly suggest a repetition of the age determination from deeper photometric measurements.

The SMC has the important property that it is the only dwarf galaxy in the Local Group known to have formed and preserved star clusters continuously over the past 12 Gyr. These clusters provide a sample of simple and powerful evolutionary tracers. However, only for six of these clusters spectroscopic metallicities have been obtained before (Da Costa & Hatzidimitriou 1998). This thesis now presents metallicities for ten additional SMC clusters and two in common with the sample of Da Costa & Hatzidimitriou (1998). From the analysis of the strong absorption features of the near IR CaII triplet we derive  $[\text{Fe}/\text{H}]$  abundances of all twelve star clusters.

Complemented by ages taken from the literature we can for the first time present an age-metallicity relation for the SMC that is purely based on spectroscopic metallicity estimates. The most striking feature in this relation is a large scatter in  $[\text{Fe}/\text{H}]$  at a given age of about 6 Gyr, indicating that the SMC was not well mixed in the past. For younger ages we find an increase in mean metallicity accompanied by a decrease of the scatter. We discuss the resulting chemical evolution history in the context of different chemical evolution models. We find that the SMC history is better reproduced by a bursting model of chemical evolution. Furthermore, we conclude that probably infall of unenriched gas has played a major role in the history of the SMC. The comparison with dynamical models of the orbital evolution of the SMC and LMC about the MW suggests that also the interaction between the components of the triple-system strongly influences the chemical appearance of the SMC.

In order to constrain the observed scatter in metallicity it is necessary to further increase the existing sample of spectroscopic metallicity estimates of SMC star clusters. Moreover, accurate age estimates based on HST observation exist only for a minority of star clusters. Better age determinations for many clusters are absolutely essential.

In a subsequent project we will apply for high resolution spectroscopy of stars in the SMC clusters. High probability members have been selected in the framework of this thesis. The advantage of targeting cluster members is that they can be associated with fairly accurate age measurements. The abundance analysis will focus on  $\alpha$ -elements and if possible  $r$ - and  $s$ - process (rapid and slow neutron capture) elements. The  $\alpha$ -elements and  $r$ -process elements are synthesized in quickly evolving high-mass stars and returned to the interstellar medium via core-collapse supernovae (SNe II). In contrast Fe is predominantly formed on longer timescales by SNe Ia. (Asymptotic giant branch stars are believed to contribute  $s$ -process elements.) Hence, the high resolution spectroscopy will allow for the estimation of the relative contribution of SN Ia to SN II ejecta. The comparison with chemical evolution models calculating detailed chemical abundances (e.g., Gilmore & Wyse 1991; Russell & Dopita 1992; Pagel & Tautvaisiene 1998) will allow to further constrain the evolution of the SMC. Furthermore, the spatial analysis will point out local enrichment by SN.

Investigations of field stars in the LMC (Cole et al. 2005) and the solar neighborhood (e.g., Feltzing et al. 2001; Nordström et al. 2004) revealed a large scatter in the age-metallicity relations. For comparison, the observation of the age-metallicity relation based on the SMC

field star population would be very interesting. This could shed light on the common past of the two galaxies. Furthermore it could help to understand how well star cluster investigations (like this thesis) trace the overall chemical evolution of a galaxy. The selection of the cluster members from the spectroscopic sample reveals that we have observed a fairly large number of spectra of probable SMC field stars. In another subsequent project we plan to determine and analyze the metallicities of the stars in the surrounding fields of each star cluster. This will require a careful estimation of an adequate reference horizontal branch magnitude for these stars, which is hindered by the depth of the SMC. We will compare the cluster and field metallicities. Ideally we also wish to achieve age estimates for these stars, which would enable the desired comparison between the age-metallicity relations based on star clusters and based on field stars.

mass and environment are required in order to analyze if there exists a critical mass for which the mixing of gas in galaxies is efficient or for which star formation occurred non intermittently.

# Appendix A

## Chemical Evolution Models

This summary of the basic inputs and assumptions of theoretical chemical evolution models applied to stellar populations is based on Tinsley (1980), Pagel (1997), and Sparke & Gallagher (2000).

### A.1 Basic assumptions and equations

For a stellar system with the total mass  $M$  we can differentiate between mass contained as gas  $M_g$  and within stars  $M_s$ :

$$M = M_g + M_s. \quad (\text{A.1})$$

The fraction of gas in the system is referred to as:

$$\mu = M_g/M. \quad (\text{A.2})$$

Assuming that the total mass changes through accretion of material from outside the system and ejection via galactic winds only, the mass and mass changes can be written as:

$$M(t) = M_g(t) + M_s(t) = M_0 + M_{acc} - M_{ej} \quad (\text{A.3})$$

$$\frac{d}{dt}M = F - E, \quad (\text{A.4})$$

where  $M_0$ ,  $M_{acc}$ , and  $M_{ej}$  are the initial, accreted and ejected masses, respectively.  $F$  and  $E$  are the infall and ejection rates of the system, respectively. The mass contained in stars changes with time due to star formation and loss of material from evolving stars:

$$\frac{d}{dt}M_s = \Psi - e, \quad (\text{A.5})$$

where  $\Psi$  is the star formation rate (SFR) and  $e$  the total ejection rate from stars of all masses and ages. Similarly the mass of the gas changes with time:

$$\frac{d}{dt}M_g = -\Psi + e + F - E = F - E - \frac{d}{dt}M_s. \quad (\text{A.6})$$

As the stellar system is evolving the abundance of the element  $Z$  in the ISM changes via star formation, stellar ejections, and gas flow. The appropriate way to describe the mass of metals in the gas ( $ZM_g$ ) is:

$$\frac{d}{dt}(ZM_g) = -Z\Psi + e_Z + Z_F F - Z_E E. \quad (\text{A.7})$$

The first term on the right hand side describes the loss of the ISM via star formation. The second is the amount of the element ejected from the stars. This implies that the material ejected from the stars is mixed throughout the ISM instantly. The last two terms describe the addition and loss of the element by infalling and outflowing material. Here the  $Z_F$  and  $Z_E$  are the mean abundances of the gas.

The ejection rates  $e$  and  $e_Z$  dependent on the initial mass function (IMF) and star formation rate (SFR) adopted. The most common parametrization is the Schmidt (1959) law where the SFR is proportional to some power ( $k=2$ ) of the gas density. A more recent suggestions is  $k=1.5$  by Kennicutt (1998) from the study of star forming galaxies. For the number distribution of stars as a function of stellar mass there exist various suggestions in the literature. The most commonly used are those by Salpeter (1955); Scalo (1986); Kroupa et al. (1993). Furthermore one assumes the approximation of sudden mass loss, which states that ejected mass of each stars is expelled instantaneously after the stars lifetime. The resulting equations are:

$$e(t) = \int_{m_t}^{\infty} (m - m_{(rem)}) \Psi(t - \tau_m) \Phi dm \quad (\text{A.8})$$

and

$$e_Z(t) = \int_{m_t}^{\infty} [(m - m_{(rem)} - mp_z)Z(t - \tau) + mp_z] \Psi(t - \tau_m) \Phi dm. \quad (\text{A.9})$$

Hereby the following parameters depend on the initial mass of the star ( $m$ ): lifetime of the star ( $\tau(m)$ ), mass loss of the star ( $m - m_{(rem)}(m)$ ), IMF ( $\Phi(m)$ ), and the stellar yield ( $p_Z(m)$ ). The latter is the fraction of the initial mass of a star that is newly synthesized and ejected.

## A.2 Instantaneous recycling approximation

The instantaneous recycling approximation states that all the stars with masses smaller than  $M_{\odot}$  live forever but also that the stars with masses larger than  $M_{\odot}$  die instantaneously after their birth, i.e., a lifetime of  $\tau \equiv 0$ . For massive stars this means that their evolution, nucleosynthesis and recycling take place at the same time. On one side this is good solution to describe the enrichment of element produced by massive stars like  $\alpha$  - and r - process elements. On the other side it is a much poorer solution for chemical elements produced on long timescales (e.g., Fe and s-process elements). However, this approximation facilitates the handling of the equation of chemical evolution as it eliminates some time dependencies. With the introduction of the return fraction  $R$  and the yield  $y$  one can further simplify the equations. The return fraction  $R$  is defined as the amount of mass ejected into the ISM by an entire stellar generation.

$$R \equiv \int_{m_{\odot}}^{\infty} (m - m_{(rem)}) \Phi dm. \quad (\text{A.10})$$

In the instantaneous recycling approximation stars with  $M > 1M_{\odot}$  are neglected. The lock-up fraction of mass in the stars can consequently be written as  $(1 - R)$ . The yield  $y$  is the mass of elements freshly produced per unit mass of matter that is locked into stars:

$$y \equiv \frac{1}{1 - R} \int_{m_{\odot}}^{\infty} mp_Z \Phi dm. \quad (\text{A.11})$$



The total ejection rate of metals can now be written as:

$$\begin{aligned} e_Z &= RZ(t)\Psi(t) + y(1 - R)[1 - Z(t)]\Psi(t) \\ &= RZ(t)\Psi(t) + y(1 - R)\Psi(t) \quad \text{since } Z \ll 1. \end{aligned}$$

The resulting equations for the changes in gaseous and stellar mass and the mass of metals in the gas of the system deduces as:

$$\begin{aligned} \frac{d}{dt}M_s &= (1 - R)\Psi, \\ \frac{d}{dt}M_g &= F - E - \frac{d}{dt}M_s = F - E - (1 - R)\Psi, \\ \frac{d}{dt}(ZM_g) &= -Z(1 - R)\Psi + y(1 - R) + Z_F F - Z_E E. \end{aligned} \tag{A.12}$$

Applying the identity  $\frac{d}{dt}(ZM_g) = Z\frac{d}{dt}M_g + M_g\frac{d}{dt}Z$  the latter equation can also be transformed into an expression for the metal abundance  $Z$  of the gas:

$$M_g\frac{d}{dt}Z = y(1 - R)\Psi + (Z_F - Z)F - (Z_E - Z)E. \tag{A.13}$$

### A.3 Simple closed-box model

The simplest way to solve the equations of chemical enrichment of the ISM of an evolving system is the so called closed-box model. This model adopts the instantaneous recycling approximation. One considers an isolated system of the initial mass  $M$ . Since no infall and outflow via galactic winds are present, i.e.,  $E = F = 0$ , the mass  $M$  is constant with time. Furthermore, the models starts as a pure, initially unenriched gaseous system ( $M_g(0) = M, M_s(0) = 0, Z(0) = 0$ ). Applying equations A.12 and A.13 one receives the simple differential equation:

$$M_g dZ/dM_g = -y, \tag{A.14}$$

which can be easily solved. The result states that the gas-phase metallicity increases monotonically with time as:

$$Z = y \ln M_g(0)/M_g(t) = y \ln M/M_g = y \ln \mu^{-1}. \tag{A.15}$$

While the abundance of the element  $Z$  increases with time the gas fraction  $\mu$  decreases. This is reasonable since more and more mass is locked up into stellar remnants and low mass stars (see Fig. A.1). The closed-box model predicts a wide distribution of metallicities.

#### A.3.1 The G-dwarf problem

A consequence of the simple closed-box model is that with increasing metallicity of the system, less and less stars are born since the available amount of gas within the system decreases. For the solar neighborhood it was found that this model fails to describe the observed metallicity distribution of stars. In comparison with the observations, the closed-box model predicts a too large number of very metal-poor stars. This disagreement is known since the G-dwarf problem as it was first discovered for these long-living stars. G-dwarfs are stars with lifetimes of the order of the age of the Galaxy or larger. The G-dwarf problem was first recognized

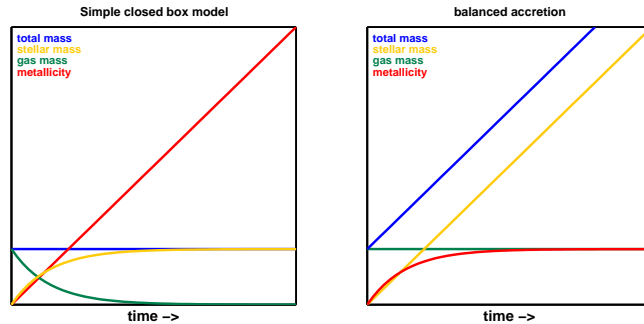


**Figure A.1:** A schematic overview of the behavior of total (blue), gas (green), and stellar mass (yellow) and the metallicity (red) for the Simple closed-box model (left) and the model of balanced accretion (right) of chemical enrichment. This figure is adopted from Pagel (1997).

by Schmidt (1963) for the solar neighborhood and later on confirmed for example by Pagel & Patchett (1975). Only 33 of 132 studied G-dwarfs were found to have metallicities smaller than  $Z_{\odot}/4$ , which is a percentage of less than 25. In contrast the simple models predict more than 50% to fall in this metallicity regime. In the meantime similar results were also observed for other systems. In a study of M 31, Espana & Worthey (2002) found that most models also overestimate the number of G-dwarf detected. More recent studies by Koch et al. (2006, 2007) revealed that a G-dwarf problem is also present in the Carina and Leo II dwarf spheroidal galaxies.

The most widely applied solutions to this problem found in the literature are: 1) The basic assumption of the closed-box model is wrong, i.e., gas infall and outflows are present. Subsequent infall of unenriched material can for example dilute the already processed material. 2) The yields are not constant over time due to a time-dependent IMF. A higher IMF in the past means that more high mass stars were present at early times whereas fewer long-living stars were formed.

## A.4 Leaky box model

One of variation of the Simple closed-box model is to give up the assumption that no gas is lost via outflow driven by galactic winds. This model starts with the same pure, initially unenriched gaseous system ( $M_g(0) = M$ ,  $M_s(0) = 0$ ,  $Z(0) = 0$ ) but now allows for gas expulsion ( $E \neq 0$ ) but still no infall ( $F = 0$ ). One assumes the ejected mass to be proportional to the SFR ( $E = \lambda(1 - R)\Psi$ ) and that the ejected gas has the same metallicity as the ISM ( $Z_E = Z$ ). Applying again equations A.12 and A.13 one receives the equation:

$$M_g dZ/dM_g = \frac{y}{-(1 + \lambda)}. \quad (\text{A.16})$$

The according solution is:

$$Z = \frac{y}{1 + \lambda} \ln \left[ \frac{1 + \lambda}{\mu} - \lambda \right]. \quad (\text{A.17})$$

Note that for  $\lambda = 0$  the equation becomes the solution for the closed-box model.

## A.5 Accreting box model

Similarly one can relax the assumption for the gas accretion from outside the system. We now consider a system with inflow of pristine gas ( $F \neq 0, Z_F = 0$ ) and no galactic winds ( $E = 0$ ). The basic equations for the gas mass and abundance then result into:

$$M_g dZ/dM_g = y(1 - R)\Psi - ZF. \quad (\text{A.18})$$

This equation can only be solved analytically if the infall rate is proportional to the SFR ( $E = \Lambda(1 - R)\Psi$ ). If  $\Lambda > 1$  this states that not all of the newly accreted material is transformed into stars and thus that the total gas fraction of the system increases. Vice-versa if  $\Lambda \leq 1$  the mass of the newly formed stars is the same or even more than the mass of the infalling system.

$$M_g dZ/dM_g = \frac{y - Z\Lambda}{\Lambda - 1}. \quad (\text{A.19})$$

The solution of this equation than is:

$$Z = \frac{y}{\Lambda} \left[ 1 - \left( \Lambda - \frac{1 - \Lambda}{\mu} \right) \right]^{-\frac{\Lambda}{1 - \Lambda}}. \quad (\text{A.20})$$

One of the most common theories to solve the G-dwarf problem is postulating a steady infall of unenriched gas ( $F \neq 0, Z_F = 0$ ) that is balanced by the gas consumption via star formation. Thus the gas mass of the system is constant with time ( $M_g = M(0) = \text{const}$ ). This means the star formation keeps up with the infall rate and the gas loss from evolving stars ( $\Psi = F + R\Psi \Leftrightarrow F = (1 - R)\Psi$ ). Therefore we derive the equation

$$M_g dZ/dM_g = y - Z \quad (\text{A.21})$$

with the solution

$$Z = y(1 - e^{-(\mu^{-1} - 1)}). \quad (\text{A.22})$$

The consequence of the assumptions in this model is that the gas phase metallicity increases more slowly than in the closed-box model. As the system evolves the amount of gas available is higher than in case of the closed-box model. This means that the number of metal-rich stars is higher and consequently the fraction of metal-poor to metal-rich stars is lower. A schematic overview of the behavior of total, gas, and stellar mass and the metallicity can be found in Fig. A.1.



# Appendix B

## List of Abbreviations

ACS	Advanced Camera for Surveys
ADS	Astrophysics Data System
ADU	Analog Digital Unit
AGB	Asymptotic Giant Branch
AMR	Age Metallicity Relation
CaT	CaII triplet
CCD	Charge Coupled Device
CMD	Color Magnitude Diagram
CN	Carbon Nitrogen, Cyanogen
dE	dwarf elliptical galaxy
dIrr	dwarf irregular galaxy
dm	distance modulus
dSph	dwarf spheroidal galaxy
DSS	Digitized Sky Survey
EFF	Elson-Fall-Freeman
ESO	European Southern Observatory
EW	Equivalent Width
FIMS	FORS Instrumental Mask Simulator
FORS	FOcal Reducer and low dispersion Spectrograph
FoV	Field of View
FWHM	Full Width Half Maximum
GC	Globular Cluster
HB	Horizontal Branch
HST	Hubble Space Telescope
IMF	Initial Mass Function
IR	Infra Red
IRAF	Image Reduction and Analysis Facility
Irr	Irregular Galaxy
ISM	Interstellar Medium
LG	Local Group
LMC	Large Magellanic Cloud
M	Messier
MC	Magellanic Clouds

---

MS	Main Sequence
MSTO	Main Sequence Turn Off
MW	Milky Way
MXU	Mask EXchange Unit
NGC	New General Catalogue
RC	Red Clump
RGB	Red Giant Branch
RMS	Root Mean Square
SC	Star Cluster
SF	Star Formation
SFH	Star Formation History
SFR	Star Formation Rate
SGB	Subgiant Branch
SMC	Small Magellanic Cloud
SN	Supernova
VLT	Very Large Telescope
WMAP	Wilkinson Microwave Anisotropy Probe

# Bibliography

- Alcaino, G., Alvarado, F., & Kurtev, R. 2003, *A&A*, 407, 919
- Alcaino, G., Liller, W., & Alvarado, F. 1997, *AJ*, 114, 2626
- Alcaino, G., Liller, W., Alvarado, F., et al. 1996, *AJ*, 112, 2004
- Alcaino, G., Liller, W., Alvarado, F., & Wenderoth, E. 1992, *AJ*, 104, 190
- Alves, D. R. & Sarajedini, A. 1999, *ApJ*, 511, 225
- Andreuzzi, G., De Marchi, G., Ferraro, F. R., et al. 2001, *A&A*, 372, 851
- Armandroff, T. E. & Da Costa, G. S. 1991, *AJ*, 101, 1329
- Armandroff, T. E. & Zinn, R. 1988, *AJ*, 96, 92
- Battaglia, G., Irwin, M., Tolstoy, E., et al. 2007, *ArXiv e-prints*, 710
- Bedin, L. R., Piotto, G., Anderson, J., et al. 2004, *ApJ*, 605, L125
- Bekki, K., Campbell, S. W., Lattanzio, J. C., & Norris, J. E. 2007, *MNRAS*, 377, 335
- Bekki, K. & Chiba, M. 2005, *MNRAS*, 356, 680
- Bekki, K., Couch, W. J., Beasley, M. A., et al. 2004, *ApJ*, 610, L93
- Bellazzini, M., Ferraro, F. R., & Ibata, R. 2003, *AJ*, 125, 188
- Bellazzini, M., Fusi Pecci, F., Montegriffo, P., et al. 2002, *AJ*, 123, 2541
- Bellazzini, M., Pecci, F. F., Ferraro, F. R., et al. 2001, *AJ*, 122, 2569
- Besla, G., Kallivayalil, N., Hernquist, L., et al. 2007, *ArXiv Astrophysics e-prints*
- Bessell, M. S. 1990, *PASP*, 102, 1181
- Bica, E., Dottori, H., & Pastoriza, M. 1986, *A&A*, 156, 261
- Bica, E. & Dutra, C. M. 2000, *AJ*, 119, 1214
- Bica, E. L. D. & Schmitt, H. R. 1995, *ApJS*, 101, 41
- Bica, E. L. D., Schmitt, H. R., Dutra, C. M., & Oliveira, H. L. 1999, *AJ*, 117, 238

- Binney, J. & Tremaine, S. 1987, *Galactic dynamics* (Princeton, NJ, Princeton University Press, 1987, 747 p.)
- Blitz, L. & Spergel, D. N. 1991, *ApJ*, 379, 631
- Boily, C. M. & Kroupa, P. 2003, *MNRAS*, 338, 665
- Briley, M. M. 1997, *AJ*, 114, 1051
- Briley, M. M., Bell, R. A., Smith, G. H., & Hesser, J. E. 1989, *ApJ*, 341, 800
- Briley, M. M., Harbeck, D., Smith, G. H., & Grebel, E. K. 2004, *AJ*, 127, 1588
- Brodie, J. P. & Strader, J. 2006, *ARA&A*, 44, 193
- Brown, J. A., Wallerstein, G., & Zucker, D. 1997, *AJ*, 114, 180
- Buonanno, R., Corsi, C. E., Pulone, L., Fusi Pecci, F., & Bellazzini, M. 1998, *A&A*, 333, 505
- Buonanno, R., Corsi, C. E., Pulone, L., et al. 1995, *AJ*, 109, 663
- Carrera, R., Gallart, C., Pancino, E., & Zinn, R. 2007, *AJ*, 134, 1298
- Carretta, E. 2006, *AJ*, 131, 1766
- Carretta, E. & Gratton, R. G. 1997, *A&AS*, 121, 95
- Chapman, S. C., Ibata, R., Lewis, G. F., et al. 2006, *ApJ*, 653, 255
- Charbonnel, C. 1994, *A&A*, 282, 811
- . 1995, *ApJ*, 453, L41
- Chiosi, C., Vallenari, A., Bressan, A., Deng, L., & Ortolani, S. 1995, *A&A*, 293, 710
- Chiosi, E. & Vallenari, A. 2007, *A&A*, 466, 165
- Chiosi, E., Vallenari, A., Held, E. V., Rizzi, L., & Moretti, A. 2006, *A&A*, 452, 179
- Cioni, M.-R. L., Habing, H. J., & Israel, F. P. 2000, *A&A*, 358, L9
- Cohen, J. G. 1978, *ApJ*, 223, 487
- . 1999a, *AJ*, 117, 2428
- . 1999b, *AJ*, 117, 2434
- . 2004, *AJ*, 127, 1545
- Cole, A. A., Smecker-Hane, T. A., & Gallagher, III, J. S. 2000, *AJ*, 120, 1808
- Cole, A. A., Smecker-Hane, T. A., Tolstoy, E., Bosler, T. L., & Gallagher, J. S. 2004, *MNRAS*, 347, 367
- Cole, A. A., Tolstoy, E., Gallagher, J. S., & Smecker-Hane, T. A. 2005, *AJ*, 129, 1465



- Cottrell, P. L. & Da Costa, G. S. 1981, *ApJ*, 245, L79
- Crowl, H. H., Sarajedini, A., Piatti, A. E., et al. 2001, *AJ*, 122, 220
- Da Costa, G. S. 1991, in *IAU Symposium*, Vol. 148, *The Magellanic Clouds*, ed. R. Haynes & D. Milne, 183
- Da Costa, G. S. & Armandroff, T. E. 1995, *AJ*, 109, 2533
- Da Costa, G. S. & Hatzidimitriou, D. 1998, *AJ*, 115, 1934
- Da Costa, G. S. & Mould, J. R. 1986, *ApJ*, 305, 214
- Da Rocha, C., Mendes de Oliveira, C., Bolte, M., Ziegler, B. L., & Puzia, T. H. 2002, *AJ*, 123, 690
- D'Antona, F., Bellazzini, M., Caloi, V., et al. 2005, *ApJ*, 631, 868
- D'Antona, F., Caloi, V., Montalbán, J., Ventura, P., & Gratton, R. 2002, *A&A*, 395, 69
- D'Antona, F., Gratton, R., & Chieffi, A. 1983, *Mem.SAI*, 54, 173
- de Freitas Pacheco, J. A., Barbuy, B., & Idiart, T. 1998, *A&A*, 332, 19
- Decressin, T., Meynet, G., Charbonnel, C., Prantzos, N., & Ekström, S. 2007, *A&A*, 464, 1029
- Denissenkov, P. A. & Herwig, F. 2003, *ApJ*, 590, L99
- Denissenkov, P. A. & Vandenberg, D. A. 2003, *ApJ*, 593, 509
- Diaz, A. I., Terlevich, E., & Terlevich, R. 1989, *MNRAS*, 239, 325
- Djorgovski, S. 1988, in *IAU Symp. 126: The Harlow-Shapley Symposium on Globular Cluster Systems in Galaxies*, ed. J. E. Grindlay & A. G. D. Philip, 333–345
- Dopita, M. A., Lawrence, C. J., Ford, H. C., & Webster, B. L. 1985, *ApJ*, 296, 390
- Durand, D., Hardy, E., & Melnick, J. 1984, *ApJ*, 283, 552
- Durrell, P. R. & Harris, W. E. 1993, *AJ*, 105, 1420
- Elson, R. A. W. 1991, *ApJS*, 76, 185
- Elson, R. A. W., Fall, S. M., & Freeman, K. C. 1987, *ApJ*, 323, 54
- Espana, A. L. & Worthey, G. 2002, in *Bulletin of the American Astronomical Society*, Vol. 34, *Bulletin of the American Astronomical Society*
- Feltzing, S., Bensby, T., & Lundström, I. 2003, *A&A*, 397, L1
- Feltzing, S., Holmberg, J., & Hurley, J. R. 2001, *A&A*, 377, 911
- Frenk, C. S. & Fall, S. M. 1982, *MNRAS*, 199, 565
- Friel, E. D., Janes, K. A., Tavaréz, M., et al. 2002, *AJ*, 124, 2693

- Fulbright, J. P. 2002, *AJ*, 123, 404
- Gardiner, L. T. & Noguchi, M. 1996, *MNRAS*, 278, 191
- Gardiner, L. T., Sawa, T., & Fujimoto, M. 1994, *MNRAS*, 266, 567
- Gascoigne, S. C. B., Bessell, M. S., & Norris, J. 1981, in *IAU Colloq. 68: Astrophysical Parameters for Globular Clusters*, ed. A. G. D. Philip & D. S. Hayes, 223
- Geisler, D., Bica, E., Dottori, H., et al. 1997, *AJ*, 114, 1920
- Geisler, D., Piatti, A. E., Bica, E., & Clariá, J. J. 2003, *MNRAS*, 341, 771
- Geisler, D. & Sarajedini, A. 1999, *AJ*, 117, 308
- Gilmore, G. & Reid, N. 1983, *MNRAS*, 202, 1025
- Gilmore, G. & Wyse, R. F. G. 1991, *ApJ*, 367, L55
- Girardi, L., Chiosi, C., Bertelli, G., & Bressan, A. 1995, *A&A*, 298, 87
- Glatt, K., Grebel, E. K., & Gallagher, J. S. 2008, *AJ*, in prep.
- Gonzalez, G. & Wallerstein, G. 1999, *AJ*, 117, 2286
- Goodwin, S. P. & Bastian, N. 2006, *MNRAS*, 1213
- Gratton, R., Sneden, C., & Carretta, E. 2004, *ARA&A*, 42, 385
- Grebel, E. K. 1999, in *IAU Symposium, Vol. 192, The Stellar Content of Local Group Galaxies*, ed. P. Whitelock & R. Cannon, 17
- Grebel, E. K. 2000, in *Astronomical Society of the Pacific Conference Series, Vol. 211, Massive Stellar Clusters*, ed. A. Lançon & C. M. Boily, 262
- Grebel, E. K. 2001, in *Astronomical Society of the Pacific Conference Series, Vol. 239, Microlensing 2000: A New Era of Microlensing Astrophysics*, ed. J. W. Menzies & P. D. Sackett, 280
- Grebel, E. K. & Richtler, T. 1992, *A&A*, 253, 359
- Grocholski, A. J., Cole, A. A., Sarajedini, A., Geisler, D., & Smith, V. V. 2006, *AJ*, 132, 1630
- Harbeck, D., Grebel, E. K., Holtzman, J., et al. 2001, *AJ*, 122, 3092
- Harbeck, D., Smith, G. H., & Grebel, E. K. 2003a, *AJ*, 125, 197
- . 2003b, *A&A*, 409, 553
- Hardy, E., Suntzeff, N. B., & Azzopardi, M. 1989, *ApJ*, 344, 210
- Harris, J. & Zaritsky, D. 2004, *AJ*, 127, 1531
- . 2006, *AJ*, 131, 2514

- Harris, W. 2003, Catalog of Parameters for Milky Way clusters: The Database, Tech. rep., Hamilton Mc Master University
- Harris, W. E. 1996, *AJ*, 112, 1487
- Hatzidimitriou, D., Croke, B. F., Morgan, D. H., & Cannon, R. D. 1997, *A&AS*, 122, 507
- Hilker, M. 2006, *A&A*, 448, 171
- Hilker, M., Kayser, A., Richtler, T., & Willemsen, P. 2004, *A&A*, 422, L9
- Hill, A. & Zaritsky, D. 2006, *AJ*, 131, 414
- Hill, V. 1999, *A&A*, 345, 430
- Hindman, J. V., Kerr, F. J., & McGee, R. X. 1963, *Australian Journal of Physics*, 16, 570
- Hirashita, H. 2000, *PASJ*, 52, 107
- Hodge, P. W. 1981, *ApJ*, 247, 894
- Ibata, R., Irwin, M., Lewis, G. F., & Stolte, A. 2001, *ApJ*, 547, L133
- Ibata, R. A., Gilmore, G., & Irwin, M. J. 1994, *Nature*, 370, 194
- Iben, Jr., I. 1968, *Nature*, 220, 143
- Karachentsev, I. D., Dolphin, A. E., Geisler, D., et al. 2002a, *A&A*, 383, 125
- Karachentsev, I. D., Karachentseva, V. E., Huchtmeier, W. K., & Makarov, D. I. 2004, *AJ*, 127, 2031
- Karachentsev, I. D., Sharina, M. E., Dolphin, A. E., et al. 2002b, *A&A*, 385, 21
- Kayser, A., Grebel, E. K., & Koch, A. 2008a, *AJ*, in prep.
- Kayser, A., Grebel, E. K., Koch, A., et al. 2008b, *AJ*, in prep.
- Kayser, A., Hilker, M., Richtler, T., & Willemsen, P. G. 2006, *A&A*, 458, 777
- Kennicutt, Jr., R. C. 1998, *ARA&A*, 36, 189
- King, I. 1962, *AJ*, 67, 471
- Kissler-Patig, M. 2000, in *Reviews in Modern Astronomy*, ed. R. E. Schielicke, 13
- Kleyna, J., Wilkinson, M. I., Evans, N. W., Gilmore, G., & Frayn, C. 2002, *MNRAS*, 330, 792
- Kniazev, A. Y., Grebel, E. K., Pustilnik, S. A., Pramskij, A. G., & Zucker, D. B. 2005, *AJ*, 130, 1558
- Koch, A., Grebel, E. K., Kleyna, J. T., et al. 2007, *AJ*, 133, 270
- Koch, A., Grebel, E. K., Wyse, R. F. G., et al. 2006, *AJ*, 131, 895

- Kontizas, E. & Kontizas, M. 1983, *A&AS*, 52, 143
- Kontizas, M. 1984, *A&A*, 131, 58
- Kontizas, M., Chrysovergis, M., & Kontizas, E. 1987, *A&AS*, 68, 147
- Kontizas, M., Danezis, E., & Kontizas, E. 1982, *A&AS*, 49, 1
- Kontizas, M., Theodossiou, E., & Kontizas, E. 1986, *A&AS*, 65, 207
- Kraft, R. P. 1994, *PASP*, 106, 553
- Kraft, R. P. & Ivans, I. I. 2003, *PASP*, 115, 143
- Kroupa, P. & Boily, C. M. 2002, *MNRAS*, 336, 1188
- Kroupa, P., Tout, C. A., & Gilmore, G. 1993, *MNRAS*, 262, 545
- Kunkel, W. E., Demers, S., & Irwin, M. J. 2000, *AJ*, 119, 2789
- Lada, E. A. 1999, in *NATO ASIC Proc. 540: The Origin of Stars and Planetary Systems*, ed. C. J. Lada & N. D. Kylafis, 441
- Lanfranchi, G. A. & Matteucci, F. 2003, *MNRAS*, 345, 71
- Langer, G. E., Fischer, D., Sneden, C., & Bolte, M. 1998, *AJ*, 115, 685
- Lee, S. G. 2000, *Journal of Korean Astronomical Society*, 33, 137
- . 2005, *Journal of Korean Astronomical Society*, 38, 23
- Lee, Y.-W., Joo, J.-M., Sohn, Y.-J., et al. 1999, *Nature*, 402, 55
- Leonardi, A. J. & Rose, J. A. 2003, *AJ*, 126, 1811
- Luck, R. E., Moffett, T. J., Barnes, III, T. G., & Gieren, W. P. 1998, *AJ*, 115, 605
- Mackey, A. D. & Gilmore, G. F. 2003a, *MNRAS*, 338, 120
- . 2003b, *MNRAS*, 338, 85
- Mackey, A. D. & van den Bergh, S. 2005, *MNRAS*, 360, 631
- Maeder, A. & Meynet, G. 2006, *A&A*, 448, L37
- Martin, N. F., Ibata, R. A., Bellazzini, M., et al. 2004, *MNRAS*, 348, 12
- Martínez-Delgado, D., Aparicio, A., Gómez-Flechoso, M. Á., & Carrera, R. 2001, *ApJ*, 549, L199
- Mateo, M. 1987, *ApJ*, 323, L41
- Mateo, M., Hodge, P., & Schommer, R. A. 1986, *ApJ*, 311, 113
- Mathewson, D. S., Cleary, M. N., & Murray, J. D. 1974, *ApJ*, 190, 291

- Mayer, L., Governato, F., Colpi, M., et al. 2001, *ApJ*, 547, L123
- McLaughlin, D. E. & van der Marel, R. P. 2005, *ApJS*, 161, 304
- Meliani, M. T., Barbuy, B., & Perrin, M.-N. 1995, *A&A*, 300, 349
- Mengel, S., Lehnert, M. D., Thatte, N., & Genzel, R. 2002, *A&A*, 383, 137
- Merritt, D., Meylan, G., & Mayor, M. 1997, *AJ*, 114, 1074
- Mighell, K. J., Sarajedini, A., & French, R. S. 1998, *AJ*, 116, 2395
- Mould, J. R. & Da Costa, G. S. 1988, in *ASP Conf. Ser. 1: Progress and Opportunities in Southern Hemisphere Optical Astronomy. The CTIO 25th Anniversary Symposium*, ed. V. M. Blanco & M. M. Phillips, 197
- Mould, J. R., Da Costa, G. S., & Crawford, M. D. 1984, *ApJ*, 280, 595
- Mould, J. R., Jensen, J. B., & Da Costa, G. S. 1992, *ApJS*, 82, 489
- Muller, E., Staveley-Smith, L., & Zealey, W. J. 2003, *MNRAS*, 338, 609
- Newberg, H. J., Yanny, B., Rockosi, C., et al. 2002, *ApJ*, 569, 245
- Nordström, B., Mayor, M., Andersen, J., et al. 2004, *A&A*, 418, 989
- Norris, J. 1987, *ApJ*, 313, L65
- Norris, J., Cottrell, P. L., Freeman, K. C., & Da Costa, G. S. 1981, *ApJ*, 244, 205
- Norris, J. & Smith, G. H. 1981, in *IAU Colloq. 68: Astrophysical Parameters for Globular Clusters*, ed. A. G. D. Philip & D. S. Hayes, 109
- Olszewski, E. W., Aaronson, M., & Schommer, R. A. 1987, *AJ*, 93, 565
- Olszewski, E. W., Schommer, R. A., Suntzeff, N. B., & Harris, H. C. 1991, *AJ*, 101, 515
- Olszewski, E. W., Suntzeff, N. B., & Mateo, M. 1996, *ARA&A*, 34, 511
- Osborn, W. 1971, *The Observatory*, 91, 223
- Pagal, B. E. J. 1997, *Nucleosynthesis and Chemical Evolution of Galaxies (Nucleosynthesis and Chemical Evolution of Galaxies, by Bernard E. J. Pagal, pp. 392. ISBN 0521550610. Cambridge, UK: Cambridge University Press, October 1997.)*
- Pagal, B. E. J. & Patchett, B. E. 1975, *MNRAS*, 172, 13
- Pagal, B. E. J. & Tautvaisiene, G. 1998, *MNRAS*, 299, 535
- Papenhausen, P. & Schommer, R. A. 1988, in *IAU Symposium, Vol. 126, The Harlow-Shapley Symposium on Globular Cluster Systems in Galaxies*, ed. J. E. Grindlay & A. G. D. Philip, 565
- Paturel, G., Dubois, P., Petit, C., & Woelfel, F. 2002, *LEDA*, 0 (2002), 0

- Penny, A. J., Smith, G. H., & Churchill, C. W. 1992, MNRAS, 257, 89
- Piatti, A. E., Santos, J. F. C., Clariá, J. J., et al. 2001, MNRAS, 325, 792
- Piatti, A. E., Santos, Jr., J. F. C., Clariá, J. J., et al. 2005a, A&A, 440, 111
- Piatti, A. E., Sarajedini, A., Geisler, D., Clark, D., & Seguel, J. 2007, MNRAS, 377, 300
- Piatti, A. E., Sarajedini, A., Geisler, D., Seguel, J., & Clark, D. 2005b, MNRAS, 358, 1215
- Pietrinferni, A., Cassisi, S., Salaris, M., & Castelli, F. 2004, ApJ, 612, 168
- Pietrzynski, G., Udalski, A., Kubiak, M., et al. 1998, Acta Astronomica, 48, 175
- Pilyugin, L. S. 1996, A&A, 310, 751
- Piotto, G., Bedin, L. R., Anderson, J., et al. 2007, ApJ, 661, L53
- Plummer, H. C. 1911, MNRAS, 71, 460
- Pont, F., Zinn, R., Gallart, C., Hardy, E., & Winnick, R. 2004, AJ, 127, 840
- Pritzl, B. J., Venn, K. A., & Irwin, M. 2005, AJ, 130, 2140
- Pryor, C. & Meylan, G. 1993, in ASP Conf. Ser., Vol. 50, Structure and Dynamics of Globular Clusters, ed. S. G. Djorgovski & G. Meylan, 357
- Rafelski, M. & Zaritsky, D. 2005, AJ, 129, 2701
- Ratnatunga, K. U. & Bahcall, J. N. 1985, ApJS, 59, 63
- Reitzel, D. B. & Guhathakurta, P. 2002, AJ, 124, 234
- Rich, R. M., Da Costa, G. S., & Mould, J. R. 1984, ApJ, 286, 517
- Rich, R. M., Shara, M., Fall, S. M., & Zurek, D. 2000, AJ, 119, 197
- Richter, P., Hilker, M., & Richtler, T. 1999, A&A, 350, 476
- Rochau, B., Gouliermis, D. A., Brandner, W., Dolphin, A. E., & Henning, T. 2007, ArXiv e-prints, 704
- Rolleston, W. R. J., Venn, K., Tolstoy, E., & Dufton, P. L. 2003, A&A, 400, 21
- Rosenberg, A., Saviane, I., Piotto, G., & Aparicio, A. 1999, AJ, 118, 2306
- Roy, J.-R. & Kunth, D. 1995, A&A, 294, 432
- Russell, S. C. & Dopita, M. A. 1992, ApJ, 384, 508
- Rutledge, G. A., Hesser, J. E., & Stetson, P. B. 1997a, PASP, 109, 907
- Rutledge, G. A., Hesser, J. E., Stetson, P. B., et al. 1997b, PASP, 109, 883
- Sabbi, E., Sirianni, M., Nota, A., et al. 2007, AJ, 133, 44

- Salpeter, E. E. 1955, *ApJ*, 121
- Sambhus, N., Gerhard, O., & Méndez, R. H. 2006, *AJ*, 131, 837
- Samus, N., Ipatov, A., Smirnov, O., et al. 1995a, *A&AS*, 112, 439
- Samus, N., Kravtsov, V., Pavlov, M., Alcaïno, G., & Liller, W. 1995b, *A&AS*, 109, 487
- Sandage, A. & Tammann, G. A. 2006, *ARA&A*, 44, 93
- Sarajedini, A. 1994, *AJ*, 107, 618
- Sarajedini, A. & Layden, A. 1997, *AJ*, 113, 264
- Sbordone, L., Bonifacio, P., Buonanno, R., et al. 2007, *A&A*, 465, 815
- Sbordone, L., Bonifacio, P., Marconi, G., Buonanno, R., & Zaggia, S. 2005, *A&A*, 437, 905
- Scalo, J. M. 1986, *Fundamentals of Cosmic Physics*, 11, 1
- Schmidt, M. 1959, *ApJ*, 129, 243
- . 1963, *ApJ*, 137, 758
- Seidel, E., Da Costa, G. S., & Demarque, P. 1987, *ApJ*, 313, 192
- Shetrone, M. D., Côté, P., & Sargent, W. L. W. 2001, *ApJ*, 548, 592
- Smith, G. H. 2002, *PASP*, 114, 1215
- Smith, G. H. & Mateo, M. 1990, *ApJ*, 353, 533
- Smith, G. H. & Norris, J. 1982, *ApJ*, 254, 149
- . 1983, *ApJ*, 264, 215
- Smith, G. H., Shetrone, M. D., Bell, R. A., Churchill, C. W., & Briley, M. M. 1996, *AJ*, 112, 1511
- Smith, H. A., Silbermann, N. A., Baird, S. R., & Graham, J. A. 1992, *AJ*, 104, 1430
- Sosin, C. & King, I. R. 1997, *AJ*, 113, 1328
- Sparke, L. S. & Gallagher, III, J. S. 2000, *Galaxies in the universe : an introduction* (Galaxies in the Universe, by Linda S. Sparke and John S. Gallagher, III, pp. 416. ISBN 0521592410. Cambridge, UK: Cambridge University Press, September 2000.)
- Spergel, D. N., Verde, L., Peiris, H. V., et al. 2003, *ApJS*, 148, 175
- Spite, F., Spite, M., & Richtler, T. 1991, *A&A*, 252, 557
- Stanford, L. M., Cannon, R. D., da Costa, G. S., Norris, J. E., & Croke, B. F. W. 2004, in *Origin and Evolution of the Elements*, ed. A. McWilliam & M. Rauch
- Stanimirović, S., Staveley-Smith, L., & Jones, P. A. 2004, *ApJ*, 604, 176

- Staveley-Smith, L., Sault, R. J., Hatzidimitriou, D., Kesteven, M. J., & McConnell, D. 1997, MNRAS, 289, 225
- Stetson, P. B., Hesser, J. E., Smith, G. H., Vandenberg, D. A., & Bolte, M. 1989, AJ, 97, 1360
- Stryker, L. L., Da Costa, G. S., & Mould, J. R. 1985, ApJ, 298, 544
- Suntzeff, N. B. 1981, ApJS, 47, 1
- Sweigart, A. V. & Mengel, J. G. 1979, ApJ, 229, 624
- Thoul, A., Jorissen, A., Goriely, S., et al. 2002, A&A, 383, 491
- Tinsley, B. M. 1980, Fundamentals of Cosmic Physics, 5, 287
- Tonry, J. & Davis, M. 1979, AJ, 84, 1511
- Tsujimoto, T., Nomoto, K., Yoshii, Y., et al. 1995, MNRAS, 277, 945
- Venn, K. A. 1999, ApJ, 518, 405
- Ventura, P., D'Antona, F., Mazzitelli, I., & Gratton, R. 2001, ApJ, 550, L65
- Vivas, A. K., Zinn, R., Abad, C., et al. 2004, AJ, 127, 1158
- Weiss, A., Denissenkov, P. A., & Charbonnel, C. 2000, A&A, 356
- Welch, D. L. 1991, AJ, 101, 538
- Westerlund, B. E. 1997, The Magellanic Clouds (Book,)
- Willemsen, P. G., Hilker, M., Kayser, A., & Bailer-Jones, C. A. L. 2005, A&A, 436, 379
- Willman, B., Dalcanton, J. J., Martinez-Delgado, D., et al. 2005, ApJ, 626, L85
- Zaritsky, D., Harris, J., Grebel, E. K., & Thompson, I. B. 2000, ApJ, 534, L53
- Zaritsky, D., Harris, J., Thompson, I. B., Grebel, E. K., & Massey, P. 2002, AJ, 123, 855
- Zinn, R. 1985, ApJ, 293, 424
- Zinn, R. 1993, in ASP Conf. Ser., Vol. 48, The Globular Cluster-Galaxy Connection, ed. G. H. Smith & J. P. Brodie, 38
- Zinn, R. & West, M. J. 1984, ApJS, 55, 45
- Zoccali, M., Renzini, A., Ortolani, S., et al. 2003, A&A, 399, 931



# Acknowledgments

Ich hatte das Glück 3 1/2 Jahre mit kompetenten und hilfsbereiten Kollegen zusammenarbeiten zu können, bei denen ich mich hier gerne bedanken möchte:

An erster Stelle möchte ich mich ganz besonders bei meiner Doktormutter, Frau Prof. Dr. Eva K. Grebel, für die exzellente Betreuung meiner Dissertation bedanken. Ich bin sehr dankbar, dass sie mir trotz der ungewissen Zukunft des Astronomischen Instituts die Möglichkeit geben hat in Basel zu promovieren.

I'm very grateful to Prof. Dr. John S. Gallagher for his second expertise, but also for the many fruitful discussions during his visits in Europe and my visit in Madison.

Ganz speziell möchte ich mich auch bei Dr. Michael Hilker für seine Unterstützung während des Kugelsternhaufen Projekts bedanken. Er ist sicherlich eine der wichtigsten Personen in meinem "astronomischen Leben".

Ein großes Danke gilt Dr. Andreas Koch, den ich während des letzten Jahres in Basel sehr vermisst habe. Unsere Zusammenarbeit hat mir immer sehr viel Spaß gemacht.

Ich danke insbesondere auch Prof. Dr. Bruno Binggeli und Prof. Dr. Roland Buser für ihre schier grenzenlose Ruhe und Geduld mit nervösen PhD Studentinnen in ihrer Endphase.

Dr. Wolfgang Löffler danke ich für das Asyl in Heidelberg und die gemütlichen Abende. Ohne dies wäre das letzte halbe Jahr meiner Promotion deutlich unangenehmer verlaufen.

Ich danke Dr. Daniel Harbeck, meine Ansprechperson in allen beobachtungstechnischen Fragen - FIMS, FPOSS, P2PP, etc..

Not to forget the other former, present and may be future PhD students at the Astronomical Institute in Basel, who have accompanied me on my way: Dr. Karin Ammon, Flavio De Lorenzi, Dr. Peter Engelmeier, Dr. Caroline Girard, Katharina Glatt, Katrin Jordi, Dr. Stefan Kautsch, Dr. Thorsten Lisker, Marco Longhitano, Dr. Niranjana Sambhus, Ayshe Siddiki, Dr. Pieter Westera and Kathrin Wolfinger. Thanks to you the institute has had its wonderful and unique atmosphere.

Ich bin dankbar für die Unterstützung des Schweizerischen National Fonds und der Schweizerischen Gesellschaft für Astrophysik und Astronomie, die mir unter anderem die Teilnahme an einigen Konferenzen ermöglicht haben.

An dieser Stelle möchte ich mich auch bei einigen Personen meines privaten Umfeldes bedanken:

Insbesondere bedanke ich mich bei meinen Eltern, Melitta und Klaus-Peter Kayser, die immer für mich da sind. Ich bin dankbar für ihre Unterstützung und die ein oder andere "Kopfwäsche".

Ich möchte mich bei Jan Brož bedanken, der immer meine Entscheidungen respektiert und unterstützt und in letzter Zeit einiges aushalten mußte. Lieber Jan: "Ich danke Dir von Herzen für Deinen Rückhalt und die Energie, die Du mir gibst."

Ausserdem möchte ich mich bei Marlen Geheb für ihre Freundschaft und ihren Blick für's wirklich wichtige im Leben bedanken.

# CURRICULUM VITAE

as of November 13, 2007

## Personal Data:

---

**Name** Andrea Kayser

**Address** Feldstrasse 1,  
CH-4123 Allschwil,  
Switzerland

**Office Address** Astronomisches Institut der Uni. Basel,  
Venusstrasse 7,  
CH-4102 Binningen,  
Switzerland

**Email** akayser@astro.unibas.ch

**Phone** home: +41 (0)61 4822404  
work: +41 (0)61 2055426  
mobile: +41 (0)79 7353862

**Date of Birth** 14.11.1977

**Place of Birth** Iserlohn/Germany

**Citizenship** German

**Gender** female

**Marital Status** single



## Current Field of Research:

---

Structure and chemical evolution of globular clusters and dwarf galaxies:

- Age-Metallicity Relation of the Small Magellanic Cloud.
- CN and CH anomalies in Galactic globular clusters.
- Shell Structures in the Fornax dSph galaxy.

## Education:

---

- Since 05/2004**      **PhD Thesis in Astronomy**  
Dept. of Physics and Astronomy, University of Basel, Switzerland  
Title of Thesis: *Chemical Evolution of Nearby Stellar Systems.*  
Supervisor: *Prof. Dr. Eva K. Grebel*
- 04/2001 – 11/2003**      Study of Physics and Astronomy  
University of Bonn, Germany  
**Degree: Diplom Physikerin (M. Sc. in physics)**  
Final mark: *sehr gut (passed with high distinction)*  
Title of Thesis: *Spectroscopy of Sub Giants in Omega Centauri*  
Supervisor: *Dr. Michael Hilker & Prof. Dr. Klaas S. de Boer*
- 03/2000 – 03/2001**      **Study abroad**  
University of New South Wales, Sydney, Australia  
**Scholarship** of the DAAD (Deutsche Akademische Austauschdienst)
- 10/1997 – 03/2000**      Study of Physics and Astronomy  
University of Bonn, Germany  
**Degree: Vor-Diplom**  
Mark: *sehr gut (passed with high distinction)*
- 08/1988 – 06/1997**      Burggymnasium der Stadt Altena  
**Degree: Abitur (high school diploma)**  
Final mark: *1.6 (on a scale 1 to 6 with 1 being the best grade)*

## Languages:

---

- German**                      Mother Tongue
- English**                     fluently spoken, read, and written
- Spanish**                    basic, since 2003 in evening school
- French**                      2 year course in school

## Relevant Work and Other Experiences:

---

- since 2005**      Leader of research project 076.0702 at the European Southern Observatory  
*Shell Structures in the Fornax dSph Galaxy: Signature of a Gas-rich Merger?*
- since 2005**      Public outreach at the Astronomical Institute of the University of Basel:
- Guided tours for school classes and adults
  - Student information days
  - Information desks at several occasions in Basel
- 2005**                      Member of the Local Organising Committee of Astronomical Meeting  
IAU Colloquium No. 198, Les Diablerets/CH
- 01–03/2004**      Research Associate  
Sternwarte of the University of Bonn, Germany
- 2002 - 2003**      Co-ordinator of the Grad. School 787 of the Universities of Bochum and Bonn
- 2002**                      Tutor for Theoretical Physics

## **Technical Skills:**

---

- Operating systems: UNIX/Linux, Mac OSX
- Software: Iraf, supermongo, Gimp, xv, MS Powerpoint, etc.
- Scripting Languages: Shell Scripts, Iraf-cl Scripts, Matlab, AWK, SED, L<sup>A</sup>T<sub>E</sub>X

## **Memberships:**

---

- Member of the Swiss Society for Astronomy and Astrophysics (SSAA)

## **Personal Interests:**

---

- Travelling and Nature
- Sport: Badminton, Climbing, Diving, Skiing, Tennis
- Musik: Piano

## Conferences:

---

- 10/2007:** Conference: General Assembly of the SSAA (Bern/CH)
- 03/2007:** Winter School: 37th Saas-Fee advanced course (Mürren/CH)
- 12/2006:** Conference: IAU Symposium 241(La Palma/E)  
Poster: *The age metallicity relation of the Small Magellanic Cloud: New Results from Ca II triplet spectroscopy*
- 09/2006:** Conference: General Assembly of the SSAA (Locarno/CH)  
Talk: *The age metallicity relation of the Small Magellanic Cloud*
- 08/2006:** NEON Observing School (Observatoire de Haute-Provence/F)
- 03/2006:** Conference: Globular Clusters - Guides to Galaxies (Conception/CL)  
Talk: *The age metallicity relation of the Small Magellanic Cloud*
- 11/2005:** Rhine Stellar Dynamics Network Meeting (Hoher List Observatory/DE)  
Talk: *CN and CH abundances in Galactic Globular Clusters*
- 07/2005:** Conference: Mass and Mystery in the Local Group (Cambridge/UK)  
Poster: *CN and CH Abundances in Globular Clusters*
- 04/2005:** Conference: Resolved Stellar Populations (Cancun/MX)  
Talk:  *$\omega$  Centauri - an accreted dwarf galaxy?*
- 02/2005:** Conference: IAU Colloquium No. 198 (Les Diablerets/CH)  
Poster: *Abundances from a large spectroscopic survey in  $\omega$  Centauri*
- 12/2004:** Basel/Heidelberg workshop (Ringberg/DE)  
Talk:  *$\omega$  Centauri - an accreted dwarf galaxy?*
- 09/2004:** Conference: Astronomische Gesellschaft - Herbsttagung (Prague/CZ)  
Poster: *Abundances from a large spectroscopic survey in  $\omega$  Centauri*
- 12/2003:** Graduiertenkolleg 787 Meeting (Bad Honnef/DE)  
Talk: *Medium resolution spectroscopy in omega Centauri*
- 10/2003:** Graduiertenkolleg 787 Meeting (Bochum/DE)
- 10/2003:** Conference: Stellar populations 2003 (Garching/DE)  
Poster: *Medium resolution spectroscopy in omega Centauri*
- 07/2003:** Graduiertenkolleg 787 Meeting (Dwingeloo/NL)

## Colloquia:

---

- 06/2007:** Zentrum für Astronomie (Heidelberg/DE)  
*Tracing the Chemical Evolution of the SMC via Star Cluster Spectroscopy*
- 06/2007:** University of Wisconsin (Madison/USA)  
*Tracing the Chemical Evolution of the SMC via Star Cluster Spectroscopy*
- 10/2004:** University of Sydney (Sydney/AU)  
*Spectroscopy in omega Centauri*
- 10/2004:** Australian National University (Canberra/AU)  
*Spectroscopy of subgiants in omega Centauri*

## **Publications:**

---

### **Refereed Publications:**

- Andrea Kayser, Michael Hilker, Philip G. Willemsen, and Tom Richtler  
Medium resolution spectroscopy in  $\omega$  Centauri:  
abundances of 400 subgiant and turn-off region stars  
2006, *Astronomy & Astrophysics*, 458, 777
- Philip G. Willemsen, Michael Hilker, Andrea Kayser, and Coryn A. L. Bailer-Jones  
Analysis of medium resolution spectra by automated methods - Application to M55 &  $\omega$  Centauri  
2005, *Astronomy & Astrophysics*, 436, 379
- Michael Hilker, Andrea Kayser, Tom Richtler, and Philip G. Willemsen  
The extended star formation history of  $\omega$  Centauri  
2004, *Astronomy & Astrophysics*, 422, L9

### **Other Publications:**

- Andrea Kayser, Eva K. Grebel et al.  
A Spectroscopy-Based Age-Metallicity Relation of the SMC  
IAU Symposium 241: Stellar Population as Building Blocks of Galaxies  
eds. A. Vazdekis and R. F. Peletier  
Cambridge University Press, 2007, 351
- Andrea Kayser, Eva K. Grebel et al.  
The Age-Metallicity Relation of the SMC  
ESO/Springer: Globular Clusters - Guides to Galaxies  
in press
- Andrea Kayser, Michael Hilker, Philip G. Willemsen, and Tom Richtler  
 $\omega$  - an accreted dwarf galaxy?  
ASP Conference Series, Vol. TBA: Resolved Stellar Populations  
in press
- Andrea Kayser, Michael Hilker, Philip G. Willemsen, and Tom Richtler  
Abundances from a large spectroscopic survey in  $\omega$  Centauri  
IAU Colloq. 198: Near-field cosmology with dwarf elliptical galaxies  
eds. H. Jerjen and B. Binggeli  
Cambridge University Press, 2005, 418

### **Publications in preparation:**

- Andrea Kayser, Michael Hilker, Eva K. Grebel, and Philip G. Willemsen  
Comparing CN and CH line strength in a homogeneous spectroscopic sample of 8 Galactic globular clusters
- Andrea Kayser, Eva K. Grebel, and Andreas Koch  
Radii and velocities for 11 clusters in the Small Magellanic Cloud
- A. Kayser, E. K. Grebel, D. R. Harbeck, A. A. Cole, A. Koch, K. Glatt, J. S. Gallagher, G. S. Da Costa  
New clues on the chemical evolution of the Small Magellanic Cloud from star clusters.
- K. Glatt, J. S. Gallagher, E. K. Grebel, G. Clementini, A. Nota, A. Kayser, A. Koch, E. Sabbi, M. Sirianni  
Age determinations of 5 clusters in the Small Magellanic Cloud



## References:

---

- Prof. Dr. Eva K. Grebel  
Astronomisches Rechen-Institut  
Mönchhofstrasse 12-14  
D-69120 Heidelberg  
Germany  
grebel@ari.uni-heidelberg.de
- Dr. Michael Hilker  
European Southern Observatory  
Karl-Schwarzschild-Strasse 2  
D-85748 Garching  
Germany  
mhilker@eso.org
- Prof. Dr. John S. Gallagher III  
Department of Astronomy  
University of Wisconsin  
475 North Charter Street  
Madison, WI 53706-1582  
USA  
jsg@astro.wisc.edu



Ich erkläre, dass ich die Dissertation “Chemical Evolution of Nearby Stellar Systems” nur mit der darin angegebenen Hilfe verfasst und bei keiner anderen Universität oder Fakultät der Universität Basel eingereicht habe.

.....  
Binningen, den 25. Oktober 2007

